2015

Field observations of wave induced coastal cliff erosion, Cornwall, UK

Earlie, Claire Siobhan

http://hdl.handle.net/10026.1/3526

http://dx.doi.org/10.24382/3339
Plymouth University

FIELD OBSERVATIONS OF WAVE INDUCED COASTAL CLIFF EROSION, CORNWALL, UK

by

CLAIRE SIOBHAN EARLIE

A thesis submitted to Plymouth University in partial fulfilment for the degree of

DOCTOR OF PHILOSOPHY

School of Marine Sciences and Engineering

Faculty of Science and Environment

May 2015

Abstract

Name: Claire Earlie

Title: *Field Observations of Wave Induced Coastal Cliff Erosion, Cornwall, UK*

Coastal cliff erosion is a widespread problem that threatens property and infrastructure along many of the world's coastlines. The management of this risk calls for robust quantification of cliff erosion rates, which are often difficult to obtain along rocky coasts. Quantification of sea-cliff rates of retreat on annual to decadal time scales has typically been limited to rapidly eroding soft rock coastlines. Rates of erosion used for shoreline management in the UK are generally based on analysis of historic maps and aerial photographs which, in rocky coast environments, does not wholly capture the detail and timing at which the processes operate and the failures occur across the cliff face.

The first stage of this study uses airborne LiDAR (Light Detection and Ranging) data at nine sites around a rocky coastline (Cornwall, UK) to gain a quantitative understanding of cliff erosion where average recession rates are relatively low (c. 0.1 m yr^{-1}). It was found that three-dimensional volumetric changes on the cliff face and linear rates of retreat can be reliably calculated from consecutive digital elevation models (DEMs) several years apart. Rates of erosion ranged between 0.03–0.3 m yr^{-1}. The spatial variability in recession rates was considered in terms of the relationship with the varying boundary conditions (rock mass characteristics, cliff geometries, beach morphology) and forcing parameters (wave climate and wave exposure). Recession rates were statistically correlated with significant wave height (*Hs*), rock mass characteristics (*GSI*) and the ratio between the two (*GSI/Hs*). Although the rates derived using airborne LiDAR are comparable to the longer term rates of retreat, the detail of erosion to the cliff-face provides additional insight into the processes occurring in slowly eroding environments, which are vital for understanding the failure of harder rock coastlines. In addition to this, the importance of the wave climate and rainfall needs further attention on a more localised scale. Monthly cliff face volume changes, at two particularly vulnerable sites (Porthleven and Godrevy, Cornwall, UK), were detected using a Terrestrial Laser Scanner (TLS). Using these volumes alongside information on beach profile, beach-cliff junction elevation changes and nearshore hydrodynamics have allowed an insight into how the cliffs respond to seasonal fluctuations in wave climate and beach morphology. Monthly variability in beach morphology between the two sites over a one-year survey period

indicated the influence that beach slope and the elevation of the beach-cliff junction have on the frequency of inundation and the power of wave-cliff impacts. Failure mechanisms between the two sites ranged from rotational sliding of superficial material to quarrying and block removal over the entire cliff elevation, according to the extent of wave-cliff interaction. This particular survey period highlighted the sensitivity of cliff erosion to the variability in wave climate and beach morphology at two different locations in the south-west of the UK, where the vast majority (over 85% of the annual value) of cliff face erosion occurs during the winter when extreme storm waves prevail.

Coastal cliff erosion from storm waves is observed worldwide but the processes are notoriously difficult to measure during extreme storm wave conditions when most erosion normally occurs, limiting our understanding of cliff processes. Over January-March 2014, during the largest Atlantic storms in at least 60 years with deep water significant wave heights of 6 – 8 m, cliff-top ground motions of a rocky cliff in the south-west of the UK (Porthleven, Cornwall) showed vertical ground displacements in excess of 50–100 μm; an order of magnitude larger than observations made previously. Repeat terrestrial laser scanner surveys, over a 2-week period encompassing the extreme storms, gave a cliff face volume loss 2 orders of magnitude larger than the long-term erosion rate. Cliff-top ground motions and erosion volumes were compared at two different locations, one a reflective beach with steeply shelving bathymetry (Porthleven, Cornwall) and the other an intermediate, low tide bar-rip beach with a wide coastal slope (Godrevy, Cornwall). Under similar wave conditions (6–8 m H_s and 15–20 s. T_p) the vertical ground motions were an order of magnitude greater at the cliffs fronted by steeply shelving bathymetry, where the breaking waves plunge right at the shoreline, with little prior dissipation, leading to large energetic runup impacting the cliff. These storm results imply that erosion of coastal cliffs exposed to extreme storm waves is highly episodic and that long-term rates of cliff erosion will depend on the frequency and severity of extreme storm wave impacts as well as the wave dissipation that occurs as a function of the nearshore bathymetry. Having recorded microseismic cliff-top motion on this scale for the first time and determined an effective method of monitoring the energetic wave impacts, this study emphasises how investigations of cliff behaviour during storms is not only obtainable, but paramount to understanding coastal evolution under extreme conditions.

Author's Declaration

At no time during the registration for the degree of Doctor of Philosophy has the author been registered for any other University award without prior agreement of the Graduate Committee.

Work submitted for this research degree at Plymouth University has not formed part of any other degree either at Plymouth University or at another establishment.

This study was financed with the aid of studentship from the European Social Fund, Great Western Research, Combined Universities of Cornwall PhD Studentship and was carried out in partnership with the University of Exeter, Penryn Campus and the National Trust.

The PhD supervisory team consisted of Prof. Gerd Masselink (Director of Studies) and Prof. Paul Russell from the School of Marine Science and Engineering, Plymouth University and Dr. Robin Shail, from Camborne School of Mines, University of Exeter and Dr Larissa Naylor, (formerly) University of Exeter.

Relevant scientific seminars and conferences were regularly attended at which work was often presented; external institutions were visited for consultation purposes and several papers prepared for publication.

Word count of main body of thesis: 48,890

Signed…….

Date……22/07/2015…….

PhD outputs

Refereed journal publications:

Earlie, C.S., Young, A.P., Masselink, G., Russell, P.E. (2015) Coastal cliff ground motions and response to extreme storm waves. *Geophysical Research Letters*, DOI: 10.1002/2014GL062534

Earlie, C.S., Masselink, G., Russell, P.E., Shail, R.K. (2014) Application of airborne LiDAR to investigate rates of recession in rocky coast environments, *Journal of Coastal Conservation*, DOI: 10.1007/s11852-014-0340-1

Earlie, C.S., Masselink, G., Russell., P.E., Shail., R.K. (2013) Sensitivity analysis of the methodology for quantifying cliff erosion using airborne LiDAR – examples from Cornwall, UK., *In:* Conley, D.C., Masselink, G., Russell, P.E., and O'Hare, T.J. (Eds), *Proceedings 12th International Coastal Symposium, Plymouth, UK. Journal of Coastal Research*, SI (65): 470-475.

Conference presentations:

Earlie, C.S., Young, A.P., Masselink, G., Russell, P.E. (2015) Coastal cliff-top ground motions and response to extreme storm waves, *Infragravity and Earth Hum workshop, IUEM, Brest, France, 12th–13th March 2015.* Oral presentation and abstract.

Earlie, C.S., Masselink, G., Russell, P.E., Shail, R.K. (2013) Terrestrial laser scanning as a method of evaluating seasonal changes to hard rock coastal cliffs, *American Geophysical Union, Annual Fall Meeting, San Francisco, 9th–13th December, 2013.* Poster presentation and abstract.

Earlie, C.S., Masselink, G., Russell, P.E., Shail, R.K., Naylor, L.A. (2013) Quantifying coastal cliff erosion in hard rock environments – examples from Cornwall, UK, *Coastal cliffs and Lake Bluffs Symposium, Llandudno, UK, 17th–18th September, 2013.* Oral presentation and abstract.

Earlie, C.S., Masselink, G., Russell, P.E., Shail, R.K., Naylor, L.A. (2013) Sensitivity analysis of the methodology for quantifying cliff erosion using airborne LiDAR – examples from Cornwall, UK, *12th International Coastal Symposium, Plymouth, UK, 8th–12th April 2013.* Oral presentation and conference proceedings. Awarded best student presentation of the conference and best overall presentation of the day.

Earlie, C.S., Masselink, G., Russell, P.E., Shail, R.K., Naylor, L.A. (2012) Coastal cliff erosion in Cornwall, *Young Coastal Scientist and Engineers Conference, Bangor, UK, 2nd–3rd April 2012.* Poster presentation and abstract.

Other presented work:

Earlie, C.S., Masselink, G. (2014) *SKY Television – documentary on the coastal erosion after the storms of 2014*. Recorded at Porthleven on the 18th February 2014, broadcast nationwide on the 19th February, 2014.

Earlie, C.S., Russell. P.E. (2014) *BBC1- 'The Storms the Shook the South-west'*. Recorded at Porthleven on the 17th March 2014, broadcast nationwide on the 11th – 18th April and 12th May 2014.

Earlie, C.S. (2014) *BBC Spotlight*, 13th April 2014. Recorded television interview.

Earlie, C.S. (2014) *BBC Radio 5*. 13th April 2014. Live radio interview.

Earlie, C.S. (2013) *Quantifying coastal cliff erosion in hard rock environments – examples from Cornwall, UK*, South-west Coastal Regional Monitoring Programme, 7th Annual Partners Meeting, Totnes, UK, 2nd October 2013. Invited talk.

Earlie, C.S. (2013) *Cliff recession and climate change in Cornwall*, University of Exeter, Geography Seminar Series, 4th February, 2013. Invited talk.

Earlie, C.S. (2012) *Coastal cliff erosion in Cornwall*, 'Pro-Geo event': Geological Society South-west region, Lifton, UK, 5th December 2012. Invited talk.

Grants awarded:

Plymouth Marine Science and Education Foundation: Grant-in-aid 2015. £400 awarded to attend the Infragravity and Earth Hum workshop, Brest, France, 2015.

Plymouth Marine Institute Education Fund: Grant-in-aid 2013. £300 awarded to attend the Coastal Cliffs and Lake Bluffs Symposium, Llandudno, UK, 2013.

Plymouth University, School of Marine Science and Engineering, School Research Committee: £2360 Small Research Grant awarded for *Storm Wave Impacts on Coastal Cliffs* project to measure, quantify and explain the effect of storm wave impacts on coastal cliffs, including visiting and collaborate with Scripps Institute of Oceanography, USA, 2013.

Contents

List of figures

List of tables

Acknowledgements

Firstly I would like to give an enormous thanks to my brilliant supervisors Prof. Gerd Masselink and Prof. Paul Russell who have provided me with no end of inspiration, enthusiasm, and excitement for the research, and for giving me the freedom and encouragement to explore wacky ideas and visit wonderful places. I met them both during my masters where they introduced me to the joys of field campaigns, at Perranporth, Cornwall, where I experienced many cold, long days running around the beach, late nights Matlabbing, drinking cheap wine and sharing a bathroom with 15 people. You have truly given me the greatest academic experience upon which to begin my journey. Thank you from the bottom of my heart, for believing in the girl who said 'crumbly stuff'. I would also like to express my sincerest gratitude to Dr. Robin Shail and Dr. Larissa Naylor at the University of Exeter. Robin, for the impromptu site visits, filled with geological wisdom, and your excitement and passion for the Cornish coastline and Larissa for her continued support and endless expertise and knowledge of rocky coastlines. Thank you both.

Sincerest thanks are also given to Dr. Andrew Wetherelt and Prof. John Coggan at Camborne School of Mines for taking the time to teach me an enormous amount of geotechnical and geological information in such a short space of time. Your time and help are greatly appreciated. I would like to acknowledge the National Trust, the University of Exeter and Great Western Research for collaborating to fund this PhD studentship and encouraging me along the way. Appreciation is also given to Plymouth Marine Institute, and the School of Marine Science and Engineering for granting me the travel funds to pursue what was quite simply an *idea*. That *idea* grew into collaboration with a world class research institute and the chance to capture some of the most exciting storm data coastal research has seen.

I would also like to give a huge thank you to Dr. Adam Young at Scripps Oceanographic Institute. I contacted Adam as a 'fan' after being impressed by his cliff-top seismic research, asking him far more questions than he probably had time for. Adam very kindly invited me to Scripps where he spent hours teaching me the wonders of seismic research and very generously lent us the infamous seismometer, with which we were able to measure the storms. I look forward to hopefully working with you on cliff research again in the future.

None of the data in this thesis would have been obtained without the help of a group of thoroughly hard working souls: Kit Stokes, Ellie Woodward, Tim Scott, Tim Poate, Antony Thorpe, Pedro Almeida, Kris Inch and Ken Kingston. I don't think any amount of sandwiches, boxes of cookies and muffins was quite enough to express my thanks and appreciation for your carrying skills, patience and eagerness to get out and help me scan in any weather; I physically couldn't have done it without your help. I will always be indebted to Peter Ganderton for his technological mastery and endless patience, helping me to understand and operate complicated equipment and always happily offering his time to help me with my research.

I also want to thank all of my office mates for constantly making me laugh and for offering suggestions, sharing knowledge and generally being the greatest bunch of people to sit down next to every day. Special thanks go to my 'first day at school' buddies, Ellie, Kit and Pedro. I wish you all the greatest success in whatever you go on to do. I'm so lucky to have gone through this journey with you and I look forward to continuing our work and friendship together in the future. As well as office friends, I would not have made it through the last few years, with as big a smile on my face, without all of my friends, both in Plymouth and far away. You know who you are, I love you loads.

A particularly massive acknowledgement goes to my incredible proof readers, Mum, Jen and Ben. Thank you for your love and support, and giving my thesis your precious time and attention. A very special thank you goes to Ben for keeping my feet on the ground and head in the clouds over the final few months and for arriving at the finish line with me, I look forward to the next adventure.

Last but by no means least I would like to thank my amazing family, Mum, Alan, Chris and Grandma. You have always encouraged and inspired me to follow my dreams. I'm not sure I would have even tried if I didn't have your support and unwavering belief in me. Thanks for everything; you are truly the greatest people in my life. My dear Dad, who is sadly no longer with us, noticed a light in me, from a young age whenever I was near the sea. His passion for all things 'ocean', fed mine and it continues to grow every time I visit the beach. This thesis is dedicated to his memory and his love for the sea.

for Dad

Chapter 1

Introduction and background to the study area

1.1 Preamble

Cliff erosion and the associated risks to coastal properties has been a topic of investigation for many decades; however, in the context of climate change, sea-level rise and the potential for increased storminess, the majority of coastal morphological literature has tended to focus on depositional, rather than erosive coasts (Emery and Kuhn, 1982; Stephenson, 2006; Naylor *et al.*, 2010). The vulnerability of different coasts can be characterised by the response to and the relaxation times between return intervals of extreme events (Pethick and Crooks, 2000). In this respect, cliffed coastlines are highly vulnerable as their erosive nature makes them non-recoverable. Naylor *et al.* (2010) identified a significant difference between the amount of research carried out on erosive compared to depositional coasts over the last 20 years, leading to a limited understanding of the vulnerability of rocky coastlines. In particular, this refers not only to rocky coastlines alone, but also erosive coastlines with complex morphologies, such as cliffs fronted by beaches or shore platforms and composite cliffs that vary in hardness throughout their vertical profile (Sunamura, 1992; Naylor *et al.*, 2010). The majority of cliff erosion studies in the UK have focused along the eastern and south-east coast of the country due to the very high rates of recession that are a consequence of the 'soft rock' geology (till, chalk, clays and heavily weathered shales) (Hall *et al.*, 2002; Damgaard and Dong, 2004; Dong and Guzzetti, 2005; Lee, 2008; Dawson *et al.*, 2009; Brooks and Spencer, 2010; Ashton *et al.*, 2011; Brooks *et al.*, 2012). Both in the UK and globally, limited literature exists on the evolution of more resistant and lesser-weathered 'harder' rock coastlines (sandstones, mudstones, shales and granite) and their response to coastal erosion.

There are a number of different variables that control the rates of and processes involved in cliff erosion. Field-based studies on rocky coastlines have attempted to consider the influence of multiple variables on the rates of erosion, e.g., geotechnical controls on slope failure (Shail *et al.*, 1998; Lee, 2008), the role of waves on the erosion and weakening of the cliff-base (Emery and Kuhn, 1982; Lim *et al.*, 2011) and/or the influence of weathering and groundwater on cliff instability (Pierre and Lahousse, 2006). Seldom have observational

studies however, been able to successfully consider the relationships between the multiple variables that can influence erosion holistically, likely due to the limitations associated with quantifying the different processes. Likewise, only recently has research has been carried out from a marine perspective; investigating the direct influence of wave impacts on cliffed coastlines (Stephenson and Kirk, 2000; Young *et al.,* 2011a; Dickson and Pentney 2012; Young *et al.,* 2012; 2013; Earlie *et al.,* 2015; Ogawa *et al.,* 2015; Van Jones *et al.,* 2015).

A large variety of methods have been used to assess cliff erosion rates and analyse cliff morphology. Cliff erosion studies in the UK have typically involved using historic mapping, photogrammetry or Terrestrial Laser Scanning (TLS) to determine cliff-face volumetric changes and rates of retreat (Rosser *et al.,* 2005; Ridgewell and Walkden, 2009; Lim *et al.,* 2010). Rates of erosion in harder rock coastlines found using these techniques range from 0.02 to 0.5 m yr^{-1}. The variation in rates depends on not only the geological characteristics, the wave exposure and meteorology, but also on the type of technique used during the analysis and the temporal and spatial scale under consideration. For example, historic map analysis of the recession of a cliff-top over decades at a coarser spatial scale will miss some of the detail of changes to the cliff-face (Earlie *et al.,* 2013), whereas bi-annual/monthly surveys of a cliff using photogrammetry or TLS will identify regions of failure across the cliff-face and will help identify any seasonality that may be apparent in the erosion activity (Rosser *et al.,* 2005; 2007). The lack of accurate data that currently captures the evolution of rocky coastlines and the parameters, which explain the variability in erosion rates, mean that most proxies for wave-cliff interaction remain theoretical.

Over the past few years (since 2010), the south-west of the UK has seen some very significant landslips, cliff falls/failures in these hard-rock environments (BBC, 2012; BGS, 2013; SWCP, 2014). Both the general public and coastal managers have begun to ask: what is causing this recent dramatic increase in cliff-failure? The winter of 2013/2014 was one of the stormiest and most energetic wave periods in over 60 years, and regions of the south-west experienced large scale erosion of many beaches and cliffs, with flooding and damage to coastal infrastructure (Masselink *et al.,* 2014; Poate *et al.,* 2014; Earlie *et al.,* 2015; Masselink *et al.,* in press). Sea-level rise and more frequent stormy conditions (heavier rain and large sea swells) induced by a changing climate have the potential to increase this rate of coastal erosion in the future. Cliff retreat, in particular, often occurs as sudden failures and

can potentially pose a great threat to public safety and existing infrastructure. Obtaining data in this dynamic environment and understanding the kinematics of the cliffs and the linkage between the forcing parameters and the rates of erosion will not only feed into cliff erosion models, but ultimately inform future coastal management strategies. It is intended that the results of this research will also help the National Trust (the largest coastal landowner in Cornwall) improve management and adaptation strategies for their coastal assets and infrastructure and contribute to the wider rocky coastal erosion research community.

1.2 Aims and Structure of Thesis

The broad aim of this study is to gain a quantitative understanding of coastal erosion along exposed cliffed coastlines characterised by a combination of harder bedrock cliffs and less resistant superficial quaternary deposits, and to assess how the spatial and temporal variability in the boundary conditions and forcing parameters affect the rates of coastal cliff erosion. In order to achieve this, the project takes a *top-down* approach, investigating the factors attributing to cliff erosion over three decreasing time and spatial scales:

1. The long term time scale quantifies rates of retreat over a period of 3–4 years at nine vulnerable locations located around the Cornish peninsula using airborne LiDAR and characterises the geological setting and wave climate at each site.

2. The medium term time scale uses TLS to obtain monthly high-resolution 3D point cloud data at two particularly vulnerable locations over one year (July 2013–July 2014). This sophisticated data set, alongside beach morphological and nearshore hydrodynamic data relates the monthly evolution of the cliffs to the weather and wave conditions.

3. On a shorter time scale, *in-situ* observations of cliff behaviour during a particularly stormy winter using a seismometer, video camera, wave buoy data, beach profiles and TLS, offers, for the first time, insight into the evolution of the cliffs and beach under extreme wave conditions.

In order to understand this spatial and temporal variability, the following specific research questions are examined throughout the thesis:

- What factors explain the spatial variability in erosion around a rocky coastline?
- How useful are remote sensing techniques, such as airborne LiDAR and terrestrial laser scanning at capturing coastal cliff change?
- What role do the nearshore hydrodynamic regime, offshore bathymetry and beach type play in the variability of cliff erosion?
- How do the cliffs respond to a highly energetic wave environment and which factors contribute to controlling the energy expended on the cliffs?
- How do wave induced cliff-top ground motions respond to waves under different coastal settings i.e., cliffs fronted by a reflective versus a dissipative/intermediate beach?

The thesis chapters are organised as follows:

Chapter 1 introduces the main research questions of the thesis and places the research into context. This chapter contains a brief overview of the broader cliff erosion literature; a theoretical framework including mechanisms of cliff failure and methods of measuring cliff erosion. Note that more detailed literature reviews specific to the research methods and time and spatial scales in question are also provided in Chapters 2, 3 and 4. Chapter 1 encompasses a detailed geological and geomorphological overview of each site, which is referred to in the subsequent chapters.

Chapter 2 considers cliff erosion over a long-term time scale where cliff erosion over a 3–4 year period is quantified using airborne LiDAR at nine locations around the Cornish coastline. A sensitivity analysis of the airborne LiDAR method and its suitability for monitoring slowly eroding 'harder rock' coastlines are also explored here.

Chapter 3 investigates cliff erosion at two vulnerable locations on opposite facing coastlines using continuous wave data, monthly point cloud cliff comparisons and beach profile surveys to determine the variability in erosion rates on a reduced time scale and relate cliff response to varying forcing and resisting factors.

Chapter 4 explores the findings of the previous two chapters by examining the geophysical behaviour of the cliffs and the cliff–top ground motions according to the wave conditions and beach morphology *in-situ* using a seismometer, video camera and continuous wave and water

level data. Intermittent terrestrial laser scanning allows for a qualitative and quantitative analysis of the changes detected under such conditions.

Chapter 5 synthesises the main findings of the thesis in the context of the research questions, drawing upon the main themes that emerge throughout. The original contributions to broader knowledge are identified and recommendations for further research are proposed.

1.3 Literature review – Theoretical Framework

1.3.1 Coastal cliff erosion – mechanisms of cliff failure

Coastal cliff erosion is understood to be due to a complex combination of sub-aerial and marine processes weakening the structural integrity of the cliffs, leading to gradual erosion and episodic mass failure (Pethick, 1984; Trenhaile, 1987; Sunamura, 1992). The variety of cliff profiles and cliff types along every cliffed coastline around the world indicates that there are a wide range of processes (both sub-aerial and marine) that are involved in shaping these coasts. These processes may include erosion due to wave-attack via abrasion, attrition, quarrying and hydraulic action, or physical and chemical weathering of cliff material as a result of rainfall, changes in temperature, biochemical and biophysical erosion (Emery and Kuhn, 1982; Trenhaile, 1987; Sunamura, 1992; Masselink and Hughes, 2003). The mechanism via which failure occurs can sometimes help indicate the cause of failure. For example, rotational landslides and mudslides often result from a period of prolonged rainfall and hence an increase in pore water pressures in the ground leading to slope failure (Wyllie and Mah, 2004). Rock falls, topples, planar and wedge failures, however, often occur more suddenly, and their failure is a result of the assailing force (e.g., waves) exceeding the resisting force (e.g., rock mass structure and the lithology) over time (Sunamura, 1992; Lee, 2002). Failed material accumulated at the toe, known as talus deposits, provide a form of protection to the base of the cliff, and is subsequently removed by waves, forming part of the nearshore sediment supply (Pethick, 1984; Sunamura, 1992). The erosive nature of cliffs makes understanding their history difficult as the stages of evolution are not preserved, but removed from the coastal ‘system’ (Masselink and Hughes, 2003). The absence of preserved evidence required by many studies makes it difficult to infer processed from cliff form. The

mechanisms of cliff failure and conditions leading to the erosion of cliffs have therefore been the topic of investigation for many decades.

The behaviour of cliffed coasts can be characterised into four main cliff system categories (Lee, 2002) (Fig. 1.1). *Simple cliffs* are cliffs where failure mechanisms and sediment inputs into the nearshore occur in a single sequence due to topples and falls, rotational landslides and mudslides. *Composite cliff* failure occurs in partly coupled sub-systems, for example, when rotational landslides occur over harder bedrock or where harder rock block slides occur over more cohesive material. *Complex cliffs* fail when strongly linked subsystems cause failure with complex feedback mechanisms. Examples of failure within this type of system are deep-seated landslides with failures throughout or seepage in an already eroding cliff. *Relict cliff systems* involve failures in pre-existing landslides where reactivation or 'slope-over-wall' failure has occurred due to progressive retreat of the current sea cliff position and subsequent failure of upper cliff material (Emery and Kuhn, 1982; Lee, 2002). Due to the geological characteristics of the cliffs along the south-west coastline, the cliff systems apparent in this study are mainly simple cliffs, (rotational land sliding and toppling of superficial deposits), composite cliff systems and relict cliff systems where rotational land sliding of weaker superficial head deposits has occurred over more resistant bedrock. Evidence of complex and relict cliffs are apparent in some locations where reactivation or seepage has occurred. The complex nature of cliff failure makes it difficult to categorise the cliffs into one specific cliff system or another, as processes and failure mechanisms vary considerably around the coastline (Emery and Kuhn, 1982). The significant lack of information and understanding of the detail in the processes involved in shaping these coastlines means that predicting failure and developing management strategies is a very complex task.

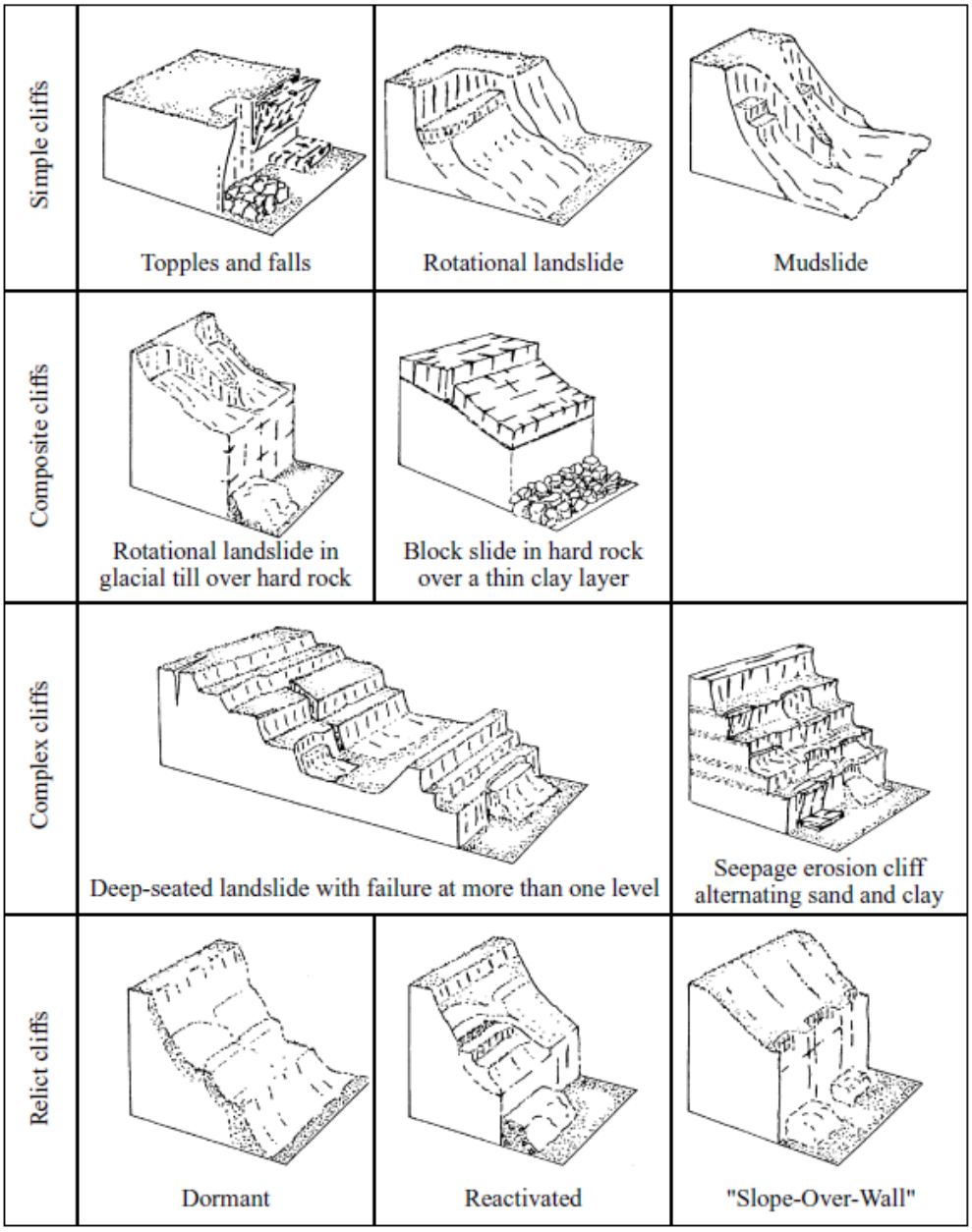

Figure 1.1. Cliff system failure categories (Lee, 2002). Many of these examples are noted around a rocky coastline such as the south-west peninsular of the UK (Arber, 1949).

1.3.2 Coastal cliff erosion – topics of investigation

The tectonic history preserved in the rocks exposed along the south-west coastline means that the stratigraphy of cliffs has been a topic of interest for many decades (Arber, 1949; Steers, 1964; Pethick, 1984; Leveridge and Shail, 2011). Numerous studies have provided evidence of the deformations that occurred during the Devonian to Carboniferous periods (Shail and Wilkinson, 1994; Alexander and Shail, 1995; 1996, among many others). These studies have

been vital in contributing toward the geological understanding of the chronology of the Variscan Orogeny; the mountain building event caused by Palaeozoic collision between Laurussia and Gondwana to form the supercontinent, Pangea (Leveridge and Hartley, 2006).

Geotechnical slope stability studies are often carried out on a site-by-site basis, analysing the geological properties and structural integrity of the cliffs for coastal or risk management and development purposes (Coggan *et al.,* 2001; Westgate *et al.,* 2003; Leveridge and Hartley, 2006; Shail and Coggan 2010). Monitoring of hard-rock coasts for these purposes has helped identify spatial and temporal patterns (magnitude-frequency relationships) in rockfall activity as a precursor to cliff or slope failure (Rosser *et al.,* 2007; Lim *et al.,* 2010; Barlow *et al.,* 2012; Norman *et al.,* 2013; Rosser *et al.,* 2013); but challenges remain linking previous failure to forcing events.

The sensitivity of cliffs to climatic variability in terms of precipitation has been considered where the hydraulic stability of cliffs has been modelled using rainfall and pore water pressures as thresholds for failure (Pierre and Lahousse, 2006; Collins and Sitar, 2008; Brooks *et al.,* 2012). The effects of wave climate variability on recession rates has also been modelled (Hall *et al.,* 2002; Damgaard and Dong, 2004; Dong and Guzzetti, 2005; Brooks and Spencer, 2010; Ashton *et al.,* 2011; Caplain *et al.,* 2011; Brooks *et al.,* 2012; Castedo *et al.,* 2012), although this research tends to focus on soft-rock, as opposed to hard-rock cliffs.

Various process-based numerical models have been developed to predict the evolution of cliffed coastlines, although many of the models often assume a vertical and lithologically homogenous cliff profile (Lee *et al.,* 2001; Milherio-Oliveira, 2007; Walkden and Dickson, 2008; Quinn *et al.,* 2010; Walkden and Hall, 2011; Barlow *et al.,* 2012) with the exception of Carpenter *et al.* (2014) who modelled the evolution of a lithologically varied soft-cliff profile. Physical process cliff recession studies have also assessed the influence of varying beach morphology (Dickson *et al.,* 2004; Lee, 2008; Walkden and Dickson, 2008; Kennedy *et al.,* 2011; Stephenson *et al.,* 2012), water levels and wave climate (Xeidakis *et al.,* 2007; Lim *et al.,* 2009; Taibi *et al.,* 2009; Nunes *et al.,* 2011), yet very few studies attempt to draw relationships between these influential variables, the rock mass characteristics and failures (Hack and Huisman, 2002; Dickson *et al.,* 2004; Dickson and Pentney, 2012;). Establishing empirical relationships between wave exposure, rock strength and cliff erosion will help to better understand the processes occurring and also predict future erosion risk.

Basal cliff erosion is largely understood to occur as a function of the interaction between the resisting force of the cliffs and the assailing force of the waves (Sunamura, 1992, Equation 1.1).

$$x = f(F_W, F_R\ , t) \qquad \text{Equation 1.1}$$

where x is the eroded distance, t is time and where erosion only occurs when the assailing force of the waves F_W is greater than the resisting force of the cliffs F_R. Wave action is understood to weaken the cliff at the toe and remove the protection that talus material provides (Sunamura, 1992; Masselink and Hughes, 2003). However, surprisingly limited research has been directed towards relating the rate of cliff-face erosion directly to the wave climate (Adams and Chandler, 2002; Adams *et al.,* 2002: 2005; Young *et al.,* 2009; Young *et al.,* 2011a; 2011b; Dickson and Pentney, 2012), particularly in the UK (Lim *et al.,* 2011; Vann-Jones *et al.,* 2015). In the last decade, seismometers buried in the cliff-top have explored the relationship between the offshore wave field and the resultant vibrating, shaking and swaying of the cliffs (Adams *et al.,* 2002; 2005; Young *et al.,* 2011a; 2011b; 2012; 2013; Earlie *et al.,* 2015, Vann-Jones *et al.,* 2015) leading to a deeper understanding of the geotechnical implications of microseisms on cliffed coastlines (Adams *et al.,* 2005; Brain *et al.,* 2014). With the potential for rising sea-levels and increased storminess, field observations of cliff-top microseisms and cliff failure in highly energetic wave and storm surge conditions have until now (Earlie *et al.,* 2015), not yet been obtained. The abundance of research in soft-rock cliffs and the investigations that have highlighted the significance of wave climate, rainfall and rock mass strength in shaping them, emphasises the opportunities for understanding harder rock coastlines in more detail. Previous investigations tend to consider failure from either a geotechnical perspective, a sub-aerial or a marine perspective, where one factor is assumed to influence cliff erosion more than another; rarely are the interactions between the systems considered holistically, especially in hard-rock cliff environments (Naylor *et al.,* 2010; Norman, 2012).

1.3.3 Quantifying coastal cliff erosion

A frequently used method of quantifying long-term shoreline change for coastal management purposes (50–150 years) involves using historic maps and aerial photos. A shoreline/cliff top/

cliff toe position is digitised using GIS software such as DSAS (Digital Shoreline and Analysis Software) tool within ArcMap (ESRI, 2011; USGS, 2012). The rate at which this 'line' retreats is determined using transects cast perpendicular to the shore at specified alongshore intervals and estimating the rate of retreat over the time period (Brooks and Spencer, 2010; Brooks *et al.,* 2012). Shoreline Management Plans in the UK use DSAS to quantify future shoreline retreat rates (Ridgewell and Walkden, 2009; Earlie *et al.,* 2012). The shoreline is divided up into 25 m lengths and a modified version of the cliff equilibrium erosion equation (Equation 1.2) for soft-rock shores (Walkden and Hall, 2005; Walkden and Dickson, 2008) is used to determine the equilibrium recession rates subjected to an increased rate in sea level rise.

$$\varepsilon_2 = \varepsilon_1 \sqrt{\frac{S_2}{S_1}} \qquad \text{Equation 1.2}$$

where the modelled cliff response to future sea level rise ε_2, is calculated using normalisation constants for the historic rate of equilibrium recession ε_1 and sea-level rise S_1 and future rates for sea-level rise S_2. This algorithm is based on recession of soft-cliffs of a vertically homogenous lithology and where beach volume is small, leading to limitations when using this technique in topographically complex hard-rock coastlines.

Maps from 100–150 years ago show coastlines which have been determined at the surveyors' discretion, with high water mark, mean sea level and position of the cliff-toe and/or cliff-top used as coastline indicators. Interpreting cliff-top lines from these coarse maps and also from recent aerial photographs means that this method, although useful in visualising change and understanding the scale of retreat, is not universally useful for determining accurate rates of retreat. Furthermore, coastline interpretation errors could occur based on the difference in surveyor's perception of the sea-cliff position during the surveying stage leading to variation in cliff position. This becomes more apparent when digitising hard-rock cliffs due to their complex three dimensional nature (Figure 1.2). Other errors may be due to different revisions, distortions in the printing process, continuity of process and also geological and environmental changes not accounted for (Lee, 2002). If the error is greater than or equal to the rate of retreat between the editions, then no reliable estimate of coastal retreat is possible (Lee, 2002; Brooks and Spencer, 2010).

Figure 1.2: (a) Digitised cliff lines from 1845-1901 (purple), 1942-1949 (red) and 2010 (yellow) for soft rock cliffs, Norfolk, UK and (b) Digitised cliff lines from 1845-1901 (purple), 1943-1995 (red) and 2010 (yellow) for hard-rock cliffs, Bedruthan Steps, UK).

The accuracy of such a method has been challenged in the past for long term trends in cliff erosion (Adams and Chandler, 2002; Hall *et al.*, 2002; Runyan and Griggs, 2003), where the amalgamation of events mean that episodic failures are often missed between surveys within the data.

1.3.4 Recent methods of monitoring change

Airborne LiDAR (Light Detection and Ranging) has been used as an accurate and reliable method of obtaining georeferenced geospatial data since the 1980's (Adams and Chandler, 2002; Young and Ashford, 2006; Young *et al.*, 2009; Lim *et al.*, 2011; Nunes *et al.*, 2011; Young *et al.*, 2012) and has proven to be useful for determining volumetric changes in a variety of different types of terrain. Large-scale data sets can be obtained at a high spatial resolution (0.5–1 m) and repetitive annual surveys can be overlain and compared to assess coastal erosion. LiDAR has been used extensively in the UK for fluvial and coastal flood risk assessment over the last decade (Geomatics Group, 2012) and is often used to assess sediment budget and pathways for coastal defence construction and for existing and future coastal developments all over the world (Sallenger *et al.*, 2003; Zhang *et al.*, 2005; Xharde *et al.*, 2006; Young and Ashford, 2006; Brooks and Spencer, 2010; Nunes *et al.*, 2011; Schmidt *et al.*, 2011; Young *et al.*, 2012). The coast of California, for instance, is frequently surveyed and monitored due to the high levels of coastal erosion and the high value of properties at risk. Here, airborne LiDAR has been used to assess volumetric changes to the cliff-face and sediment inputs into the nearshore (Young and Ashford, 2006; Young *et al.*, 2009, 2011b,

2012) and also to determine a linear rate of retreat (c. 0.03–0.13 m yr^{-1}). The public availability of LiDAR data in the UK makes this an ideal method of assessing coastal change at a range of spatial scales, from metres to tens or hundreds of kilometres. LiDAR data also makes coastal change assessments possible in inaccessible/unsafe regions.

Another common method to monitor cliff changes has been to use photogrammetry (Buckley *et al.,* 2002; Waters and Payne, 2006; Wangensteen *et al.,* 2007) to develop Digital Elevation Models (DEM) of the cliff face and identify regions of change. In complex topography, however, such as rocky coasts, the accuracy of this method (10's of cm) can inhibit the capture of small scale change and the determination of precise volume differences (Adams and Chandler, 2002). More recent techniques such as 'structure-from-motion' range imaging may overcome this accuracy issue, where a 3D structure can be obtained with high accuracy from a high resolution 2D image sequence (Westoby *et al.,* 2012).

The development of sophisticated technologies such as TLS, used alongside Global Positioning Systems (GPS) and survey data, enables the collection of highly accurate topographic data. Its applications have been used as a means of mapping and identifying regions of topographic change in a number of environments. Examples include dune morphological analysis (Montreuil *et al.,* 2013), fluvial morphology (Jaboyedoff *et al.,* 2009; Alho *et al.,* 2011; Schurch *et al.,* 2011; Lague *et al.,* 2012), beach morphology (Poulton *et al.,* 2006), rocky platform analysis (Dewez *et al.,* 2009) and recently TLS has been adopted for monitoring both hard and soft-rock cliffs (Rosser *et al.,* 2005; Poulton *et al.,* 2006; Rosser *et al.,* 2007; 2013; Abellan *et al.,* 2010; 2011; Brodu and Lague, 2012; Lague *et al.,* 2012; 2013; Santana *et al.,* 2012; Dewez *et al.,* 2013; Rohmer and Dewez, 2013). Using methods such as LiDAR, aerial photography or photogrammetry, means that the detail of the complex nature of cliff topography is often missed as such detail is often smoothed during the data processing. TLS is able to capture data to millimetre resolution and repetitive surveys can be compared to obtain overall volumes of change. Sensitive regions of failure can be detected and probability-density functions of rockfalls can help determine failure likelihood and scale for risk management purposes (Rosser *et al.,* 2007; Vaaja *et al.,* 2011; Dewez *et al.,* 2013).

The origin of microseisms (the displacement of the ground due to waves) and their interference with terrestrial seismic investigations has been a topic of interest for many years since Longuet-Higgins (1950). More recently, this research has been taken into the nearshore

to investigate the influence waves and shear stresses have on cliff flexing and the strength of the cliff using seismometers in the cliff-top and water level data at the toe of the cliff (Adams *et al.,* 2002, 2005; Young *et al.,* 2011a; 2012; 2013; Dickson and Pentney, 2012, Norman, 2012; Brain *et al.,* 2014; Earlie *et al.,* 2015; Vann Jones *et al.,* 2015). This has been highly significant in highlighting the influence wave energy has on the integrity of cliffs. Wave-induced vertical cliff-top ground motions have been measured in a number of international locations (California and Hawaii, USA, Australia, New Zealand and the east coast of the UK) and found displacements of 0.5–10 μm under wave climates < 5 m H_s (significant wave height). Such investigations have suggested that this repetitive flexure of the cliff is conducive to the growth of microcracks and ultimately triggers cliff failure (Adams *et al.,* 2005). Cliff-face rockfall activity has also been correlated with cliff-top ground motions (Lim *et al.,* 2011; Vann Jones *et al.,* 2015), however, more recently (Brain *et al.,* 2014; Earlie *et al.,* 2015) research has suggested that it is the larger-scale displacements (50–100 μm) that occur as a result of extreme storm wave activity, as opposed to ongoing, repetitive small scale flexing that is responsible for sudden and substantial failure (Earlie *et al.,* 2015).

1.3.5 Cliff erosion in the south-west UK

Although there is an absence of recent research into cliff erosion in Cornwall, localised and regional studies into the geology, hydrodynamics and beach morphology have been useful in contributing toward the broader understanding of cliff erosion processes in the south-west UK (Arber, 1949; Buscombe and Scott, 2008; Ridgewell and Walkden, 2009; Shail and Coggan, 2010; Leveridge and Shail, 2011; Poate *et al.,* 2014; Masselink *et al.,* in press). The second generation Shoreline Management Plan (SMP2) for Cornwall and the Isles of Scilly (Ridgewell and Walkden, 2009) provides a high-level overview of the historic evolution, geomorphology, wave climate, tides, sediment sources and transport pathways. In order to understand the erosion of a rocky coast environment and its variability with the resisting and assailing forces, more localised, detailed investigations are necessary (Sunamura, 1992; Lee, 2002; Naylor *et al.,* 2010).

1.4 Study sites

Cornwall forms the south-west peninsula of the UK, with a 525-km long rugged coastline protruding into the Atlantic (Shail *et al.*, 1998). The coastline has relatively low rates of erosion in comparison to the rest of the UK; however, a high spatial variability in these rates has been noted with elevated rates in local 'hot spots' (Cosgrove *et al.*, 1998). Nine sites were selected initially (Chapters 1 and 2) to represent a range of rock mass characteristics and varying wave exposures (Fig 1.3). These sites, which are all owned by the National Trust, were also identified as having particularly pressing issues with coastal erosion, where property and/or infrastructure (i.e. access roads, coastal paths) are at risk. Two of these nine sites have been used for more detailed monitoring on a finer temporal scale (Chapters 3 and 4).

The variability in geology around the south-west of England (the Cornish coastline in particular) and the spatial differences in the resistance of rock to erosion (Bird, 1998), means that the region experiences localised rates of erosion which result of a combination of episodic failures and gradual erosion over the longer term (Shail *et al.*, 1998; Ridgewell and Walkden, 2009). The rugged nature of the Cornish coastline is a product of not only the hard-rock geology, but also the highly energetic wave climate from the Atlantic Ocean (Scott *et al.*, 2011).

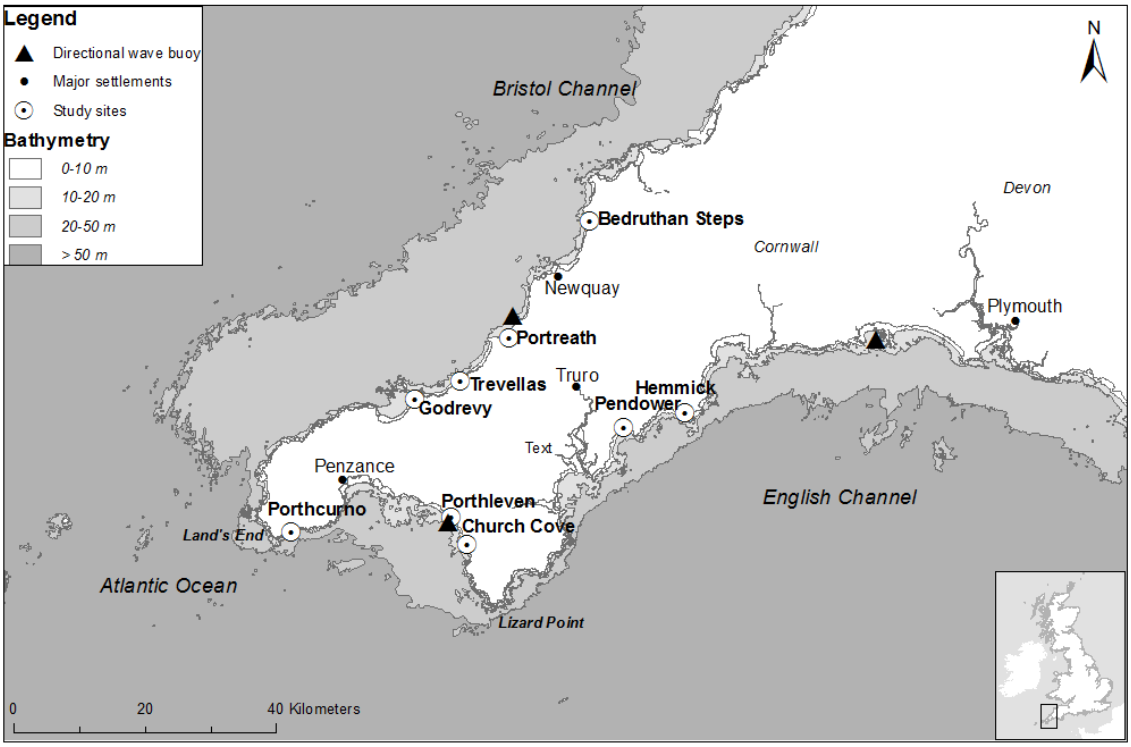

Figure 1.3: Locations of study sites around the south-west peninsula of the UK

Coastal landsliding in Cornwall has recently been of interest due to specific active regions placing the coastal path and other valuable assets at risk. The National Trust own 420 miles of the 630 mile long south-west coast path; stretching from Minehead in Somerset around the Devon and Cornwall coastline to Poole in Dorset. This footpath is an integral part of the Cornish coastline, not only providing access to the beaches, coves and historic and natural sites of interest but is economically important, drawing millions of visitors each year, generating about £300 million a year and supporting about 7500 jobs (Ridgewell and Walkden, 2009). Understanding the changing coastline and anticipating the impacts these changes have on the coast path will be vital in its long term sustainability.

1.4.1 Geological and geomorphological setting of Cornwall

Cornwall is one of the most complex geological regions in England (Bird, 1998). The coastline is dominated by marine basin sediments, formed in the Devonian and Carboniferous periods, and subsequently metamorphosed by intrusions during the Carboniferous to Permian times. Metasedimentary rocks developed during the Devonian to Carboniferous rifting (Bird, 1998) are present in most of the cliffs around the coastline, mainly formed of sandstones, mudstones, shales and slates. The deformation of these rocks during the Variscan Orogeny

and the horizontal stresses exerted on the rocks led to the folding, faulting, thrusting and regional low-grade metamorphism noted in the exposed cliffs along the coast (Leveridge and Shail, 2011). Following this period, these rocks were all cut by a variably reactivated network of Carboniferous-Triassic faults, formed as a result of the vertical pressures applied during the late Carboniferous.

Figure 1.4: Simplified map of the geological setting of the south-west of England, with study sites marked by red dots (Shail and Leveridge, 2009). Granites are in magenta and the different intrusions are denoted as LEG, Land's End; CG, Carnmenellis; SAG, St Austell; BMG, Bodmin Moor; DG, Dartmoor; SM, St Mellion klippe; SPZ, Start-Perranporth Zone.

All sites are situated on the Gramscatho Basin and the Looe Basin, both formed of sedimentary/metasedimentary bedrock, with the exception of Porthcurno at Land's End peninsular, which is a granite outcrop (Fig 1.4). Nearly all of the sites, including Bedruthan Steps, Trevellas Porth, Portreath and Godrevy on the north coast, and Porthleven and Church Cove on the south coast, are characterised by Lower Devonian lithology comprising medium to coarse-grained sandstones or dark grey mudstones/shales interbedded with fine-grained silty sandstones. Porthcurno on the south coast is an igneous intrusion, a granite headland from the Permian to Carboniferous age. Pendower, Hemmick and Seaton, all on the south coast, are characterised by Upper, Middle and Lower Devonian lithology with fine to medium sandstones or mudstones/shales interbedded with coarse sandstones (Shail *et al.*, 1998; Westgate *et al.*, 2003; Leveridge and Hartley, 2006). Most of the sites are capped with a layer of superficial Quaternary deposit (poorly consolidated periglacial sedimentary head deposits comprising clay, silt, sand and gravel), the thickness of which varies around the coast from 0 to 15 m (Shail *et al.*, 1998; Westgate *et al.*, 2003).

The spacing, frequency and orientation of the principal discontinuities that formed during the post-Variscan deformation towards the upper Carboniferous (Leveridge and Hartley, 2006; Shail *et al.,* 1998; Leveridge and Shail, 2011), as well as the subsequent joints and cleavages within the rock, are all important for dictating the potential for cliff failure and the mechanism via which it may occur (Wyllie and Mah, 2004). Cliff failure or mass wasting tends to occur through different mechanisms characterised by different *cliff systems* (Fig. 1.1). Typical failure mechanisms noted around the Cornish coastline are either translational (planar or wedge failure), rotational or toppling (Shail *et al.,* 1998; Westgate *et al.,* 2003; Leveridge and Hartley, 2006).

1.4.2 Wave climate and tidal regime

The wave climate around the Cornish coastline is the most energetic of UK coastal waters (Ridgewell and Walkden, 2009; Scott *et al.,* 2011) and derives all its waves, both sea and swell, from the Atlantic. The north-west (from the Cornwall Devon border to Land's End), south-west (from Land's End to Lizard Point) and south (from Lizard Point to Rame Head) coastlines experience varying wave climate. The north-west coast is exposed to swells from the west and north-west (2.5–3 m 10% exceedance significant wave height H_s), with south and south-westerly swells refracting around Land's End Peninsular around to the west-facing beaches. The south-west coast tends to be more sheltered from westerly and northerly Atlantic swell (2–2.5 m 10% exceedance H_s). Southerly and south-westerly swells affect the south-west coast more than the south coast. To the east of Lizard Point the wave climate is significantly less energetic (1–1.5 m 10% exceedance H_s), with locally fetch limited wind waves generated in the English Channel. All of Cornwall's beaches are macrotidal with spring tidal ranges between 4–7 m. The north coast generally experiences greater tidal ranges than the south coast, with the south and south-west coast varying between 4–4.8 m, and between 5.4–6.5 m along the north coast (UKHO, 2012) (Fig 1.5).

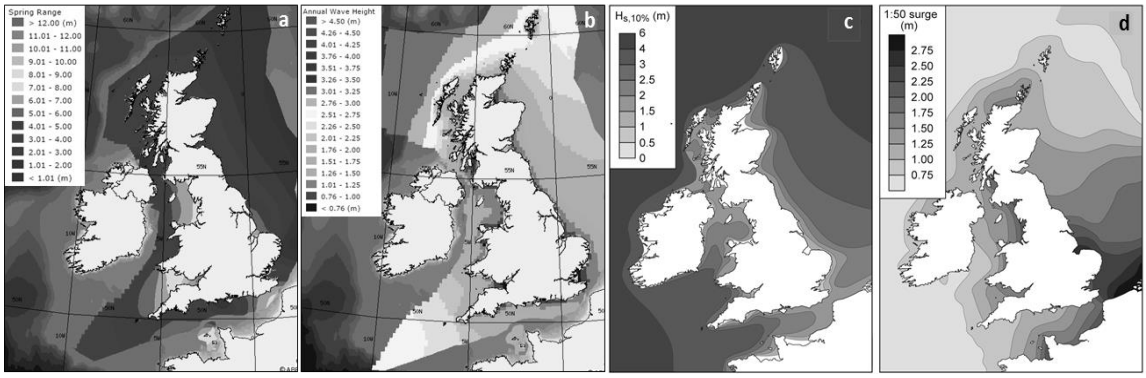

Figure 1.5: Maps of the UK with a) Spring Tidal range (ABPMer, 2015), b) Annual significant wave height (H_s), c) 10% exceedance significant wave height, and d) 1-in-50-yr storm surge level (taken from Masselink and Russell, 2013)

1.4.3 Climate

The climate of Cornwall is influenced for the most part by temperate maritime air. Temperatures in the south-west are generally warm compared to the rest of the country, with mean annual temperatures (between 1981 and 2010) of 9–11 °C (Fig 1.6). The south-west is one of the wetter regions of the country with annual averages (1981 – 2010) of 1000–1500 mm with little variability around the Cornish coastline. Compared with the rest of the UK, temperatures that are cold enough to bring ground frost are only found 15–20 days out a year and are rarely found at sea level (Met Office, 2012).

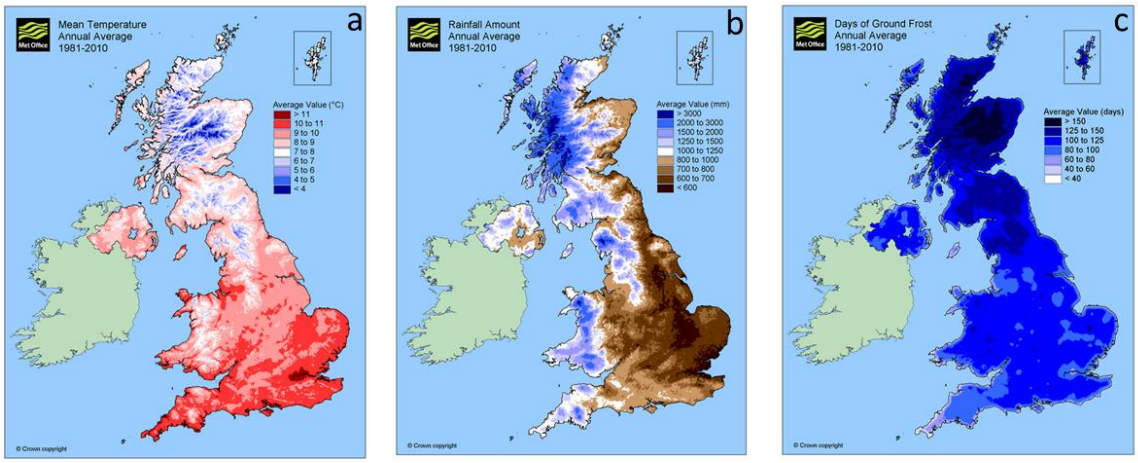

Figure 1.6: Annual average a) mean temperature for the UK, b) rainfall totals and c) days of ground frost. (Met Office, 2012).

1.4.4 Hemmick cove – 50°13'44.84"N 4°48'51.77"W

Hemmick cove is a remote pocket beach situated along the south facing coast of Cornwall, to the west of 'Dodman Point' headland (Fig 1.7a). The tidal regime is macrotidal with a Mean Spring Range (MSR) of 4.7 m. The cliffs are fronted by a swash aligned, intermediate low-tide terrace beach (tan β = 0.05) facing south-west into the English Channel. Sheltered from easterly waves from the English Channel by Dodman Point, Hemmick cove is mostly exposed to waves from the south-west and west. Average wave statistics (2009–2015) measured at the Looe Bay wave buoy (30 km to the east) show significant wave heights H_s of 1 m during the winter (Oct–Mar) and 0.67 m in the summer (Apr–Sept) and peak wave periods T_p of 9 seconds and 8 seconds respectively.

Figure 1.7: Hemmick cove a) aerial perspective of study site, b) beach and cliffs looking west and c) section of failing cliff at the upper western end of the beach.

The cliffs rise up to >30 m towards the east of the cove and 10–15 m ODN (Ordnance Datum Newlyn) to the west (Fig 1.7 b and c). They are formed of mainly two units, a lower bedrock formed of calciferous slates (De la Beche, 1839) from the Dodman Phyllite series thrust over the Pendower formation (brecciated slates and limestones) (Bird, 1998), capped by a layer of superficial Quaternary deposit and wind-blown sand. The cliffs towards the western end of Hemmick Cove are undergoing ongoing erosion of the upper Quaternary material (Fig 1.7b and c). Very little infrastructure is at risk here, but the National Trust owned property, situated behind a small seawall at the back of the beach has experienced land-loss issues, related to erosion.

1.4.5 Pendower - 50°12'18.95"N 4°56'43.33"W

Pendower is a 2.5 km beach situated along the south coast of Cornwall, facing south-east into the English Channel. These cliffs are fronted by a wide intermediate low-tide terrace beach

with an exposed shore platform to the west and a thin sandy medium to coarse grained beach to the east (tan β = 0.09). The tidal regime is macro-tidal (4.6 m MSR) and the bay is protected from south-westerly and westerly swells by Land's End peninsula and mainly exposed to lower energy waves from the east-south-east (Ridgewell and Walkden, 2009).

Figure 1.8: Pendower a) aerial perspective of study site, b) beach and cliffs looking west and c) wave-undercutting of the cliffs.

The cliffs rise 10–15 m ODN above the beach in this section (Fig 1.8a) and 10–20 m ODN towards the eastern and the western ends of the beach. These cliffs are formed of three major units; Quaternary head deposits (well-stratified brown and grey earthy gravel) (5–8 m thick) overlying a late Pleistocene emerged beach (1–2 m thick layer of quartz pebbles and sandy material with faint beach bedding inclined seaward), sitting above an emerged shore platform (1–2 m thick), dissected into the slates of the Pendower Formation (Bird, 1998). Evidence of cliff-toe undercutting due to waves is apparent in the caves that have formed in the slates (Fig 1.8c). Local landowners have noted rotational sliding of the head deposit and occasional failure due to undercutting of the emerged shore platform, placing at risk the coast path, an access road and the car park.

1.4.6 Church Cove - 50°02'18.70"N 5°16'01.11"W

Church Cove is a small pocket beach situated to the north-west of Lizard Point (Fig 1.3 and Fig 1.9a) facing south-west towards the Atlantic Ocean. The tidal regime is macro-tidal (4.7 m MSR) and the beach experiences higher energy wave conditions from the south-west and west. The beach is borderline intermediate/reflective low-tide bar/rip, low-tide terrace, with a tan β of 0.05. The bathymetry here is very steep, with the 20 m contour, less than 1 km from the shoreline (Orford *et al.*, 2002). Average significant wave heights (2011–2015) (H_s), taken from the Porthleven wave buoy (3 km to the north-west) are found to be 1.52 m in the winter and 0.9 m in the summer, and wave periods (T_p) are 11 seconds and 9 seconds respectively.

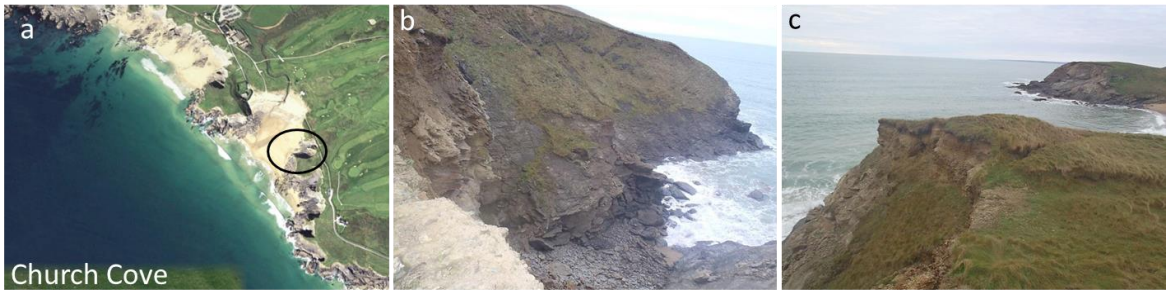

Figure 1.9: Church cove a) aerial perspective of study site, b) view of the southern side of the beach and cliffs from the coast path and c) evidence of rotational failure in upper quaternary head.

The cove has been cut out of low lying head deposits and soft weathered rock by marine erosion (Bird, 1998). The cliffs at either end of the cove rise high above the beach (20–30 m ODN) and are formed of two units, a lower bedrock unit of schists and shales of the Lizard series, overlain by significant (5–10 m thick) head deposits (Bird, 1998). Ongoing erosion of the cliff-toe (Fig 1.9b) and rotational landsliding of the upper Quaternary material in the cliff-top (Fig 1.9c) has placed the coastal footpath and wall at risk.

1.4.7 Porthleven - 50°04'26.18"N 5°18'04.95"W

Porthleven beach is an exposed swash-aligned beach, facing directly south-west towards the Atlantic (Fig 1.3 and 1.10a). The tidal regime is macrotidal with a MSR of 4.7 m. The cliffs are fronted by a reflective, steeply-sloping (tan β = 0.14) beach formed of coarse-to very coarse sand (1–2 mm) and fine to medium gravel (2–16 mm) (Buscombe and Scott, 2008). Much like Church Cove, the bathymetry is fairly steep here with the 20 km contour approximately 1 km from the shoreline. Wave statistics are taken from the Porthleven wave buoy and are similar to those noted at Church Cove (section 1.4.6).

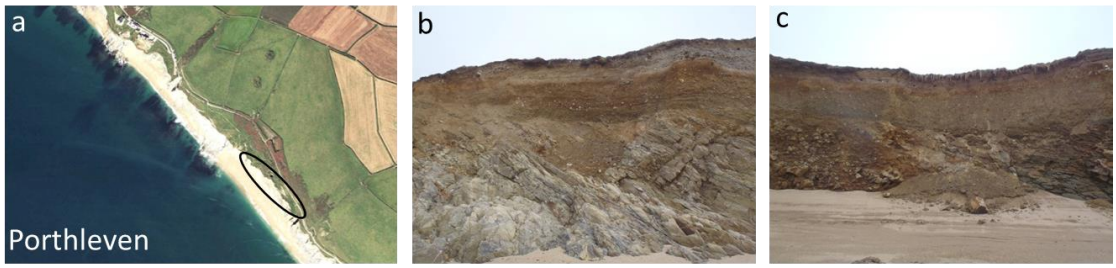

Figure 1.10: Porthleven a) aerial perspective of study site, b) section of cliffs towards the southern section of interest showing the two major units and c) evidence of rotational failure in upper quaternary head.

The cliffs are formed of Devonian Mylor slates, (grey-blue slates with interbedded sandstones and mudstones), overlain by a layer of quaternary head deposits (2–4 m thick poorly consolidated sand, silt, clay and gravel) (Bird, 1998; Leveridge and Shail, 2011) capped by a thin layer (0.5–1.5 m) of 'made ground'; a remnant of 19th century mining activity. The cliffs along this section of the coast rise 8–10 m above the beach (10–12 m ODN) and are bounded at either end of the bay by Porthscatho beds of grey-green sandstone and dark-grey mudstone (Leveridge and Shail, 2001). Above the Porthscatho beds, the cliffs rise steeply to 20–25 m ODN. Porthleven cliffs are geologically important as they provide evidence of the order of the deformation phases (faulting and folding) that occurred during the Variscan Orogeny. The cliffs dip gently south-eastwards and have been cut by a network of late Carboniferous–Triassic joints and faults dipping SSW and NNE (Fig 1.10b).

This site has been noted to have ongoing issues with erosion of the upper Quaternary head deposits, and failure along the shore perpendicular faults (Zawn) at either end of the bay (Shail and Wilkinson, 1994), placing the coast path at risk.

1.4.8 Porthcurno - 50°02'36.35"N 5°38'39.70"W

Porthcurno is a large southerly-facing pocket beach, situated to the east of Gwennap Head, 5 km from Land's End, the south-western most point in the UK (Fig 1.3 and Fig 1.11a). The tidal regime here is slightly more macro-tidal than the south coast with a MSR of 5.4 m. The beach is an intermediate low-tide terrace and rip/low-tide terrace (low and high energy beach types respectively) (tan β and D_{50} unknown). Located on the south-western most point of the peninsula, Porthcurno is highly exposed to westerly and south-westerly waves from the Atlantic Ocean.

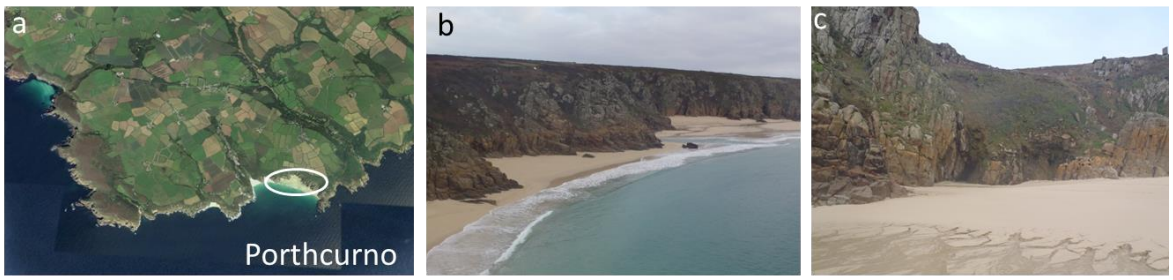

Figure 1.11: Porthcurno a) aerial perspective of study site, b) cliffs looking eastwards and c) evidence of cave formation at the toe of the cliffs.

Although this is one of the most exposed sites in this study, it is also one of the most resistant in terms of geology. The cliffs at Porthcurno rise up to 70–80 m above the beach and are mainly blocky, coarse grained megacrystic Land's End Granite, formed during large-scale igneous intrusions during the Carboniferous to early Permian times (Leveridge and Hartley, 2006). This site has been identified as having issues with weathering and erosion of the upper face of the cliff and concern has been raised over the stability of the caves formed at the toe of the cliffs.

1.4.9 Godrevy - 50°13'57.84"N 5°23'31.04"W

Godrevy, situated on the northern coast of Cornwall faces directly west, towards the Atlantic. The cliffs are located at the western side of St. Ives Bay, a deep concave bay formed from marine erosion cutting into less resistant Devonian slates, mudstones and sandstones, between the more resistant headlands of St Ives Head and Godrevy Head (Ridgewell and Walkden, 2009) (Fig 1.12a). The tidal regime becomes more macro-tidal along the north coast, with a MSR of 5.88 m. The beach is a wide, gently-sloping (tan β = 0.02) intermediate low-tide bar/rip and is highly exposed to Atlantic swell waves from the west and south-west. The coastal slope is relatively wide and shallow-sloping with the 20 m contour 10 km from the shoreline (UKHO, 2012). Average significant wave heights (H_s) taken from the Perranporth wave buoy (20 km to the north-west, from 2011–2015) are 1.91 m in the winter and 1.22 m in the summer, with wave periods (T_p) of 12 seconds and 11 seconds respectively (CCO, 2015).

Figure 1.12: Godrevy a) aerial perspective of study site, b) beach and cliffs c) evidence of failure of superficial head deposit.

The cliffs rise 8–15 m above the beach and are formed of two major units, underlying bedrock of weakly metamorphosed Devonian sandstones and mudstones (Shail and Coggan, 2010), with evidence of Carboniferous deformation during the Variscan Orogeny, much like

most of the cliffs in this study. These bedding planes dip gently towards the south-east and are cut by a network of ENE-WSW, NE-SW and NW-SE oriented joints and faults (Bird, 1998). The bedrock is overlain by a layer of superficial head deposit of a poorly sorted silty cohesive matrix, varying in thickness along the cliff frontage as the boundary between the two units rises from almost beach level at the northern end of the cliffs to 15 m ODN at the southern end. Towards the northern end of the cliffs, the superficial units lay above an emerged Pleistocene beach, situated at about 0.5–1 m above beach level. Godrevy is one of the most visited National Trust properties in SW England (Shail and Coggan, 2010) attracting more than 250,000 people per year. The access road to a car park which generates a high amount of revenue for the National Trust is situated alongside the south-west coast path at the very edge of the cliff-top. Ongoing erosion of the cliffs at Godrevy has placed this road and footpath at immediate risk over the last few years.

1.4.10 Portreath - 50°15'41.05"N 5°17'46.99"W

Portreath is a north-west facing pocket beach along the north coast of Cornwall, 7 km to the north-east of Godrevy Head (section 1.4.9). The tidal regime is macro-tidal, with a MSR of 6.1 m. The cliffs towards the west of the harbour are sheltered from southerly and south-westerly Atlantic swell by Western Hill, yet exposed to swell from the west and north-west Atlantic. The beach is a gently sloping (tan β = 0.03) intermediate low-tide terrace and bar/rip (Buscombe and Scott, 2008), with the 20 m coastal slope contour 2 km from the shoreline. Average wave conditions obtained from Perranporth wave buoy (12 km to the NNE) are comparable to those in section 1.4.9.

Figure 1.13: Portreath a) aerial perspective of study site, b) beach and cliffs with 'Battery House' situated above c) evidence of cave formation due to a mining activities exacerbated by wave-action

The cliffs are Upper Devonian (Frasnian) slate, siltstones and fine sandstones of the Porthtowan Formation with evidence of uplift and erosion from plate collision during the

Variscan Orogeny (Bird, 1998). The deformation occurring during the later Variscan led to low and high angled faults where the bedding dips about 10° towards the west and is intersected by steep NW-SE faults and N-S joints. The relationships between these intersecting faults have led to the variation in the cliff instability (Marks, 1999). Historic quartz mining activity of the cliff beneath 'Battery House' (Fig 1.13b and c) exacerbated by wave action has caused overhanging of the cliffs. This has led to periodic slips, placing the property and road at the top of the cliff at risk.

1.4.11 Trevellas Porth - 50°19'23.36"N 5°11'46.81"W

Trevellas Porth is a small cove to the north-east of St Agnes (Trevaunance Cove) at the mouth of the Trevellas Coombe stream, an area historically used for mining. The beach faces towards the west and is exposed to Atlantic swell from the south-west to the north-west. The tidal regime is macrotidal (6.1 m MSR) and the beach is mostly a rocky shore platform covered with a thin veneer of sand and variably sized boulders at the toe of the cliffs. The bathymetry shelves fairly steeply with the 20 m contour less than 2 km from the shoreline.

Figure 1.14: Trevellas Porth a) aerial perspective of study site, b) beach and cliffs looking north-east from southern headland. Evidence of undercutting present in the cliffs above the beach c) ongoing failure of material via weathering and erosion of the cliff toe.

The cliffs are formed of predominantly metamorphic Devonian slates with interbedded sandstones and limestones of the Gramscatho group. The cliffs have been cut into marine erosion platforms, uplifted during the Tertiary period (Bird, 1998), rising about 70 m to the south of the cove and about 20 m to the north. The erosion processes appear to differ within this bay, where weathering of the cliffs to the south, combined with wave attack of the toe, leads to rotational slips of the cliff. Towards the north, evidence of wave attack is apparent in the undercut, overhanging sections of cliff (Fig 1.14b). The coast path and the small car park are at risk of erosion.

1.4.12 Bedruthan Steps - 50°29'09.85"N 5°02'05. 51"W

Bedruthan Steps forms a series of rocky headlands and stacks along the north coast of Cornwall, facing west towards the Atlantic. Macro-tidal, with a MSR of 6.5 m, the beach is fine-grained, wide and gently sloping (tan β = 0.01). Bedruthan Steps is classified as intermediate low-tide bar/rip to dissipative, and is exposed to swell from the south-west, west and north-west. The bathymetry shelves steeply, with the 20 m contour about 1 km from the shoreline. Average wave conditions obtained from Perranporth wave buoy (17 km to the south) are comparable to those in section 1.4.9.

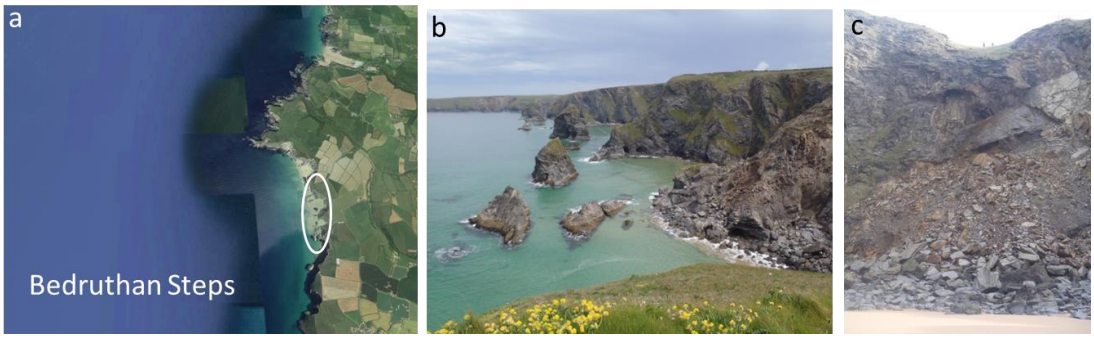

Figure 1.15: Bedruthan Steps a) aerial perspective of study site, b) cliffs and stacks looking northwards from southern headland, c) ongoing failure of material via weathering and erosion of the cliff toe.

The cliffs rise high above the beach along the frontage, (75–80 m) and have been cut by marine-action into grey and green Devonian slates with bands of limestone and quartz veins (Bird, 1998). The stacks visible on the beach contain remnants of slope-deposited late Pleistocene periglacial head and indicate the coastline has retreated about 250 m over the last 6000 yrs.

Bedruthan Steps is an important geological feature of the coastline owned and managed by the National Trust. Cliff falls appear to have been a problem regarding access to the beach via a staircase and cliff stabilisation and engineering measures have been taken to protect the steps and allow access onto the beach. This measure has temporarily halted the erosion around the steps, however the highly active nature of the cliffs hints towards a potential larger slip in the future. The stability of the cliffs here will determine whether continued access onto the beach is possible.

1.5 Summary

This wide range of geomorphological characteristics around the coast of Cornwall provides an ideal a setting upon which to draw comparisons and explain the spatial variability in erosion around the coastline. The sites selected for this study are either currently experiencing issues related to coastal cliff erosion or have been identified as regions where infrastructure is threatened by potential failure in the future. The sites chosen also provide a range of coastal orientations (S, SW, W, NW), offshore bathymetric profiles, and beach types, (e.g., reflective, intermediate, low-tide terrace and low-tide bar/rip) with different geomorphological settings (i.e., pocket beaches, coves, rocky platforms and wide sandy beaches); which will help explain the influence of various wave exposures on cliff erosion rates. Seven out of the nine sites (excluding Portreath and Porthcurno) are characterised as complex cliffs, with a unit of softer superficial head deposit overlaying a more resistant bedrock unit. Cliff heights vary from 8–80 m and although all sites (apart from Porthcurno) are mostly meta-sedimentary/sedimentary, they differ in their resisting force - the rock mass characteristics (spacing, orientation and frequency of joint sets and fractures).

This study uses two different techniques to quantify cliff volume erosion under varying temporal and spatial scales:

1. Airborne LiDAR data allows for large scale, high-resolution (0.5 m) quantification of cliff erosion volumes at nine sites over a 3–4 year time scale (Chapter 2). These data are used alongside rock mass characteristics and wave exposures to explore the spatial variability in erosion around the coastline.

2. Monthly Terrestrial Laser Scanning (over 12 months) at two particularly active and vulnerable locations (Porthleven and Godrevy) facilitates a high temporal and spatial resolution (10 cm) chronology of cliff face erosion (Chapter 3). Previous research has suggested the morphology of the beach and nearshore hydrodynamic regime plays a vital role in controlling cliff erosion rates (Trenhaile, 1987; Sunamura, 1992; Masselink and Hughes, 2003; Ashton *et al.*, 2011; Caplain *et al.*, 2011; Brooks *et al.*, 2012), however most field studies (and as a result, most theoretical models) are based on the erosion of soft-rock cliffed coastlines. This study uses monthly quantification of cliff volume erosion, combined with

beach profiles and continuous wave and water level data, to explore these forcing parameters in a harder rock environment.

Monitoring and quantifying the impacts of high-energy extreme storms on coastal cliffs is hindered by the difficulties associated with deploying instrumentation in such conditions. Therefore, most models for wave-cliff interaction under elevated water level and high energy wave conditions remain theoretical. This study employs, for the first time, *in-situ* observations of cliff-top ground motions, waves and water levels and subsequent cliff erosion and beach morphology (Chapter 4). The forcing parameters (waves, water levels) and boundary conditions (lithology, beach morphology, bathymetry) explored in this study will aim to explain the spatial and temporal variability in harder rock cliff erosion in the south-west UK and ultimately contribute towards the broader understanding of the oceans' role in shaping our coastlines.

Chapter 2

The spatial variability in cliff erosion around the south-west UK coastline

2.1 Introduction

2.1.1 Measuring rates of retreat

Cliff erosion studies have typically involved historic mapping, photogrammetry, LiDAR (Light Detection and Ranging) or terrestrial laser scanning to determine cliff face volumetric changes and rates of retreat. Rates of erosion used for shoreline management purposes for rocky coastlines using these techniques range from 0.02 to 0.5 m yr^{-1} (Rosser *et al*., 2005; Ridgewell and Walkden, 2009; Lim *et al*., 2010), and in rocky coast environments, do not tend to wholly capture the detail in the processes and the failures occurring across the cliff-face. This chapter examines the usefulness of airborne LiDAR technology to gain a quantitative understanding of cliff erosion along rocky coastline where recession rates are relatively low (c. 0.1 m yr^{-1}) and determine linear retreat rates. In this chapter, the relative resistance of rocks is characterised by the lithology of the rock as well as the rock mass characteristics that control the intrinsic resistance to erosion. The variation in the erosion rates depends largely on the local geological characteristics, wave exposure and meteorology. The spatial and temporal variations in the type of analysis technique will also influence the resultant rate of erosion, and hence the interpreted amount of vulnerability, due to the resolution of data capture in the method itself.

In many shoreline management strategies, historic shorelines are digitised and recession rates calculated using the ArcGIS DSAS tool (Ridgewell and Walkden, 2009; USGS, 2012). The site-specific detail is missed using this method as the rates are summarised on a larger scale (10's 100's km) and, for the purposes of policy formulation and development, only the cliff top position is considered. The nature of rocky coastlines and the modes in which failure occurs (often on the cliff face) calls for a more detailed understanding of the way in which the cliffs behave (Rogers *et al.*, 2009). Erosion rates derived from historic mapping techniques are often the only data available and are consequently used in coastal management

strategies. The spatial scale at which this technique quantifies the rates of erosion alongside the low rates noted in slowly eroding harder rock coastlines, means this method has a tendency to over-estimate rates of change, only capturing larger changes over a longer time period (Lim *et al.,* 2010). Although sporadic failures on a large magnitude are very difficult to predict, smaller rock falls can often be a precursor to these larger failures (Rosser *et al.,* 2007). It is important to identify areas of weakness to attempt to manage this risk.

With advances in technology, the three-dimensional nature of the evolution of cliffs has become easier to capture. Terrestrial Laser Scanning (TLS) and photogrammetry are methods that allow for very high-resolution georeferenced data to be obtained for cliff faces (Rosser *et al.,* 2005; Young *et al.,* 2009). However, there are often issues with photogrammetry regarding accuracy (Adams and Chandler, 2002). TLS is useful for more site-specific and localised changes (10–100 m), yet such methods may not be feasible in some difficult to reach locations.

2.1.2 Applications of airborne LiDAR

Airborne LiDAR has been used as an accurate and reliable method of obtaining georeferenced geospatial data since the 1980s (Wood and Fisher, 1993; Cosgrove *et al.,* 1998; Adams and Chandler, 2002; Hall *et al.,* 2002; Young and Ashford, 2006; Young *et al*., 2009; Lim *et al*., 2011; Nunes *et al*., 2011; Young *et al*., 2011b; Jaboyedoff *et al.,* 2012) and has proven to be useful for determining volumetric changes in a variety of coastal landscapes. Large scale data sets can be obtained at a high spatial resolution (0.5 m^2) and repetitive annual surveys can be compared and used to assess coastal erosion. The application of LiDAR in the coastal zone has allowed for future coastal erosion rates to be projected to account for sea-level rise (Walkden and Hall, 2005; Ridgewell and Walkden, 2009), and for local and regional sediment budgets to be quantified via volumetric beach, dune, gulley and cliff change over time (Young and Ashford, 2006; Young *et al.,* 2009). Other uses have included; analysing coastal response to extreme events (Zhang *et al.,* 2005), habitat mapping (Schmidt *et al.,* 2011), coastal and fluvial flood risk analysis (Brock and Purkis, 2009; Ridgewell and Walkden, 2009), coastal defence construction, and for existing and future coastal developments all over the world (Sallenger *et al*., 2003; Zhang *et al*., 2005; Xharde *et*

al., 2006; Young and Ashford, 2006; Brooks and Spencer, 2010; Nunes *et al*., 2011; Schmidt *et al*., 2011; Young *et al*., 2011b).

Detection of beach changes in terms of shoreline position (HW mark) and dune dynamics has successfully been monitored using LiDAR (Zhang *et al.*, 2005; Young and Ashford, 2006); however, its application in cliffed environments has typically been limited to rapidly eroding soft-cliff regions (Kidner *et al.*, 2004; Xhardé *et al.*, 2006). Erosion of hard-rock coasts is understood to occur episodically and at a slower rate. The ephemeral nature of the erosion in these environments means that the perceived risk is lower and therefore studies looking at the evolution of hard-rock erosive coasts are limited (Xhardé *et al.*, 2006; Naylor *et al.*, 2010). The high resolution of LiDAR (footprint of 0.5 m^2) means that in coastal slopes and non-vertical cliffs, the face of the cliff can be surveyed and changes occurring on the cliff face can be captured. Cliff erosion can take place via a number of different modes of failure, translational, toppling, rotational, slumping, depending on the lithology of the rock and the rock mass characteristics (Wyllie and Mah, 2004). Using LiDAR data to analyse changes over relatively short periods of time, in this case a few years, provides a method of understanding of the variety of these failure mechanisms that occur spatially. The public availability of LiDAR data makes this an ideal method of assessing coastal change at a range of spatial scales, from metres to tens or hundreds of kilometres. LiDAR data also enables the assessment of coastal change at inaccessible/unsafe regions.

2.1.3 Using airborne LiDAR to measure slowly eroding coastlines

Digital Elevation Models (DEMs) produced using airborne LiDAR data allow a comparison between years to be made to generate a volume difference surface plot and highlight sensitive regions. The accuracy of these DEMs has been greatly improved over the years as the technology has developed. Advances in computer capabilities and laser ranging technology, alongside increasingly accurate kinematic global positioning system (GPS) technologies (Brock and Purkis, 2009) has meant that vertical Root Mean Squared Errors (RMSE) between the LiDAR acquisition data and ground survey data obtained using Real Time Kinematic GPS are in the order of 0.03–0.1 m (Young and Ashford, 2006; Young et al., 2011b; Geomatics Group, 2012).

Erosion rates in softer rock coastlines are typically higher than this RMSE value (Walkden and Hall, 2011); however, the rates observed in more slowly eroding harder rock coastlines may potentially be lower or of the same magnitude (Ridgewell and Walkden, 2009; Shail and Coggan, 2010, Lim *et al.*, 2010). This, then, begs the question whether LiDAR data can actually be used to quantify cliff recession rates along such slowly eroding hard-cliff coasts. If so, how confident can we be of the derived recession rates? The need for robust erosion rates is vital to accurately quantify historic morphology of the coast and evaluate and manage future risk.

This study uses LiDAR data from two different periods (2007/2008 and 2010/2011) to derive rates of retreat from volumetric changes to the cliff face, top and toe at 9 coastal sites in the south-west of England. Firstly, this chapter aims to quantify the spatial variability of coastal cliff erosion at these different sites, which are located around a lithologically resistant, highly energetic coastline with three different coastal orientations. These rates are also considered in terms of their relationships with the spatial variability in boundary conditions and forcing parameters (rock mass characteristics and wave climate). Secondly, this chapter investigates the accuracy of using airborne LiDAR technology to derive linear rates of retreat in a slowly eroding coastline and tests the sensitivity of the data to varying thresholds of error removal that may be inherent in using such a technique. Thirdly these annual cliff retreat rates are compared with the annual rates obtained from longer time periods (used for shoreline management purposes) to evaluate whether short-term LiDAR data can be used as a suitable method to estimate long-term cliff recession along rocky cliffed coastlines.

2.2 Study Area

2.2.1 Geological setting

All sites are situated on sedimentary/metasedimentary bedrock, with the exception of Porthcurno on Land's End peninsular, which is a granite outcrop. Nearly all of the sites, including Bedruthan Steps, Trevellas Cove, Portreath and Godrevy on the north coast, and Porthleven and Church Cove on the south coast, are characterised by Lower Devonian lithology comprising medium to coarse-grained sandstones or dark-grey mudstones/shales interbedded with fine-grained silty sandstones. The Porthleven site incorporates an additional

site, Caca Stull Zawn, which is a shore-perpendicular thrust fault formed as a result of deformation processes during the Variscan Orogeny (Leveridge and Shail, 2011). Porthcurno on the south coast is an igneous intrusion, a granite headland from the Permian/Carboniferous age. Pendower, Hemmick and Seaton, all on the south coast, are characterised by Upper, Middle and Lower Devonian lithology with fine to medium sandstones or mudstones/shales interbedded with coarse sandstones (Shail *et al*., 1998; Westgate *et al.,* 2003; Leveridge and Hartley, 2006). Most of the sites are formed of two geological units, with Carboniferous to Devonian bedrock overlain by a layer of superficial Quaternary deposit (poorly consolidated periglacial sedimentary head deposits comprising clay, silt, sand and gravel), the thickness of which varies around the coast from 0 to 15 m (Shail *et al*., 1998; Westgate *et al.,* 2003). A detailed description of the geological and geomorphological characteristics and hydrodynamic setting of each site is provided in Chapter 1, section 1.4.

2.3 Method

2.3.1 Quantification of geological parameters

Typical methods of quantifying the rock mass strength characteristics include statistically analysing results from multiple triaxial tests on core samples or using a Schmidt hammer to determine the compressive strength of a rock sample (Wylie and Mah, 2004). In rocky coastal environments, studies have highlighted how it is primarily the intrinsic structural controls on the rock mass that ultimately determine its vulnerability to erosion more than the compressive strength of the rock itself (Shail *et al.,* 1998; Wyllie and Mah, 2004; Dornbusch and Robinson, 2005). The spacing, frequency and orientation of the principal discontinuities that formed during the post-Variscan deformation towards the Upper Carboniferous (Shail *et al*., 1998), as well as the subsequent joints and cleavages within the rock, are all important for dictating the potential for cliff failure and the mechanism via which it may occur. The Geological Strength Index (GSI) classification proposed by Hoek *et al.* (1998) (Fig. 2.2), is a method of quantifying the rock mass strength (dimensionless) and deformability parameters based on a visual impression of the rock structure. It allows an assessment of the condition of the rock surface based on the extent of weathering apparent and the level of alteration the surface of the rock has undergone. The classification scheme also considers the spacing,

frequency, roughness and orientation of the visible discontinuities to determine the kinematic stability of the rock (Cai *et al.*, 2004; Wyllie and Mah, 2004).

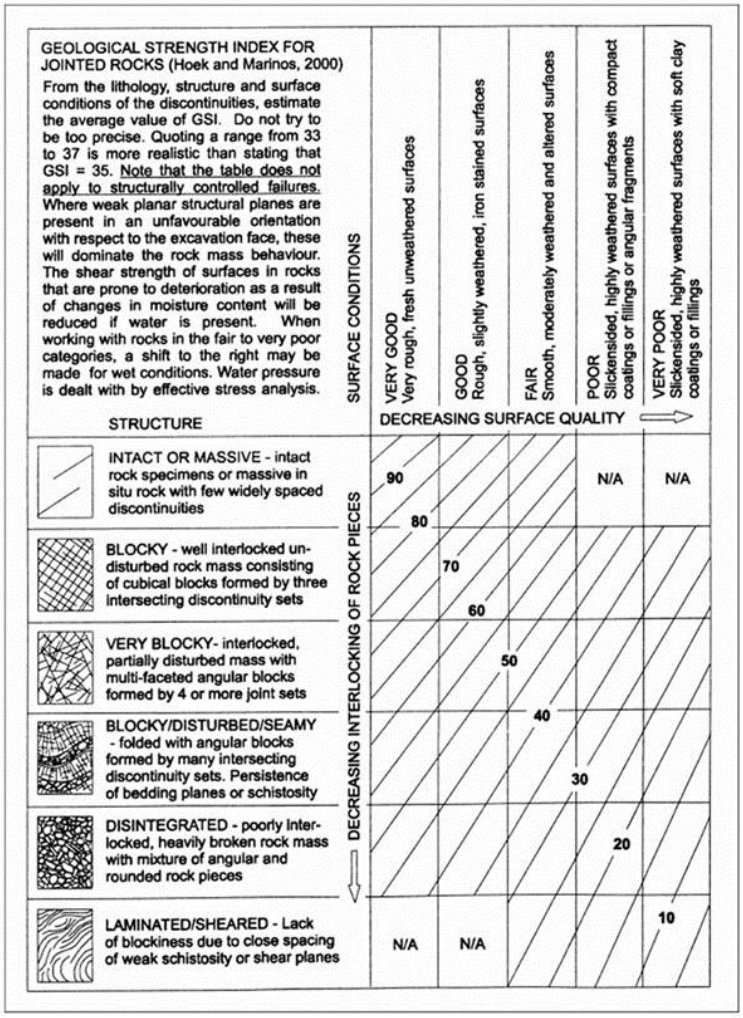

Figure 2.2: Geological strength index, taken from Hoek *et al.*, 1998 used to quantify and characterise rock mass characteristics.

The GSI produces high values (100–70) along a contour system (Fig 2.2) for rocks that have an unweathered or unaltered surface condition and a well interlocked rock mass with few discontinuities and a low GSI value (0–20) for highly weathered, heavily broken rock mass with numerous poorly interlocked discontinuities. As it was not possible to obtain core samples for triaxial testing or carry out extensive *in-situ* kinematic analysis, rock mass characteristics obtained from field observations were applied to the GSI method as a simplified means of determining the relative strength of the bedrock at each site (Table 2.1).

2.3.2 *Wave climate analysis*

Cliff erosion studies have previously focused on the following cliff failure factors: rainfall, strength of rock, rock mass characteristics and slope stability. Aside from the general understanding that waves tend to weaken the cliff at the toe and remove the protection talus material provides (Chapter 1), only recently has research been directed towards linking the potential for weakening of the rock mass structure with exposure to waves (Adams and Chandler, 2002; Adams *et al.*, 2005; Young *et al.*, 2009; Young *et al.*, 2011b; Dickson and Pentney, 2012, Lim *et al*., 2011). It was not possible in this stage of the study to compare a time series of wave climate with cliff failure as the time period between consecutive LiDAR flights was too long to identify individual failures with a particular event. However, the relationship between the spatial variability in erosion rates and that of the wave exposure around the south-west peninsular was worth considering.

A SWAN regional wave model for the south-west peninsula of the UK, provided hindcasted wave statistics for the study area. The model outputs significant wave height (H_s) peak spectral wave period (T_p) and wave direction (θ) (Austin *et al*., 2012) every 30 minutes, with data for a 3-year period statistically analysed. These values were used to determine the percentage occurrence statistics for wave heights and periods from different directions. The purpose of using these data was to characterise the nearshore wave climate at each of the sites and determine the variability in energy that is delivered to the cliffs around the coast.

2.3.3 *Rocky Coast Evolution Model*

Rock coast evolution is typically understood to be a function of wave height, and relative rock strength, as proposed by Sunamura's rocky coast evolution model (1992).

$$\frac{Sc}{\rho g H_1} \qquad \text{Equation 2.1}$$

Where S_c represents the resisting forces (compressive strength of the cliff material (MPa)) and $\rho g H_1$ represents the assailing forces (where ρ is the density of water (1025 kgm^{-3}), g is the gravitational acceleration (9.81 ms^{-2}) and H_1 the height of the maximum significant wave height (max H_S in the area under consideration (in m)) (Sunamura, 1992). Five wave breaking

scenarios are considered in Sunamura's model, and rock strength is qualitatively categorised into three categories; very strong, moderately strong and weak. Although it assumes the rocks are insoluble and uniform, and no sediment accumulation takes place in the nearshore, Sunamura's model is applicable in the rocky coast environment as it effectively captures the relationship between the boundary conditions (rock strength) and forcing (wave climate). In our study, GSI was substituted for compressive rock strength in order to account for the discontinuities and rock mass characteristics and the average significant wave height (H_s), to represent the wave climate (Eqn 2.2).

$$\frac{GSI}{H_S} \qquad \text{Equation 2.2}$$

2.3.4 LiDAR data collection and analysis

The LiDAR surveys were carried out by the Environment Agency Geomatics Group and were provided in raster format by the Channel Coastal Observatory. The surveys were flown using different instruments for 2007/2008 and 2010/2011; however, the flights were all based on a laser scan rate of 34 Hz with a swath angle of 25° and flight altitude of 900–1000 m (Geomatics Group, 2012). In 2007/08 the LiDAR data was acquired using the Optech ALTM 2033 and 3100 LiDAR instruments and in 2010/11 the Optech ALTM Gemini 06SEN191 and 08SEN230 LiDAR instruments were used.

Prior to publication, the LiDAR data underwent a series of checks and quality controls (Geomatics Group, 2012). These included checking the data against the aircraft trajectory using the Global Navigation Satellite System (GNSS), smoothing and interpolating to output a georeferenced point cloud. Flight line overlaps were checked to be less than 0.1–0.15 m and if greater they were then recomputed with corrections for systematic errors. Alongside the LiDAR flights, RTK-GPS surveys were undertaken over a paved, unchanged surface and used to ground truth the LiDAR data (Geomatics Group, 2012). A bare earth Digital Elevation Model (DEM) was generated by passing the point cloud data through classification routines and interpolated using specialist software (Geomatics Group, 2012). A ground truth check was repeated, the Root Mean Squared Error (RMSE) calculated and the DEMs edited to provide a more realistic bare earth. Last returns were used here as they produce the most accurate bare earth DEMs (Leigh *et al.*, 2009; Hladik and Alber, 2012). Once removed of

error and any vegetation filtered, the data are provided to the Channel Coastal Observatory for publication in georeferenced raster format (CCO, 2015).

The downloaded raster tiles for each site were processed using ArcGIS version 10 (ESRI, 2011). The raster data were compared with georeferenced aerial photography (CCO, 2015). The purpose of this was to 'mask' the cliff toe and the cliff top, so volume differences unrelated to cliff processes (e.g., due to beach change) could be excluded, and only changes to the cliff toe, face and top were considered. The masked regions were converted into ASCII format and exported for volume difference calculations.

2.3.5 Sensitivity analysis

Normally when considering magnitude of change between two DEMs it is standard procedure (Zhang *et al.*, 2005) to remove any data that fall within a certain threshold that may be attributed to error (e.g., acquisition errors, positional errors, or post processing errors). As the actual accuracy of the LiDAR data itself has already been checked and errors removed, the relative change between flights as opposed to the relative accuracy of data to the ground truth survey is of interest to determine volumes of change. For each LiDAR tile, a paved surface (about 10 m^2) was selected to represent zero change between flights. The RMSE of the paved surface (control RMSE) represents an average of error between the two years, and the RMSE of the masked data (cliff RMSE) represents an average magnitude of change between the two years z_a (2010/11) and z_b (2007/08) (Zhang *et al.*, 2005).

$$RMSE = \sqrt{\sum_{i=1}^{n} \frac{(za_i - zb_i)^2}{n}} \qquad \text{Equation 2.3}$$

The ratio between the two values was calculated for each site to give the percentage error in the data.

$$Percentage = \frac{RMSE_{(control)}}{RMSE_{(cliff)}} \, x \, 100 \qquad \text{Equation 2.4}$$

The 'control RMSE' calculated for each site was used as a threshold above which data were removed. Only values larger than the positive RMSE value or smaller than the negative value

were considered. This provided a new difference grid which was used to sum all the differences to obtain an overall net erosion volume. Positive values represent slumped material on the cliff face. This material essentially still forms part of the cliff volume, yet accumulation of eroded material at the cliff toe that may be considered to be removed from the system by waves was 'masked out' of the cliff area. The rates of retreat were calculated using the following equation

$$R = \frac{V}{(H_c \ L_c \, T)} \qquad \text{Equation 2.5}$$

where R = linear rate of retreat (m yr^{-1}), V = net volumetric erosion (m^3), H_c = average cliff height (m), L_c = longshore length of cliff (m) and T = time interval between consecutive surveys (yr.) (Young and Ashford, 2006). The longshore length was estimated across the masked area using ArcGIS and the cliff height was deduced by calculating the mean elevations along the cliff-top in each particular masked section of data.

The LiDAR surveys are carried out over the UK coastline annually; however, only certain sections of the coast are flown each year and therefore it was not possible to compare all sites within the exact same time frame. For the purpose of this study this is not an issue as we are attempting to understand the variability in recession rates on a larger spatial scale and not relate failure events to each other or individual storm events. Intermediate values are not available for these sites as there is no current method of continual monitoring. Apart from the long-term rates in the Shoreline Management Plan (SMP2) (Ridgewell and Walkden, 2009), LiDAR data are the only easily accessible means of assessing the evolution of the Cornish coastline.

The DEM of difference plots allowed for both a quantitative and qualitative view of the changes occurring to the cliff face. Cliff profiles were interpolated along the face of the cliff to provide a visualisation of the failure mechanisms occurring at the different sites. Frequency distribution plots provide information on the varying magnitudes of change detected at each site.

An important parameter to consider with respect to the various processes occurring at each site was the frequency and extent of inundation of the cliffs to the waves. The exposure of the

toe of the cliff (Z_b) was determined at each site from the LiDAR data, where elevation of the beach relative to the toe of the cliff was compared with mean sea levels.

2.4 Results

2.4.1 Rock mass characteristics

Cliff failure or mass wasting tends to occur through different mechanisms, according to the rock mass characteristics and principal discontinuities. Typical failure mechanisms noted around the Cornish coastline are varied and range from translational (planar or wedge failure), rotational to toppling and rockfalls as described in Chapter 1 (Shail *et al*., 1998; Westgate *et al.*, 2003; Leveridge and Hartley, 2006). Alongside terrestrial processes leading to slumping of superficial material, wave-induced block removal or quarrying at the toe of the cliffs tends to be apparent at all of the sites. A summary of the geology, failure mechanisms and coastal recession potential, based on site visits and a national shoreline behavioural study carried out by Orford *et al. (*2002) for each stretch of coast is presented in Table 1. What is interesting to note is how the sites are identified as active or inactive according to their recession potential values (<0.1 m yr^{-1} for 5 of the 9 sites and 0.1–0.5 m yr^{-1} for 4 out of the 9 sites) and classified according to Emery and Kuhn (1982). The GSI values identified from recent field observations in this study provide additional detail of the potential for recession, suggesting that the cliff surfaces exposed at sites have a much lower rock mass strength at Porthleven (25–30), Bedruthan Steps (30–34) and Trevellas (33–36) compared to Hemmick (55–58) and Porthcurno (70–75) (Table 2.1).

Table 2.1: Characteristics of the study sites. Average cliff height determined from LiDAR data; lithology taken from Ridgewell and Walkden (2009); and failure information (activity) based on Emery and Kuhn (1982), Bird, (1998), Orford *et al.*, (2002) and Leveridge and Shail (2011). GSI values calculated from recent (2012) field observations

Location	Average cliff height (m)	Lithology	GSI	Failure mechanism	Activity	Recession potential (m yr^{-1})	Site photo
Hemmick	11	Hard sandstones and mudstones with some superficial deposits. Cliffs (Dodman Phyllites) thrust over Pendower Formation (brecciated slates and limestones with igneous intrusions)	55-58	Mainly rotational failure of superficial material, block removal or planar failure unlikely. Debris slides and rockfalls possible	Inactive	<0.1	
Pendower	20	Superficial head deposits above emerged beach, above emerged shore platform, above Pendower formation bedrock	37-40	Undercutting, some block removal and collapsing, low potential for planar failure or slippage	Inactive	0.1 – 0.5	
Church Cove	20	Sandstones and mudstones overlain by head deposits	30-35	Block removal, of toe material and wedge and planar failure of upper cliff material. Topples occurring in superficial deposits	Inactive	<0.1	
Porthleven	5-25	Sedimentary gramscatho beds with interbedded slates and sandstones. Mylor slates overlain by head of clay, silt, sand and gravel. Porthleven cliffs are SSSI, Devonian sediments with basaltic intrusions	25-30	Mainly block removal and wedge failure leading to slumping or collapse of superficial material. Block removal in fault (Caca Stull Zawn) leads to toppling and planar failure	Inactive	<0.1	
Porthcurno	50	Mostly granite	70-75	Block removal rarely, some topples and rockfalls	Inactive	<0.1	
Godrevy	15	Rubbly head, varying from 3-8 m over pebbly emerged beach, sitting upon Pleistocene emerged shore platform, cutting over Porthtowan slates with interbedded sandstones	40-50	Block removal of bedrock and toppling leading to slumping or rotational failure of superficial deposits. Also terrestrial processes leading to slumping of head	Active	0.1 – 0.5	
Portreath	25	Porthtowan formation slate with mudstones and sandstones	45-50	Failures look more fault controlled than block removal, orientation of discontinuities suggests toppling failures or undercutting within faults leads to collapse	Active	0.1 – 0.5	
Trevellas Porth	50	Metasedimentary Devonian slate with sandstones and limestones some superficial deposits	33-36	Block removal at the toe of the cliffs have led to material above translating down the cliff slope. Rotational sliding and slipping apparent in superficial material	Active	<0.1	
Bedruthan Steps	50	Large exposed slate outcrops on the beach, cliffs are grey and green slates with limestone bands some head	30-34	Block removal of lower material leading to rotational sliding of upper cliff, rockfalls, topples and slipping apparent	Active	0.1 – 0.5	

2.4.2 Waves, tides and beach morphology

Wave rose diagrams illustrate the SWAN output for the mean significant wave height H_s at certain nodes around the coastline (Fig. 2.3). The north coast experiences a spatially-varying mean significant wave height ranging from 1 m for the north-facing (more sheltered) stretches of coast and 1.42 m along the more exposed west and north-west regions, with 10% of the waves during this period exceeding 2–3 m at all three nodes. Statistics for the south-west coast showed a mean H_s of 1.33 m, with 10% of the waves exceeding 2–3 m. The south-facing coast is less energetic, with a mean H_s of 0.87 m and a 10% exceedance H_s of 1–2 m. The peak wave periods tend to average 9 s for the north and south-west coast, and 5 s on the south coast. The maximum wave period reaches a maximum of 16 s around the whole coastline. For Porthcurno, wave climate is determined from the Loe Bar node (Fig. 2.3). This is because the nearest node (Penzance) is situated in a sheltered region and would not accurately represent the wave climate in Porthcurno. One would, however, expect to see a slightly less energetic wave climate than depicted by the Loe Bar node, because Porthcurno is south facing and is therefore, slightly more sheltered. Therefore an average between the Loe Bar and Loo Bay node has been used to characterise the wave climate here. The exposure of the cliffs to the waves and the vertical runup extent will vary locally and seasonally according to the tidal range, beach morphology, surge and significant wave height. The local tidal ranges and mean beach/cliff junctions presented in Table 2.2 provide a general indication of the frequency of tidal inundation of the cliffs. The greatest tidal ranges are seen on the north coast with mean spring ranges in the region of 6 m. The coincidence of the tidal levels with the cliff toe will depend on the beach elevation and beach morphology. The sites that experience the greatest water inundation in terms of still water levels in relation to beach/ cliff junction levels are Bedruthan Steps, Porthcurno and Trevellas, and the least ‘exposed’ sites are Porthleven, Godrevy and Hemmick.

Table 2.2 Beach/cliff elevations (obtained from LiDAR data) and tidal levels and ranges for the nearest secondary ports (UKHO, 2012), and mean significant wave heights from the nearest SWAN output nodes.

	Beach/Cliff elevation (m ODN)	MHWS (m ODN)	Tidal Range (m)	H_s (m)
Hemmick	2.7	2.4	4.7	0.87
Pendower	1.7	2.5	4.6	0.87
Church Cove	1.8	2.4	4.7	1.33
Porthleven	5.3	2.5	4.7	1.33
Caca Stull Zawn	*4.4*	*2.5*	*4.7*	*1.33*
Porthcurno	0.7	3.0	5.4	1.1
Godrevy	4.8	3.2	5.8	1.01
Portreath	3.5	3.5	6.1	1.36
Trevellas	2.7	3.5	6.1	1.36
Bedruthan Steps	0.5	3.5	6.5	1.42

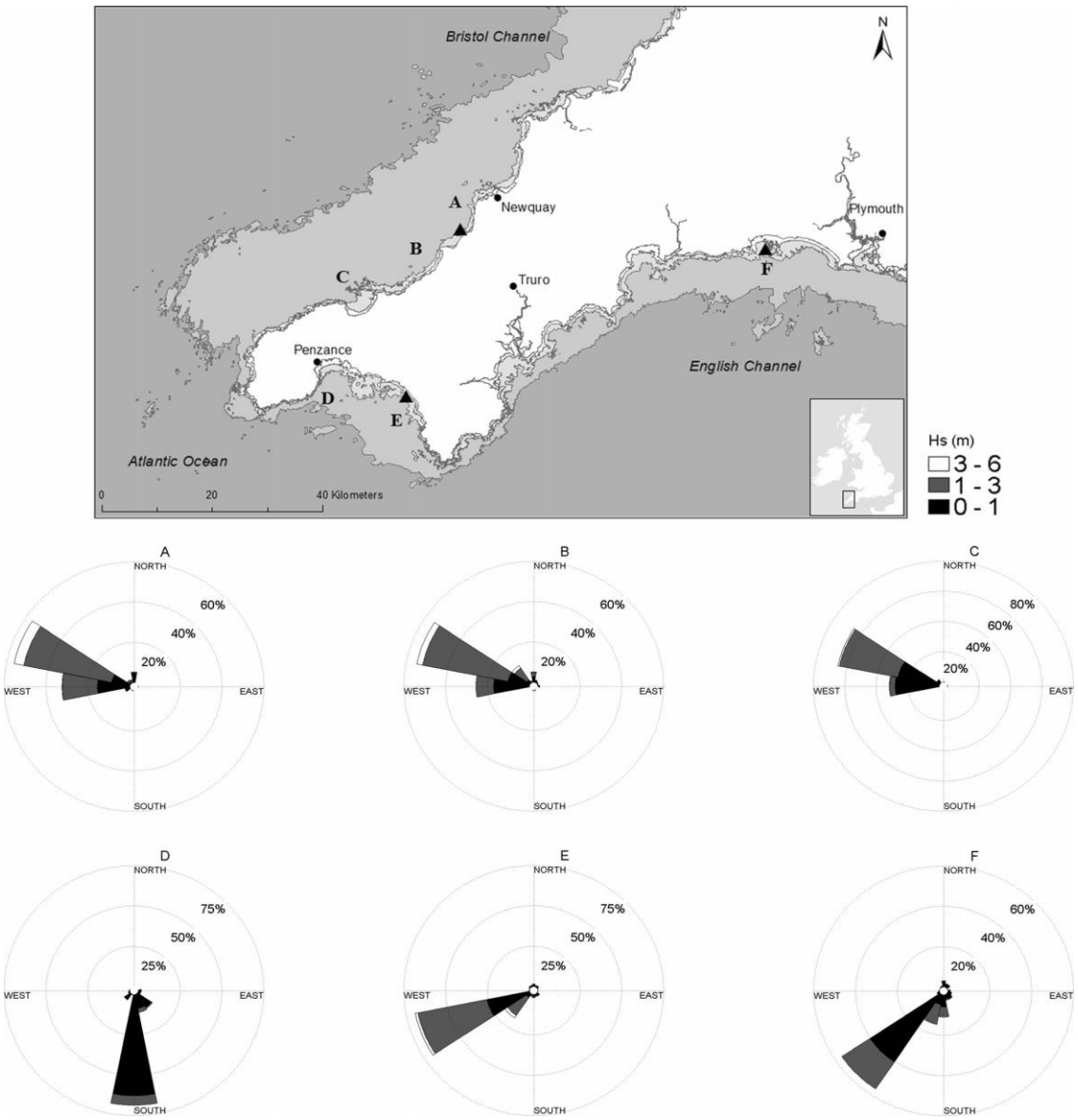

Figure 2.3 Wave climate around the coastline derived from SWAN wave model data (Austin et al., 2012). Roses represent percentage occurrence statistics for H_s from different directions at various nodes around the coastline. Nearest nodes for each site; ***A*** for Bedruthan Steps, ***B*** for Trevellas and Portreath, ***C*** Godrevy and, ***D*** for Porthcurno, ***E*** for Porthleven and Church Cove, ***F*** for Hemmick and Pendower. Wave buoy locations are noted as triangles within the map.

2.4.3 LiDAR Survey Accuracy

The root mean squared difference between the two surveys was calculated to check that no large systematic offset exists between the two surveys (Table 2.1). With an average mean difference of -0.06 m this suggests that this is not the case (Zhang *et al.,* 2005). The magnitude of error between flights ('control RMSE') is of the same order of magnitude at each site, ranging again from 0.03–0.11 m (Table 2.3). This, then, is the limit to which LiDAR technology is capable of detecting change.

Table 2.3: Study areas, mean differences and RMSE values used as error thresholds for each site.

Site	**Area (m^2)**	**Mean difference (m)**	**Control RMSE (m)**
Hemmick	201	-0.11	0.07
Pendower	3734	-0.13	0.11
Church Cove	2332	-0.11	0.09
Porthleven	1665	-0.03	0.04
Caca Stull Zawn	1219	-0.03	0.04
Porthcurno	62446	0.07	0.05
Godrevy	6512	0.05	0.04
Portreath	1591	-0.05	0.05
Trevellas	14929	-0.05	0.07
Bedruthan Steps	16296	-0.04	0.05

2.4.4 DEM's of difference and rates of retreat

The DEMs of difference plots not only provide an illustrative method of highlighting active regions within the vulnerable sites, but also allow for the changes that have occurred over the time period to be quantified and erosion rates calculated (Eqn 2.5). Two sites have been presented here (Fig. 2.4) to demonstrate the capability of LiDAR data in capturing changes to the cliff face and highlight the variability in the magnitudes of failure noted around the coastline. At Bedruthan Steps, the erosion/accretion patterns along the cliff face are spatially highly variable, and, as illustrated in the large mass movement in the centre of the study area (Fig. 2.4b and e; cross section B-B'), negative changes greater than 10 m in the vertical can be seen. This event is largely responsible for the large long-term recession rate deduced from these data, highlighting the sensitivity of the result on single events. In addition to the large mass movement, various smaller changes are obvious along the upper cliff edge. The cliff profile at Godrevy is much steeper (69°) than Bedruthan Steps (43°), therefore, the footprint of the DEM from the LiDAR is much narrower. Plotting profiles across the cliff, however,

shows how the volume change is still captured and a net loss of material can be quantified even on steeply sloping cliff faces.

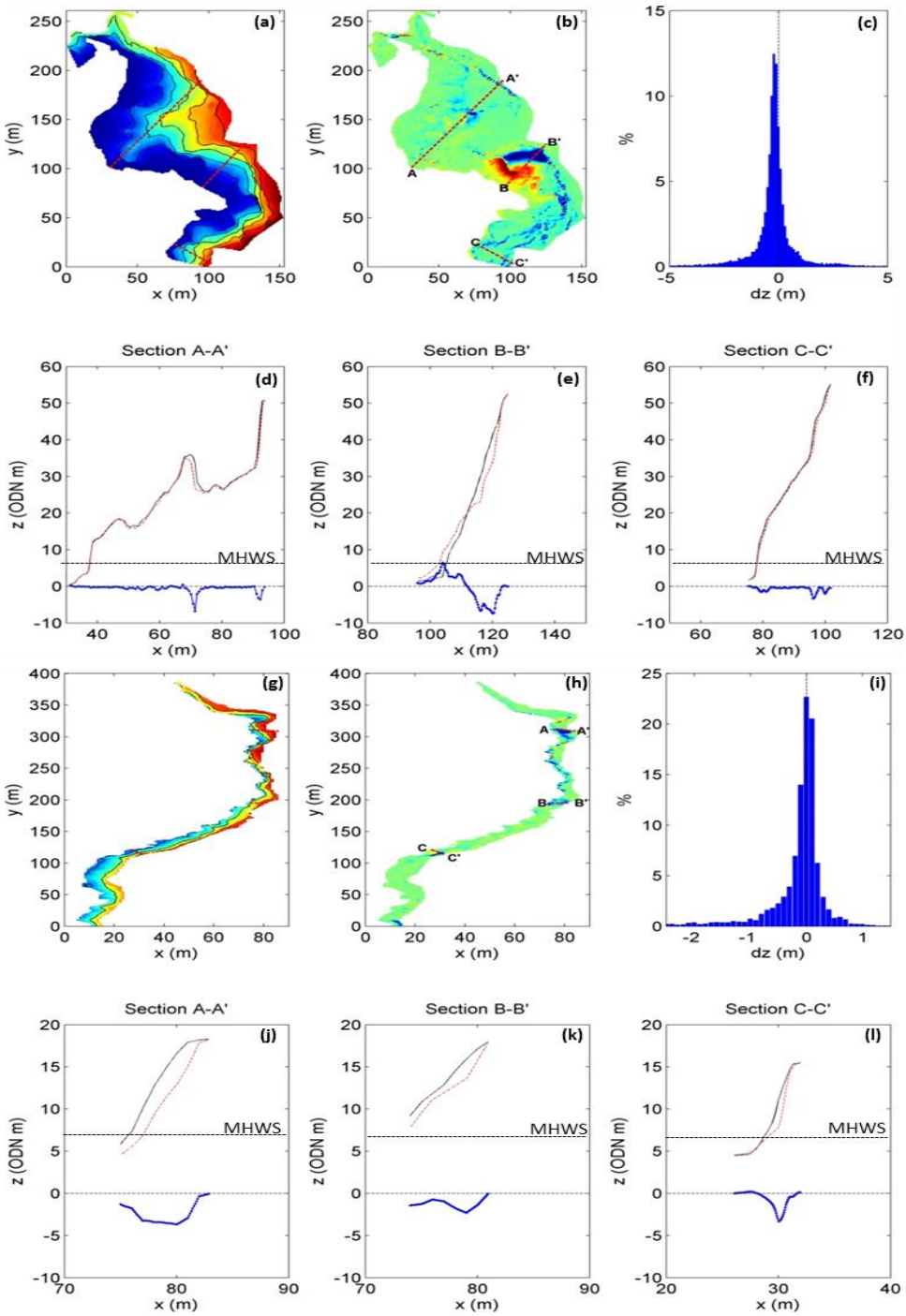

Figure 2.4: DEMs, frequency distributions and cross-shore profiles for Bedruthan Steps (a-f) and Godrevy (g-l). Figures a and g show contoured DEM with the x-axis as cross shore distance and the y-axis, longshore distance. Colour bar shows elevations from 0 m (blue) to 50 m (red). Figures b and h are DEMs of difference, with the colour bar indicating surface change (erosion) of up to -8 m (blue) and accumulation of material (red) of up to +5 m. Frequency distributions of the percentage of vertical change (dz) between the two years are illustrated in Figures c and i. The A-A', B-B' and C-C' profiles are plotted in Figures d-f and j-l with the solid line indicating the 2008 profile and the dotted indicating the 2010/11 profile in relation to MHWS. The bold line in these plots indicates the difference in elevation between the two years across these profiles

The changes to the cliff-face are further illustrated in cross-shore profile lines interpolated from the DEMs, where removal of material higher up the cliff-face and deposition of this material lower down is apparent. Gradual erosion of material across the whole vertical profile of the cliff face is also shown in the cross-shore profiles of Godrevy and in the high percentage of smaller changes in the frequency distributions.

Table 2.4 Cliff dimensions and resultant rates of retreat obtained from LiDAR-derived DEM comparisons

	Net Volume loss (m^3) (V)	Ave cliff height (m) (H_c)	Average slope (°)	Longshore length (m) (L_c)	Time interval (yrs) (T_c)	Rate of Retreat (m yr^{-1}) (R)
Hemmick	40.37	11	68	40	3.8	0.03
Pendower	39.66	10	66	370	3.8	0.01
Church Cove	1091.80	20	42	64	3	0.29
Porthleven	1373.50	17	73	265	3.5	0.09
Caca Stull Zawn	642.00	24	60	20	3.5	0.37
Porthcurno	0.053	50	73	780	3	0.00
Godrevy	677.83	15	69	660	2	0.04
Portreath	623.54	26	75	135	3	0.06
Trevellas	1078.50	70	51	200	1	0.08
Bedruthan Steps	5422.10	45	43	380	2.5	0.17

The highest cliffs in the study are found at Porthcurno (50 m), Trevellas (70 m) and Bedruthan Steps (45 m), and the smallest at Hemmick (11 m), Pendower (10 m) and Godrevy (15 m) ; the steepest cliffs are found at Porthleven (73°), Portreath (75°) and Godrevy (69°). The sizes of the regions of interest at each site (longshore length of cliff (L_c)) vary, but this does not affect the rate of retreat as this figure is normalised to the length of cliff (in m). The largest volume changes during this 3–4 yr period occurred at Bedruthan Steps (5422 m^3), Porthleven (1374 m^3), Church Cove (1092 m^3) and Trevellas (1079 m^3), with little change noted at Hemmick, Pendower and Porthcurno (all < 40 m^3). With information about the area of the region of interest (H_c and L_c) and the time period between consecutive surveys (Eqn 2.5) (T_c), the rate of recession of the cliff (R) can be calculated (Table. 2.4). These rates vary by an order of magnitude around the coastline, from 0.00 at Porthcurno to 0.37 m yr^{-1} at Caca Stull Zawn.

2.5 Discussion

Fig. 2.5 provides the DEMs of difference between, and the frequency distributions of the vertical surface elevation change for all ten sites. Although the coastline of the south-west of the UK is characterised as a slowly eroding coastline in comparison to the south and eastern

coasts of the country, variability in the magnitude of erosion that is apparent using this method is suggestive of some of the processes occurring at each site. The DEMs and the frequency distributions very clearly highlight the sites that experienced greater activity during the study period. For example, Bedruthan Steps, Porthleven, Caca Stull Zawn and Church Cove prove to be much more active (more negatively skewed distributions; meaning more losses than gains) than Pendower and Porthcurno. This suggests that there are regions where failure occurs and material remains part of the system (e.g., at Bedruthan Steps where positive and negative changes are noted), whereas at other sites material that is removed from the cliff face is removed by waves (e.g., at Godrevy and Porthleven where there distributions are more negatively skewed).

The accuracy of LiDAR is understood to decrease as cliff slope angle increases (Adams and Chandler, 2000; Xharde *et al.*, 2006). It is not possible to test this notion in this situation as the only locations within the LiDAR tile that are certain to have not changed between the LiDAR surveys are on flat ground. A method of assessing whether the change seen on sloping surfaces is actual change or error inherent in the LiDAR method, is by applying a gradually increasing threshold (0 to 10 m at 10 cm intervals) to the volume differences to remove any data that may potentially be construed as error (Earlie *et al.*, 2013). This allows us to determine whether the net rate of retreat is influenced by this 'cut-off' (Figure 2.5c (i-v)). This sensitivity testing allows us to assess how the resultant rate of retreat will change according to how much of the data is considered error; hence, how much valid data are eliminated (Earlie *et al.*, 2013).

All ten sites (nine plus Caca Stull Zawn) are presented here to demonstrate the sensitivity analysis process. All plots show a decrease in net erosion with an increasing threshold. The point at which this value reaches zero varies, depending on the size of the failures noted in relation to the threshold (Figure 2.5c (i-v)). What is apparent from these plots is that LiDAR is able to accurately detect failure on sloping surfaces, as even if the conservative cut-off threshold of 0.5 m is used to eliminate potential error, very little reduction in the net volume difference is seen, compared to using no threshold. Using this method allows for the smaller changes that are often difficult to detect using historic mapping or photogrammetry to be accountable for the change in volume, as well as the larger mass failures

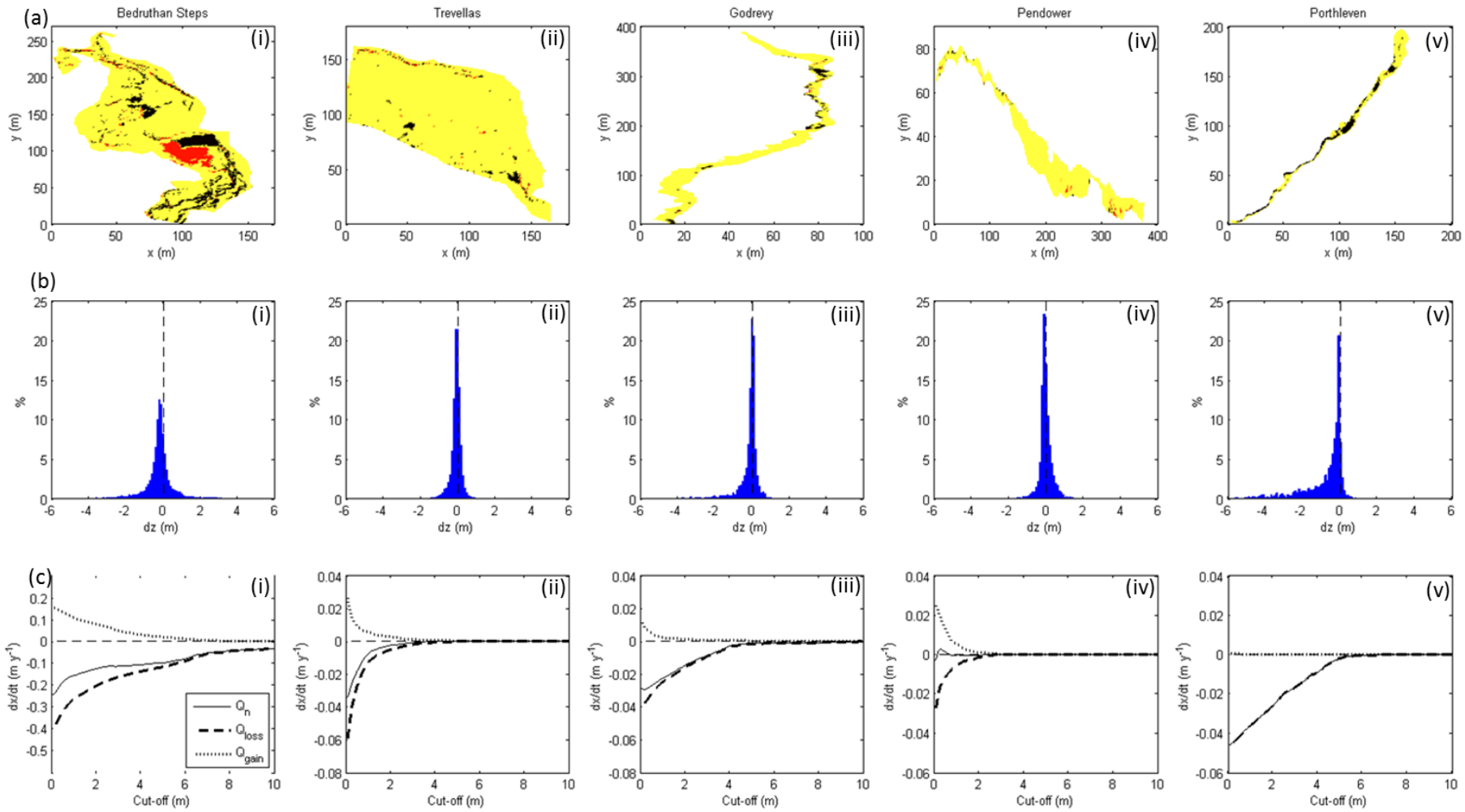
(a)
Bedruthan Steps
Trevellas
Godrevy
Pendower
Porthleven
(i)
(ii)
(iii)
(iv)
(v)
y (m)
x (m)
(b)
%
dz (m)
(c)
dx/dt (m y-1)
Cut-off (m)
Qn
Qloss
Qgain

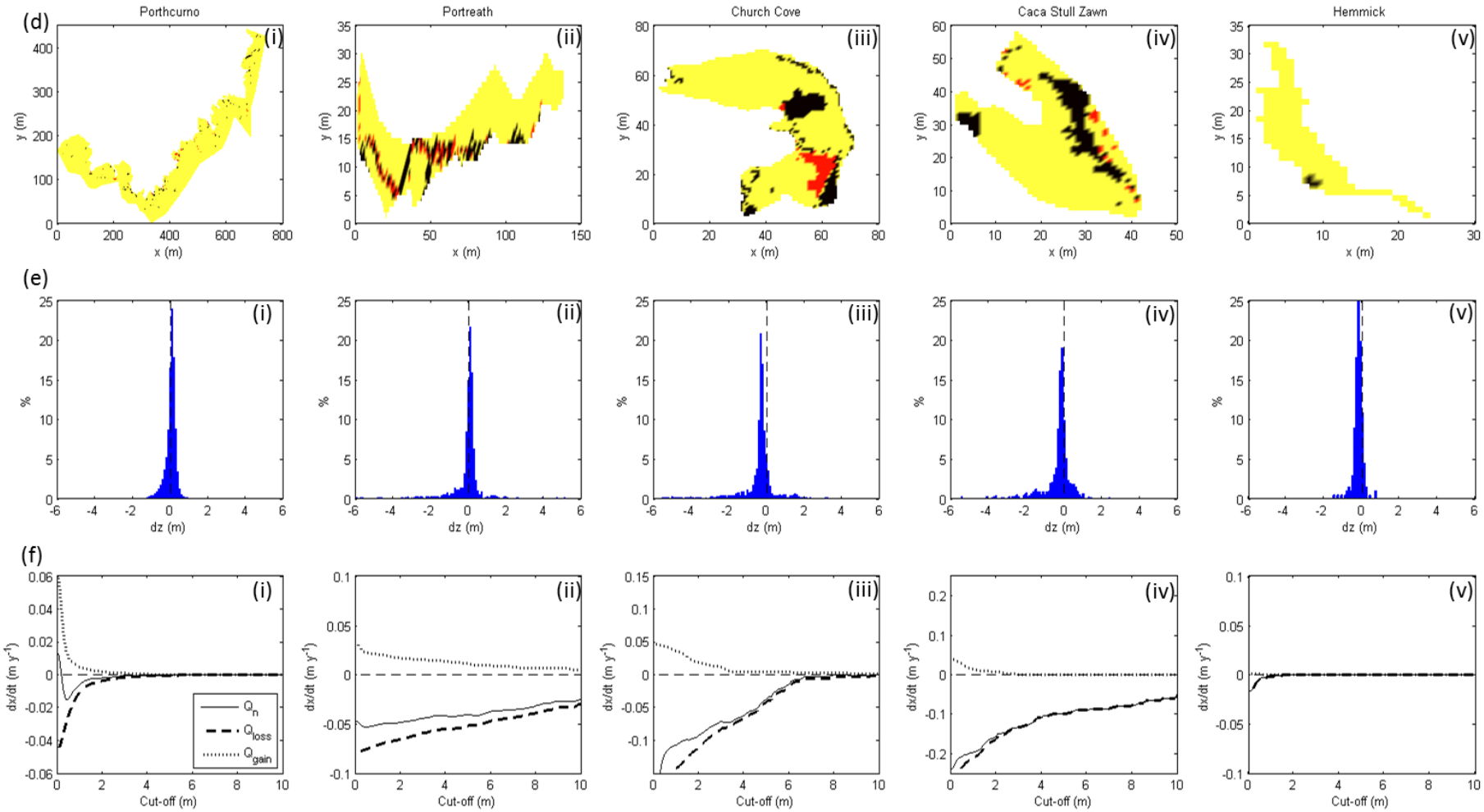

Figure 2.5: Panels a and d (i-v) - DEM's of difference (x-axis; cross-shore, y-axis; longshore); where red regions represent accumulation of material, black regions represent erosion and yellow shows no change. Panels b and e (i-v) - frequency distribution (vertical change, dz versus %). Panels c and f (i-v) - sensitivity analysis of recession rate (y-axis) to a gradually increasing error threshold (x-axis) for all ten sites. The small dashed line in these plots represents the total positive changes (accumulation of material), the thick dashed line represents total negative changes (erosion) and the solid line represents the net change (*V*)

2.5.1 *Physical parameters and rates of retreat*

It is rare for both the geotechnical resisting forces (lithology and rock mass characteristics) and the erosive forces (tide data, wave climate) to be included in process-based cliff erosion studies (Rosser *et al.*, 2005; Rosser *et al.*, 2007; Naylor *et al.*, 2010). Many investigations are site-specific and, although in this study a relatively small data set has been obtained, it represents one of the first longitudinal data sets that considers both the boundary conditions and the forcing parameters, and attempts to draw relationships between these spatially-varying parameters (Fig. 2.6).

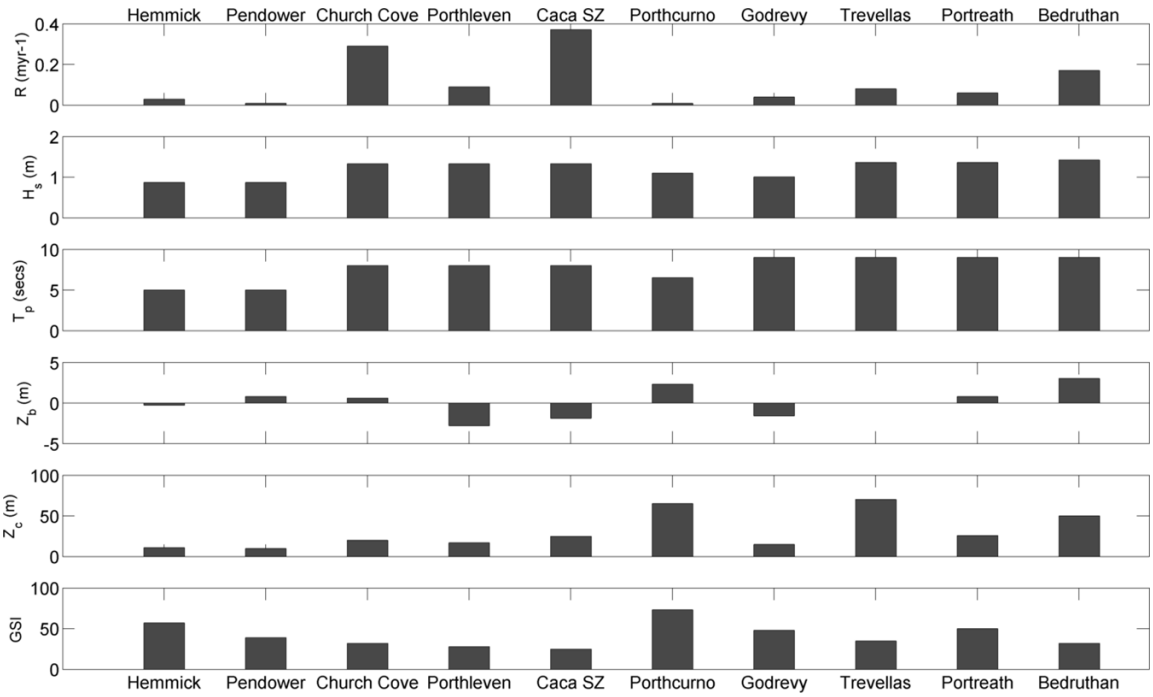

Figure 2.6: Rates of retreat, mean H_s, mean T_p, toe exposure (elevation of beach level above/below MHWS (Z_o)), cliff height (Z_c) and GSI at each site. Wave statistics are taken from nearest SWAN output node locations, representative of the regional wave climate

What is initially apparent from Figure 2.6 is that the sites along the west, north-west and south-west facing coast (Church Cove, Porthleven, Caca S.Z., Porthcurno, Godrevy, Trevellas, Portreath and Bedruthan Steps) experience greater rates of erosion than the sites along the south-east coast (Hemmick and Pendower), varying by almost an order of magnitude from 0.00–0.03 m yr^{-1} to 0.05–0.37 m yr^{-1}. The more sheltered sites along the south-east coast experience smaller significant wave heights and peak wave periods than those along the north-west coast. The wave exposure values (Z_o) refer to the average elevation of the beach at the cliff toe relative to mean high water springs (MHWS). Negative

values indicate that the cliff base is located above MHWS and therefore not affected by wave action over most of the tidal cycle, whereas positive values indicate that the cliff base is located below MHWS and is subjected to wave action over most of the tidal cycle. This parameter varies around the coastline, with the majority of the toe of the cliffs (6 out of 10 sites) undergoing regular inundation. The beach levels are extracted from the LiDAR data and therefore represent an average between two points in time. It is important to note however, that these levels are subject to seasonal variation and the beach slopes and beach/cliff junction elevations can change according to the wave climate by several meters (Ridgewell and Walkden, 2009).

Some preliminary inferences can be drawn from Fig. 2.6. For example, sites with higher GSI values appear to be more resistant to erosion: Porthcurno has a GSI of 70–75 and a 0.01 m yr^{-1} rate of erosion, whereas Church Cove has a GSI of 30–35 and an erosion rate of 0.29 m yr^{-1}. However, there are also regions where low rates of erosion are apparent in cliffs with a low rock mass strength: Pendower has a GSI value of 37–40, yet a relatively low erosion rate of 0.01 m yr^{-1}. Clearly, other variables are influential, for example, wave exposure parameterised by H_s and the protection afforded to the cliff toe due to the elevation of the beach (Z_o).

Erosion rates identified in this study are not only a function of the boundary conditions and wave forcing, but also the scale at which the data are captured. The variables that are investigated and the associated scale at which they occur have strong bearing on the results (Naylor *et al*., 2010). The two most active areas detected in the LiDAR data (Church Cove and Caca Stull Zawn), characterised by erosion rates of 0.2–0.4 m yr^{-1}, are related to the presence of very localised regions of structural weakness or faults. Therefore, the associated erosion rates are perhaps not representative of the stretch of coastline as a whole. For the purposes of statistical analysis, these two sites have been removed to ensure the correlations represent the changes occurring due to processes such as abrasion, quarrying and erosion due to weathering. This produces a limitation in the data set, where only considering eight sites produces 6 degrees of freedom. With a 0.05 alpha level, this gives a critical value of 0.707, meaning only variables whose correlation coefficients exceed this value are statistically significant.

2.5.2 *Statistical relationships*

It is important to consider the relationships between the various boundary conditions and forcing factors at each site to understand what is causing failure on a local scale. The correlation coefficients (*r* values) between the various parameters and cliff erosion rates allows for these relationships to be drawn. Although this is a relatively small data set, correlations are apparent between the rates of retreat and the variables acting to control them.

Cliff height is generally considered to play a significant role in the rate of erosion, e.g., along the south coast of the UK; (Pethick, 1984), yet, some studies have proved cliff height to be a poor predictor of cliff retreat (Dornbusch and Robinson, 2005). The fact that both the highest and the lowest rates of retreat are found in cliffs of the same average height (20–25 m) emphasises how this variable tends to be influenced by the rock mass structure that controls the failure mechanisms of the cliffs rather than the height of the cliff itself.

Table 2.5: *r* values for correlations between rate of retreat and variables of significant wave height (H_s), the 10% exceedance wave height (H_{10}), peak spectral wave period (T_p), the elevation of the beach relative to the cliff (Z_o), the cliff height (Z_c), the Geological Strength Index (GSI), and a simplification of Sunamura's ratio (GSI:H_s)

Variable	Correlation coefficient (*r* value) of variable to rate of retreat (removing Caca Stull Zawn and Church Cove)
H_s	**0.78**
H_{10}	**0.76**
T_p	0.64
Z_o	-0.40
Z_c	0.29
GSI	-0.66
GSI /H_s	**-0.77**

The highest *r* values (also the only relationships that exceed the critical value (0.707)) between the variables and the rates of retreat were found between the significant wave height (H_s) (0.78) the 10% exceedance wave height (H_{10}) (0.76), the GSI values (-0.66), and the ratio of the GSI to the significant wave height (-0.77) (Fig. 2.7). The high r-value (-0.77) for rate of retreat and a simplified version of Sunamura's rock coast evolution model (Equation 1b) supports the notion that the ratio of the rock strength to the wave exposure is highly influential in the rate of erosion.

Fig. 2.6 illustrates a number of variables that influence and control hard rock cliff dynamics. It is unlikely that any one factor on its own explains the cliff behaviour and it is more likely

that a combination of the different factors should be considered. This indicates how these relationships can only really be drawn between failures and processes in the longer term. Directly linking large scale failures and forcing would require more detailed, perhaps even *in-situ*, investigations of the variables at a particularly vulnerable site.

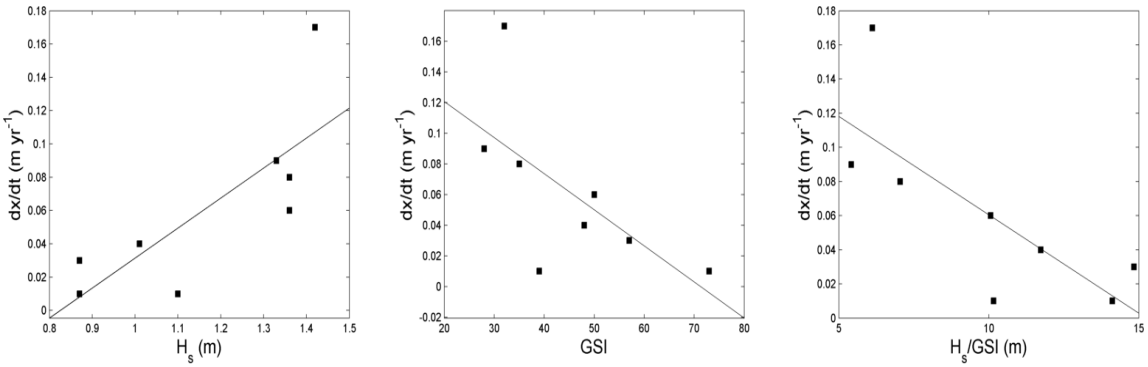

Figure 2.7: Relationship between rates of retreat and significant wave height (H_s), GSI and the ratio H_s: GSI. These three plots represent some of the strongest correlations between the variables and observed recession

2.5.3 Comparison with existing rates of retreat

One of the aims of this study was to compare the rates derived using LiDAR data with the rates used in shoreline management (Table. 2.6) and evaluate whether LiDAR data can be used as a suitable tool to estimate longer term rates of retreat. The rates derived from historic maps and the LiDAR rates tend to agree on the whole, however statistically, the two methods have a low correlation (r value of 0.5). As there are no SMP2 erosion rates for Hemmick and Bedruthan, this leaves eight sites for comparison. With an alpha value of 0.05 and 6 degrees of freedom, this produces a critical value of 0.7, therefore the r value found from comparing the two data sets does not satisfy this requirement. Using this method across more sites in the region could potentially improve this correlation as the failures noted at each of these sites are very locally variable and site specific. There are regions where large failures have occurred during the time period of the LiDAR study, causing the LIDAR-obtained average retreat rates to be close to the upper bound of the range of the longer term recession rates (e.g., at Church Cove, Porthleven and Caca Stull Zawn). Likewise, there are regions where the rate of retreat is much lower than that detected using historic maps, perhaps due to the time constraint of using a relatively modern technology, when only a shorter time period of data are available (e.g., Godrevy and Portreath). Larger scale failures are not detected during this time meaning that an epoch of a few years may not be sufficient. Rates of retreat may be too

slow to be captured using historic maps, and not accounted for within the existing rates of retreat. LiDAR data is however able to provide recession data in regions that are not identified in large scale coastal behaviour analyses (e.g. Hemmick and Bedruthan Steps).

The uncertainty of the recession rates associated with the SMP2 method (Ridgewell and Walkden, 2009) (indicated with a range of values for each site) is decreased with the LiDAR method as the rate of change to the cliff face over a period of time can be accurately quantified with some degree of certainty (Earlie *et al.*, 2013; 2014). These retreat rates differ slightly to those derived in Earlie *et al.*, (2013; 2014) as a higher threshold of error was used in this study, to derive more robust erosion rates and eliminate any data that may be attribute to error (Zhang *et al.*, 2005).

Table 2.6: Comparison of recession rates derived in this study, using airborne LiDAR with the existing rates of retreat used for shoreline management (SMP2 rates).

Site	SMP2 (historic rate (m yr^{-1}))	LiDAR method (m yr^{-1})
Hemmick	n/a	0.03
Pendower	0.02	0.01
Church Cove	0.15-0.25	0.29
Porthleven Caca Stull Zawn	0.10-0.25	0.09 0.37
Porthcurno	0-0.10	0.00
Godrevy	0.10-0.50 0.02-0.06 (Shail and Coggan, 2010)	0.04
Portreath	0.40-0.50	0.06
Trevellas	0-0.02	0.08
Bedruthan Steps	n/a	0.17

The processes involved in the evolution of rocky coastlines are not entirely captured with current methods used for shoreline management purposes. Casting a line along the top of the cliff to represent change does not wholly capture the three-dimensional detail of the important changes occurring to the face of the cliff which contribute to overall failure. LiDAR data provides a means of obtaining large scale, high resolution geospatial data sets and can be used to accurately and confidently quantify rocky coast evolution for the purposes of informing coastal management and coastal conservation policies and practices.

2.6 Conclusion

In the first part of this study we have tested the suitability of using Airborne LiDAR on a regional scale over 3–4 yrs at nine different sites, to determine volumetric changes to the cliff-face and calculate linear rates of retreat for a slowly eroding geologically 'resistant' coastline exposed to a highly energetic wave climate.

Digital Elevation Models (DEMs) of difference provide volumetric change information for a variety of cliff geometries and allow for not only frequency distributions of failure but also cross-sectional detail on the types of failure mechanisms occurring. Rates of retreat around the Cornish coastline range from 0.01–0.37 m yr^{-1} and were found to vary according to the spatially varying boundary conditions (rock mass characteristics, beach elevation/ cliff toe exposure) and forcing parameters (significant and maximum wave height and peak wave period). The strongest correlations were apparent between the rate of retreat and a) the significant wave height (H_s) (0.78) b) the 10% exceedance wave height (H_{10}) (0.76) and c) the ratio between the rock mass strength and H_s (0.77) (GSI/H_s).

It is well understood that the accuracy of LiDAR decreases with an increasing slope angle (Adams and Chandler, 2002); however, the sensitivity analysis carried out here and by Earlie *et al.* (2013) shows that even if vertical changes in excess of 0.5 m are disregarded, this has a minor effect on the computed recession rates.

The overall rates of retreat determined using LiDAR data are similar to the long term rates developed in the SMP2, yet has provided an additional level of detail that the historic map analysis method is not able to provide. This method has indicated that localised studies are vital to obtaining a more accurate understanding of the rates of erosion on a shorter time scale, especially in hard rock coastlines where failure is often episodic. In terms of understanding hard rock cliff erosion, this study has emphasised the complexity of these coastal systems. The variety of factors that influence the rates of erosion means there is no single factor causing cliff erosion; the whole system of the physical interactions must be considered holistically in order to understand their evolution.

Chapter 3

Quantifying cliff erosion on a monthly time scale

3.1 Introduction

Investigating hard-rock cliff erosion using airborne LiDAR data on an annual timescale has highlighted the importance of localised studies and data collection methods which encompass the complexity of coastal cliff systems. Chapter 2 provides one of the first erosion rate investigations in hard rock coasts along the south-west coast of England, where cliff erosion has quite recently posed a significant threat to infrastructure (SWCP, 2012). Although the rates derived using LiDAR are comparable to the longer term rates of retreat, determined by analysing decades of change using historic mapping, Chapter 2 has indicated how capturing the detail of the cliff-face that is lacking from map analysis is vital to understanding the failure mechanics of harder rock coastlines. In addition to this, the importance of the beach morphology, wave climate and rainfall, alongside an understanding of the lithology and cliff failure mechanisms, needs further attention on a more localised scale.

Typical methods of obtaining information about coastal change for coastal management purposes include readily available airborne LiDAR data and aerial photography or photogrammetry (Ridgewell and Walkden, 2009; Young *et al.*, 2006, 2009, 2011b). These techniques have proved highly valuable for identifying flood risk zones, or regions sensitive to coastal erosion on a large scale (hundreds of meters to kilometres) and over a long time period (years to decades) as highlighted in Chapter 2. For rocky coast geomorphology in particular, the time scales addressed with such methods allow for both the smaller scale continuous and the larger scale episodic changes to be captured within a longer frame (Naylor *et al.*, 2010). These changes are then averaged out to provide an indication of the change to a cliff per year based on numerous years of change (rate of erosion in m yr^{-1}).

Long-term retreat rates of rocky coasts in the UK, such as the south-west peninsular, are currently understood to be in the order of 0.01 to 0.10 m yr^{-1} (Ridgewell and Walkden, 2009; Earlie *et al.*, 2014). These values are based on the landward migration of the cliff edge over decades. Shoreline Management Plans in the UK, which inform local and regional management decisions, are based on these rates of retreat. When this method is applied to

rocky coastlines, erosion of the cliff face as well as the cliff toe is missed. The failure mechanisms occurring in such a complex three-dimensional environment are important to capture as they contribute to the overall cliff failure. To consider the more imminent risks to infrastructure in particularly vulnerable and eroding stretches of coastline, displaying dynamics on a much smaller time and spatial scale (months to years, over tens of metres) that cannot be covered by map analysis, an *in-situ* method that is confidently able to quantify change at a higher temporal (monthly or weekly) and spatial scale (centimetres to metres) is required.

It is typically understood that wave action leads to erosion of the cliff-toe and subsequent cantilever failure (Trenhaile, 1987; Sunamura, 1992), and that rainfall and ground saturation are responsible for a great deal of coastal landsliding (Wyllie and Mah, 2004). Annual monitoring of cliff morphology is not suitable for investigating inter-annual dynamics related to, for example, wave height and rainfall variability. With the potential for increased storminess and sea level rise in the future (Dodet *et al.,* 2010) this begs the question of 'how will the cliffs stand up to more extreme and frequent assailing forces?' Monitoring the evolution of the cliffs at a high spatial and temporal resolution will help to fill in the gaps that currently exist in our understanding of the processes leading to cliff erosion. Specifically, it will help with understanding the processes that govern short-term cliff dynamics (waves, rainfall, water level) – it is the integration of these short-term cliff dynamics that determine long-term cliff recession.

Terrestrial Laser Scanning (TLS) has been selected as a method for investigating short-term (monthly) cliff dynamics, due to its high-resolution data capture and suitability for rapid deployment in the field. Coastal retreat and threats to property and infrastructure on a more immediate timescale can be understood with greater confidence and detail using methods such as TLS. Its applications have been used as means of mapping and identifying regions of topographic change in a number of environments. Examples include dune morphological analysis (Montreuil *et al.,* 2013) fluvial morphology (Jayboyedoff *et al.,* 2009; Alho *et al.,* 2011; Schurch *et al.,* 2011; Brodu and Lague, 2012; Lague *et al.,* 2012), beach morphology (Poulton *et al.,* 2006) and rocky platform analysis (Dewez *et al.,* 2009). Recently, TLS has been adopted for monitoring both hard and soft-rock cliffs (Rosser *et al.,* 2005; 2013; Poulton *et al.,* 2006; Rosser *et al.,* 2007; Abellan *et al.,* 2011; Dewez *et al.,* 2013; Rohmer and Dewez, 2013).

Obtaining an accurate three-dimensional surface of a cliff face may provide insight into where failures are occurring and when (Rosser *et al.,* 2005; 2007; Norman, 2012; Kuhn and Prufer, 2014; Travelletti *et al.,* 2014), and frequent surveys provide a chronology of material failure relative to the forcing conditions (Lim *et al.,* 2011). Obtaining a record of wave and weather conditions may help to identify this relationship between assailing forces and failure events, allowing the exploration of the notion that material is removed from the top of the cliff during rainy conditions, and bedrock and cliff-toe material are removed during periods of energetic wave conditions.

The development of sophisticated technologies such as TLS has meant that topographic data can now be captured at a very high resolution; when used alongside global positioning systems (GPS) and survey data, the TLS data are also highly accurate. TLS is able to capture data to millimetre resolution, providing additional detail that contributes to understanding the erosion of the cliffs. Many TLS are equipped with a high resolution camera and, when viewing the data, the imaged can be draped over the point cloud, providing further detail on dynamic features such as the surface roughness, beach elevations and talus deposits. Repetitive surveys can be compared to obtain overall volumes of change. Sensitive regions of failure can be detected and help determine failure likelihood and scale for risk management purposes (Rosser *et al.,* 2007; Vaaja *et al.,* 2011; Dewez *et al.,* 2013).

In order to understand the relationship between the assailing forces and cliff failure mechanisms an accurate quantification is also needed of nearshore wave energy and water levels, the morphology of the beach and meteorological conditions (Ruggerio *et al.,* 2001; 2004). Studies have previously related the interplay between wave runup, offshore wave climate and beach levels using models (Shih *et al.,* 1994; Lee, 2008; Young *et al.,* 2013); yet, few studies use *in-situ* observations, and those that do tend to use proxies or modelled data for wave conditions and water levels (Lim *et al.,* 2011; Norman 2012). Recent studies (Rosser *et al.,* 2013; Brain *et al.,* 2014; Vann Jones *et al.,* 2015) found that as well as cliff toe erosion, rock falls propagating progressively upwards are a result of marine processes and result in failure extending the full height of the cliff. Cliff-toe inundation *duration* was not found to be responsible for increased rock fall activity in the Vann Jones *et al.,* (2015) study, however the relative wave energy expended on the cliffs during these inundation periods although not considered here, was believed to be influential. TLS has been used in coastal settings in many different countries (Rosser *et al.,* 2005; 2007; Abellan *et al.,* 2010; Lague *et*

al., 2013; Travelletti *et al.*, 2014; Vann Jones *et al.*, 2015); however, no studies as of yet compare erosion volumes and locations directly with the nearshore hydrodynamics and beach morphology.

This chapter firstly introduces the two study sites, (Porthleven and Godrevy) their coastal, geological and hydrodynamic setting (section 2) and describes the field instrumentation deployment and data processing methodology (section 3). Observations of cliff face erosion beach morphology, beach-cliff junction elevation, wave climate and water levels are presented in section 4 and a discussion of the relationships between the variables and the geomorphic implications of the findings is provided in section 5.

3.2 Study area

This chapter focuses on two particularly vulnerable sites situated on the south-west peninsula of the UK, facing south-west (Porthleven) and west (Godrevy) towards the Atlantic Ocean (Fig 3.1). Both sites are subject to a highly energetic wave climate being exposed to both locally generated wind waves and Atlantic swell from the south and south-west (Scott *et al.*, 2011).

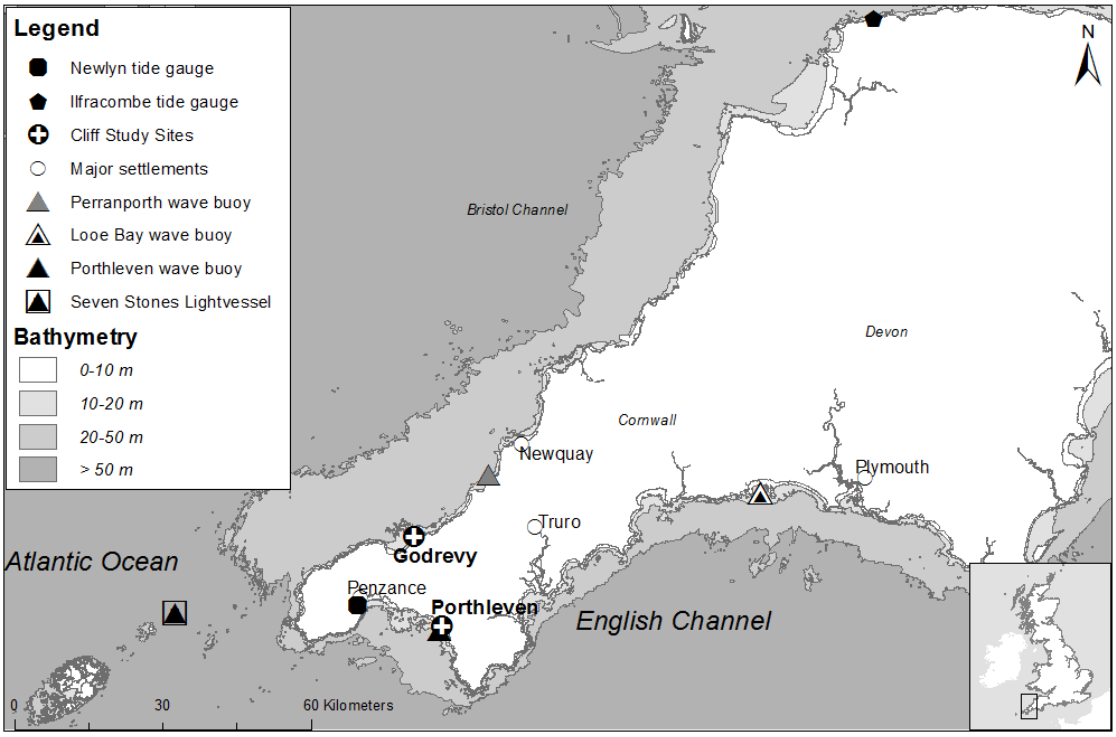

Figure 3.1. Location of study sites, wave buoys and tide gauges.

The two sites, along with many others around the south-west, experience current management issues due to recent and ongoing cliff instability impacting on infrastructure and posing risks to beach and coast path users. These two sites have similar geology (e.g., cliff height, lithology and rock mass characteristics), but differ in their coastal settings, where the beach morphology and offshore bathymetry influence the dissipation of wave energy differently.

3.2.1 Porthleven

The study site at Porthleven (Fig. 3.1) is situated along a 300-m stretch of uninhabited cliffed coastline just southeast of the small town of Porthleven, UK. The tidal regime is macrotidal with a mean spring range of 4.7 m. The cliffs rise 8–10 m above a steeply-sloping (tanβ = 0.12) beach (Poate *et al.*, 2009), and the beach elevation at the cliff-toe varies from anywhere between 2.5 m and 4.5 m seasonally (in m Ordnance Datum Newlyn (ODN) which is c. 0.2 m above MSL). The coastal slope at Porthleven is relatively steep, with the 10 m contour about 1 km offshore and the 20 m contour about 2.5 km offshore (Lee, 2002; CCO, 2015).

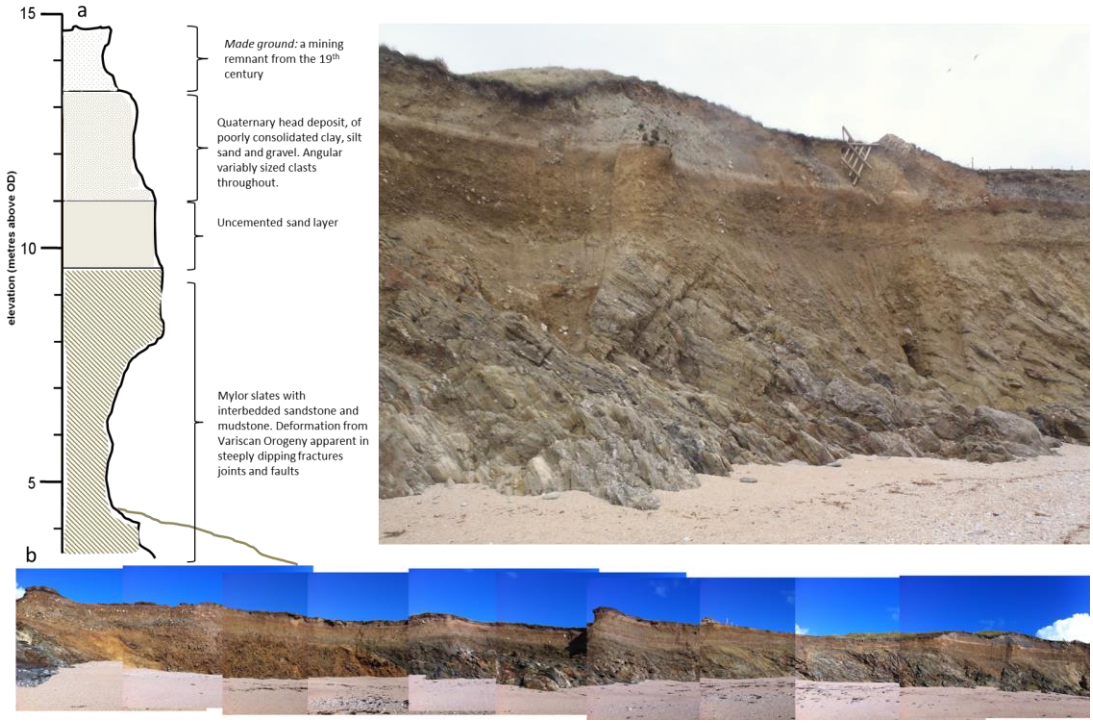

Figure 3.2: (a) Sketch and photograph of a profile through a section of cliff at Porthleven summarising the stratigraphic sequence of bedrock and superficial units; and (b) panoramic perspective of the cliff frontage.

The cliffs are mainly formed of Late Devonian Mylor slate lithofacies and comprise pale grey-green mudstone with interbedded-siltstone and fine-grained sandstone (Leveridge and

Shail, 2011) (Fig. 3.2). These cliffs are bounded at either end of the bay by Porthscatho lithofacies of alternating beds of green-grey sandstone and dark-grey mudstone (Leveridge and Shail, 2011). The Porthleven cliffs are geologically important as they provide evidence of the order of the deformation phases that occurred during the Variscan Orogeny (Leveridge and Shail, 2011). The cliffs are oriented at 200°, dipping gently south-eastwards and exhibit evidence of deformation during this period (Alexander and Shail, 1996); cut by a variably reactivated network of late Carboniferous – Triassic fractures, joints and faults steeply dipping SSW and NNE (Fig 3.2a). It is the orientation, spacing, roughness and frequency of these features that ultimately dictate the likelihood and mode of failure (Wyllie and Mah, 2004). The Mylor slates are overlain by a *c.* 2–4 m thick Quaternary head deposit of poorly-consolidated clay, silt, sand and gravel capped with a thin layer of 'made ground' (0.5–1.5 m); a remnant of mining activity in the late 19th century (Bird, 1998).

3.2.2 Godrevy

Also situated on the south-west peninsula, but along the west-facing coast, lies the settlement of Godrevy. Exposed to a similarly energetic wave climate, the cliffs are subject to both south-westerly and westerly Atlantic swell. The tidal regime at Godrevy is macrotidal with a mean spring range of 5.88 m. The cliffs are fronted by a gently sloping beach ($\tan\beta = 0.02$) composed of well-sorted medium sand (D = 0.25–0.5 mm) with a slightly steeper upper beach ($\tan\beta = 0.06$) composed of mixed sand and gravel/ pebbles (D = 16–30 mm) (Scott, 2012). The cliffs rise 8–15 m above the beach and the beach elevation at the cliff toe varies seasonally by 3–6 m ODN.

The geological units at Godrevy consist of underlying, more resistant bedrock of weakly metamorphosed sandstones and mudstones overlain by superficial head deposits, varying in thickness along the cliffs. The boundary between the two major units rises from beach level at the northern end of the embayment to an elevation of about 15 m ODN at the southern end (Fig 3.3). The bedrock (Porthtowan formation) comprises weakly metamorphosed Upper Devonian sandstones and mudstones (Shail *et al.*, 1998).

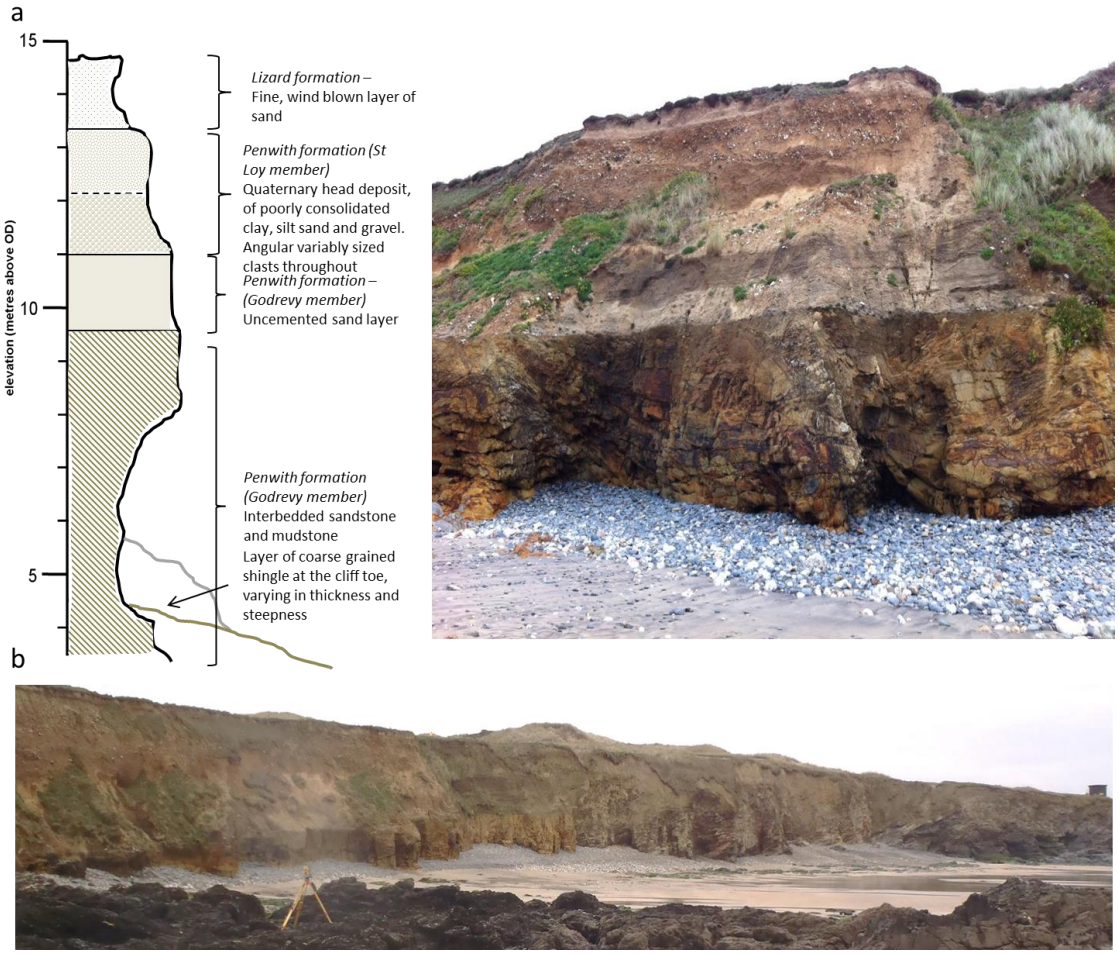

Figure 3.3: a) Sketch and photograph of a profile through a section of cliff at Godrevy summarising the succession of bedrock and superficial units and b) panoramic perspective of the cliff frontage.

Much like the cliffs at Porthleven, this bedrock displays evidence of complex deformation during the late Carboniferous tectonic evolution of the southwest of the UK (Shail *et al.*, 2010). The bedding planes are gently inclined towards the southeast and the main fractures (joints and faults) cutting the rocks are oriented ENE-WSW, NE-SW and NW-SE (Fig. 3.3a). A unit of superficial head deposit overlying the bedrock is composed of a poorly sorted mixture of variably sized fragments in a silty cohesive matrix overlain by a layer of wind-blown sand (Shail *et al.*, 2010). The coastal slope offshore of Godrevy is very wide and flat, with the 10 m contour about 1–2 km offshore. The seabed then slopes gently out to the 30 m contour which lies at about 15 km offshore to the WNW (Lee, 2002; CCO, 2015).

Table 3.1 Summary of physical characteristics at each site. Cliff heights, beach-cliff elevation and tidal elevation (Mean High Water Springs (MHWS)) are shown in meters relative to Ordnance Datum Newlyn (m ODN). Tidal elevations (MHWS) are also presented in metres relative to Chart Datum (m CD).

Site characteristic	Godrevy	Porthleven
Cliff height	15 – 17 m ODN	17 – 20 m ODN
Length of cliff	~300 m	~300 m
Lithological units	Devonian sandstones and mudstones (2 – 15 m) overlain by Quaternary head deposit (2 – 12 m)	Mylor slates (5 – 10 m) overlain by Quaternary head deposit (2 – 4 m)
Beach – cliff elevation	2.5 – 4.5 m ODN	3 – 6 m ODN
Beach slope (tan β)	0.01	0.12
Offshore slope	0.02	0.05
Tidal range	5.88 m	4.7 m
MHWS	3.2 m ODN (6.6 m CD)	2.5 m ODN (5.5 m CD)
Winter H_s (Oct - Mar)	1.7 m (*mean*) 5.6 m (*max*)	1.4 m (*mean*) 10 m (*max*)
Summer H_s (Apr - Sep)	0.8 m (*mean*) 3.6 m (*max*)	0.7 m (*mean*) 3.8 m (*max*)
Winter T_p (Oct - Mar)	12 s (*mean*) 22 s (*max*)	9 s (*mean*) 28 s (*max*)
Summer T_p (Apr - Sep)	9 s (*mean*) 20 s (*max*)	7 s (*mean*) 22 s (*max*)

3.3 Method

3.3.1 Site setup

The same site set up was adopted at both sites for a survey period of one year (July 10th 2013 – July 17th 2014). Inshore waves and nearshore water levels were measured continuously using directional wave buoys, tide gauges and pressure transducers, and the cliffs and beach were surveyed every month during a spring tide. Extreme storm conditions between December and March led to damage of the wave and water level monitoring instruments and alternative data were used in place. Surveys during this time were carried out when beach levels and wave and water level conditions permitted access.

3.3.2 Wave climate

3.3.2.1 Inshore wave climate

Inshore wave conditions were obtained from directional Waverider wave buoys located directly offshore of Porthleven in 10 m water depth and Perranporth, located 20 km to the north of Godrevy, in 10 m water depth (Figure 3.1) (CCO, 2015). Bad data were flagged and removed from both time series and half-hourly statistics of significant wave height (H_s), peak

wave period (T_p) and wave direction (°) were derived. During the extreme energetic wave conditions over February 2014, both wave buoys malfunctioned, causing a 34-day data gap between 8th Feb and 12th March at Godrevy and a 28 day gap between 4th Feb and 5th March at Porthleven.

To extend the Porthleven wave record, a nearby wave buoy located at Looe Bay, 70 km from the site (Figure 3.1) was used as an alternative source of wave data. Over a three-year (2011-2014) wave record, significant wave heights at Looe Bay (under southerly and south-westerly swell directions; 180° – 240°) were 5% smaller than those at Porthleven. During this 28-day missing data period, 87% of the waves originated from this quadrant with a mean θ of 200°. Significant wave height statistics for Looe Bay were increased by 5% for this period and used to represent the nearshore wave climate at Porthleven.

No alternative wave buoy data were available for Perranporth (representing nearshore conditions at Godrevy); therefore, regional SWAN modelled data were used to extend the Perranporth wave record. The model is run daily and is forced by initial wind and wave output from the NOAA Wave Watch III Global wave model, providing half-hourly statistics of H_s and T_p from a 2D spectra, at 30-minute intervals at a number of output *nodes* around the coastline (Austin *et al.*, 2012). Data from the same SWAN model was also run at Gwithian (2 km from Godrevy) between 2011 and 2012. The two wave data sets were compared for the 2011 – 2012 record to estimate the suitability of using the Perranporth wave buoy to represent inshore wave conditions at Godrevy. For this period, significant wave heights from westerly and west north-westerly swell directions (270° and 325°) (the dominant swell direction: 98% at Gwithian) were found to be 26% bigger at Perranporth than those at Gwithian and the correlation between the two gave an R^2 of 0.93. The combined Perranporth wave buoy and SWAN data wave record (for the 34-day data gap) were therefore reduced by 26% to represent nearshore wave conditions at Godrevy.

The inshore data for both sites (using a combination of Porthleven and (adjusted) Looe Bay wave buoy data for Porthleven and a combination of Perranporth and SWAN modelled Perranporth data for Godrevy (both adjusted)) were de-shoaled to 100 m depth according to linear wave theory (a detailed explanation is provided in Chapter 4) to obtain deep-water wave conditions.

3.3.2.2 Nearshore hydrodynamics

Linking the response of the cliffs to the wave climate over the period of one year requires reliable water level data. Using a combination of nearshore water levels and inshore wave data it was possible to obtain a comprehensive picture of the wave climate over the year and the hydrodynamics at the coast. Nearshore water levels were obtained at each site using two self-logging RBR tide wave recorders (TWR 2050) deployed for the duration of the survey period (Jul 2013 – Jul 2014). Holes were drilled into a nearby section of rock using a heavy-duty drill and in-filled with a quick drying anchor adhesive resin holding the anchor sockets in place. Each sensor was placed inside a length of scaffold tube and bolted to the rock anchors.

Figure 3.4: Rock mounted pressure sensors held within scaffold tubes, deployed at Godrevy and Porthleven.

The sensors were configured to burst-sample waves at 2 Hz for 17 minutes (1024 burst length) every 38 min 24 s and average tidal elevation at 2 Hz over 2 min every 4 min 16 s. At this configuration, the battery and memory of the sensor allowed for a 35-day deployment, and data were downloaded every month during the cliff scanning survey.

The RBR processing software *Ruskin* (RBR, 2013) calculates water depth using a default value for atmospheric pressure. Limited availability of meteorological data at both sites (daily averages, when available) meant that the atmospheric pressure record was interpreted from the low-tide (i.e. dry) pressure sensor readings and the water pressure record were adjusted

according to these values. After adjusting for atmospheric pressure, the corrected pressure was converted to depth using the simple approximation (SBE, 2002);

$$depth(metres) = pressure(decibars) * 1.019716 \qquad \text{Equation 3.1}$$

The nearshore pressure sensor at Godrevy functioned for the duration of the survey period, yet during the stormy period the Porthleven sensor was lost to the sea. Access to replace the sensor was hampered by large waves for the month of February, thus leaving a large data gap at Porthleven of 43 days between 20th January and 5th March 2014.

3.3.2.3 Tidal levels

Measured water levels were obtained from the nearest National Tidal and Sea Level Facility tide gauge: The Newlyn tide gauge (20 km distant) for Porthleven and the Ilfracombe tide gauge (130 km distant) for Godrevy (NTSLF, 2014). The nearshore pressure sensors at the study sites were both deployed above mean low water neaps (MLWN), therefore only capturing mid-high-mid tide and were exposed to bores and broken waves in the swash zone at lower tidal elevations. To obtain a full tidal record, without the effects of bores and broken waves, mean half-hourly water levels for a 2-hr period either side of high-tide from the pressure sensors were compared with measured tidal level. The average ratio between the nearshore sensor and the tide gauge was applied to the whole time series of measured tide gauge data to represent measured tidal levels at each site. The water levels at Porthleven were 10% larger than those at Newlyn and Godrevy water levels were on average 35% smaller than those at Ilfracombe, and the gauge data were adjusted accordingly.

3.3.2.4 Wave runup

The total measured water level is made up of the tidal elevation and the wave runup which includes both the infragravity and incident components of the wave setup and swash fluctuations (Ruggerio *et al.*, 1996). Estimates of the 2% exceedance level for vertical wave runup (R_2) (for intermediate beaches) were calculated using the Stockdon *et al.* (2006) equation for runup;

$$R_2 = K\left(0.35\tan\beta\,(H_0L_0)^{\frac{1}{2}} + \frac{[H_0L_0(0.563\tan\beta^2 + 0.004)]^{\frac{1}{2}}}{2}\right) \qquad \text{Equation 3.2}$$

Where tan β is the slope of the beach face, and H_0 and L_0 are the deep-water wave height and length, respectively, obtained from the deshoaled inshore wave record (section 3.2.1). Stockdon *et al*. (2006) concluded that this equation was suitable for beaches where the Iribarren number (Eqn. 3) (ξ) (Battjes, 1974) lies between 0.3 and 1.25, representing intermediate beach conditions, i.e., those at Godrevy.

$$\xi = \frac{\tan\beta}{\sqrt{\frac{H_0}{L_0}}} \qquad \text{Equation 3.3}$$

However, recent field investigations of extreme wave runup on gravel beaches under energetic conditions (Masselink *et al.*, in press) have revealed that the Stockdon equation under predicts the runup by almost a factor of 2. Therefore, for Porthleven, an adjusted version of Stockdon *et al.* (2006), proposed by Masselink *et al.* (in press) was used where the fitting parameter (K) (K = 1.1 in Stockdon *et al.* 2006) when applied to gravel beaches (calculated for Porthleven beach), was increased to $K = 2$ for Porthleven.

3.3.3 Beach morphology

Monthly beach surveys at both sites were conducted using real time kinematic global positioning systems (RTK dGPS). At each site a 300 m alongshore section of beach was surveyed, from the toe of the cliff to the shoreline, using cross-shore transects at 50 m spacing at Godrevy and 10 m at Porthleven. The cross-shore profiles were used to determine the average slope of the beach for each month and the beach volume differences between surveys. As each survey area differed from month-to-month, the beach volume differences were normalised by the surveyed area to represent the vertical volumetric erosion/accretion per m to represent an average change in beach level.

The GPS beach profiles began in September; therefore, the elevations of the beach for the initial three months of the survey are unknown. As no other data were available, the beach slope from September was used for these summer months for the wave runup calculations. Difficulties associated with poor precisions due to reduced satellite coverage when surveying within close proximity to the base of the cliff meant that it was not possible to obtain a full profile towards the cliff-toe at every survey. Therefore, the beach-cliff junction elevation was

extracted from the monthly point cloud data as these could be confidently obtained for every survey (Jul 2013–Jul 2014).

3.3.4 Cliff volume loss

3.3.4.1 Point cloud data acquisition

Both sites were surveyed using a Leica ScanStation 2 Terrestrial Laser Scanner (TLS) (Leica, 2015) for the first 5 months of the year (Jul–Nov 2013) and a faster and more lightweight Leica P20 for the following 8 months (Dec 2013–Jul 2014) (Fig 3.5). Both are 'time-of-flight' laser scanners and provide high-resolution high-range point cloud data. The ScanStation 2 scans at 50,000 points/sec scan rate, and the P20 has a 1,000,000 points/sec scan rate. A similar set up was adopted for all of the monthly scans at both sites, where point clouds of the cliff face were obtained at 2 cm resolution at a 40 m range. The scanners were mounted on a survey tripod, levelled and situated about 20–30 m from the cliff face. To acquire optimum coverage of the cliff face and minimise occlusion effects due to shadowing/ blinding of complex surfaces, the scanner was repositioned 4–5 times along the beach (Fig 3.6). A full scan of the 300 m length of cliff at each site took about 5–6 hrs using the ScanStation 2 and 3–4 hrs using the P20.

Technical issues with surveying equipment at Godrevy in Sep 2013 caused the entire cliff face to shift forwards by 20–30 cm. As this site had no known positions within the scan area and the survey was georeferenced using mobile targets (surveyed using a total station from known benchmarks at the top of the cliff), it was not possible to re-register the Sep 2013 scan using alternative benchmarks. Instead of attempting to shift the face of the cliff to, essentially, an unknown position, this month was removed from the data set, as the true position of the cliff was unknown. At Porthleven, low beach levels, and large waves hindered scanning for most of December. Therefore, this month is also missing from the data set. Storm-impact related research during Feb 2014 (Chapter 4) provided interim scans at Porthleven, providing an insight into the impacts of particularly high-energy storms on the erosion of the cliffs (Chapter 4).

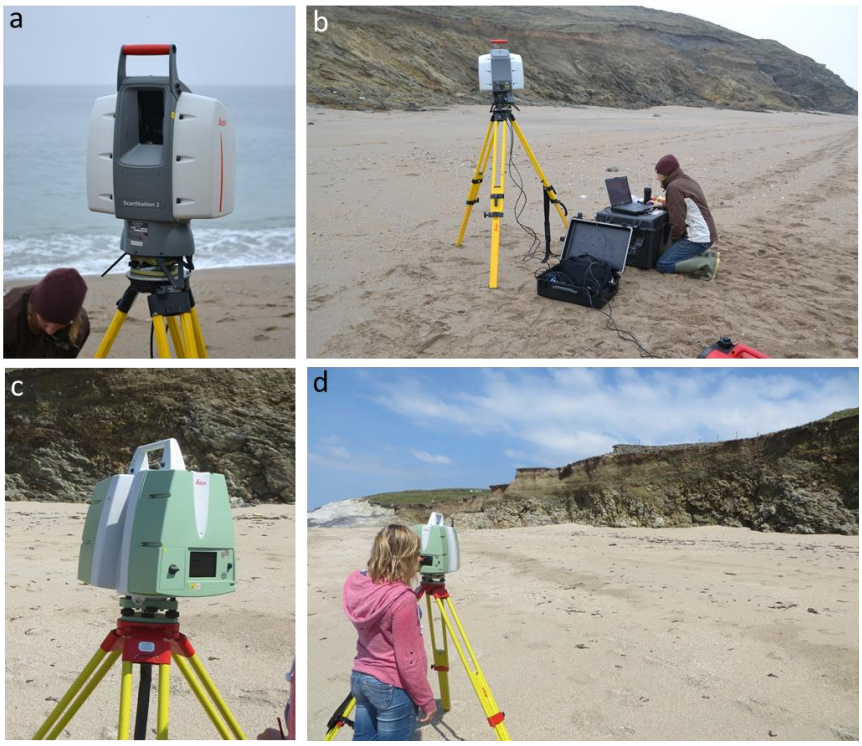

Figure 3.5 a) and Leica ScanStation 2 and b) scanner set up using generator for power and laptop for user interface. c) and d) P20 laser scanner, powered by internal battery and controlled using touch screen interface on scanner

3.3.4.2 Point cloud data georeferencing

Each individual scan (ScanWorld) contains common points that are used to 'stitch' the point clouds together. The Leica scanner software *Cyclone* (Leica, 2015) performs this registration of the ScanWorlds using a system of *constraints* which are pairs of equivalent or overlapping objects that appear in two scan worlds. The optimal alignment transformation for each component is computed, resulting in one single georeferenced ScanWorld point cloud. As the cliffs were constantly changing from month-to-month, features such as rock corners/ faces were not suitable to use as common points as in previous studies (Rosser *et al.*, 2005; 2007; Norman, 2012). High Definition Surveying (HDS) targets were situated within the scan, providing *constraints* and remained in place as the scanner was repositioned along the beach (Fig 3.6c and d).

At Porthleven, the HDS targets were fitted to fixed brackets along the cliff top (Fig 3.6d) and at Godrevy the targets were attached to weighted magnetic mounts and placed on the beach (Fig 3.6c). The central points of the targets were surveyed using a total station and using these known positions, the point cloud was retrospectively registered and geo-referenced using Leica Cyclone software.

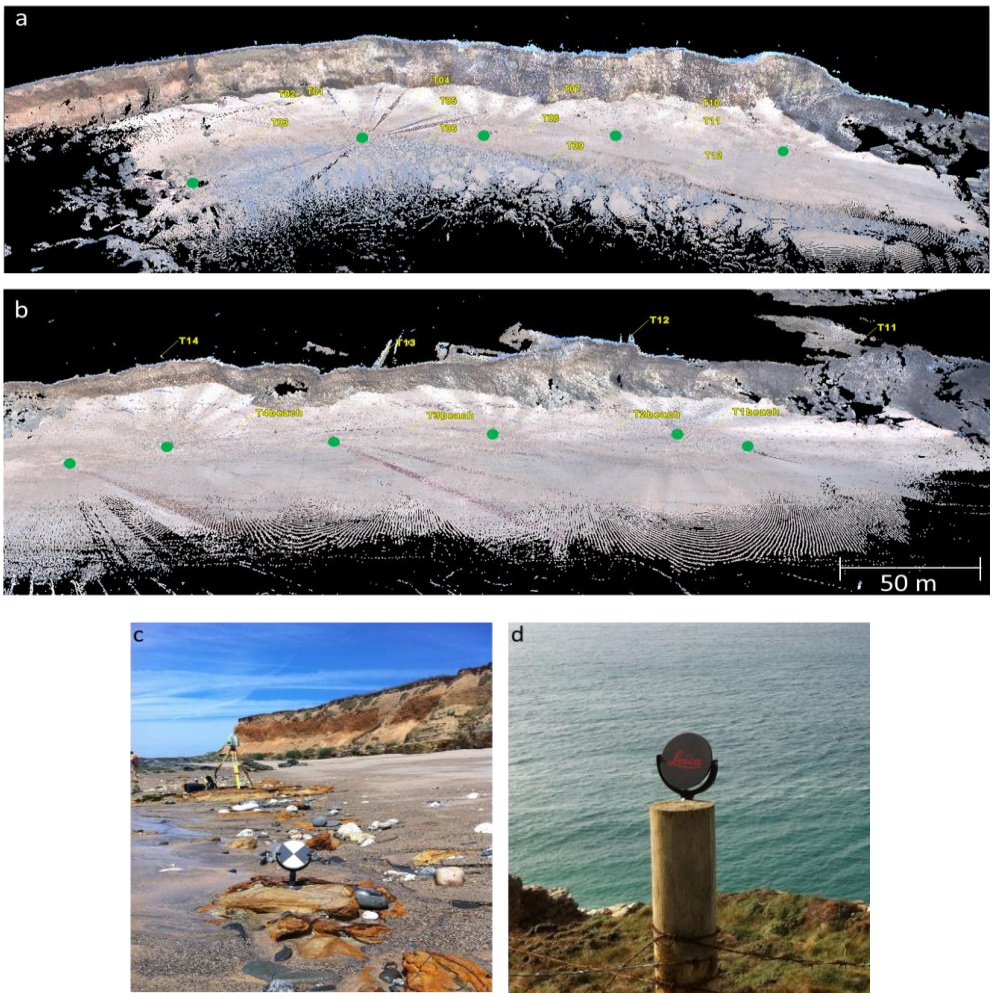

Figure 3.6: Point clouds of a) Porthleven and b) Godrevy with the image from the camera within the scanner draped over the point cloud. The fixed target locations are identified by yellow T values and scanner set-up positions are represented by green dots. HDS targets at c) Godrevy, attached to a magnetic weighted mount and positioned on the beach, and d) in fixed brackets (facing towards the scanner) at Porthleven

3.3.4.3 Point cloud data processing

The geo-referenced registered point clouds were removed of any noise (i.e. birds, people, dogs) manually and exported as .xyz files for further analysis. The first step in performing point cloud difference analysis is typically to create a mesh of the point cloud surface (Rosser *et al.*, 2005; Dewez *et al.*, 2013). A number of approaches were used to attempt this stage, ranging from using various meshing software to using the raw data in programs such as Matlab to manually create meshed surfaces. However, these methods highlighted a number of difficulties and sources of inaccuracy. In complex surfaces such as rocky cliff faces, meshing becomes inaccurate due to the errors involved in interpolating across regions that may show occlusion (Lague *et al.*, 2013). Unless the different surveys are carried out from the exact

same location (highly unlikely in such an environment) there is often overestimation of volume change due to the surface roughness, creating differences in occlusion patterns as a result of varying scanner position during different survey periods. Most point cloud meshing software does not allow for such sources of uncertainty and are therefore not entirely appropriate for complex topographies.

3.3.4.4 Point cloud data comparison: The M3C2 algorithm

Multiscale Model to Model Cloud Comparison (M3C2) is an algorithm developed to overcome issues associated with comparing complex surfaces and computing accurate point cloud to point cloud distances (Lague *et al*., 2013). It uses surface normal estimations along the 3D surface, with orientations varying according to the surface roughness, and computes the distances between two point clouds along these normal directions. Typically, meshing/gridding techniques are unable to account for vertical or overhanging parts and tend to reduce the resolution of fine-scale details due to grid size. Eliminating the need for surface meshing, the software reduces computation time and retains the high-resolution detail of the cliff-face. TLS point clouds of complex surfaces often contain occluded patterns due to the viewpoint of the scanner and variations in ground surface topography (Girardeau-Montaut *et al.*, 2005). Directly comparing point-to-point cloud, as opposed to meshing across blinded regions makes volume calculations more robust as the algorithm is only able to compare two surfaces where data are present. Each point cloud distance is provided along with a confidence interval, which is related to the surface roughness and the point cloud registration error (Lague *et al*., 2013).

The algorithm requires two user-defined parameters in order to compute distances between the point clouds: the *normal scale* (D) and the *projection scale* (d) (Figure 3.7). The basic principles of the algorithm are discussed in this section, and a more detailed description of the algorithm and a discussion on the validity of the method compared with meshing techniques is provided by Brodhu and Lague (2012) and Lague *et al.* (2013).

Prior to running the algorithm, the first point cloud is subsampled to 10 cm and used as a ‘core point’ file. This simplifies the point cloud and rapidly enables the algorithm to calculate the relevant normal scale and determine point cloud distances based on a coarser resolution file. The two point clouds are compared based on this information and no subsequent detail is

lost. Further details of the M3C2 algorithm and the definitions and sensitivity analysis of the normal and projection scales are provided in the Appendix 1.

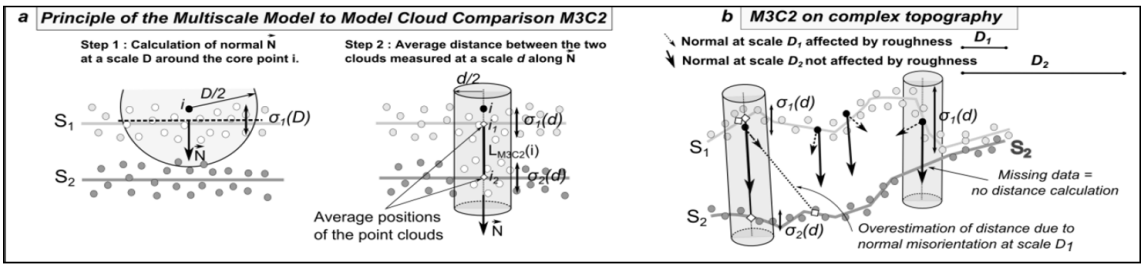

Figure 3.7: Principles of the M3C2 algorithm, taken from Lague *et al.* (2013)

3.3.4.5 Point cloud data comparison: volume change analysis

Volumes of change are calculated by multiplying the distances computed by the M3C2 algorithm by the area of the cylinder surface and then by the number of cylinders. The projection scale (Fig. 3.7a) was tested between 0.05–0.5 m and optimum scale was defined as 0.3 m to provide the most robust difference calculation (details of the sensitivity analysis is provided in Appendix 1). As the core point cloud upon which the projection is based is spaced at 0.1 m, this means that there is a significant overlap in the projection 'cylinders' (Fig 3.7). Using smaller projection cylinders, however, reduces the number of points per cylinder (and hence the statistical significance of the calculation) and also results in gaps across the surface (Fig 3.8a). To account for this tessellation issue, the projection cylinder volume was based on *squared* cylinders, where, instead of multiplying the distance of the change by πr^2 it was multiplied by $(2r)^2$. The optimum projection scale of 0.3 m results in a 'cylinder' whose cross-sectional area is 9 times greater than the resolution of the core subsampled point cloud it is calculated on (0.1 m). Therefore, the sum of the differences is largely overestimated and as a result is divided by 9 ($30^2/10^2 = 9$) (Girardeau-Montaut, 2014).

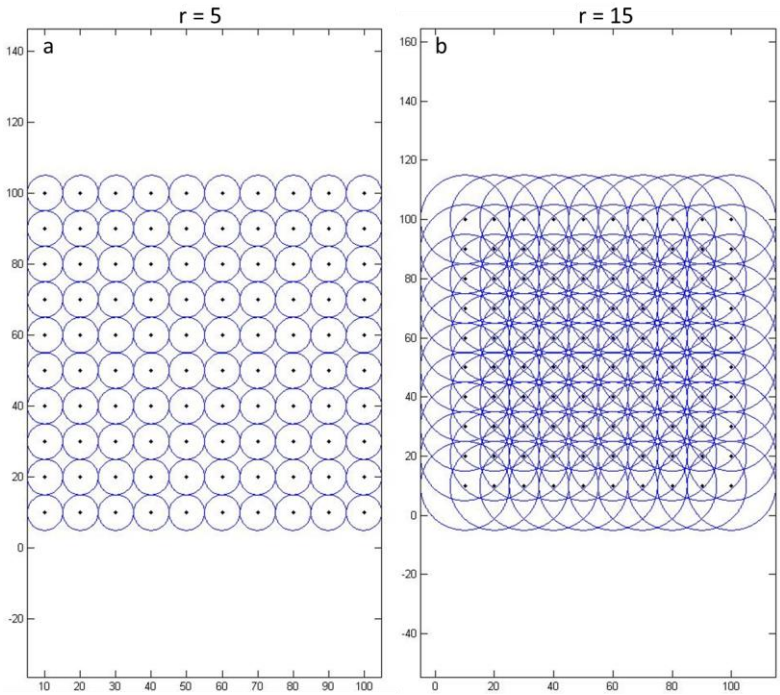

Figure 3.8: Projection cylinder areas illustrating the challenges associated with calculating the volume difference using (a) 5 cm and (b) 30 cm diameter cylinders. Squares were used instead of circles in the volume calculations to minimise loss of cliff coverage.

3.3.5 Meteorological conditions

Meteorological controls on cliff erosion are typically a function of ground temperatures where repetitive freezing/warming of the ground leads to instability of the soil (Durperret *et al.*, 2005) and an increase in pore water pressures from precipitation (Sunamura, 1992). In the southwest UK, temperatures very rarely fall below freezing at the coastline (< 5 days a year) (Met Office, 2014), therefore, the variability of air/ ground temperature is not considered here. Cornwall is however, one of the wettest regions in the country with rainfall totals of 1000 – 1500 mm yr^{-1} (Met Office, 2012). Monthly rainfall totals were obtained from nearby weather stations; Camborne (7 km from Godrevy) and Culdrose (3 km from Porthleven) as a proxy for ground saturation (and hence instability) due to rainfall. The monthly totals represent values for the same time periods as the scan and survey periods.

3.3.6 Time series

The nature of monitoring processes in a dynamic environment presents difficulties with selecting temporal and spatial scales at which to capture change. Wave buoys and tide gauges provide a continuous time series of data for one year at hourly or half-hourly intervals. This affords a detailed quantification of the behaviour of the waves and water levels at the nearshore over an extended period of time. Cliff falls and changes to beach morphology tend to occur either sporadically via topples, rockfalls or landslides or over a prolonged period via spalling (Sunamura, 1992), dependant on the forcing conditions. To capture the activity at both sites, monthly surveys were carried out over a one-year period. This provided a time series consisting of 12 cliff erosion volumes and 12 beach profiles. In order to draw relationships between forcing (waves, water levels and rainfall) and failure (cliff erosion volumes), monthly total wave energy values (for periods where water levels exceeded the beach-cliff junction) and monthly rainfall totals were compared with the volume of material lost from the cliff face.

3.4 Results

3.4.1 Wave climate

The wave climate at both sites was highly variable over the year, with inshore significant wave heights ranging from 0.5 to > 6 m and wave periods between 5 and 22 s along both the north and the south coast. Spring/summer wave conditions between Jul and Oct 2013 and May and Jul 2014 were much calmer than the rest of the year with significant wave heights less than 3–4 m and wave periods less than 12 s, whereas between Nov 2013 and Apr 2014 wave heights ranged from 4 to 9 m and periods from 15 to 25 s. The winter of 2014 was one of the most energetic periods the region has experienced in over 60 years (see Chapter 4 for further details) with inshore significant wave heights exceeding 5 m and wave periods between 12 and 22 s. at both sites on more than five occasions (Fig 3.9 and 3.10) between Dec 2013 and Mar 2014. The durations of the storms were relatively short, lasting from 4 to 8 hrs; however, the persistent nature and frequency of the storms provided the coast limited opportunity for recovery between events.

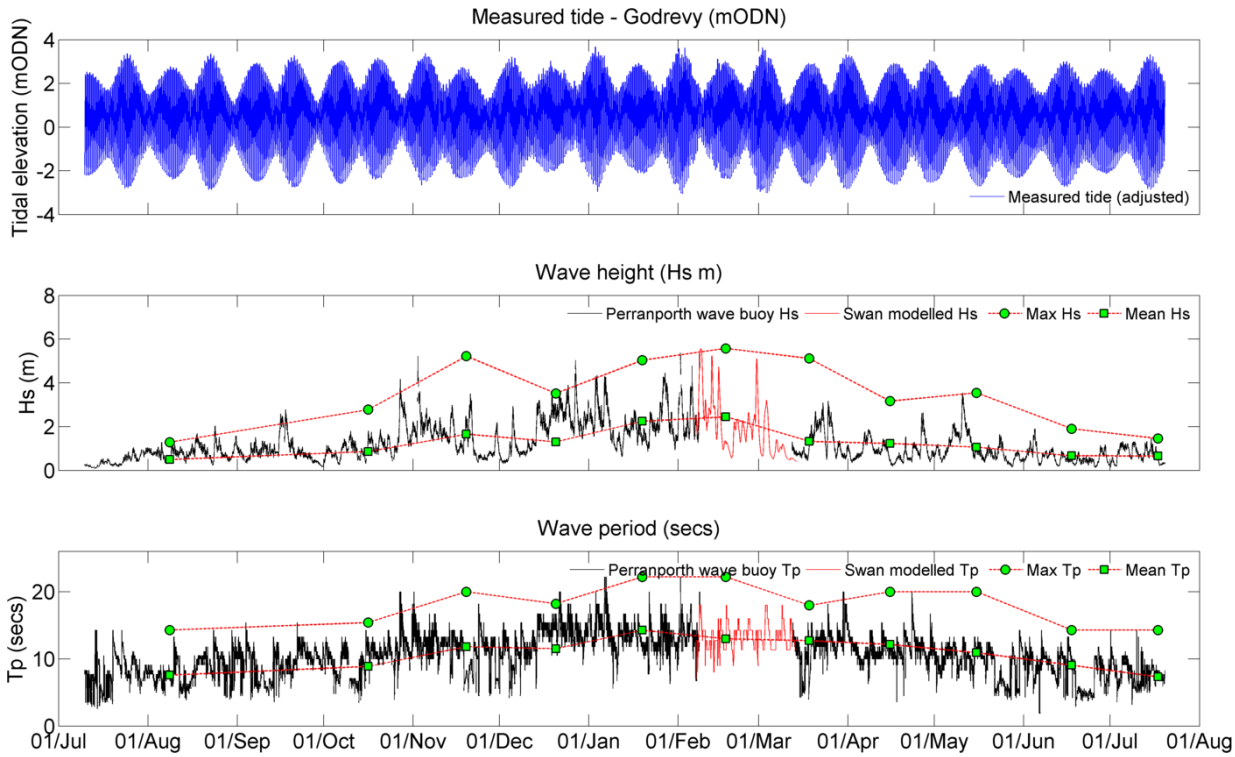

Figure 3.9: Wave and water level data for Godrevy. Measured tide data obtained from Ilfracombe and adjusted according to the ratio between the mean values over a 4hr high tide period at the Godrevy pressure sensor and the Ilfracombe tide gauge. Significant wave height (H_s) and peak spectral wave period (T_p) for the survey period from directional Waverider wave buoy deployed in 10 m water depth 1 km offshore of Perranporth. Red data indicates SWAN modelled data for the missing data period. The full wave data time series was adjusted according to the ratio between the SWAN modelled Perranporth and Gwithian (2 km from Godrevy) data. Significant wave heights at Perranporth for waves from W-NW (98% of the dominant swell direction) were 26% percent greater than those at Gwithian, and were therefore reduced to represent conditions offshore of Godrevy. Monthly mean and maximum values are illustrated in the legend.

The mean significant wave height (H_s) at Godrevy over the year was 1.3 m with a standard deviation of 0.6 m. Wave periods (T_p) averaged 11 s with a standard deviation of 2 s. At Porthleven, average conditions over the year were similar with a mean H_s of 1.1 m and a standard deviation of 0.5 m and a mean T_p of 9 s with a standard deviation of 3 s. Monthly mean significant wave heights reached their maximum in Feb 2014 at both sites with H_s of 5.8 m and T_p of 22 s at Godrevy and a maximum H_s of 10.3 m and T_p of 22 s at Porthleven. Although the average significant wave heights and wave periods indicate that whilst Porthleven was overall slightly calmer over the year than Godrevy, there were much more energetic extreme conditions at Porthleven. Maximum monthly significant wave heights exceeded 8 m and wave periods were greater than 20 s on three occasions (Jan 2014, Feb 2014 and Mar 2014) (Fig 3.10). In comparison with Porthleven, maximum wave statistics at Godrevy indicated calmer extreme conditions, with significant wave heights exceeding 5 m and wave periods exceeding 18 s during the same three winter months (Fig. 3.9).

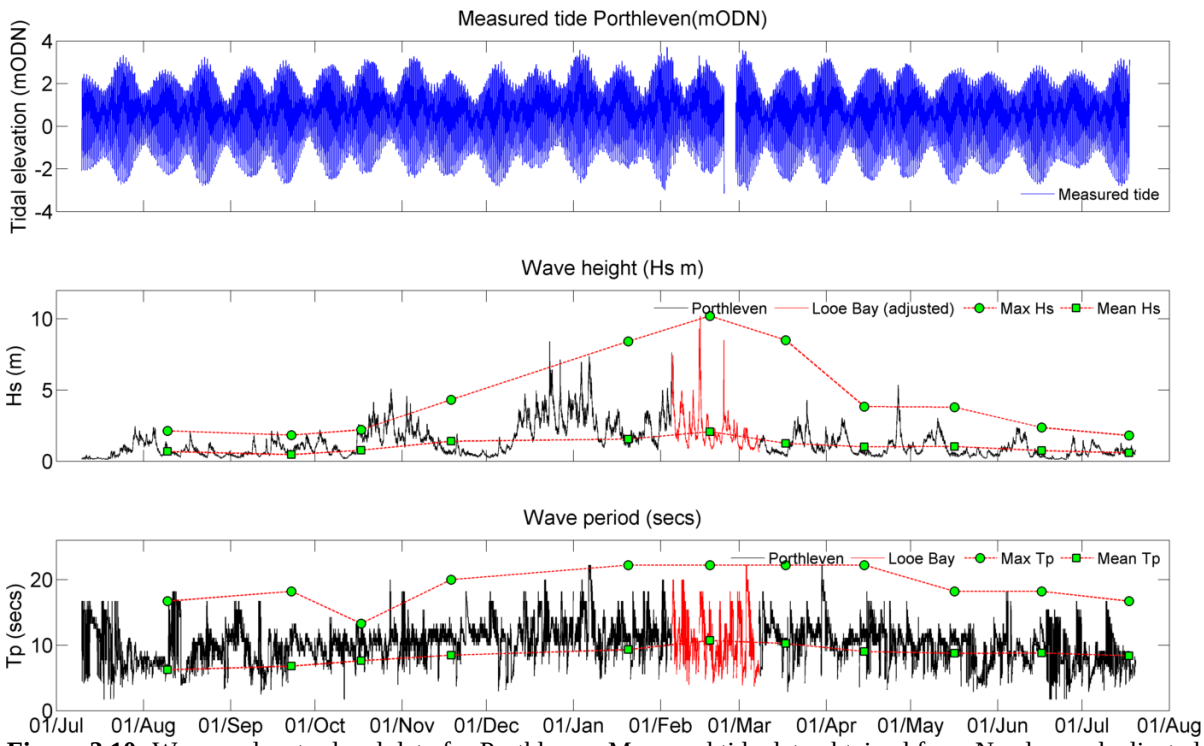

Figure 3.10: Wave and water level data for Porthleven. Measured tide data obtained from Newlyn and adjusted according to the ratio between mean values over a 4hr high tide period at the Porthleven pressure sensor and the Newlyn tide gauge. Significant wave height (H_s) and peak spectral wave period (T_p) for the survey period from directional Waverider wave buoy deployed in 10 m water depth 1 km offshore of Porthleven. Red data indicates Looe Bay wave buoy data for the missing data period. The Looe buoy wave data were adjusted according to the ratio between the Porthleven data. Significant wave heights at Porthleven for waves from S-SW (87% of the dominant swell direction) were 5% percent greater than those at Looe Bay, and were therefore reduced to represent conditions offshore of Porthleven. Monthly mean and maximum values are illustrated in the legend.

3.4.2 Water levels

Adjusted water levels were derived from offsetting the measured levels at the nearest tide gauge by the ratio between it and water levels (2 hrs either side of high tide) at the nearshore pressure sensor. The values were adjusted accordingly (Newlyn to Porthleven; + 10% and Ilfracombe to Godrevy; - 35%) and represent nearshore water levels at each site, minus the influence of breaking waves and bores. Both sites are macro-tidal with the greatest measured tides occurring during the winter months (Dec 2013 – Mar 2014).

3.4.3 Monthly rainfall totals

The wettest periods at both sites correspond with the most energetic periods in terms of wave climate. Greatest monthly total rainfall values were recorded between Oct–Nov 2013 (> 170 mm) and Dec 2013–Feb 2014 (> 200 mm at Godrevy and > 170 mm at Porthleven)

(Fig 3.11). The annual variability of rainfall is fairly similar between the north and south coast however the north coast is on average wetter than the south. Over the year Godrevy experienced total of 1324 mm with mean monthly rainfall total of 110 mm and standard deviation of 67 mm. Porthleven was somewhat drier with a total annual rainfall of 1055 mm, mean of 88 mm and standard deviation of 54 mm. On average, the north coast was 22 mm a month wetter than the south coast. The driest period for both sites was Aug–Sep 2013 (65 mm at Godrevy and 25 mm at Porthleven) and the wettest period for Godrevy was Dec 2013–Jan 2014 (250 mm) and Oct–Nov 2014 at Porthleven (180 mm).

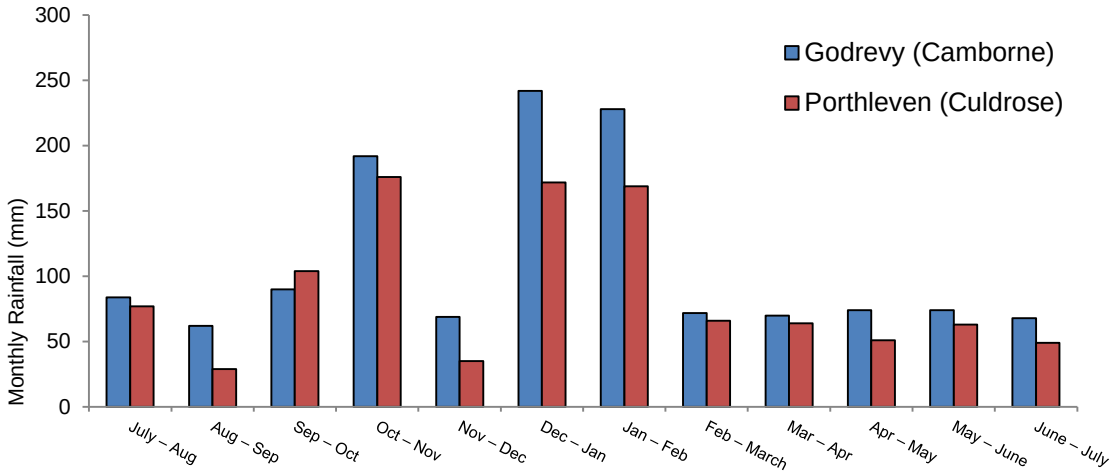

Figure 3.11: Monthly rainfall totals for Godrevy (Camborne) and Porthleven (Culdrose) from Jul 2013 – Jul 2014. Monthly periods correspond to monthly survey periods.

3.4.4 Beach morphology

At Godrevy, the beach elevation varied by up to 2 m at the toe of the cliff and in the lower intertidal zone (Fig 3.12a–c). Alongshore, the elevation of the beach tended to remain fairly constant where an increase or decrease in elevation occurred across the whole beach face, with no beach rotation apparent within the bay; however, changes tended to be slightly emphasised at the northern end of the beach. The slope of the beach at Godrevy remained around 0.02 (standard deviation 0.005) throughout the year; yet, the elevation of the beach-cliff junction varied by up to 2.5 m at the toe (Fig 3.12d).

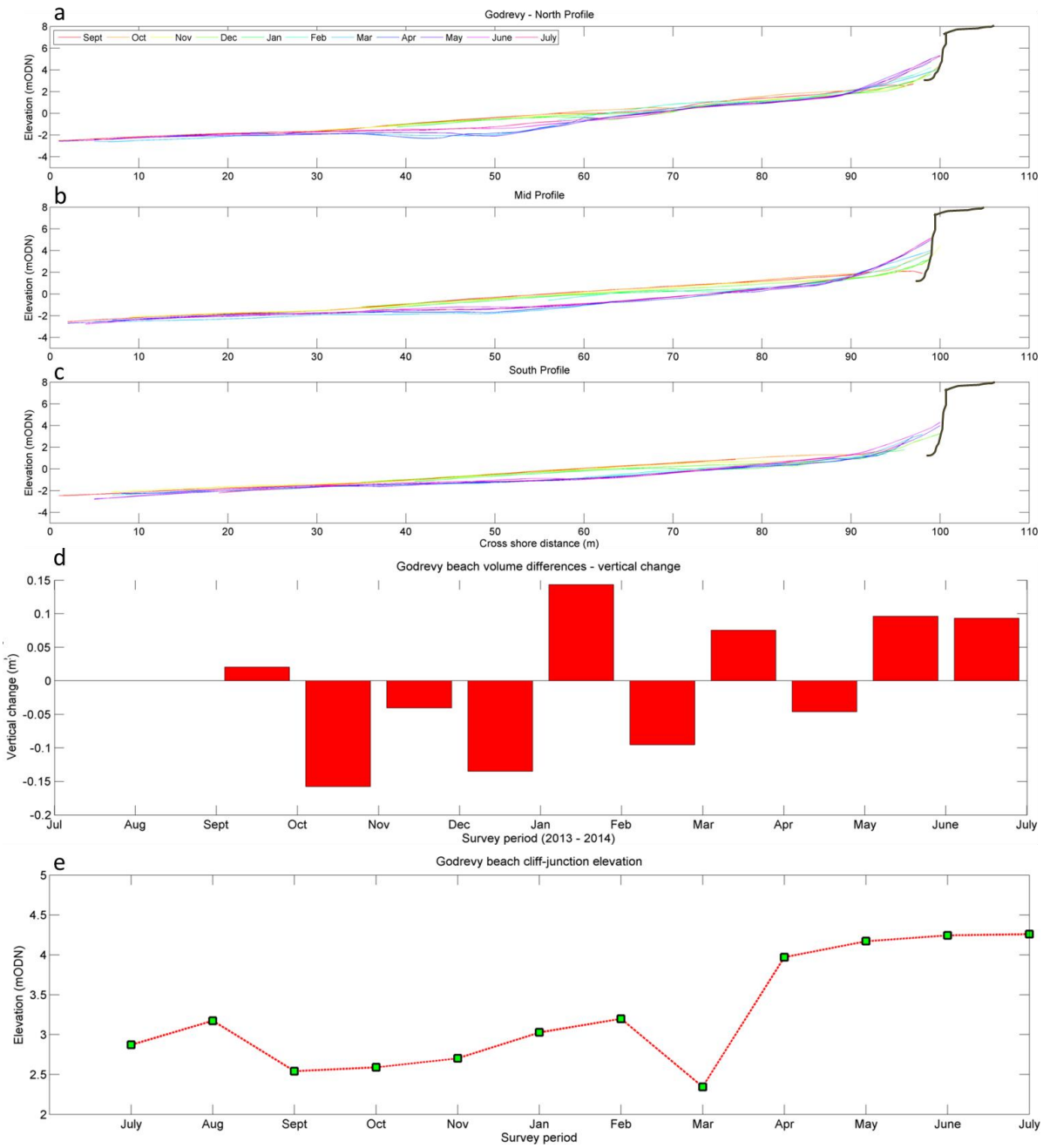

Figure 3.12: Cross-shore profiles for Godrevy from either end of the bay (a) and (c) and the centre of the beach (b). d) Beach volume differences from one survey period to the next obtained from beach profiles between Sept 2013 and July 2014. Beach-cliff junction (e) obtained from an average of the junction across the whole cliff frontage from combining the beach survey data with the cliff face point cloud.

Towards the beginning of the survey period, the beach elevation at the cliff-toe fluctuated between 2.5 and 3.5 m until after the winter, when the junction was as its lowest following extreme storm conditions (Mar 2014; 2.2 m). The beach-cliff junction elevation rapidly increased to 4 m ODN in Apr 2014 and remained at this elevation for the rest of the survey period.

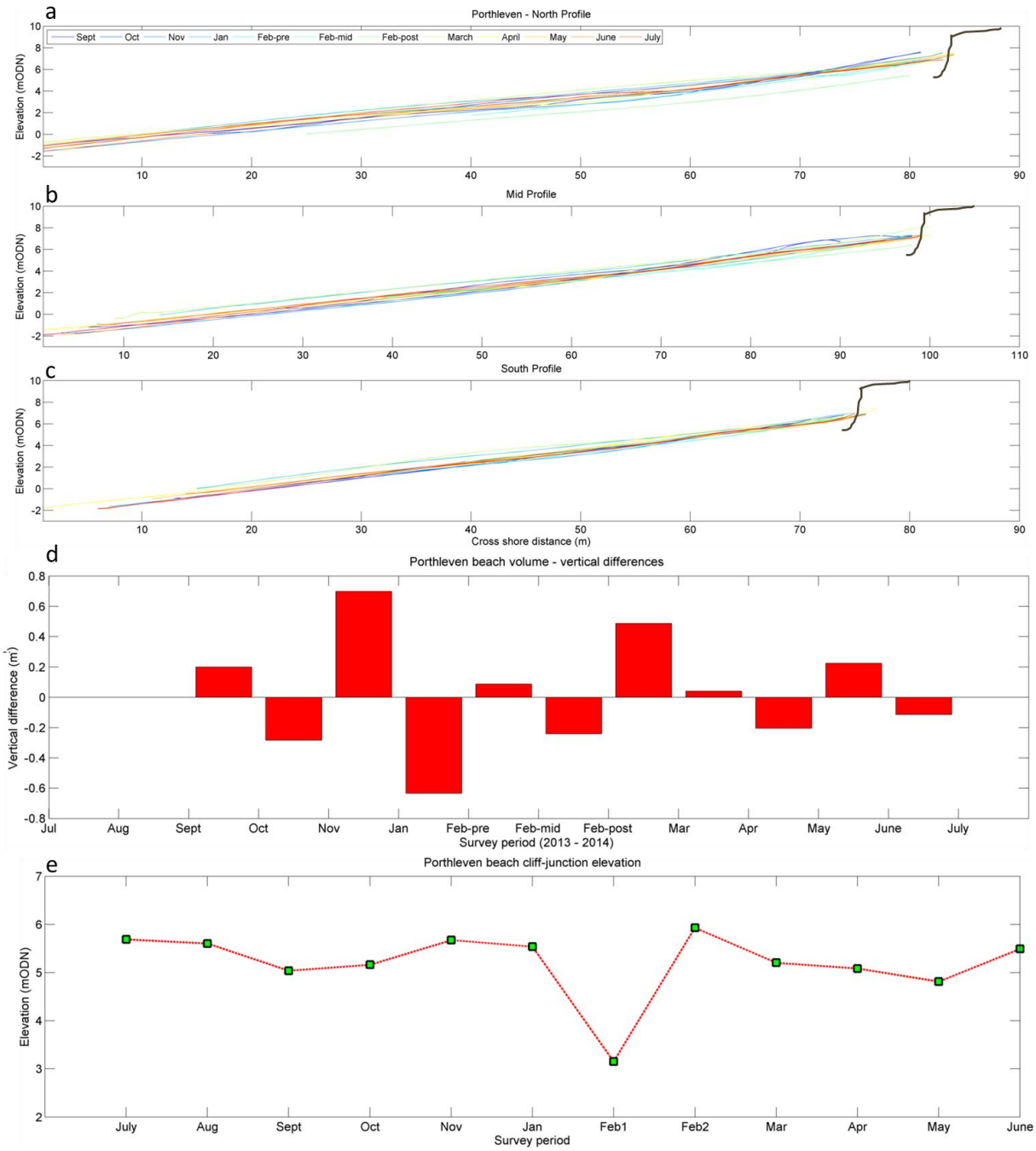

Figure 3.13: Cross-shore profiles for Porthleven from either end of the bay (a) and (c) and the centre of the beach (b). d) Beach volume differences from one survey period to the next obtained from beach profiles between Sept 2013 and July 2014 (Feb-pre relates to a survey on the 1st Feb (am), pre-storm, Feb-mid; the 1st Feb (pm), Feb-post; 2nd Feb (pm)). Beach-cliff junction (e) obtained from an average of the junction across the whole cliff frontage from combining the beach survey data with the cliff face point cloud (Feb1 relates to TLS survey on the 2nd Feb, Feb2; TLS survey on the 18th feb).

The beach at Godrevy is subject to substantial volume changes from one survey to the next. The beach experienced maximum erosion between Oct and Nov 2013 with a loss of 6848 m^3 over the survey area. Normalised to the beach area this equates to erosion of 0.16 m. Further erosion occurred over the winter with an additional 5724 m^3 between Nov 2013 and Jan 2014

(0.04 m (Nov–Dec 2013) and 0.14 m (Dec 2013–Jan 2014)). Following the stormy period of Jan–Feb 2014 the beach recovered by 3000 m^3, however the volume of sand removed during the stormy period in Feb 2014 is unknown due to the timing of the surveys. For the remainder of the year Feb–July 2014 the beach experienced both erosion and accretion from month-to-month with the overall beach elevation fluctuating around +/- 0.15 m per month. The beach elevation at Porthleven fluctuated by up to 2–3 m across the whole beach face, cross-shore and alongshore, with more emphasised changes towards the northern end of the bay (Fig 3.13a–c). In terms of volume, this equates to a fluctuation of up to +/- 0.8 m (+/- 10,000 m^3) from month to month. Between Oct and Nov 2013 the beach eroded by 4290 m^3 (0.29 m) yet recovered by 12,580 m^3 (0.7 m) the following period, between Nov 2013 and Jan 2014. The beach-cliff junction fluctuated between 4.5 and 6 m throughout the year, apart from in February when elevations were at their lowest (2.8 m). The stormy conditions in February led to considerable changes in the beach-cliff junction elevation and beach volume of +/- 0.5 – 0.6 m (+/- 10,000 m^3) over a 12 hr period, suggesting the temporal resolution of surveying for this beach was too low to capture the significant beach changes at Porthleven. Although these monthly surveys provide an indication of the fluctuation in beach elevation at each site, they do not adequately capture the changes which occur on a daily/hourly time scale.

3.4.5 Cliff volume changes

Overall, from Jul 2013–Jul 2014 the cliffs at Porthleven experienced more than twice as much erosion as Godrevy, with a total volumetric cliff loss of 3326 m^3 compared with 1579 m^3 (Table 3.2). Normalised according to the length of the cliff face (~ 300 m at each site), this equates to a total annual volume loss of 11 m^3 per m length of cliff at Porthleven and 5.26 m^3 per m length of cliff at Godrevy. Assuming a cliff height of 10 m and averaging this erosion over the year, this equates to an equivalent cliff retreat rate of 1.1 m yr^{-1} at Porthleven and 0.5 m yr^{-1} at Godrevy. Erosion at Porthleven although higher, was more variable than Godrevy with a standard deviation of 650 m^3 compared with 213 m^3 (Table 3.2). During the summer months, Godrevy was more susceptible to erosion than Porthleven with monthly total volumes ranging between 8 and 29 m^3 compared with volumes between 1 and 17 m^3 at Porthleven. At both sites, the erosion volumes were greatest in the winter of 2013–2014, with the largest losses measured between Dec 2013 and the end of Feb 2014. Comparing the means of erosion at two sites proves the data to be highly variable from month to month

(variance) and therefore a difference between the means that is not significant. A t-test produces a t-value between the means of 0.78, which at the 95% probability level (p = 0.05) with 20 degrees of freedom ((n1+n2)-2) is lower than the value of t required to prove the difference as significant (2.09).

Table 3.2: Net cliff erosion volumes for Godrevy and Porthleven from July 2013 – July 2014

Survey Period 2013 – 2014	Godrevy erosion (m^3)	Porthleven erosion (m^3)
Jul – Aug	27	4
Aug – Sep	51	1
Sep – Oct		3
Oct – Nov	88	35
Nov – Dec	54	1184
Dec – Jan	499	
Jan – Feb	629	1958
Feb – Mar	148	140
Mar – Apr	28	10
Apr – May	20	18
May – Jun	8	6
Jun – Jul	30	4
Total	**1582**	**3363**
Mean	144	306
Standard deviation	213	650
Equivalent annual cliff retreat rate	0.5 m yr^{-1}	1.1 m yr^{-1}

The point cloud comparison plots not only provide quantitative volume differences, but are also a qualitative means of determining the locations of failure across the face of the cliff. Figures 3.14 and 3.16 compare the cliff surfaces between Jul 2013 and Jul 2014 and Figures 3.15 and 3.17 compare the cliff surfaces from month-to-month. Over the one-year survey period (Jul 2013–Jul 2014) at Godrevy, the majority of failure occurred at three locations, the northern extent of the cliffs, the middle of the bay and at one particularly steep region of cliff at the southern end. Smaller scale failures of both the bedrock and the head deposit can also be seen across the cliff face. Towards the northern end of the cliffs, where the boundary between the bedrock and quaternary unit falls to beach level, erosion of the entire cliff face has occurred via rotational sliding of superficial material. This has led to steepening of the cliff face and a cliff-normal retreat, mid-way up the cliff elevation by a maximum of 2.3 m (Fig 3.14bi). Failure in the central section of the cliff (Fig 3.14bii) has occurred via 'slope-over-wall' failure where superficial material has been removed above the underlying bedrock by a maximum of 2 m. Towards the southern end of the cliffs, the cliff has retreated in the upper superficial unit by 0.9 m and in the bedrock at the cliff toe by 1.1 m.

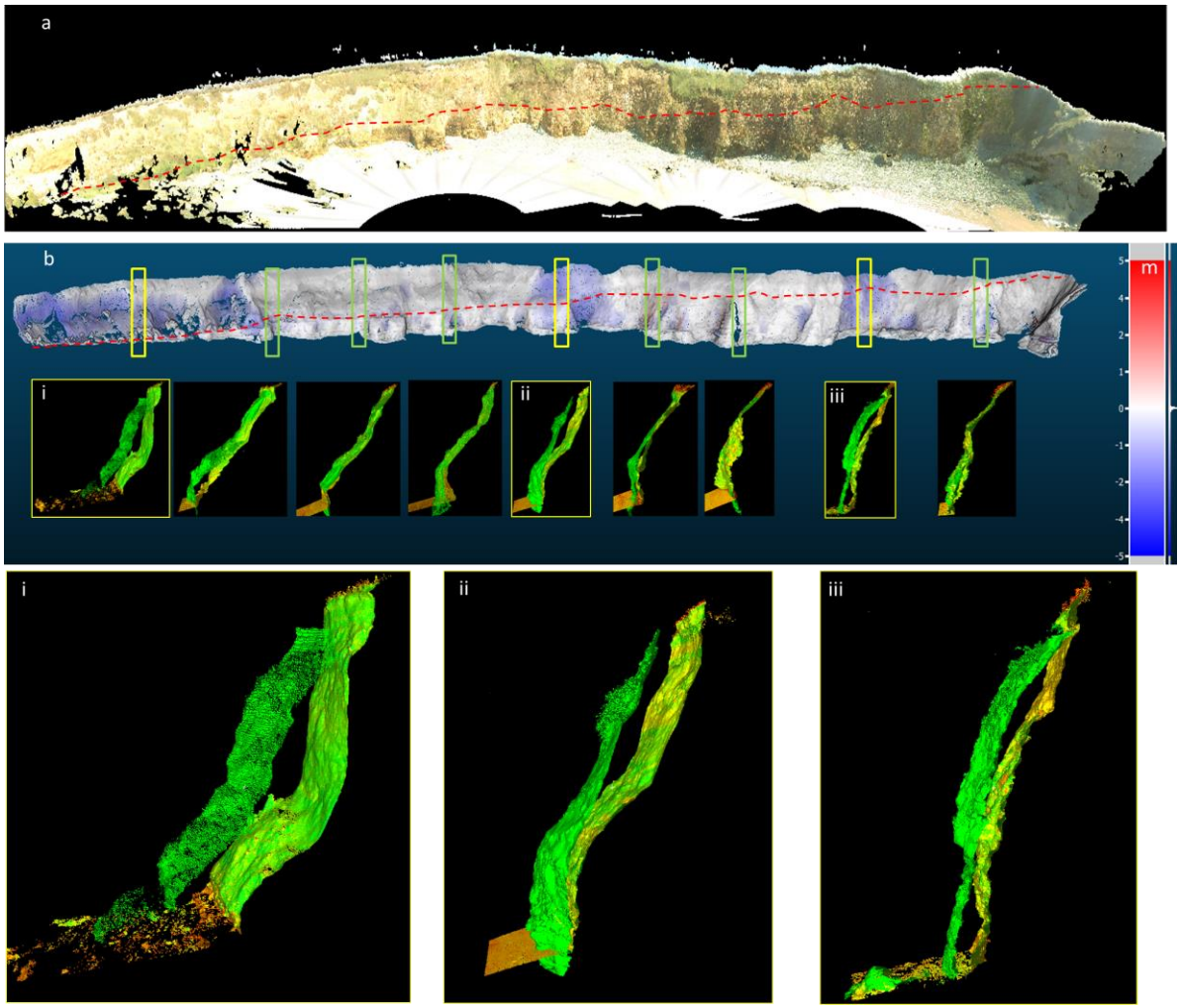

Figure 3.14: a) Point cloud of Godrevy cliff face in July 2013 with colours from the scanner camera draped over the point cloud. Dotted red line indicates the boundary between underlying bedrock of Mylor slates and overlying, less resistant quaternary head deposit. b) Point cloud comparison plot for July 2013 – July 2014, with colour bar scale ranging from blue (- 5m) to red (5 m). i – iii) 3-D sections through the cliff at three locations where the majority of failure has occurred. Initial surface (July 2013) is depicted in brighter green, superimposed over the later scan (July 2014, yellow-green).

The monthly comparison plots indicate that the failure of these three sections took place during the winter months. Between Dec 2013 and Jan 2014 slope-over-wall failure can be seen in the upper unit of the central and southern sections of the cliff (Fig 3.15). The majority of failure at the northern end of the cliffs occurred during Jan–Feb 2014 and then Feb–Mar 2014. Erosion of the bedrock at the central and southern sections of cliff can be seen again between Jan–Feb 2014. The volumes of erosion for all the other months do not appear to be in the form of a sudden failure, and are likely to be from a gradual spalling of material from the cliff face.

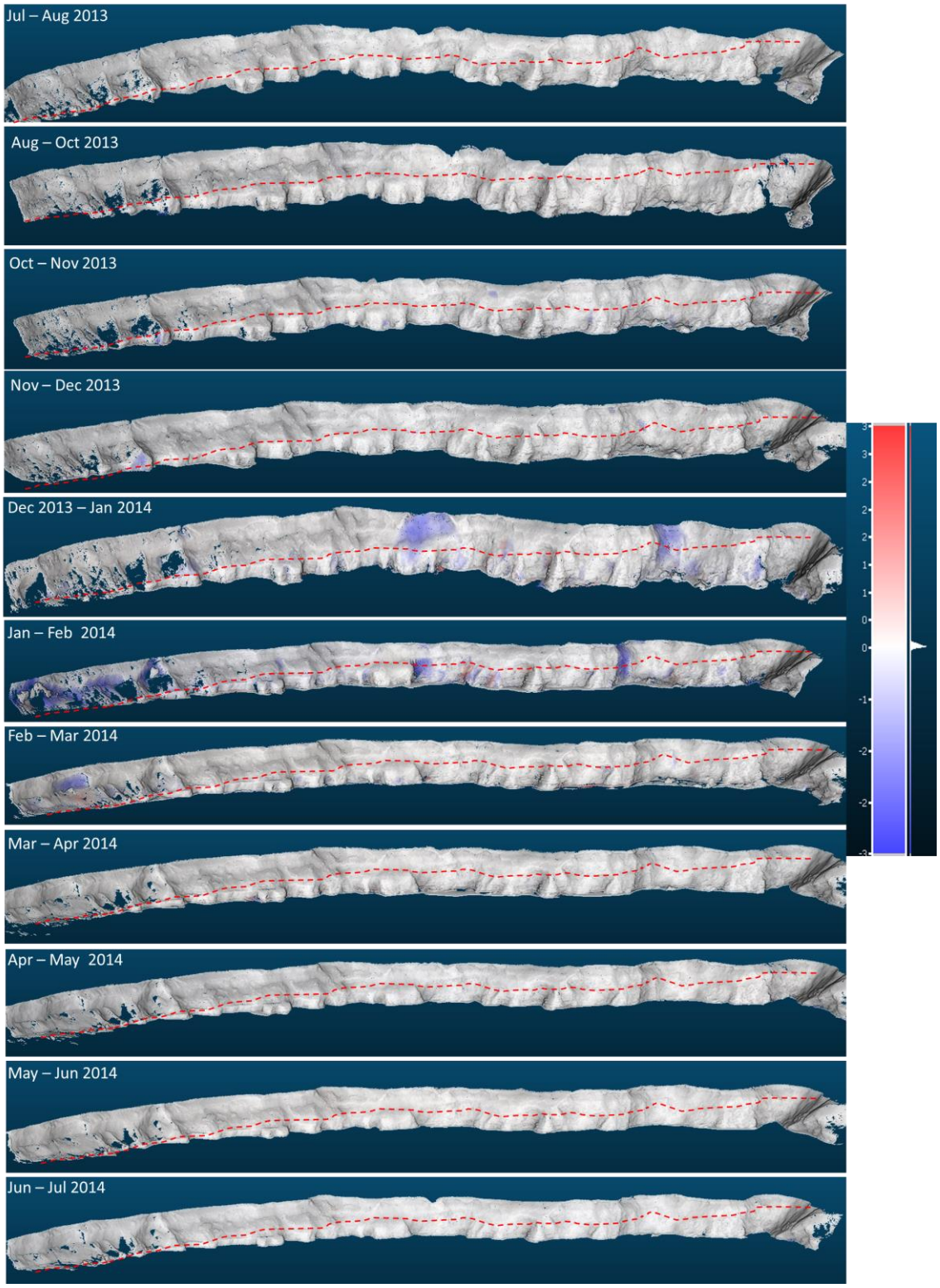

Figure 3.15: Point cloud comparisons for each survey period at Godrevy, erosion/accretion is scaled from blue/red (-3 to 3 m). Boundary between geological units denoted by dotted red line.

At Porthleven, the retreat of the overall cliff face was a lot more dramatic and the annual difference plot indicates failure occurred in almost all regions of the cliff, both in the alongshore and the vertical profile, with erosion visible in the upper superficial and lower

bedrock units (Fig 3.16). Three sections selected in Figure 3.16 indicate a horizontal retreat of the cliff face by 2 m towards the northern extent of the cliffs (Fig 3.16bi), 2.3 m in the central section of cliffs and up to 4.8 m horizontally towards the south. The failure mechanisms via which these failures have occurred are difficult to determine from the annual difference plots as there is no remaining material (i.e., talus deposit) present to indicate rotational sliding or slope-over-wall failure. The entire cliff elevation has retreated almost homogeneously alongshore.

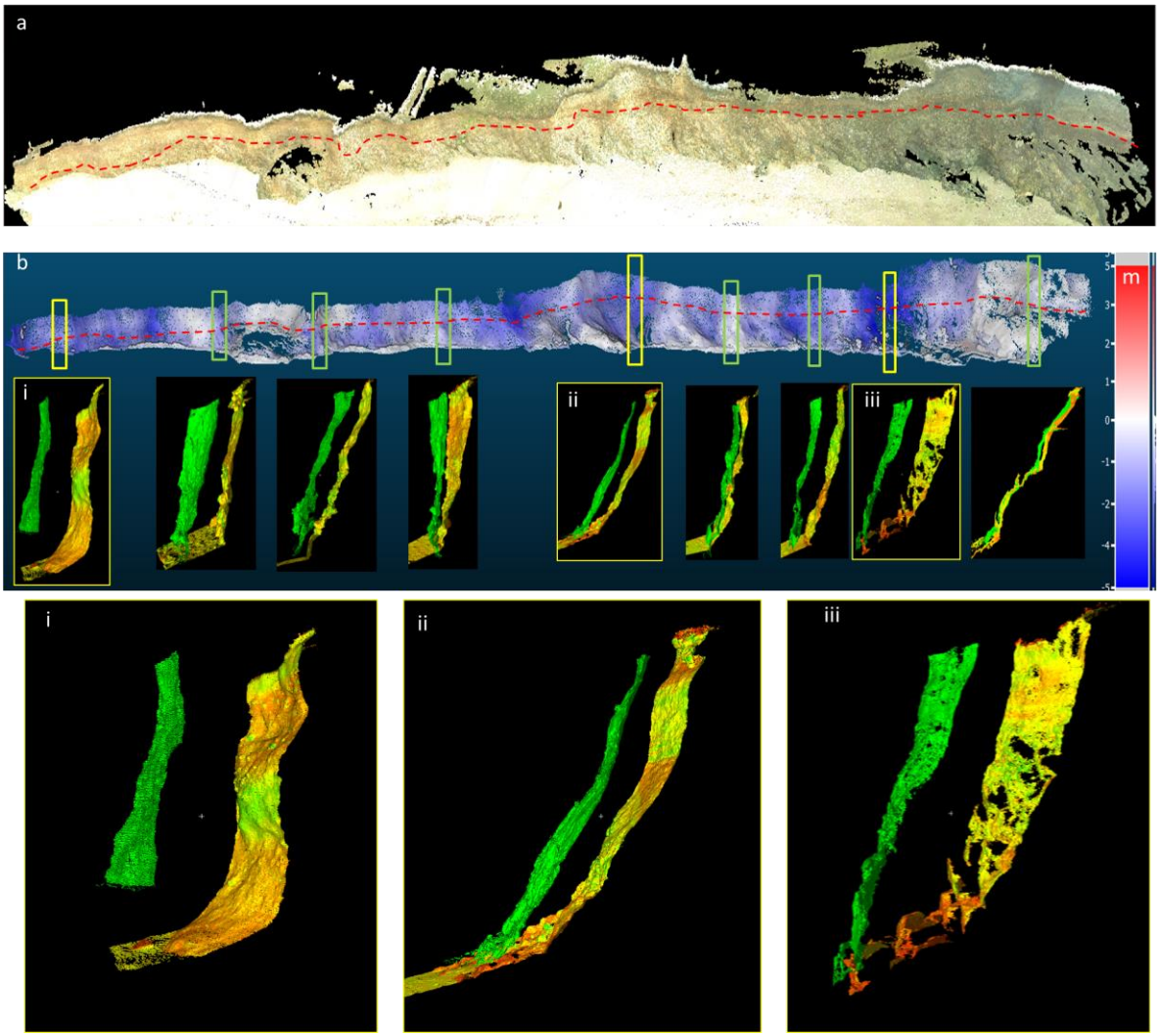

Figure 3.16: a) Point cloud of Porthleven cliff face in July 2013 with colours from the scanner camera draped over the point cloud. Dotted red line indicates the boundary between underlying bedrock of Mylor slates and overlying, less resistant quaternary head deposit. b) Point cloud comparison plot for July 2013 – July 2014, with colour bar scale ranging from blue (- 5m) to red (5 m). i – iii) 3-D sections through the cliff at three locations where the majority of failure has occurred. Initial surface (July 2013) is depicted in brighter green, superimposed over the later scan (July 2014, yellow-green).

Much like Godrevy, the majority of failure at Porthleven occurred during the winter months between Nov 2013 and Mar 2014. The period Nov 2013–Jan 2014 shows a large amount of erosion across the entire cliff face over a period of two months.

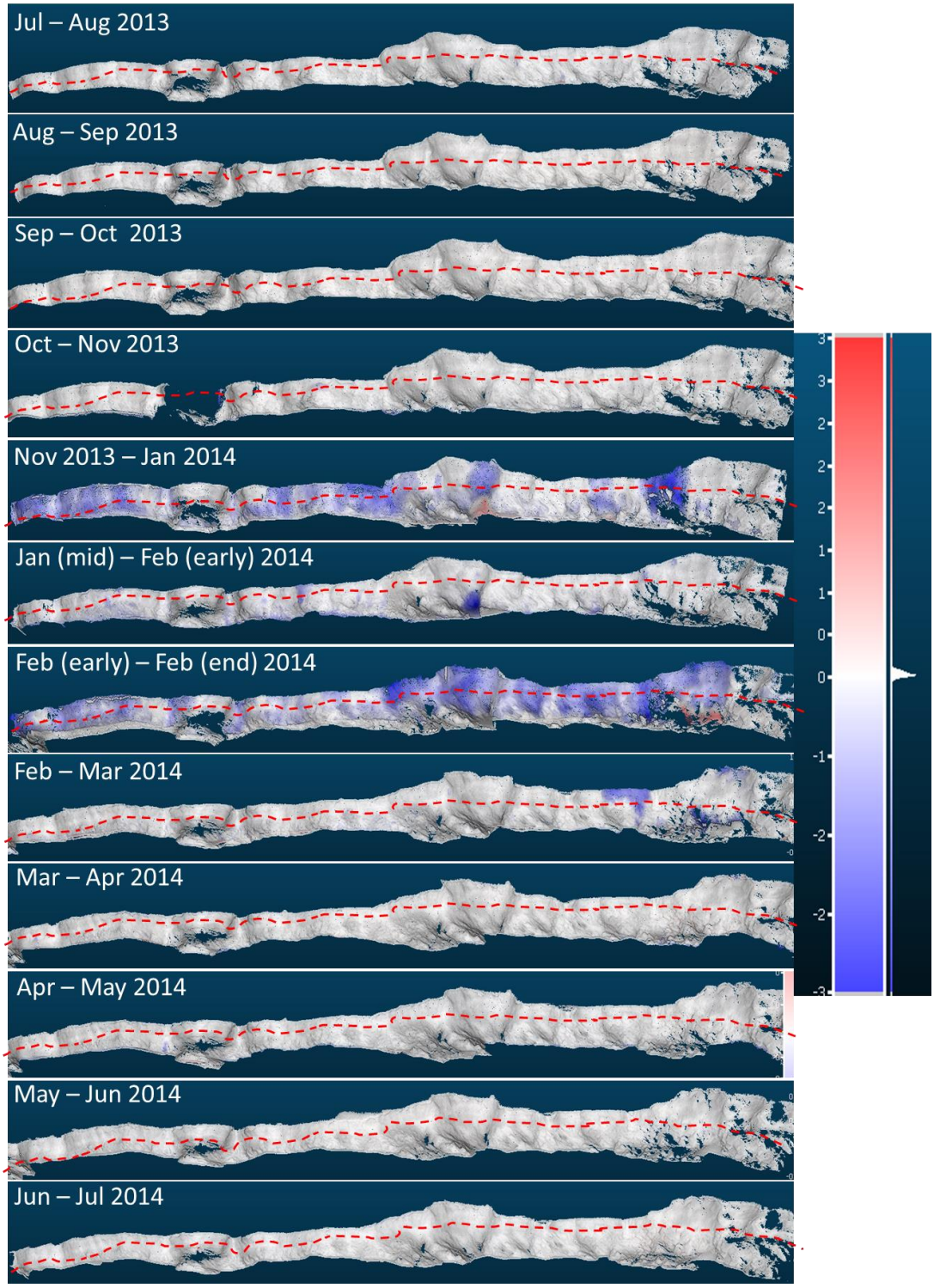

Figure 3.17: Point clouds comparisons for each survey period at Porthleven, accretion/erosion is scaled from red/blue (-3 to 3 m). Boundary between geological units denoted by dotted red line.

Further erosion can be seen in the two week period Jan (mid)–Feb (early 2014) in both the lower bedrock (towards the centre of the cliffs) and in the upper material at certain locations across the cliff face. In the following two week period (Feb (mid)–Feb (end) 2014) an overall volume of 1770 m^3 was lost over almost the entire cliff elevation across the whole cliff face (Fig 3.17). Further failure of the upper superficial material from overhanging material occurred towards the southern end of the cliffs following this particularly active period (Feb – Mar 2014).

3.5 Discussion

Wave and weather conditions over the study period proved to be spatially and temporally consistent between the two sites yet the difference in erosion volumes, cliff failure patterns and timings tend to suggest a disparity in assailing and/or resisting forces. Seasonally and monthly, wave heights and rainfall totals showed the same trend on the north and south coasts with more energetic and wetter conditions in the winter compared with the summer. Yet cliff erosion volumes over the year at Porthleven were almost double those at Godrevy (1580 m^3 compared with 3362 m^3).

Average seasonal wave conditions tended to be higher at Godrevy in both the winter (Oct 2013–Mar 2014); 1.7 m H_s and 12 s T_p and the summer (Jul–Sep 2013 and Apr–Jul 2014); 0.8 m H_s and 9 s T_p, than at Porthleven (1.4 m and 9 s (winter) and 0.7 m and 7 s (summer)). Monthly rainfall totals also indicated that Godrevy experienced wetter conditions compared to Porthleven in both the winter (totalling 803 mm compared with 618 mm) and the summer (74 mm compared with 62 mm). In contrast, the total cliff erosion volume for the same winter months at Godrevy was half that of Porthleven (1418 m^3 compared with 3317 m^3) yet over the summer, the total erosion volume at Godrevy was three times greater (164 m^3) than at Porthleven (46 m^3) (Fig 3.18). This then raises the question; what is causing the considerable difference in cliff erosion volumes between the two sites when the data suggest the north coast is exposed to on average, greater assailing forces than the south coast? Recent studies have highlighted the importance of the elevation of the beach in relation to the cliff-toe (Lee, 2008; Young *et al.*, 2014; Vann Jones *et al.*, 2015) and the influence of extreme wave conditions on the resultant erosion of sea-cliffs (Young *et al.*, 2013; Brain *et al.*, 2014; Vann Jones *et al.*, 2015). The elevation of the beach-cliff junction proved to be highly variable at

both Godrevy and Porthleven, fluctuating between +/- 2 – 3 m at both sites elevations ranging between 2.5–4.5 m ODN at Godrevy and 3–6 m ODN at Porthleven. Beach volumes however were much more variable from month-to-month at Porthleven (- 0.3 to 0.7 m) compared with Godrevy (-0.16 to 0.1 m) (Fig 3.18).

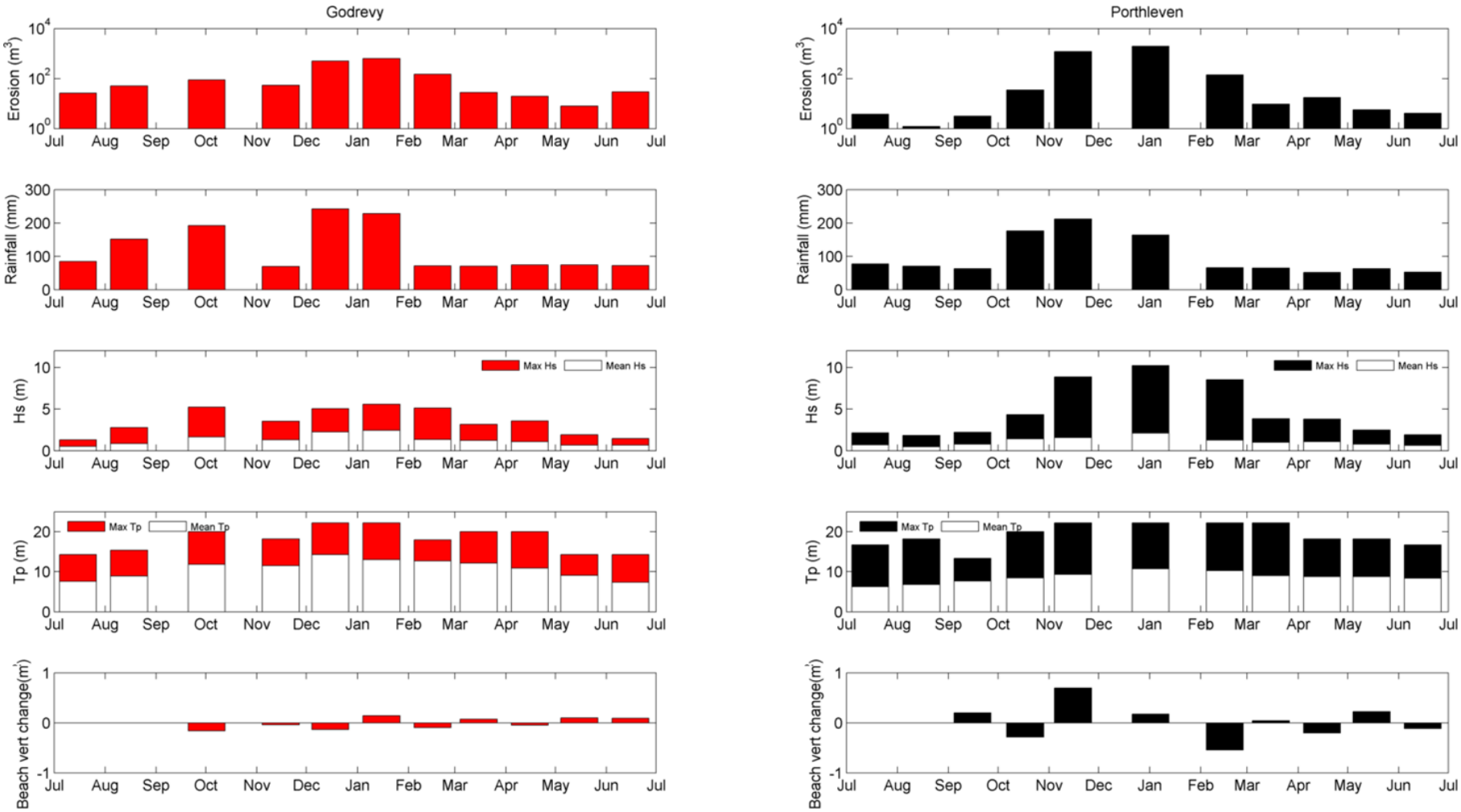

Figure 3.18: Summary of results from the monthly surveys, i.e., total erosion volumes, total rainfall, maximum and mean monthly significant wave heights (H_s) and wave periods and normalised vertical beach volume change (m) for Godrevy and Porthleven.

The maximum significant wave heights and wave periods for each month indicate that although the average monthly values for Godrevy are greater than Porthleven, the extreme values are typically much greater at Porthleven than Godrevy in both the winter (10 m H_s and 28 s T_p compared with 5.6 m H_s and 22s T_p) and the summer (3.8 m H_s and 22 s T_p compared with 3.6 m H_s and 20 s T_p).

Tables 3.3 and 3.4 compare the variables in Fig. 3.18. With n = 12 (months), therefore 10 degrees of freedom, at the 0.05 significance level, the critical value for R is 0.576. Therefore all variables apart from beach volume satisfy these criteria. At both sites, the highest correlation is found between cliff erosion and significant wave height (H_s), with R values of 0.89 for Godrevy and 0.84 for Porthleven. At Godrevy, rainfall tends to bear stronger significance with cliff erosion than at Porthleven with an R value of 0.82 compared with 0.71. This implies that the rainfall totals are almost as significant in determining erosion volumes as the wave climate. At Porthleven, however, a strong correlation exists between erosion volumes and maximum wave heights (0.82), implying that the erosion at Porthleven is strongly related to the nearshore wave climate. Under a similar forcing conditions (waves and rainfall), Porthleven is therefore more sensitive to the wave climate than Godrevy.

Table 3.3: Correlation matrix for all variables at Godrevy.

	Erosion	Rainfall	H_s	Max H_s	T_p	Max T_p	Beach volume
Erosion	**1.00**						
Rainfall	**0.82**	1.00					
H_s	**0.89**	0.80	1.00				
Max H_s	**0.68**	0.65	0.90	1.00			
T_p	**0.65**	0.52	0.88	0.91	1.00		
Max T_p	**0.69**	0.61	0.91	0.86	0.92	1.00	
Beach volume	**0.03**	-0.23	-0.22	-0.45	-0.40	-0.30	1.00

Table 3.4: Correlation matrix for all variables at Porthleven

	Erosion	Rainfall	H_s	Max H_s	T_p	Max T_p	Beach volume
Erosion	**1.00**						
Rainfall	**0.71**	1.00					
H_s	**0.84**	0.76	1.00				
Max H_s	**0.82**	0.65	0.91	1.00			
T_p	**0.61**	0.35	0.79	0.82	1.00		
Max T_p	**0.53**	0.52	0.70	0.78	0.72	1.00	
Beach volume	**0.49**	0.46	0.16	0.14	-0.03	0.00	1.00

3.5.1 Beach morphology and tidal elevations

The variability in beach volume and beach-cliff elevation over the year and from month-to-month suggests that the temporal resolution of the monthly beach surveys was too coarse to capture the rapid nature of beach response to incident wave conditions. The complex nature of these rapid changes implies that wave set-up and swash appear to be more influential than a single value for beach volume. This is further supported by the beach response under highly energetic wave conditions at Porthleven in Feb 2014. Three surveys were carried out over three consecutive low-tides during the storm on the 1st–2nd Feb 2014 (6.5 m H_s and 15 s T_p). The beach volume from the first (low tide on 1st Feb 2014 (am)) to the second survey (low tide on 1st Feb 2014 (pm)) showed 0.7 m of accretion and then 0.6 m of erosion between low tide on the 1st Feb 2014 (pm) and the low tide on the 2nd Feb 2014 (pm). This change to the beach is also noted by a sudden drop from 5.5 to 2.5 m and then an increase in beach-cliff elevation to 6 m ODN over a two week period. During low tide on the 2nd Feb (am) access to the beach was hindered by a substantial drop in beach levels beyond the point of access. This implies that the minimum beach volume, beach-cliff junction and beach slope are underestimated here and under certain storm conditions levels are much lower than recorded, by possibly up to 1–2 m.

The variability in the slope of a beach, will ultimately dictate the vertical extent of the wave runup (Shih *et al.*, 1994; Stockdon *et al.*, 2006; Masselink *et al.*, in press) as the vertical runup is a function of the square of the beach slope (tan β) (Eqn 3.2); therefore the steeper the beach, the greater the runup. A steeper beach is also associated with a higher beach-cliff junction; and this in turn affords the cliffs more protection from wave attack. Due to the highly variable nature of the beach at both sites relative to the low temporal resolution of the surveys, three *scenarios* have been derived, where the beach slopes and beach-cliff elevations are based on a minimum, maximum and mean value to calculate wave runup and determine scenarios when the wave runup exceeds the beach-cliff junction. Maximum beach slope is associated with the maximum beach-cliff junction, minimum slope with the minimum junction and mean slope with the mean beach-cliff junction (Fig 3.19). From this, three different wave energy impact scenarios can be drawn, providing the number of hours per month where the waves exceed a mean maximum and minimum beach-cliff junction.

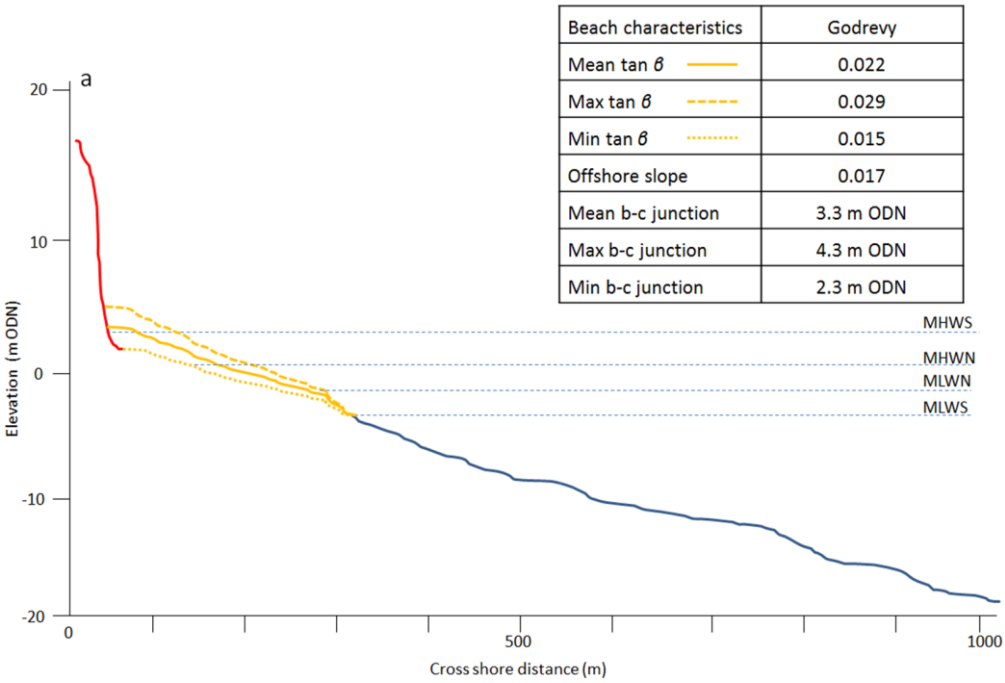

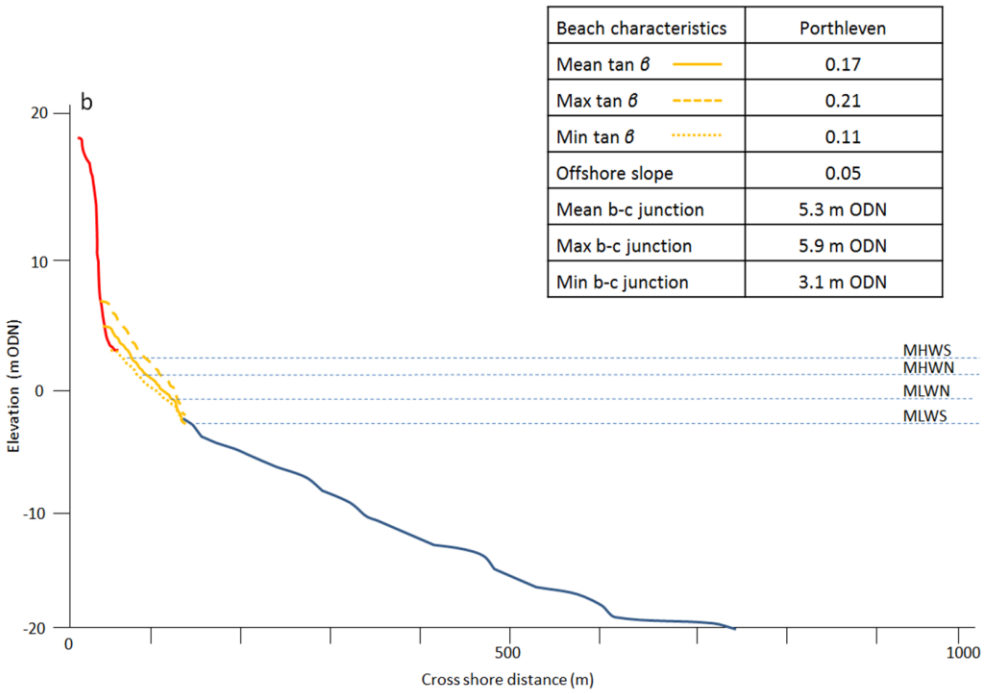

Figure 3.19: Cross shore profile of the cliffs, beach slope, and tidal elevations for a) Godrevy and b) Porthleven with mean maximum slopes and beach-cliff junctions provided in the tables

The elevation of the beach-cliff junctions relative to tidal levels imply that Godrevy is exposed to more frequent inundation than Porthleven (Fig 3.19). Under a mean and minimum beach slope and cliff junction scenario, the cliffs at Godrevy are inundated every spring high-tide; however, tidal levels only reach the base of the cliff at Porthleven under a minimum beach slope and beach cliff junction elevation. A recent study along coastal cliffs in the north

of England has suggested that cliff failure is not a function of cliff-toe inundation duration (Vann Jones *et al.,* 2015) or frequency, however, the energy expended on the cliffs during inundation periods could be responsible for failure progressing upwards on the cliff-face. The results from the volumes of erosion at Porthleven, compared with Godrevy agree with this notion as inundation duration and frequency are higher at Godrevy, i.e., the site with lower erosion volumes, suggesting cliff failure is not a function of cliff-toe inundation duration or frequency. Although a range of wave conditions are captured in Vann Jones *et al.* (2015) significant wave heights were < 6 m and wave periods < 18s, therefore no extreme storm events were captured. As both studies agree that cliff-toe inundation duration and frequency is not directly linked to cliff failure, it is possible that the massive increase in erosion detected at Porthleven and to a lesser extent, Godrevy during the stormy periods is a product of sudden and dramatic changes to the morphology of the beach combined with the energy expended on the cliffs during these extreme storm conditions.

3.5.2 Beach morphology and wave runup

The runup measured at Godrevy is approximately 60% of the offshore significant wave height (H_s) (Fig 3.20a) which agrees with the understanding that runup on intermediate to dissipative beaches tends to be approximately 60–70 % of the significant wave height (Ruggerio *et al.,* 1996; Stockdon *et al.,* 2006). At Porthleven, using the adjusted equation for runup (Masselink *et al.,* in press) wave runup values are 2.2–2.5 times greater than the significant wave height (Fig 3.21a), which agrees with the notion that wave runup on reflective beaches can be > 2 times the offshore significant wave height (Masselink *et al.,* in press).

The slope of the beach at Porthleven is considerably steeper than the slope of the beach at Godrevy (mean $\tan\beta$ = 0.17 compared with mean $\tan\beta$ = 0.02). The slope of the beach and offshore bathymetry ultimately dictate the dissipation of wave energy and hence the amount of residual wave energy expended on the cliffs. On more dissipative beaches, vertical runup is less dependent on the slope of the beach and more-so on the offshore significant wave height (Ruggerio *et al.,* 1996). This implies that the vertical runup extent and therefore the times when the water level exceeds the beach-cliff junction are more sensitive to the slope of the beach at Porthleven than at Godrevy.

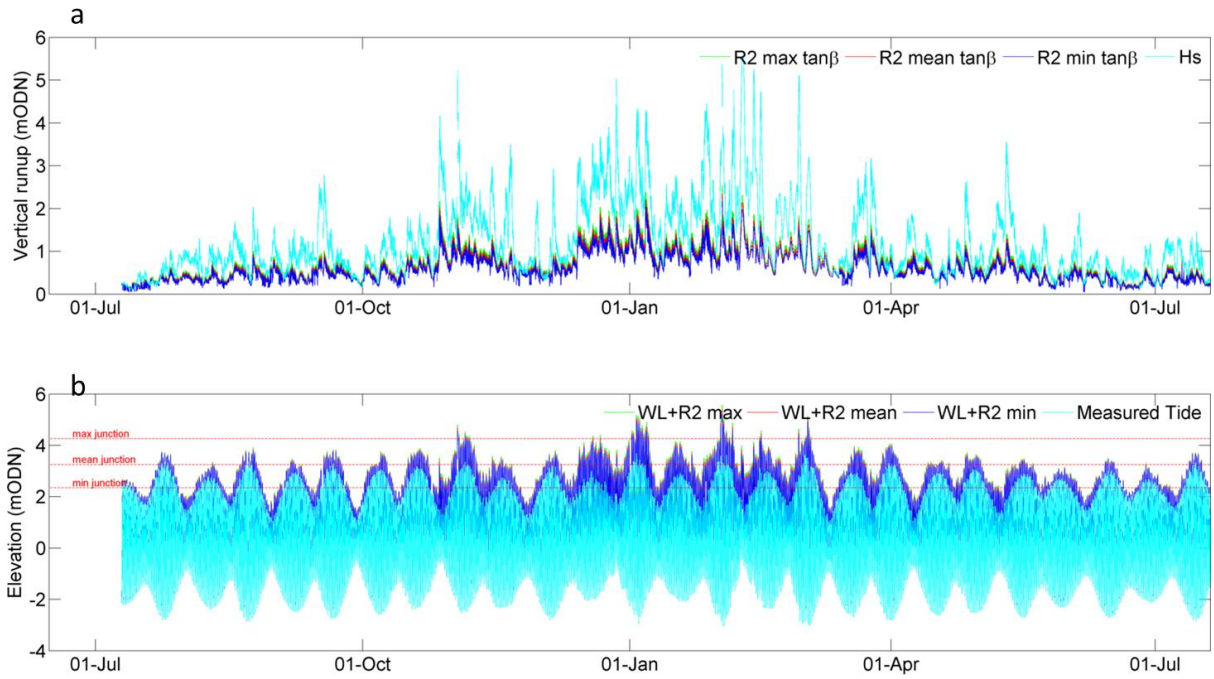

Figure 3.20: a) Time series of vertical runup under the three beach slope scenarios for Godrevy. b) Combined measured tide and runup for all three beach slopes. The relevant beach-cliff junctions are depicted across the time series to illustrate frequency of cliff inundation.

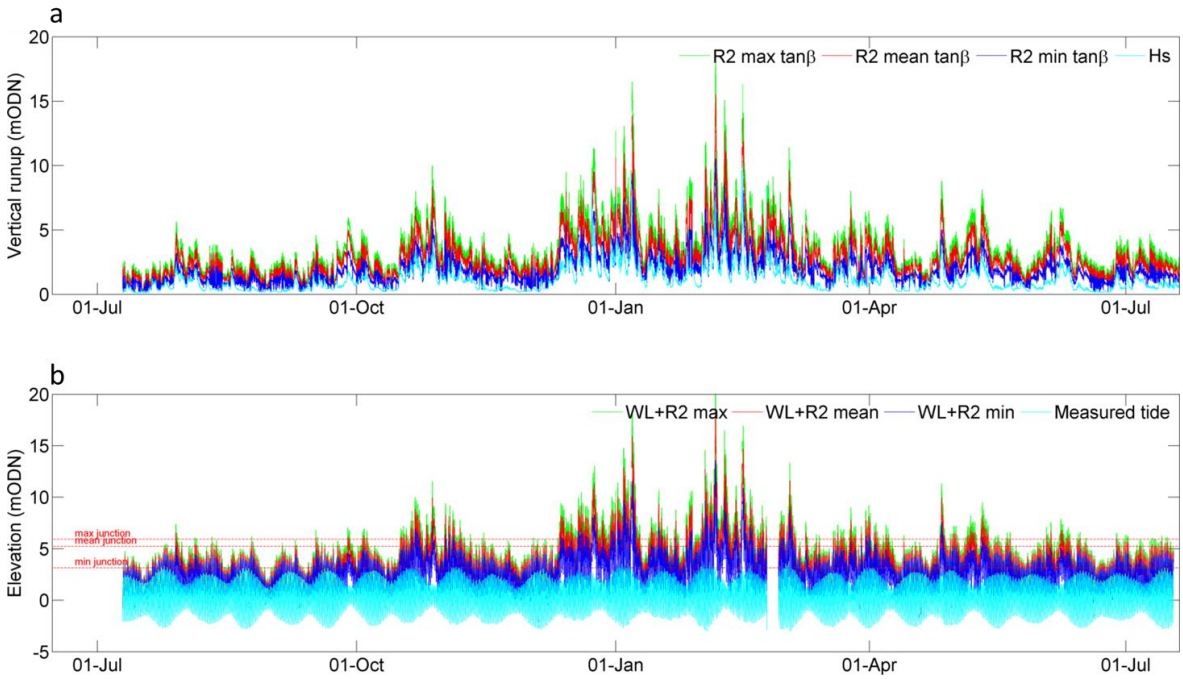

Figure 3.21: a) Time series of vertical runup under the three beach slope scenarios for Porthleven. b) Combined measured tide and runup for all three beach slopes. The relevant beach-cliff junctions are depicted across the time series to illustrate frequency of cliff inundation.

This is illustrated in Figs 3.20a and 3.21a with a noticeable difference between the vertical runup at Porthleven. The vertical runup predicted using Eqn 3.2 with a fitting parameter (*K*) of 1.1 for intermediate beaches (i.e., Godrevy) shows an average increase in vertical runup of 0.1 m between the maximum and minimum slope with a standard deviation of 0.06 m. At

Porthleven, using a fitting parameter of K = 2 for gravel beaches (Masselink *et al.*, in press) the average difference in runup between the minimum and maximum slope values is 1.4 m with a standard deviation of 0.9 m. Combining the predicted runup values (based on the three beach slope scenarios) with the measured tidal levels provides an indication of the water level conditions at the toe of the cliffs (Fig. 3.22b and 3.23b). At Godrevy, the total water level tends to depend on the tidal elevations and the contribution of the runup component to the total water level is minimal, whereas at Porthleven, the total water level is highly dependent on the offshore wave conditions and the tidal modulation of the signal is dampened, especially under energetic wave conditions. At Godrevy with the combined measured tidal levels and wave runup, the beach-cliff junction is exceeded every high tide. At Porthleven however the minimum beach-cliff junction is only exceeded when water levels exceed 3.1 m ODN and the maximum water level required to exceed the maximum beach-cliff junction is 5.9 m ODN. The minimum elevation is exceeded during most spring high tides; however the mean and maximum elevations are exceeded only under highly energetic wave conditions in the winter months (Dec 2013 – Mar 2014). The mean and maximum levels are exceeded at some points during the spring/summer months, however only when significant wave heights are greater than 3 m H_s (Fig 3.21b).

3.5.3 Cliff erosion volumes and wave energy

As cliff-toe inundation duration and frequency has not been found to be responsible for cliff failure along other coastlines (Vann Jones *et al.*, 2015), the amount of energy expended on the cliffs during these inundation periods may however explain the elevated volumes of erosion under storm conditions. The inundation durations were calculated by summing the periods when the runup extent exceeds the beach-cliff junction. The assumption was then made that when this junction was exceeded, all offshore wave energy was expended on the cliffs and this energy was integrated across the time where the cliffs are affected by the runup. Therefore the wave energy values in Fig 3.22c and 3.23c signify deep water wave energy flux values and do not take wave dissipation into account. Further modelling of wave dissipation across the two beaches would be required for accurate quantification of the residual wave-cliff impact energy.

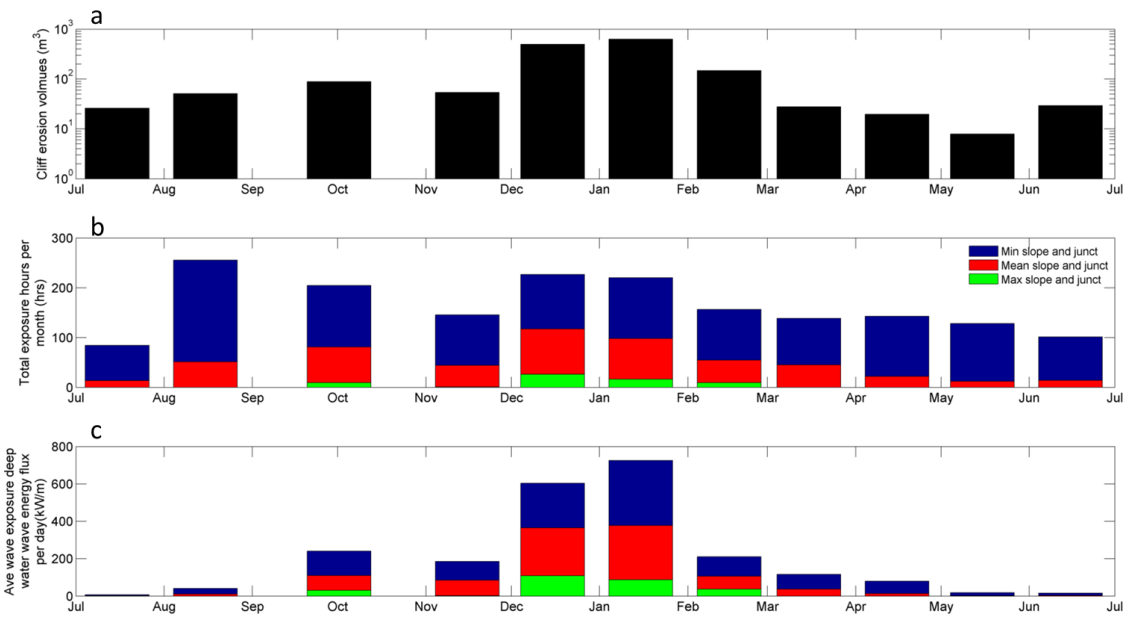

Figure 3.22: a) Cliff erosion volumes for each survey period for Godrevy (scaled logarithmically), b) the total number of hours per month where water levels exceed a minimum (blue), mean (red) and maximum (green) beach cliff junction, and c) the total deep water wave energy flux during the relevant exposure scenarios, scaled by the number of days in the survey period.

The number of hours per month where the water levels are exceeded at Godrevy gradually increases with a decrease in beach slope and beach cliff junction elevation. The greatest cliff-toe inundation period is between Aug and Oct 2013 (260 hrs), however this is also because this is the longest survey period. Normalising the deep water wave energy flux by the number of days in the survey period indicates that during Dec 2013 to Feb 2014 the cliff received the highest deep water wave energy flux values with an average of 200 kW/m/hr for a total of 80 hrs in from Dec 2013 – Jan 2014 under a maximum beach elevation scenario, and approximately 600 kW/m/hr for 200 hrs under a minimum beach scenario. Between Jan – Feb 2014 (i.e. the storm period), when the cliffs experienced the maximum erosion volume (629 m^3) the deep water wave energy values were also at their maximum, with approximately 700 kW/m/hr for 220 hrs under a minimum scenario and 200 kW/m/hr for 50 hrs under a maximum scenario. The higher erosion volumes tend to agree with the periods where the maximum deep water wave energy reaches the cliffs. The wave exposure at Godrevy depends linearly on the slope of the beach and the elevation of the beach cliff junction. A gradual increase in slope and junction results in a decrease in the duration of inundation along with a decrease in the wave energy expended on the cliffs.

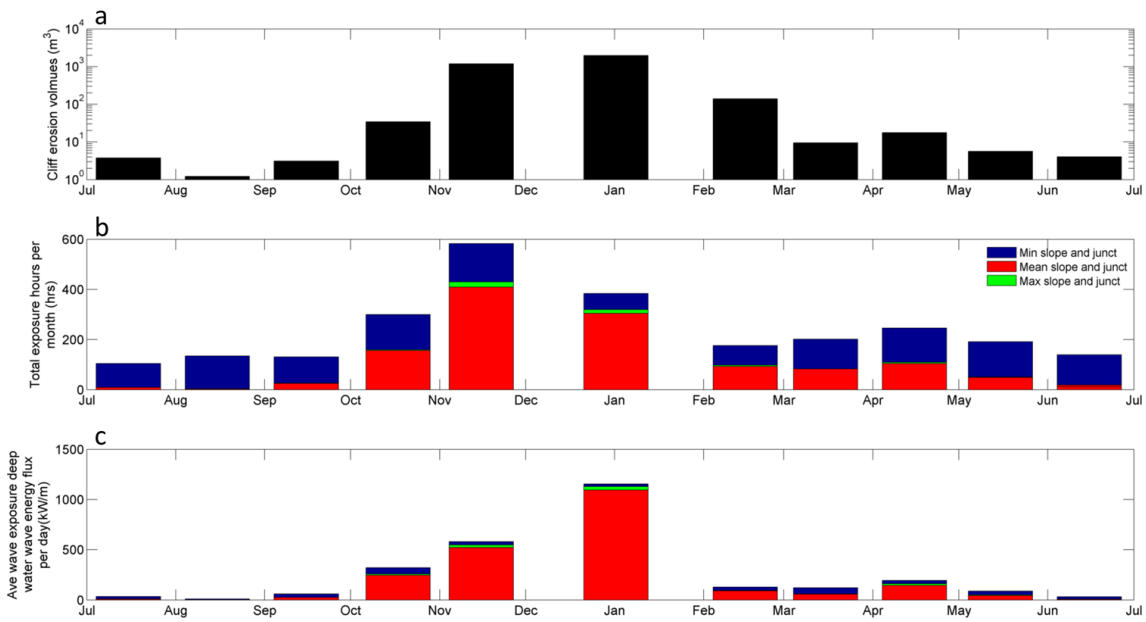

Figure 3.23: a) Cliff erosion volumes for each survey period for Porthleven (scaled logarithmically), b) the total number of hours per month where water levels exceed a minimum (blue), mean (red) and maximum (green) beach cliff junction, and c) the total deep water wave energy flux during the relevant exposure scenarios, scaled by the number of days in the survey period.

At Porthleven, the cliff erosion volumes also tend to agree with the deep water wave energy values, and the duration of exposure. Maximum erosion volumes measured between Nov 2013 – Jan 2014 (1184 m^3) and Jan – Feb 2014 (1958 m^3) occurred when the wave climate was at its most energetic (500 kW/m/hr for 300 – 500 hrs and 1000 kW/m/hr for 280 – 300 hrs). Although the vertical runup extent is more sensitive to the variability of the slope of the beach at Porthleven (Fig 3.23a), the variation in beach-cliff junction does not tend to influence the duration of wave-cliff exposure as linearly as at Godrevy. Comparing the mean, minimum and maximum beach-cliff junction and beach slope scenarios suggests that the influence of the beach morphology is important in dictating the runup extent. Due to the amplification that occurs with wave runup on reflective beaches (Masselink *et al.*, in press), the resultant increase in beach-cliff junction elevation then plays a minor role in the protecting of the cliffs from wave energy. This amplification in runup therefore results in a greater number of hours where the total water level reaches the cliffs combined with higher average wave power, especially during the winter months.

3.5.4 *Wave breaker type*

The average monthly Iribarren numbers are a dimensionless means of using the ratio between the beach slope and the square root of the offshore wave steepness to determine the wave breaker type. This was calculated according to Battjes (1974) (Eqn 3.3) and characterises the difference in wave breaker types over time between the sites. Spilling waves tend to dominate at Godrevy ($\xi < 0.4$) under a minimum and mean beach *scenario* and on the boundary between spilling and plunging under a maximum scenario (Fig. 3.24a). Waves on a reflective beach however tend to break as plunging waves and under higher beach elevation and slope scenarios, waves tend to surge onto the beach or at the toe of the cliffs (Fig 3.24b).

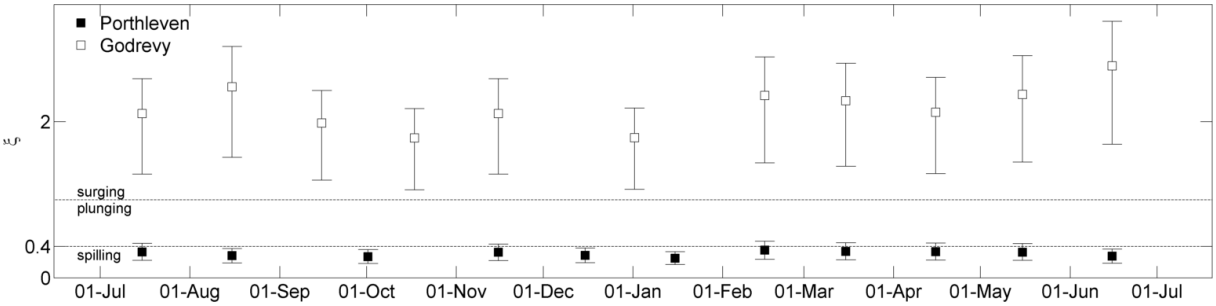

Figure 3.24: Mean Iribarren numbers for Godrevy and Porthleven. The mean, max and min beach scenarios are depicted with error bars. Wave breaker types have been calculated using Battjes (1974) equation for Iribarren numbers (Eqn 3.3).

3.4.5 *Geomorphic implications and conclusions*

Monthly surveys of cliff erosion volumes at two particularly vulnerable sites indicate that the variability from month-to-month is dependent on a combination of rainfall totals and offshore wave climate (Fig 3.18), where stormy conditions during the winter months produce an increase in rainfall together with an increase in wave energy leading to elevated rates of erosion.

As well as considering the influence of offshore wave conditions, this study has examined the interplay between the morphology of the beach and the wave climate. It has been found that although Porthleven and Godrevy have similar physical settings, i.e., similar lithology, cliff height, exposure to waves and weather conditions (exposed to highly energetic Atlantic swell), the beaches fronting the cliffs are very different; with a reflective beach at Porthleven and dissipative – intermediate beach at Godrevy.

The implications of this are as follows;

The slope of the beach at Porthleven and the variation in beach-cliff junction elevation is highly variable over a short period of time. Higher beach-cliff elevations under calm conditions provide protection to the cliffs from wave attack. The elevation of the beach-cliff junction relative to tidal levels means that the cliffs are only exposed to inundation during spring high tides and under a minimum beach-cliff elevation. This is illustrated in the monthly erosion volumes where under calm conditions (regardless of beach cliff elevation and slope), the cliffs experience erosion in the order of 0.003 – 0.12 m^3 per m length of cliff. Under extreme storm conditions however, the reflective nature of the beach with deep water offshore delays the onset of wave breaking so that plunging waves break right at the shoreline with little prior dissipation, leading to amplified wave runup (Masselink *et al.,* in press) and frequent beach-cliff junction exceedance. This mechanism explains the massive and sudden nature of cliff erosion which took place over these survey periods, where erosion increased to 6.5 m^3 per m length of cliff during the stormy period of Jan–Feb 2014. Under these stormy conditions cliff material was removed from the entire elevation and width of the cliff, homogeneously (also apparent in supplementary material of Earlie *et al.,* 2015).

At Godrevy, under similar forcing conditions, the volume of cliff erosion was half the volume measured at Porthleven. Much like the cliffs at Porthleven, the cliffs at Godrevy are formed of two units, a lower more resistant bedrock unit capped by poorly consolidated, less resistant superficial head deposit, so there is nothing that suggests the cliffs at Godrevy are more resistant to erosion. The gently sloping beach fronting the cliffs at Godrevy, however, plays an important role in influencing the extent of wave energy reaching the cliffs. Vertical wave runup on intermediate-dissipative beaches is 60 – 70% of the offshore significant wave height (Ruggerio *et al.,* 1996; Stockdon *et al.,* 2006) and much wave energy is dissipated across a wide surf zone before reaching the cliffs. The erosion volumes measured at Godrevy during the same stormy period (Jan–Feb 2014) were three times smaller than those measured at Porthleven and failure was concentrated to the superficial unit of the cliff (Fig 3.15).

The results imply that two important parameters need to be considered when investigating monthly/seasonal changes to the cliffs. Firstly the morphology of the beach fronting the cliffs (i.e.; the slope of the beach, the volume of the beach and the elevation of the beach at the toe of the cliffs), and secondly the influence these parameters have on the resultant nearshore

hydrodynamics, particularly wave breaking patterns and surf zone dissipation under extreme storm conditions.

Erosion volumes were found to greatly increase in winter when wave conditions are more energetic and accompanied by more rainfall. Beach slope, wave breaker type and the elevation of the beach-cliff junction were found to directly control the extent of wave energy flux reaching the cliff toe and resultant erosion volumes at both sites. Cliffs fronted by an intermediate/dissipative beach were less vulnerable to wave energy reaching the cliffs as wave energy under larger wave conditions is dissipated offshore, before reaching the cliff toe. Cliffs fronted by a reflective beach, however are more vulnerable under highly energetic wave conditions as beach elevations fluctuate about the cliff toe and waves with greater energy are able to reach the toe of the cliffs.

Chapter 4 – Cliff top ground motions and cliff face erosion under extreme wave conditions

4.1 Introduction

Coastal cliff erosion in response to storm waves is observed worldwide, but is notoriously difficult to measure, especially during extreme wave conditions when most erosion is likely to occur (Chapter 3). Periodic terrestrial scanning surveys are an effective method of quantifying cliff face volume losses (*response*) from such events, (Rosser *et al.,* 2005; Poulton *et al.,* 2006; Norman 2012) while inshore wave buoys characterise the wave climate (*forcing*) (Young *et al.,* 2011a; 2012; 2013). Direct observations of the energy expended from extreme waves as they impact coastal cliffs are hindered by the difficulties associated with deploying instrumentation in extreme conditions. In this chapter we use seismically detected cliff-top ground motions alongside remotely sensed (terrestrial laser scanning and video footage) and *in-situ* (wave data and beach profiles) measurements of the inshore and offshore hydrodynamics to allow, for the first time, an insight into the processes occurring real-time under extreme wave events.

4.1.1 Cliff top microseismic ground motions

Wave pressure fluctuations on the ocean floor generate microseismic ground motions both at the coast and hundreds of kilometres inland. When orbital water particle motions come into contact with the seabed, pressure fluctuations of the same amplitude and frequency as ocean waves cause what are known as *primary* microseisms (Longuet-Higgins, 1950; Bromirski and Duennebier, 2002). Interference of waves with the same wavelength travelling in opposite directions creates pressure fluctuations that do not attenuate with depth. As a result, these propagate to the seafloor and create microseisms *double* the frequency of the waves creating them (because the opposing waves have the same wavelength) (Longuet-Higgins, 1950).

Seismologists and oceanographers have used this ocean-driven microseismic activity as a proxy for hindcasting wave climate (Zopf *et al.*, 1976; Tillotson and Komar, 1997) since as far back as the 1930's (Gutenberg, 1931; Ramirez, 1940; Longuet-Higgins, 1950). More recently, combined observations of coastal ground motions and *in-situ* nearshore

hydrodynamic data have advanced our understanding of the impacts of wave energy on different coastal morphologies and shelf bathymetries under varying tidal and wave conditions (Adams *et al.,* 2002; 2005; Young *et al.,* 2011a; Dickson and Pentney, 2012; Young *et al.,* 2012; 2013; Norman *et al.,* 2013; Brain *et al.,* 2014) (Table 4.1). In most instances considered, cliff top ground motions increase with increasing wave height and with the exception of elevated shore platform fronted cliffs (Dickson and Pentney, 2012), tidal elevations.

The cliff top ground motion generated from local ocean waves can be categorized into three major frequency bands: (1) high frequency (HF) 1 – 50 Hz (1 – 0.02 s), reflecting the natural frequency of the ground as it 'rings' in direct response to wave impact and breaking waves (Young *et al.,* 2013); (2) low-frequency cliff motion or 'flexing' generated by individual sea-swell or single-frequency waves associated with the dominant nearshore wave period (SF) 0.1 – 0.05 Hz (10 – 20 s.) (Adams *et al.,* 2005); and (3) infragravity frequencies (IG) < 0.05 Hz (> 20 s) (Young *et al.,* 2011) which load the foreshore, causing pressure fluctuations (Agnew and Berger, 1978). Microseisms are also detected at double-frequencies (DF, twice the primary sea swell frequency) (0.1 – 0.2 Hz, 1 – 5 s) and exhibit similar amplitude at the coast and tens of kilometres inland (Young *et al.,* 2011a; Norman, 2012; Young *et al.,* 2013). As DF microseisms are created by waves of the same wavelength, their source is difficult to identify as they can originate globally as well as locally. Their generation is not linearly related to ocean wave height and can therefore occur with a group of interacting waves with the same wavelength but small amplitude (Bromirski *et al.,* 1999; Traer *et al,* 2012).

4.1.2 Geomorphic implications of cliff-top ground motions

Locations for previous cliff top microseismic experiments have included southern and northern California (Adams *et al,* 2002; 2005; and Young *et al.,* 2011a; 2012; 2013), eastern Australia (Young *et al.,* 2013), northeast New Zealand (Dickson and Pentney, 2012 and Young *et al.,* 2013), northeast UK (Lim *et al.,* 2011; Norman, 2012 and Brain *et al,*. 2014, Vann Jones, *et al.,* 2015) and Hawaii (Young *et al.,* 2013). Seismometers and *in-situ* hydrodynamic instrumentation has been deployed in a variety of coastal morphologies, tidal regimes and wave climates (Table 4.1).

All previous cliff top ground motions measured under wave conditions with significant wave height H_s less than 3 m show vertical ground displacements in the region of 0.5 – 10 μm during each wave loading cycle (Adams *et al.,* 2005; Young *et al.,* 2011a; Young *et al.,* 2013). It has been suggested that this repetitive flexure of the cliffs may ultimately fatigue rock strength and lead to cliff failure (Adams *et al.,* 2005). Furthermore, an increase in cliff face rockfall activity has been found to correlate with an increase in preceding seismic events (Lim *et al.,* 2011, Vann Jones, *et al.,* 2015), indicating a lag in the geomorphic response of the cliff. Experiments using cross-shore seismometer arrays show an exponential decay in the ground motion signal (in the infragravity IG and single frequency SF bands) with distance inland (Adams *et al.,* 2005, Young *et al.,* 2011a; Dickson and Pentney, 2012; Norman, 2012; Young *et al.,* 2012). The stresses created by the decrease of displacement inland are thought to be responsible for potentially weakening the integrity of the rock structure (Adams *et al.,* 2005). Brain *et al.* (2014) revisited this theory and argued that 'background' microseismic cliff top motion caused by cyclical loading is usually not of sufficient amplitude to drive growth of microcracks. However, Brain *et al.* (2014) also suggest larger displacements associated with episodic wave events can be responsible for less frequent, cliff-normal displacements, leading to an interaction between groups of microcracks that could ultimately damage the integrity of the rock structure.

Cliff face volume change related to microseismic activity was monitored during three experiments carried out in the north-east UK (Lim *et al.,* 2001; Norman 2012, Vann Jones *et al.,* 2015). Monthly terrestrial laser scan surveys over an 8 month (Lim *et al.,* 2001) and 2-year (Norman, 2012, Vann Jones *et al.,* 2015) period were related to tidal elevations and prevailing wind speeds and directions (Lim *et al.,* 2010) and nearshore wave climate (Norman, 2012). A recent study (Vann Jones *et al.,* 2015) investigating marine controls on cliff erosion found that whilst nearshore wave conditions were correlated with rockfall activity, the distribution of rockfalls extended above the inundation zone, and wasn't directly related to inundation durations alone. All experiments found an increase in the normalized volumes of cliff change with an increase in shaking from direct wave impacts and quarrying of material across the cliff face during higher tides and energetic conditions.

Table 4.1: Summary table of cliff top microseismic studies

Author	Setting	Duration	Tidal Regime	Max wave conditions	Instrumentation	Frequencies considered	Maximum displacements and main findings
Adams *et al.*, 2002	Monterey Bay, California, cliff height ~10 m. Upper Miocene mudstone bedrock capped by marine terrace deposits (1-2 m thick), fronted by submerged shore platform	*133 days* (Jan–May)	Micro tidal MSR – 2.5 m. Mixed semi diurnal	5 m, 20 s (deep water)	Broadband velocity seismometer in cliff top, sampling frequency 50 Hz. Hourly Offshore deep water (~2000m) wave buoy data transformed nearshore Tide gauge	Total velocities were squared to gain energy per unit mass and then summed over each hour.	146 μJ/kg (vertical), 633 μJ/kg (N-S) 1000 μJ/kg (E-W)
Adams *et al.*, 2005	As above	*40 days* (April–June)	As above	1.5 m, 15 s (nearshore)	Cross shore array of three broadband velocity seismometers 2 m, 13m and 33 m from the cliff edge sampling at 50 Hz Hourly Offshore deep water (~2000m) wave buoy Nearshore wave data (pressure sensors) 17 min bursts at 2 Hz. Tide gauge for water levels	Considered frequencies > 0.033 Hz (30 s). Found agreement with 0.1- 0.05 Hz (10-20 s) and incident wave period. Investigated the cyclical flexing motion of cliff top ground displacement.	50 μm horizontal 10 μm vertical
Lim *et al.*, 2011	Staithes, Yorkshire, UK 70 m high Jurassic sedimentary cliffs capped with 10 m of glacial till fronted by a 200 m wide shore platform	*8 months* (Sept–April)	Macro tidal MSR – 5 m semi diurnal	Tidal elevations, wind speed and direction. No wave data used.	Seismic triaxial geophone Airborne LiDAR Terrestrial Laser Scanner Uses wind characteristics and water levels as a proxy for wave climate	Considered the number of seismic events per hr and related to tidal cycle, wind conditions and directions. Compared total seismic events per month with volume loss above and below cliff inundation level and found the cliff responded to the microseismic events in the preceding month.	n/a
Young *et al.*, 2011b	Del Mar, California 24 m cliffs formed of Eocene sandstone capped with Pleistocene deposits fronted by a narrow sand beach	*64 days* (Feb–April)	Micro tidal MSR – 2.5 m. Mixed semi diurnal	3 m	Broadband velocity seismometer sampling at 100 Hz 26 m shoreward of the pressure sensor Nearshore wave data from a pressure sensor sampling at 8 Hz on the shore platform 10 m wave climate from virtual wave buoy network	Found shaking in HF (> 0.3 Hz), swaying at incident frequencies (0.05-0.1 Hz) and slow swaying at infragravity frequencies (0.006 – 0.05 Hz) and double frequency levels were the same inland as cliff top (0.1-0.3 Hz). Found ground displacements increased with H_s and tides.	5 – 10 μm vertical
Young *et al.*, 2012	As above	*2-4 week deployments* (November 2010 – April 2011)	Micro tidal MSR – 2.5 m. Mixed semi diurnal	2 m	3 broadband velocity seismometers located at 7 different locations in a cross shore array 2-4 week deployments 10 m wave climate from virtual wave buoy network Tide gauge	Frequencies from (0.1 – 0.01). SF = 0.04-0.1 Hz, IG = 0.01 – 0.04 Hz. DF = twice the sea swell frequency. HF = 0.2-0.5Hz. Suggests that at lower frequencies (0.001 – 0.01 Hz) vertical ground motions were caused by pressure loading and gravitational attraction of low frequency ocean waves Agnew and Berger (1978)	5 – 10 μm vertical

Dickson and Pentney, 2012	Okakari Point, New Zealand rocky coastline, 35 m cliffs of flysch and alternating mudstone and sandstone fronted by 100 m wide shore platform	*20 days*	Meso tidal MSR 3 m semi diurnal	3 m	2 broadband velocity seismometers in the cliff top, one on the cliff toe and one 75 m inland sampling at 100 Hz and 250 Hz Cross shore array of 4 RBR pressure sensors on the shore platform 30 -40 m apart and one 20 m seaward of the outer edge of the platform (17 min bursts at 4 Hz) ADCP deployed 30 m offshore in 12 m water depth (17 min bursts at 4 Hz)	Investigated frequencies between 1-100 Hz, hourly mean absolute voltage values for each channel were computed. Horizontal motion dominates at the cliff top, vertical at the toe. Ground motions were greatest at low rather than high tide. Waves impact shoreward platform edge, over the cliff toe.	Voltage values instead of displacement. Lower frequencies dominated at cliff top, higher at cliff toe. Horizontal displacement greater at cliff top than toe, vertical dominant at toe.
Norman, 2012	Boulby cliff, Yorkshire, UK 70 m high Jurassic sedimentary cliffs capped with 10 m of glacial till fronted by a 200 m wide shore platform	2 years	Macro tidal 6 m semi diurnal	5.m	5 velocity seismometers in a cross shore array Terrestrial Laser scanner scanned cliff surface every 1-2 months. Modelled wave climate from an offshore wave buoy in 65 m depth of water 18 km NW of the site Monitored wind data Tide gauge	Long period peak (0.01 Hz) Microseismic band (1-0.07 Hz). Anthropogenic band (1.1-25 Hz and 1.1-2Hz due to people and farm machinery) High tide (12.5 Hz), wind frequency band (45 Hz)	Largest vertical energy component in the 0.2 Hz and 0.014 Hz frequencies
Young *et al.*, 2013	8 different sites; 4 cliff top locations in southern California fronted by submerged platforms, (see Young *et al.*, 2011) , another cliff top in NZ and Australia (with elevated platforms) and Hawaii (fronted by rocky reef) and three beach sites (2 in California, one in North Carolina)	Over 3 yrs, 8 deployments ranging from *13 – 52 days*	All micro-meso tidal regimes (0.7 – 2.6 m)	4.5 m	Broadband velocity seismometer (see Young *et al.*, 2011), offshore wave buoys and nearshore pressure sensors at all sites except NZ, Australia and Hawaii. ADCP used in NZ.	At all sites – 0.01 – 40 Hz. Between 0.01 and 0.1 Hz ground flexing is seen at all sites in phase with IG and sea swell waves, shaking at higher frequencies (0.5 – 40 Hz). Displacement amplitudes greater at flexing than shaking frequencies.	Greatest displacements at Hawaii under ~5 m waves in the order of several mm.
Brain *et al.*, 2014	Staithes, Yorkshire, UK 70 m high Jurassic sedimentary cliffs capped with 10 m of glacial till fronted by a 200 m wide shore platform	*32 days*	Macro tidal 6 m semi diurnal	5 m	Broad band velocity seismometer sampling at 100 Hz Weather station data (wind direction and velocity, rainfall, atmospheric pressure) Tide gauge Wave climate from an offshore wave buoy in 65 m depth of water 18 km NW of the site	Due to tilt effects, only considers the 0.14 – 1 Hz (1-7secs) .Ground tilt increases with increasing period (Webb and Crawford, 1999). Tilt contamination in the vertical is minimal (Grazier, 2006)	Maximum peak in calm conditions 0.3 – 3 μm in the vertical and (apparent) horizontal and 1.5 – 3 μm in the vertical and 10 – 16 μm in the horizontal during storms.
Vann Jones *et al.*, 2015	N Yorkshire, UK, 55 m high near vertical Lower Jurassic mudstone, shale, siltstone and sandstone cliff	*2- yrs* (25 July 2008 – 28 June 2010)	Macro tidal 6 m semi diurnal	6 m	Broadband seismometer in cliff-top, measured tide gauge, offshore wave buoy, wave modelling to monitor conditions close to the cliff, TLS at 4–8 week intervals.	Signal power and energy obtained from 3 frequency bands (12.5–50 Hz), (1.1–50 Hz), (1–0.1 Hz)	Found statistically strong correlations between rockfalls and distally measured wave conditions, marine influence on rockfall extends above the inundation zone. Rockfalls not found to be a function of inundation duration alone.

4.1.3 Chapter layout

In this chapter, we firstly introduce the two study sites, (Porthleven and Godrevy). A detailed description of their coastal, geological and hydrodynamic setting is provided in Chapter 3. Section 3.4 describes field instrumentation deployment and data processing methodology. Observations of the ground motions in relation to the inshore and deep water wave conditions, beach morphology and cliff face erosion are presented in section 4.4. Ground motions under extreme conditions are compared with those detected under 'calm' conditions at both sites under a range of tidal elevations (section 4.5). In this section (4.5) we also examine the physical conditions that may have resulted in the distribution of energy across the frequency spectrum at each site. Cliff-top displacements under extreme wave conditions are also examined closely. Finally, in section 4.6, the cliff-top observations are subsequently placed in a longer-term context by comparing cliff face changes that occurred over this extremely energetic period, obtained from terrestrial laser scanning, with the annual cliff face development.

Previous studies primarily focus on low to moderate incident ocean wave conditions and observations of the impacts of extreme wave events are rare. Observations of extreme wave events in coastal processes are hampered by problems associated with instrumentation deployment and damage. The winter of 2014 was one of the most energetic periods in the southwest UK since the 1950's (NOAA, 2014) and brought c. 15 storms with significant wave heights (H_s) in excess of 6 m (the 1% exceedance limit). This study explores a unique set of cliff-top seismic observations made during extreme wave events and relates them to visual observations of storm wave activity using both *in-situ* and remote instrumentation.

4.2 Study area

In this chapter we focus on two particularly vulnerable sites situated on the southwest peninsula of the UK, facing southwest (Porthleven) and west (Godrevy) towards the Atlantic Ocean (Fig 4.1). Both sites are subject to a highly energetic wave climate being exposed to both locally generated wind waves and Atlantic swell from the south and southwest (Scott *et al.*, 2011).

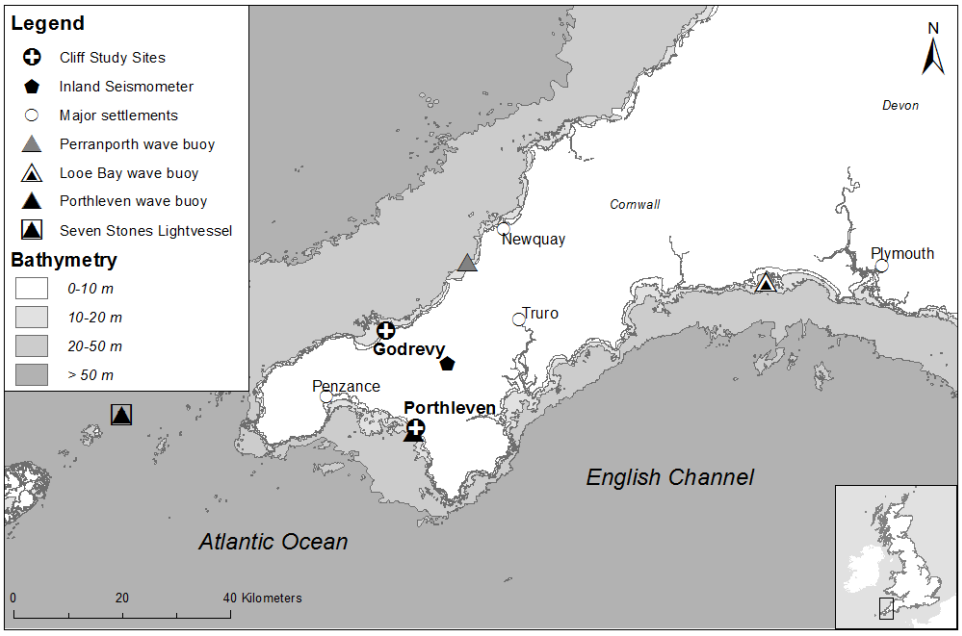

Figure 4.1: Study sites with locations of inland seismometer, nearshore and deep water wave buoys.

Detailed information of the beach and cliff characteristics at the two sites is presented in Chapter 1 and Chapter 3.

4.3 Method

To capture the variability in cliff response to differing wave conditions, three separate instrument deployments were made over a two-month period during the winter of 2014 (Figure 4.2). The first deployment was made at Porthleven under highly energetic conditions (herein referred to as PLV1) for a 7-day period (31st Jan – 6th Feb 2014), the second at Godrevy (GOD) for a 13-day period (6th – 19th Feb 2014) including both stormy and calm conditions, and the third at Porthleven (PLV2) for 16 days (5th – 21st March), under mainly

calm conditions. The difficulties associated with deploying *in-situ* instrumentation during storms are highlighted by the various periods of missing data.

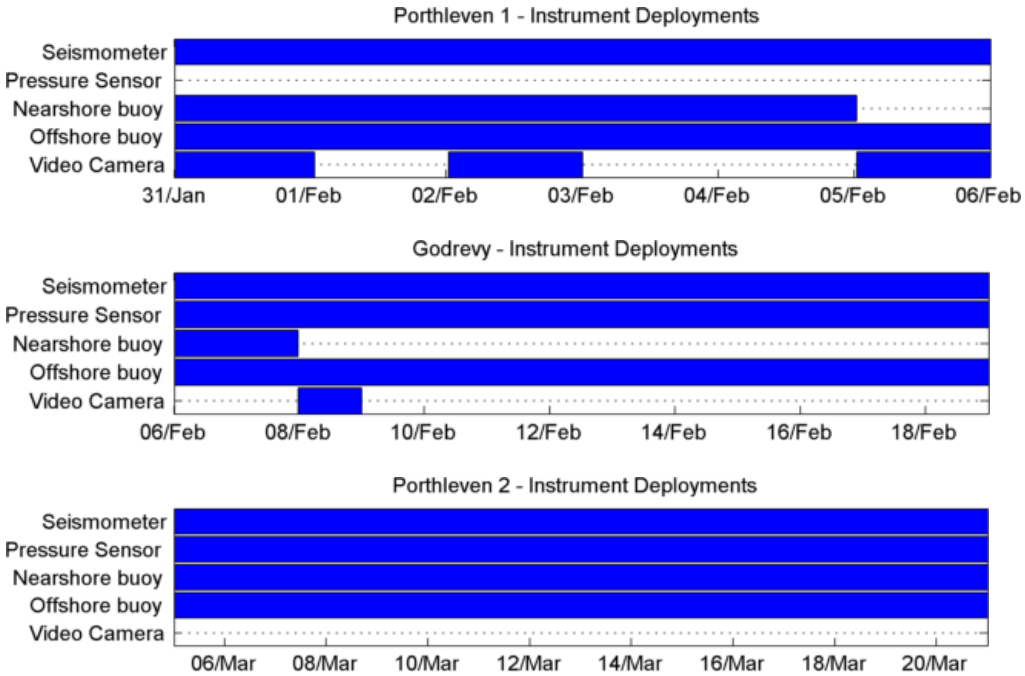

Figure 4.2: Schedule of instrumentation deployments during each experiment. Beach profiles were taken at Porthleven on the 20th Jan, the 1st Feb (both low tides), 2nd Feb and the and the 18th Feb and at Godrevy on the 16th Jan, 17th Feb and 18th March (2014).

4.3.1 Site setup

A similar site set-up was adopted at both sites including a seismometer buried in the cliff-top, a pressure sensor attached to a nearby rocky outcrop, a tripod mounted video camera positioned on a headland facing the cliffs and inshore and offshore wave buoy data. Gaps in the deployments are due to instrumentation malfunctioning during extreme events. A 4.5-hour video deployment over a high-tide captured the impacts of the waves during the largest extreme event at each site. Beach profiles and terrestrial laser scanning of the cliff face was undertaken pre and post-deployment at both sites, and additional low-tide profiles when conditions permitted (Figure 4.3). Figures 4.4 and 4.5 illustrate the site set-up adopted at each site with locations of the seismometer and video camera in relation to the cliff and beach.

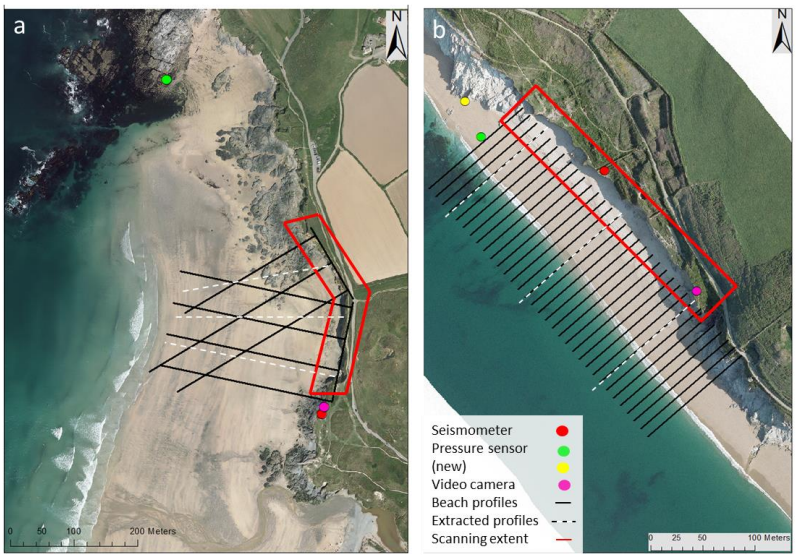

Figure 4.3: Aerial photographs of the coastal site set up with instrument deployment locations at a) Godrevy and b) Porthleven.

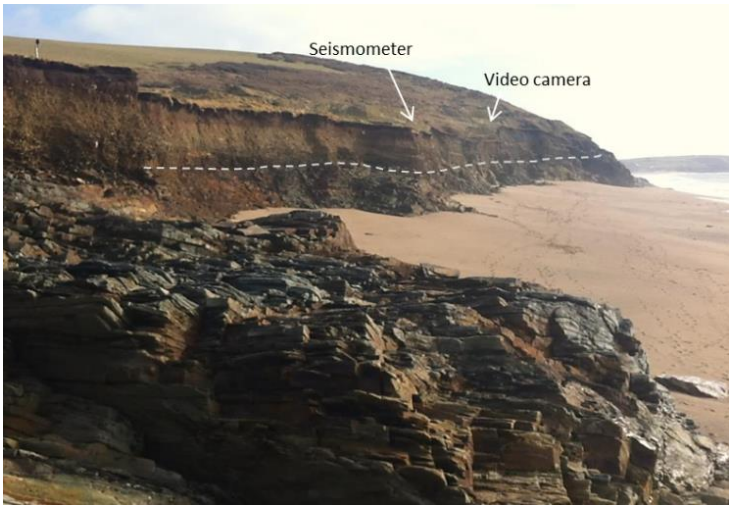

Figure 4.4: Photograph of cliffs at Porthleven, and locations of seismometer and video camera. The boundary between the two major geological units (Mylor slates and overlying Quaternary head deposits) is identified with a dotted line. Mylor spate characteristics are shown in the outcrop in the foreground.

Figure 4.5: Photograph of cliffs at Godrevy, and locations of seismometer and video camera. The boundary between the two major geological units (Porthtowan formation and overlying Quaternary head deposits) is identified with a dotted line.

4.3.2 Wave climate

4.3.2.1 Deep water wave climate

Deep water wave conditions were obtained from the Sevenstones offshore light vessel located 55 km to the west of Porthleven and 52 km south west of Godrevy (Fig. 4.1) with a water depth of approximately 60 m (NOAA, 2014). Hourly statistics of significant wave height (H_o) and zero crossing wave periods (T_z) were derived for all three deployments, providing an overview of the offshore wave conditions for the entire study period.

4.3.2.2 Inshore wave climate

Although deep water wave power provides an indication of hourly wave energy, the wave direction, in relation to the coastal orientation of the sites plays a role in the energy delivery to the coast. Inshore directional wave buoys, situated 1 km off the coast of Porthleven and 20 km to the NNE of Godrevy (at Perranporth), both with approximate water depths of 10 m, provided half hourly significant wave height, peak spectral wave period and wave direction. Under extreme storm conditions, on the 4th February at Porthleven and on the 8th February at Perranporth, the wave buoys were badly damaged and both malfunctioned (Fig. 4.2).

In order to extend the Porthleven wave record, the closest alternative inshore buoy situated 70 km ENE from the study site (Looe Bay directional wave buoy deployed in *c.* 10 m water depth; Fig 3.1) was used. Over the available data period (2011 – 2014) significant wave heights at the Looe Bay buoy under southerly and south-westerly swell directions (180 – 225°) were only 5% smaller than the wave height measured at the Porthleven wave buoy. The inshore Looe Bay wave data were therefore considered representative for the wave conditions at Porthleven.

A SWAN regional wave model (Austin *et al.*, 2012) covering the Perranporth inshore wave buoy location was run for the periods of missing data for the Perranporth wave buoy as no alternative nearby wave buoy was available. The SWAN model runs daily, and is forced by initial wave and wind output data from the NOAA Wave Watch III Global wave model. The model output provided significant wave height (H_s) and peak spectral wave period (T_p) from 2D spectral data at 30 minute intervals. The difference between SWAN modelled data for a

model run 2011-2012 at Gwithian (1km from Godrevy) and Perranporth (26% decrease in H_s) was applied to both the modelled and measured wave buoy data (Chapter 3 for further details).

All the wave buoy and modelled wave data were deshoaled using linear wave theory (equations 1 - 6) to obtain deep water wave conditions according to the relationship (Komar, 1998);

$$H_0 = \left(\frac{C_1 n_1}{C_0 n_0}\right)^{\frac{1}{2}} H_1 \qquad \text{Equation 4.1}$$

where H_0 and H_1 represent the deep and intermediate (10 m buoy water depth) significant wave heights, C_1 and C_0 the intermediate water and deep water wave speed where in intermediate water;

$$C_1 = \frac{L}{T_p} \qquad \text{Equation 4.2}$$

Wave length is calculated using the following function derived by Fenton and McKee (1990), which is a simplified alternative to solving the dispersion equation iteratively.

$$L = L_0 \left(\tanh \left[\left(\frac{4\pi^2 h}{gT^2} \right)^{\frac{3}{4}} \right] \right)^{\frac{2}{3}} \qquad \text{Equation 4.3}$$

$$n_1 = \frac{1}{2}\left[1 + \frac{2kh}{\sinh(2kh)}\right] \qquad \text{Equation 4.4}$$

h is the tidally dependent water depth at the wave buoy, g is acceleration due to gravity (9.81 m/s^2) and k is the wave number defined by

$$k = \frac{2\pi}{L} \qquad \text{Equation 4.5}$$

In deep water, group wave speed, C_0, is calculated as;

$$C_0 = \frac{gT}{2\pi} \qquad \text{Equation 4.6}$$

Where n = 0.5 in deep water.

The deep water wave energy flux was calculated from the deshoaled inshore data using;

$$P = \frac{1}{16}\rho g {H_0}^2 C_0 \qquad \text{Equation 4.7}$$

where ρ is the density of seawater (1025 kg/m^3) and the significant *offshore* wave height (H_0). The deep water wave energy flux was used to compare the cumulative wave power per hour with the cumulative cliff-top vertical displacement power per hour.

4.3.2.3 Nearshore hydrodynamics

At each site a TWR-2050 pressure sensor was secured to a rock in the intertidal area for the period of one year. The sensors were configured to sample at 2 Hz for 17.4 min bursts (2048 data points) every 35 minutes. The pressure sensor deployment and configuration methods are provided in further detail in Chapter 3. The Godrevy sensor functioned for the entire year; however, the sensor deployed at Porthleven was lost under extreme conditions during the first deployment (on the 4th Feb 2014). A replacement sensor was redeployed at Porthleven on the 5th March 2014. Both pressure sensors were deployed in the intertidal zone, meaning they only captured wave and water level data from mid–high–mid tide at both sites. Under neap tides, with stormy conditions, the full tidal cycle was captured at Godrevy. The nearshore pressure sensor data were used to compare the wave energy spectra with the cliff-top velocity energy spectra.

4.3.3 Tidal levels

Predicted tide elevations were obtained for each site from the nearest secondary ports at Porthleven and St Ives (UKHO, 2012). These half-hourly tidal levels were compared with the water levels recorded by the nearshore pressure sensors (where data were available).

4.3.4 Seismometer deployment

The cliff-top ground motion was recorded using a Nanometrics Compact Trillium broadband velocity seismometer sampling at 100 Hz (Fig. 4.6a). The instrument was buried in the cliff-top, about 1 m from the ground surface and about 7 m from the cliff-edge at both sites (Fig. 4.6b). The seismometer was placed upon a smooth concrete paving slab at the base of the hole, levelled and aligned to the North (true north, corrected for magnetic declination) (Figure 4.6). The hole was back filled with soil to minimise disturbance due to ground settling and ensure insulation from extreme changes in temperature. The seismometer was connected to a data logger/digitizer, situated in a weather-proof box, and secured about 20 m away from the seismometer (Fig 4.6d) to prevent interference with the signal when configuring and checking the instrument. A similar burial was adopted at both sites and the seismometer was re-deployed in the same location as the previous deployment at Porthleven.

Figure 4.6: a) Nanometrics broadband seismometer (background) and digitiser (foreground); b) burial of seismometer 1m in the cliff top, 7 m from cliff edge on the 31st Jan 2014; c) seismometer was placed upon a smooth surface inside the hole in the cliff top; d) once buried the digitiser was accessible from inside a weather proof case, situated 20 m away from the seismometer to minimise disturbance.

4.3.5 *Seismic data processing - Transfer function correction*

The seismometer response has -3dB corners at 0.009 and 108 Hz. The raw velocity data were corrected for phase and magnitude for frequencies above 0.005 Hz according to the instrument response curve.

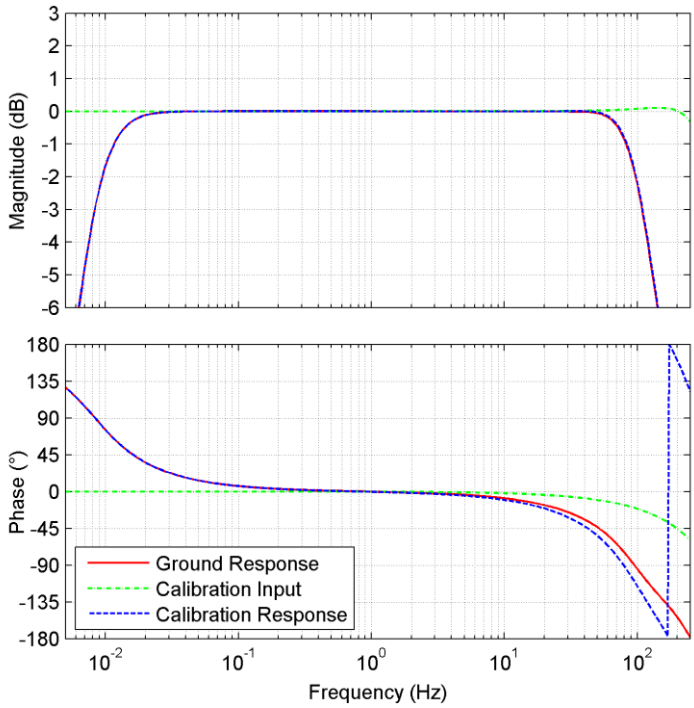

Figure 4.7: Transfer function for Nanometrics Trillium broadband seismometer (Nanometrics, 2011).

According to the bode plot provided in the instrument manual (Fig. 4.7), the sensor response output signal decreases (at lower frequencies) between 0.03 and 0.005 Hz in magnitude and phase. As we are considering frequencies up to the Nyquist frequency (50 Hz), no corrections were necessary for data at higher frequencies. The bode plot also demonstrates the -3dB corners of the ground motion response at 0.009 Hz and 108 Hz. Beyond these frequencies energy is attenuated or reflected by the instrument rather than passing through it. Only the magnitudes and phases for the frequencies between 0.005 and 50 Hz were corrected; no correction was applied to the values lower than 0.005 Hz and they therefore remained attenuated. To correct the raw velocity output according to the curve, the data were divided into 24-hourly files, detrended and transformed into the frequency domain using standard Fourier methods (Jenkins and Watts, 1968). Transforming the time series into the frequency domain allows us to understand the amplitude and phase of a signal from the output complex conjugate, containing two numbers, a real and an imaginary part (Eqn. 4.8).

$$P(f) = \underbrace{Ao\cos(\sigma t)}_{\text{Real}} + \underbrace{j\,Ao\sin(\sigma t)}_{\text{Imaginary}}$$ Equation 4.8

Where the real component is a function of the cosine of the angle and the imaginary part a function of the sin of the angle:

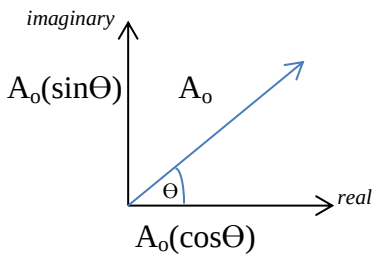

To calculate the magnitude and the phase:

$$Magnitude\ (dB) = \sqrt{real^2 + imaginary^2}$$ Equation 4.9

$$Phase\ (\theta) = tan\theta = \frac{imaginary}{real}$$ Equation 4.10

In order to correct the signal at each frequency in the Fourier transform, the complex poles and zeros provided in the instrument handbook were used to digitise the bode plot, interpolated to an equivalent frequency scale. Details of the complex poles and zeros coefficients and the equations for the digitised bode plot are provided in Appendix 2. To apply the corrections the magnitude units were converted from dB to amplitude and phase units from degrees to radians using equations 4.11 and 4.12:

$$Mag = 10^{\left(\frac{dB}{20}\right)}$$ Equation 4.11

$$\theta c = \theta \times \left(\frac{\pi}{180}\right)$$ Equation 4.12

The corrections were then applied to the magnitude (*abs* function in Matlab (MathWorks, 2013)) and phase (*angle* function in Matlab (MathWorks, 2013)) by converting the correction values into a complex conjugate using Eq. 4.13 and dividing the complex conjugate from the Fourier transform by the correction complex conjugate (Eq. 4.14). The fast Fourier transform was then transformed into the time domain for comparison with the wave time series (Vetterling *et al.*, 1988).

$$G(f) = Mag \times e^{-i\theta c}$$ Equation 4.13

$$Calibrated = P(f)\,/G(f)$$ Equation 4.14

Upon deployment, the seismometer is aligned towards the north. The coastline at Porthleven faces SW (230°), meaning horizontal components needed to be resolved to represent the cross shore and longshore ground motion.

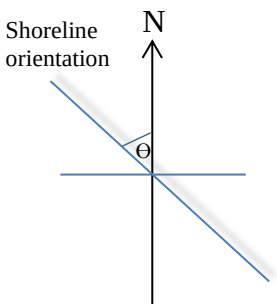

Cross shore resolved velocity

$$Xv = (EW \times \cos\theta) - (NS \times \sin\theta) \qquad \text{Equation 4.15}$$

Longshore resolved velocity

$$Lv = (NS \times \cos\theta) + (EW \times \sin\theta) \qquad \text{Equation 4.16}$$

For the Godrevy deployment (GOD), the shoreline faces west (270°) therefore the easting component represents cross shore horizontal displacement and the northing component, long shore horizontal displacement.

Once the raw data were corrected and rotated, the data were band passed in the frequency domain to identify the magnitude of shaking within three major frequency bands (Table 4.2). Energy within the double frequency band was identified and excluded from the spectrum where necessary. These bands were chosen according to the difference in spectra at each site compared with inland levels.

Table 4.2: Frequency bands for seismometer data at each site. The band limits are chosen based on the output of the spectral analysis and the concentration of energy across the spectrum.

Site	Infragravity frequency (IG)	Single frequency(SF)	High frequency (HF)	Double frequency (DF)
Porthleven 1	0.005 – 0.04 Hz	0.08 – 0.04 Hz	5 – 50 Hz	0.08 – 5 Hz
Godrevy	0.005 – 0.05 Hz	0.09 – 0.05 Hz	1 – 50 Hz	0.09 – 1 Hz
Porthleven 2	0.005 – 0.04 Hz	0.09 – 0.04 Hz	5 – 50 Hz	0.09 – 5 Hz

Observed horizontal ground motions at low frequencies are in fact ‘apparent’ ground motions as the gravitational acceleration is ‘mapped’ onto the horizontal component due to ground tilt (Rodgers, 1968). Young *et al.* (2012) found that near a cliff edge, ground tilt dominates the observed large (relative to vertical) cross-shore acceleration at infragravity frequencies, contributes significantly to cross-shore acceleration at swell frequencies, and is a small fraction of cross-shore acceleration at higher frequencies. A cross shore array of seismometers was used in Young *et al.* (2012) to derive these ratios through the analysis of cross shore decay in vertical and horizontal velocities. In our study, only one cliff top

seismometer was used and therefore the cross shore decay in ground motion under energetic conditions was not investigated. The tilt contamination in the vertical is minimal (Grazier, 2006) therefore, for the sake of clarity, only vertical velocities and displacements are discussed in this chapter. The apparent horizontal velocities and displacements are presented in Appendix 2.

4.3.6 Inland seismic data

The coastal cliff top ground motions were compared with data obtained from the British Geological Survey inland broadband seismometer located at Carmenellis, Cornwall 17 km inland from the site, sampling at 50 Hz (ORFEUS, 2014) (Fig. 4.1). The data were corrected according to the instrument's transfer response curve. The poles and zeros used to calculate the transfer function are provided in Appendix 2 and the magnitudes and phases were corrected using the same method as the cliff top seismometer (section 4.3.5).

The inland data were used to help eliminate ground motion that might be from a regional or global source such as earthquakes or earth hum (Bromirski, 1999; Traer *et al.*, 2012; Ardhuin, *et al.*, 2015). Spikes in the vertical inland spectra were compared with corresponding spikes in the cliff top data and then identified as either earthquakes in the USGS earthquake database (USGS, 2014) or human-induced noise to the seismometer (people walking around or near the instrument).

The daily files of corrected, resolved and cleaned velocity were integrated in the time domain to obtain displacement and split into hourly files for analysis with the half-hourly wave data.

4.3.7 Cliff volume loss

4.3.7.1 Point cloud data acquisition

Alongside monthly scanning of the cliffs at both sites (Chapter 3), pre- and post-storm interim scans were undertaken to assess any cliff change caused by the storms. The cliffs were scanned using a Leica P20 Terrestrial Laser Scanner from five different scanning

positions along the beach approximately 20 m from the cliff face at each site. The scanner was mounted and levelled on a tripod with the dual-axis compensator activated in case of any disturbance caused by settling of the tripod in the sand. Each scan consisted of two scans, a 360° coarse resolution scan at 12 mm at a distance of 10 m and finer scan of the region of interest (cliff face and fronting beach) at a resolution of 3 mm at 10 m. The consecutive scans were registered together using georeferenced targets, fixed at Porthleven and mobile at Godrevy. A full description of the scanning method is provided in Chapter 3.

The point clouds were post-processed using Leica software *Cyclone*, georeferenced, registered and checked for errors (Porthleven; 0.007 m, Godrevy; 0.004 m). As the data sets contain a very large number of data points (>4,000,000 points per ScanWorld), the registered scans were unified to remove any duplicate points, re-sampled at a 10 cm resolution and exported as .xyz files for analysis in 3D point cloud processing software, CloudCompare (EDF, R&D, 2011).

Terrestrial laser scanning requires dry weather and calm winds. This limitation, alongside scanning on a macro-tidal beach under stormy conditions, meant that surveys were somewhat restricted during the seismometer deployments. Monthly volume changes noted in Chapter 3 highlighted the dramatic increase in erosion over the winter of 2014 and these particular monthly changes are considered here in more detail.

4.3.7.2 Point cloud data processing

A typical method of detecting changes between point clouds involves meshing the data to create a surface (Dewez *et al.*, 2013). In complex surfaces such as rocky cliffs and beaches, meshing tends to lead to interpolation inaccuracy across surfaces that show occlusion or ‘blinding’ due to varying scanner positions (Lague *et al.*, 2013). Most meshing software cannot account for this source of uncertainty and are not entirely appropriate for complex topographies. Multiscale Model to Model Cloud Comparison (M3C2 (Lague *et al.*, 2013)) is an algorithm developed to overcome these issues and accurately compute direct point-to-point directions and distances. A detailed description of how volume change is detected using M3C2 is provided in Chapter 3. The point-to-point distances obtained using this technique were summed to give a total volume change over the cliff face.

4.3.8 Beach morphology

At Porthleven the cliffs are fronted by a fairly narrow reflective gravel beach (Scott *et al.*, 2011). At Godrevy a wide intermediate low tide bar rip beach (Masselink and Hughes, 2003) provides a natural buffer for wave energy reaching the cliffs. The beaches tend to vary in profile quite considerably throughout the year (Chapter 3) and hence were monitored for the period of the seismometer deployment when conditions permitted access to the beach. Beach profiles were measured using a Trimble 5800 Receiver and T2C2 handset attached to a surveying staff, carried and positioned at a 5 m cross-shore spacing along the lines depicted on Fig. 4.3. Tide and time constraints meant the sample spacing was much coarser at Godrevy (50 m longshore) than Porthleven (10 m longshore) due to the difference in the size of the intertidal area. The data were checked for errors using Trimble Business Centre (Trimble, 2012) and exported as .csv files for analysis. At each site, three cross-shore profile lines were extracted from the data; at either end and the centre of the cliff section.

4.3.9 Video capture

The embayed nature of the cliffs provided a promontory from which a GoPro® waterproof video camera inside a closed circuit television casing was deployed, facing north alongshore, towards the cliffs (at both Porthleven and Godrevy). The videos were GPS time-synced and closely inspected for cliff collapses, large wave impacts, and wave overtopping events for a 4:30 hour period from high to mid-tide on the 6th day of the PLV1 deployment (5th Feb 2014) and from mid to high tide on the 8th Feb at GOD, during the most energetic of the extreme storm events. The video camera was not deployed during PLV2. The video camera provided a qualitative, but detailed account of the hydrodynamics during the seismometer deployment.

4.4 Results

4.4.1 Wave climate

The observed wave climate during the winter of 2014 was one of the most energetic periods the southwest of the UK has seen since the 1950's (Fig. 4.8a). These remarkable conditions

brought more than 10 storms with deep water significant wave heights in excess of 6 m (the 1% exceedance limit) measured off the southwest tip of the UK (Sevenstones Lightvessel (Fig. 4.1)) over a four month period (Fig 4.8 b) (1st December 2013 – 31st March 2014).

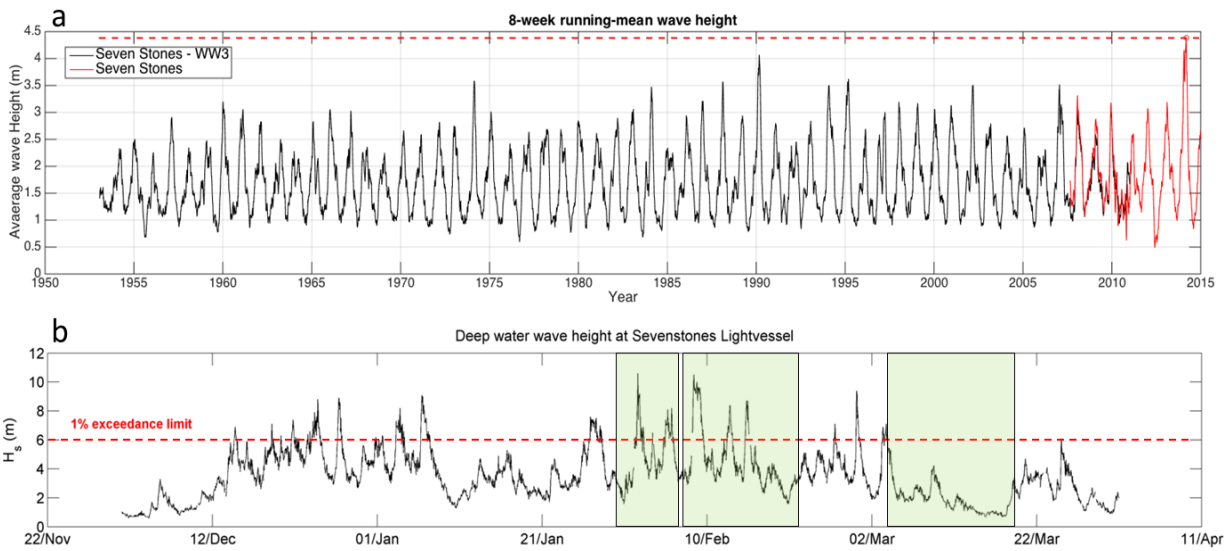

Figure 4.8: – Sevenstones light vessel data; a) 8 week running mean H_s from 1954 – present (Masselink *et al.*, in press). Black line represents modelled Wavewatch 3 data and red line represents measured values. b) H_s for the winter of 2014 from 1st December 2013 – 31st March 2014 with 1% exceedance limit. The shaded boxes represent each of the seismometer deployments chronologically.

The first deployment (PLV1) coincided with two extreme events exceeding 4 m (inshore *Hs*), the first on the 2nd February 2014 with an inshore significant wave height (H_s) of 4 – 5 m, peak wave period (T_p) of 18 – 22 s from a WSW direction (240 – 250°). The second storm on the 5th February 2014 had an inshore significant wave height of 6 – 8 m and a wave period increasing from 10 to 20 s. (Met Office, 2014; CCO, 2014). The second storm was not only more energetic but it took a more southerly track (SSW 200 – 220°) (Fig 4.9c) than typical winter weather systems making the south coast of the peninsula much more vulnerable.

The second deployment (GOD) coincided with another three energetic storms, exceeding the 1% exceedance limit on the 8th, 12th and 14th February. The SWAN modelled data for Perranporth estimated an inshore H_s of 6 – 8 m for all three storms, and a T_p of 20 s, 15 s and 17 s respectively. The first two storms were from a westerly direction (275°) and the storm on the 14th of Feb was south-westerly (220°). This is also reflected in the PLV inshore wave buoy data, where the latter storm was greater on the south coast than the north (Fig 4.9a and b).

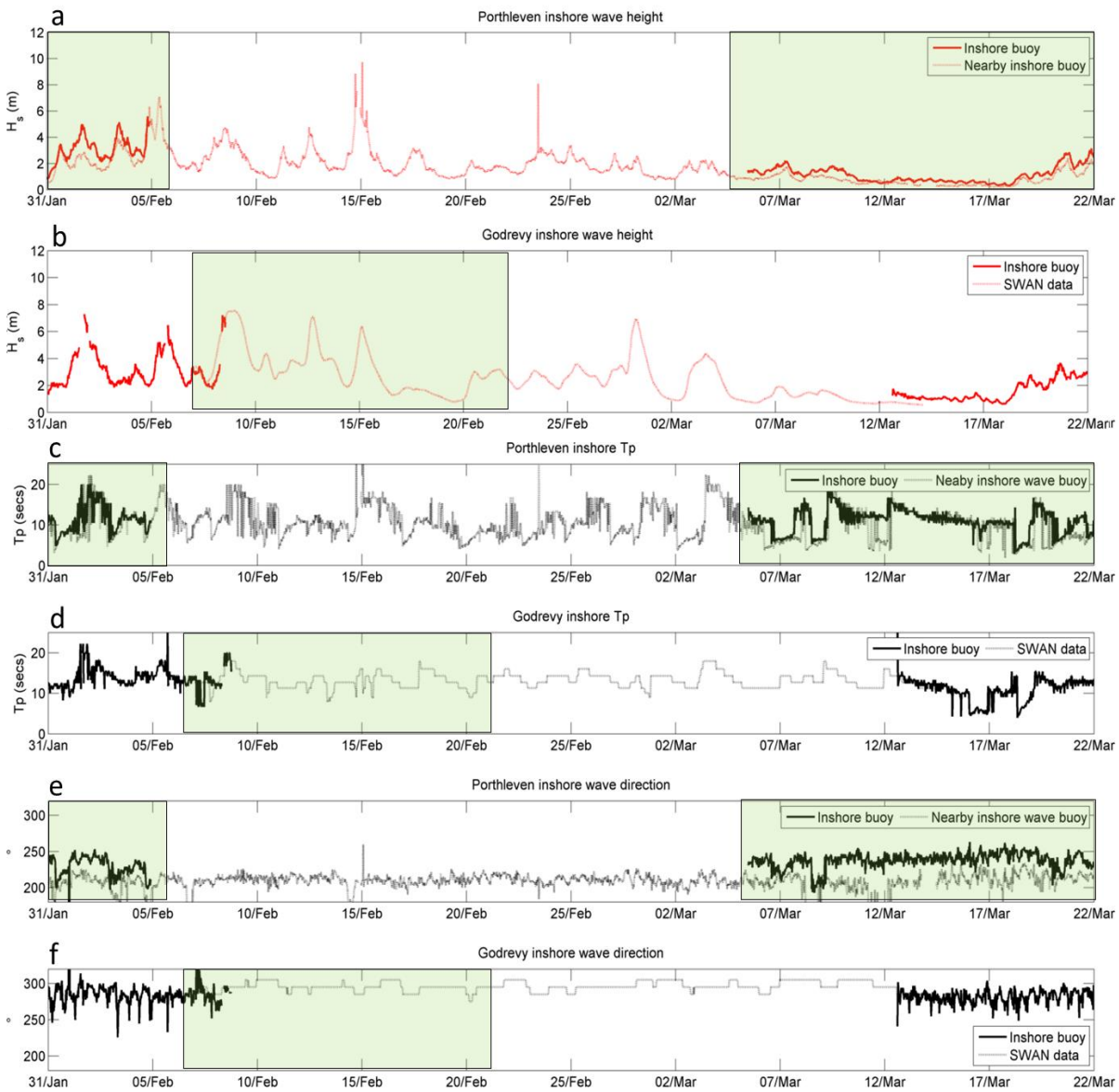

Figure 4.9: a) H_s, c) T_p and e) wave direction for Porthleven wave buoy (bold line) and Looe Bay wave buoy (dotted line); b) H_s, d) T_p and f) wave direction for Perranporth buoy (bold line) and estimated from SWAN modelled data (dotted line). The shaded boxes represent the seismometer deployments at the relevant site.

The third deployment (PLV2) occurred during comparatively calm conditions < 4 m H_s with a T_p between 8 – 16 s mostly from a SSW direction (210° - 260°). Although this period was calm compared to the storm deployments, the H_s was greater during some periods than most previous cliff top ground motion experiments (Table 4.1). Maximum wave energy during all of the storms coincided with spring high tide with the exception of the storm on the 8th Feb, which coincided with neap high tide. The variability of the wave climate during the 4 month period meant that both extreme and calm conditions under spring and neap tides were captured at both sites.

4.4.2 Cliff-top vertical ground velocities

The cliff-top ground velocities for all deployments increased with increasing incident wave height and tide level (Fig. 4.10 – 4.12). The largest velocities occurred at Porthleven (PLV1) during the two extreme storm wave events on 1st and 5th Feb when significant wave heights offshore reached 6 – 8 m (Fig. 4.10b). Vertical velocities towards the beginning of this deployment (PLV1) fluctuated around 20 to 30 μm/sec under 'calmer' conditions (H_s < 4 m). The increase in velocity was more closely associated with the inshore wave buoy H_s more than the offshore (Sevenstones) wave height as the velocities during the second storm on the 5th were much greater than the first (> 50 μm/sec compared with 40 – 50 μm/sec) when the inshore H_s exceeded 6 m. The tidal modulation is very clear in this signal, and even under moderately stormy conditions (4 – 6 m H_s) the velocities exceeded 40 – 50 μm/sec due to the higher spring tidal elevations (Fig 4.10b).

Comparison with inland seismic vertical velocity energy data (Fig. 4.10, 4.11 and 4.12d) helped identify local and non-local sources of energy. Elevated HF signals were detected at the coast during all deployments yet not inland, indicating a locally generated signal. At PLV1 the HF signals exhibited tidal modulation and double energy peaks around 10 Hz and 20 Hz suggesting a possible primary normal site frequency of 10 Hz. Throughout this deployment, inland and coastal DF signals were similar suggesting a dominance of non-local signals at the coast, again, consistent with previous studies (e.g. Young *et al*,. 2013). At the coastal site, elevated SF ground motions (not detected inland) coincided with the storm events. The inland seismometer detected three peaks in the infragravity frequency range on the 1st, 2nd and 4th of February that were not detected at the coast, suggesting a local inland source. The spectral peak located around 0.1 Hz on the 3rd Feb was present in both the inland and the coastal spectra and coincided with a magnitude 5.7 earthquake located at Lixourion, Greece (USGS, 2014). A clear IG energy peak occurred during the storm periods only in the coastal spectra (Fig. 4.10c).

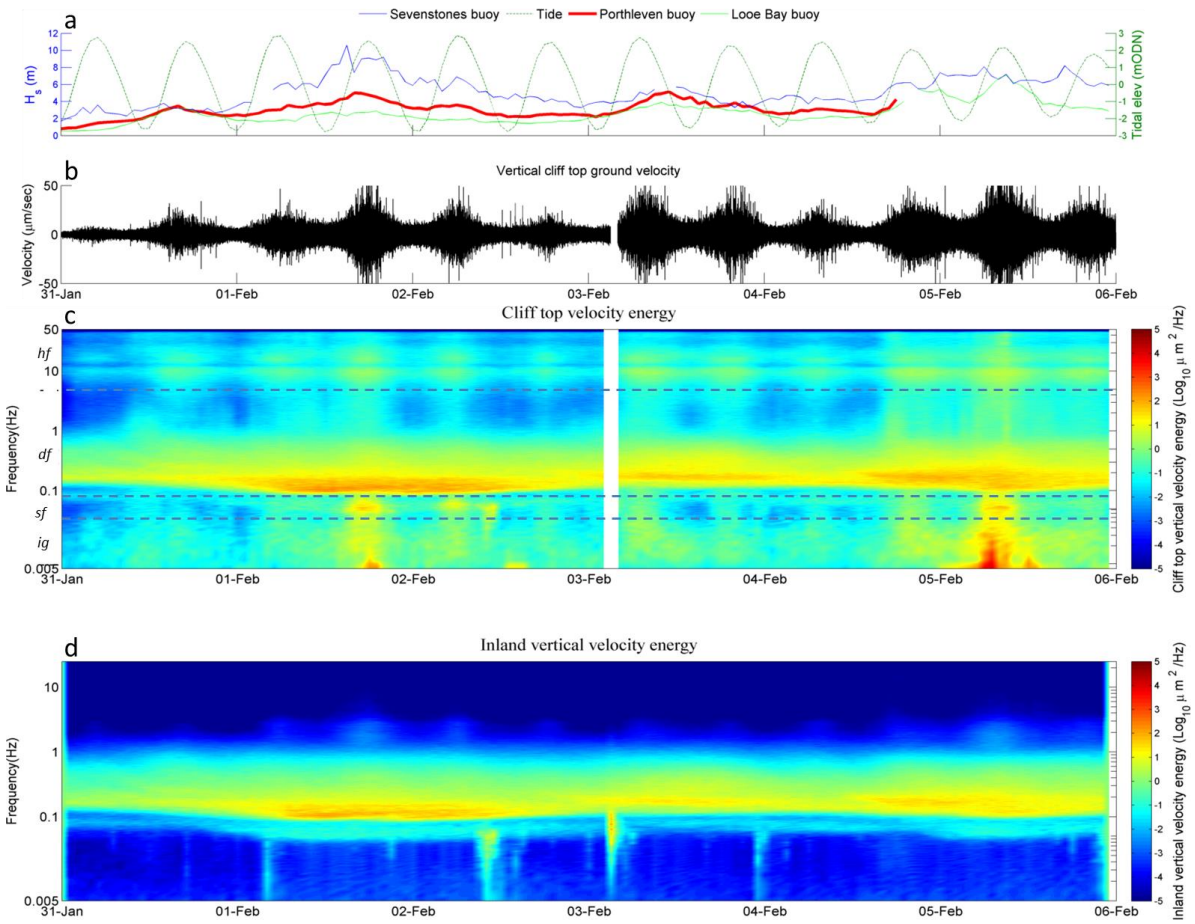

Figure 4.10: a) Porthleven deployment 1: Tidal elevations (predicted) and significant wave heights from offshore wave buoy (blue) nearshore wave buoy at Looe Bay (green) and recorded (solid red line) and interpolated (dotted red line) Porthleven wave buoy. (b) Time series of vertical cliff top ground velocity. (c) Spectra of vertical cliff top velocity energy and (d) spectra of vertical velocity energy inland.

The GOD deployment captured half a spring-neap cycle. The peak of the first storm (also the largest of the three storms on the north coast) (8th Feb) coincided with a neap high tide, and the vertical velocities were around 20 – 50 μm/sec. The second storm (12th Feb) showed much less energetic ground velocities (< 20 μm/sec) coinciding with a high tide between spring and neaps with H_s ~ 6 m. The third storm (14th Feb), coincided with (almost) spring high tide, although slightly smaller (H_s ~5 m) generated ground velocities between 20 – 30 μm/sec. Under calm conditions (< 5 m H_s), the tidal signal and the vertical velocities were dampened to 5 – 10 μm/sec during neap tides. During the spring tide, with these same calm conditions, the tidal signal became much more obvious and velocities increased at high tide to their maximum at about 30 – 50 μm/sec. There appeared to be no tidal signal in the high frequency band under neap tide and a faint tidal signal during springs (Fig 4.11c). At this site, the majority of the energy lay within the infragravity frequencies (< 0.05 Hz) and was clearly modulated by the tide. The extreme events were also detected in the IG band with the highest

energy during the first storm. Much like the first deployment (PLV1) the double frequency band peaks are present in both the coastal and inland spectra and coincide with the extreme events.

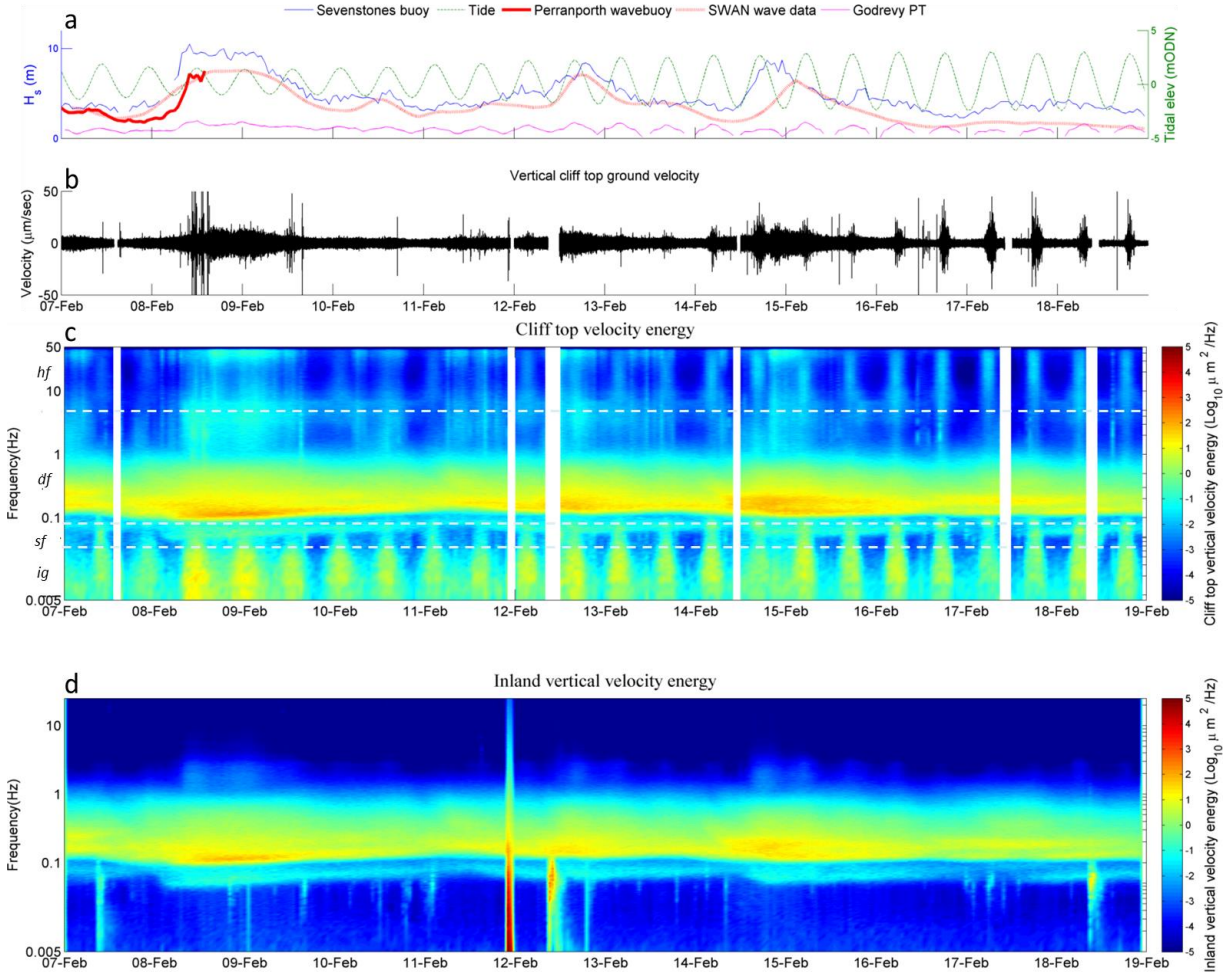

Figure 4.11: a) Godrevy deployment: Tidal elevations (predicted) and significant wave heights from offshore wave buoy (blue) and recorded (solid red line) and modelled (dotted red line) Perranporth wave buoy. Nearshore water levels measured with a pressure sensor are shown in magenta. (b) Time series of vertical cliff top ground velocity. (c) Spectra of vertical cliff top velocity energy and (d) spectra of vertical velocity energy inland.

The second deployment at Porthleven (PLV2) was over a 3-week period, and almost a full spring neap cycle, under mainly calm conditions (< 5 m H_s). The vertical velocities during this deployment were almost an order of magnitude smaller than the previous deployment at Porthleven (5 – 10 μm/sec). The tidal modulation was apparent in the signal and especially the spring tidal elevations. Two moderately stormy events (4 – 5 m H_s) occurred (9th March and the 19 – 21st March); the former during neaps with velocities of 10 – 15 μm/sec and the latter during springs with velocities of 20 – 30 μm/sec. The spectra indicate that there is no tidal signal in the IG frequency band under calm or energetic conditions during this

deployment. The tidal signal in the double peak at higher frequencies is still apparent however, and amplified under more energetic conditions (Fig 4.12c).

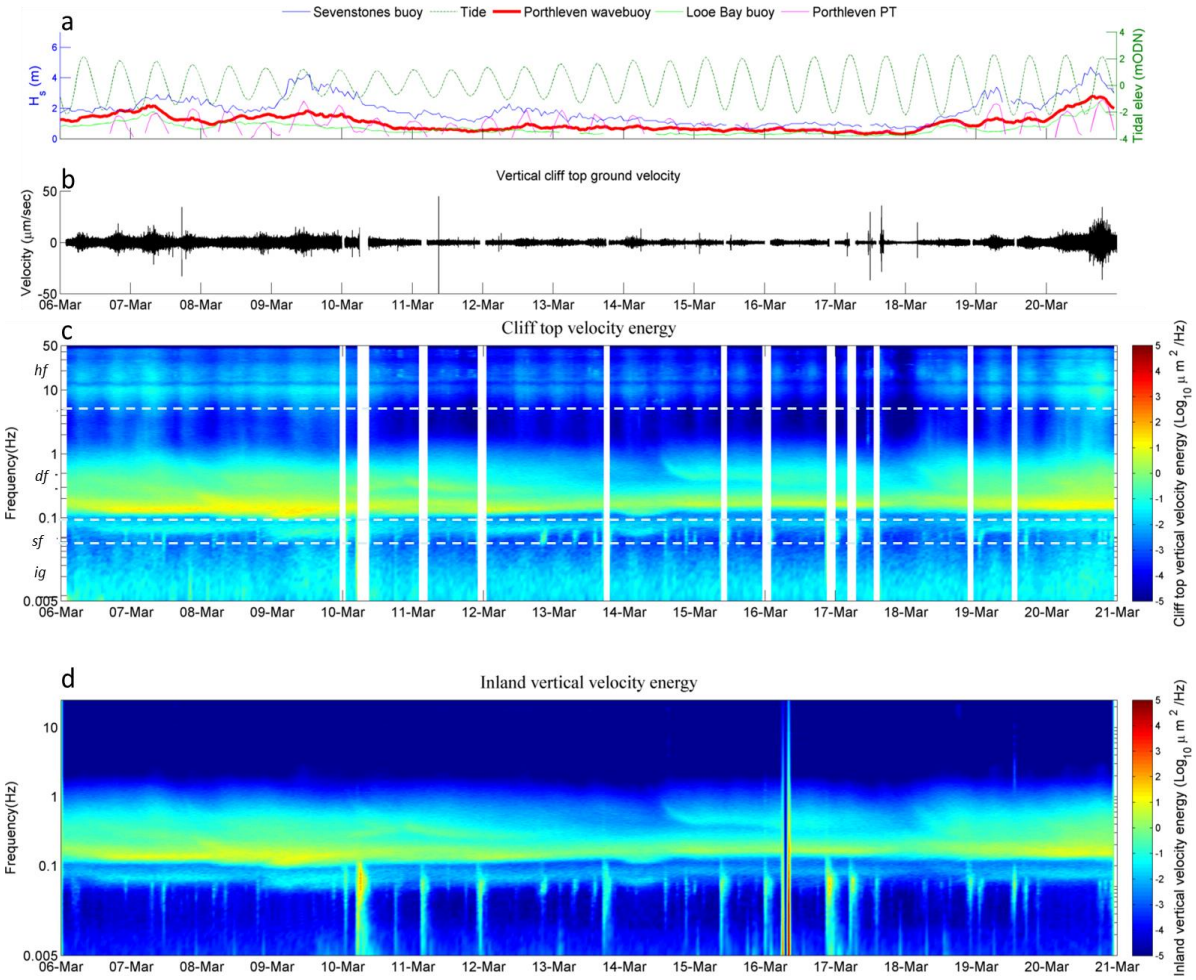

Figure 4.12: a) Porthleven deployment 2: Tidal elevations (predicted) and significant wave heights from offshore wave buoy (blue) nearshore wave buoy at Looe Bay (green) and recorded (solid red line) Perranporth wave buoy. Nearshore water levels measured with a pressure sensor are shown in magenta. (b) Time series of vertical cliff top ground velocity. (c) Spectra of vertical cliff top velocity energy and (d) spectra of vertical velocity energy inland.

4.4.3 Beach morphology

Over the period of one year the elevation of the beach changed quite dramatically at both sites. Godrevy underwent a gradual lowering of the lower intertidal area and accretion of the upper beach (by up to 2 m), with fine sand gradually burying the shingle ridge at the toe of the cliff (Chapter 3). At Porthleven the elevation of the beach tended to erode/accrete by up to 2 m according to the incident wave conditions rather than the longer term seasonal conditions.

The energetic wave conditions at Porthleven during the first deployment lowered the overall elevation of the beach by about 2 m at the northern end of the embayment (Fig 4.13a) and by about 1 m at the southern end. The sediment drift pattern along this stretch of coastline can be both easterly and westerly dependant on the short-term wave conditions (Ridgewell and Walkden, 2009). The dominant wave direction during this period was WSW 200° – 250° consistent with the pattern of greater erosion towards the NW end of the beach. Following the two extreme events the beach recovered very quickly. Over a period of one week, the elevation at the northern end of the beach accreted by about 2.2 m and 1 m towards the south (Fig 4.13).

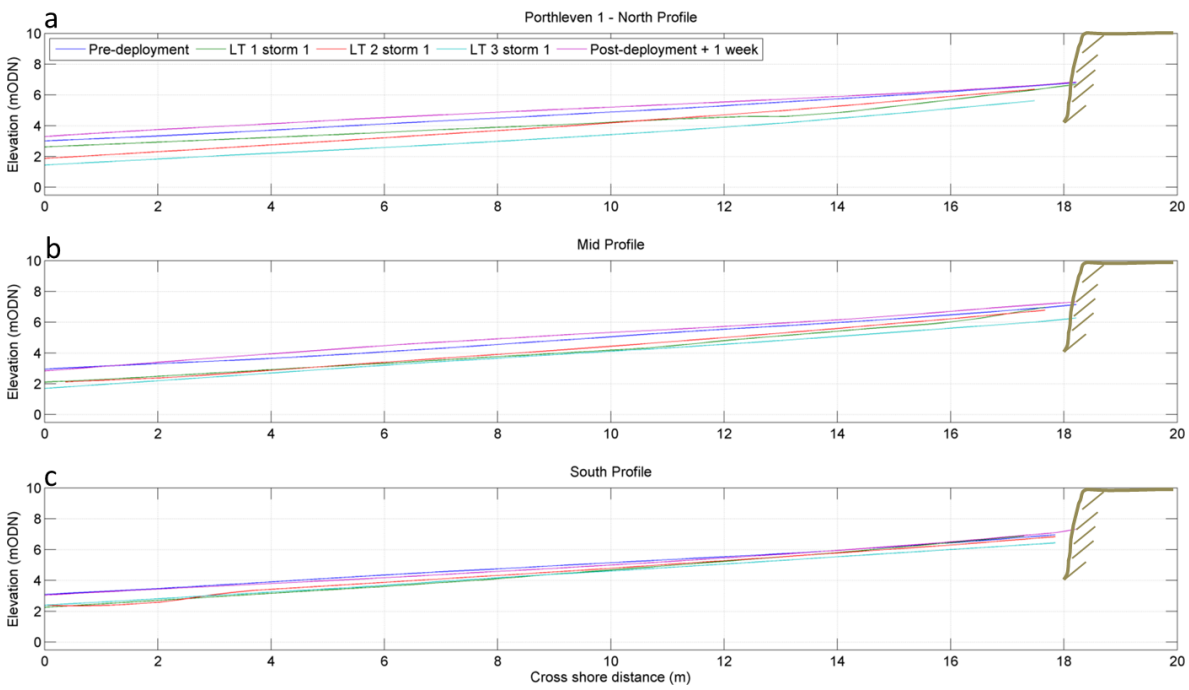

Figure 4.13: Beach profile changes over PLV1 deployment at 3 locations alongshore (Fig 4.3a). Three low tide surveys were carried out during the first storm; however conditions hampered surveys until one week after seismometer retrieval. Cliff height not to scale.

Compared to Porthleven, the beach at Godrevy was much more dissipative with a much wider intertidal zone and less responsive/dynamic. The beach elevation change over short periods of time (days–weeks) was much less noticeable at Godrevy. Over the deployment period the intertidal area of the beach underwent a gradual lowering by 0.5–0.8 m and the upper beach gradually accreted towards the mid and southern end of the bays by about 2 m (Fig 4.15 and 4.16).

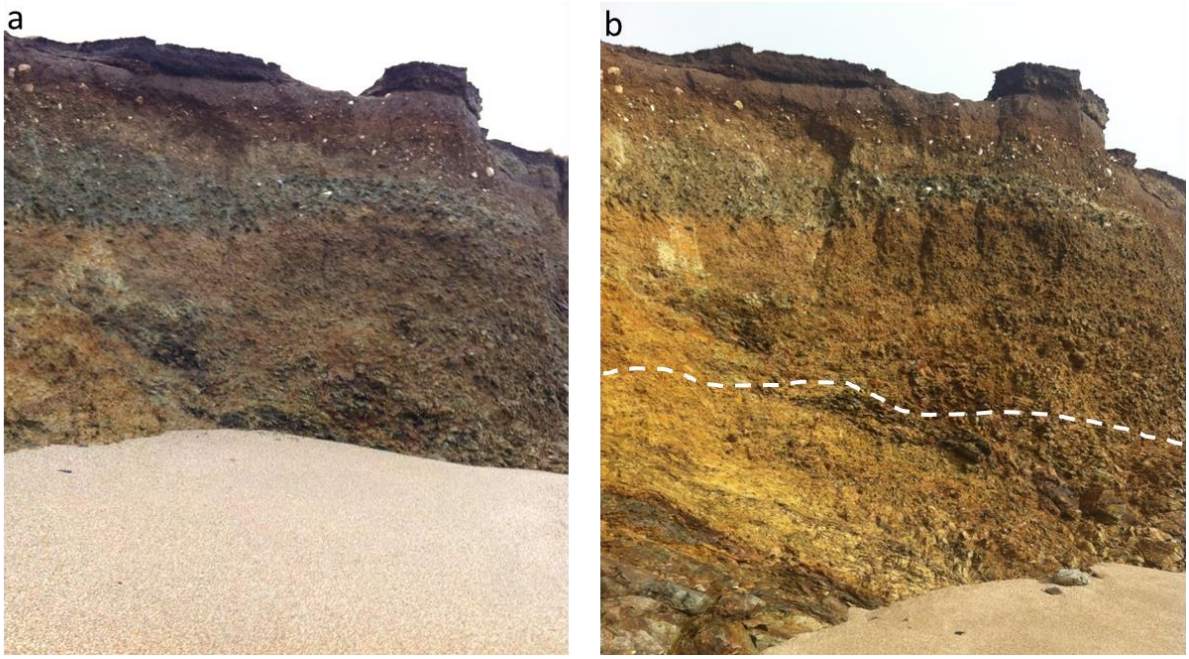

Figure 4.14: Photograph of the beach elevation at the toe of the northern end of the cliffs at Porthleven on a) 31st Jan 2014 (pre-deployment profile in Figure 4.13a) and b) on the 2nd Feb with the previous beach level indicated by a dotted line (Fig 4.13a LT3 storm 1 profile).

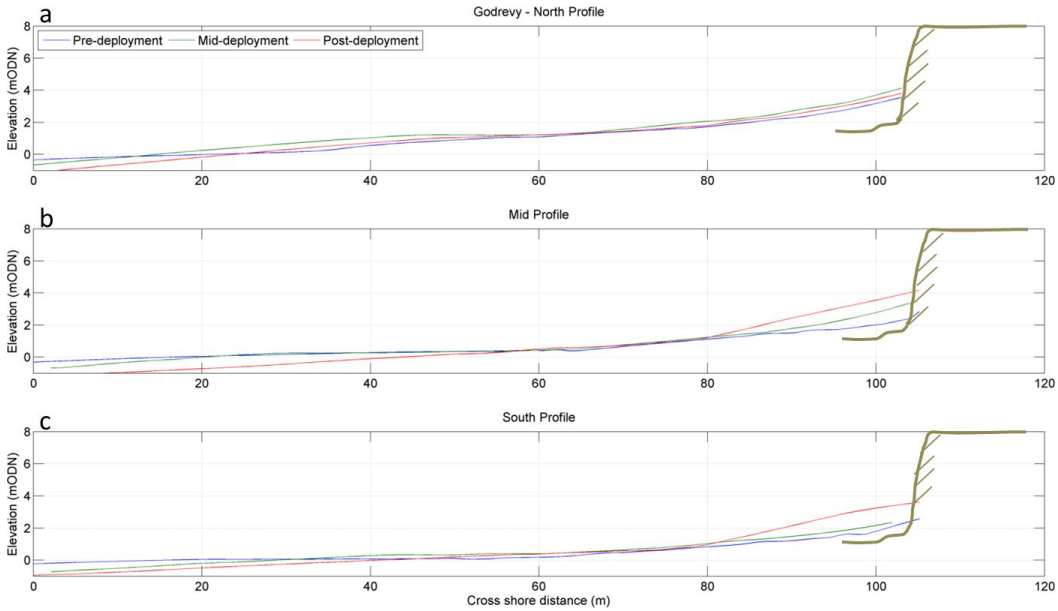

Figure 4.15: Beach profile changes over GOD deployment at 3 locations alongshore (Fig 4.3).Cliff height not to scale.

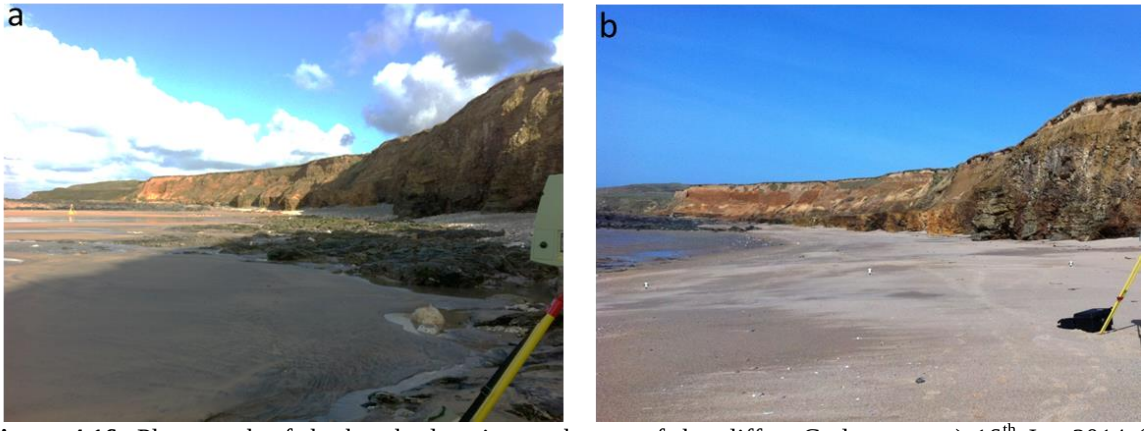

Figure 4.16: Photograph of the beach elevation at the toe of the cliff at Godrevy on a) 16th Jan 2014 (pre-deployment profile in Figure 4.15b) and b) on the 3rd March (Fig 4.15b post-deployment profile).

During the second deployment at Porthleven (PLV2) the beach increased in elevation by about 2 m towards the northern end of the bay, 1 m in the middle and 0.5 m at the southern end of the bay (Fig 4.17). The time period between these surveys were about 1 month and as this beach varies according to the incident wave climate it is difficult to relate the beach volume to seismic ground motion or cliff erosion for this deployment.

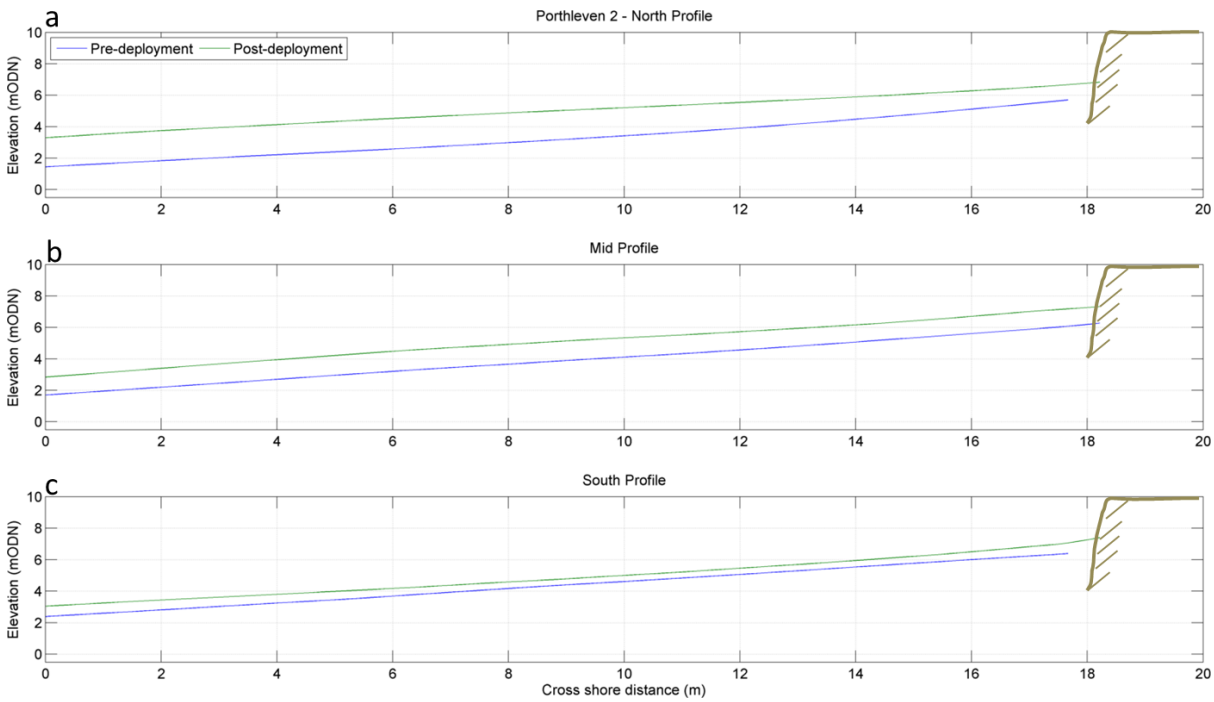

Figure 4.17: Beach profile changes over PLV2 deployment at 3 locations alongshore (Fig 4.3a). Cliff height not to scale.

4.4.4 Cliff volume changes

The cliff volume changes during the seismometer deployments are placed into context when compared with typical monthly erosion volumes at both sites. At Porthleven, stormy conditions hindered scanning during December; therefore the erosion volume over this period is representative of two months. Over the 2 week stormy period in early February (including PLV1) the volume of eroded material contributed to 49% of the annual erosion or the equivalent of 113 m^3 erosion per m of cliff per year (for a 10 m high cliff). This 2-week period is 16% greater in erosion volume than the two month winter period (Nov–Jan). In comparison, the second deployment at Porthleven (PLV2) saw only 0.3% of the annual erosion or 0.3 m^3 per m of cliff per year. At Godrevy, there have been two months over the year that have proved significantly more active than others (32–40 % for Dec–Jan and Jan–Feb) (Chapter 3). The deployment period, and the stormiest period that year (Fig 4.8b) contributed towards 40 % of the total erosion for the year, equating to 16 m^3 erosion per m of cliff per year (for a 10 m high cliff) (Table 4.3).

Table 4.3: Monthly cliff volume changes at both sites over a one year period from July 2013– July 2014. Shaded areas represent deployment periods.

	Porthleven (300 m length, 10 m height)		**Godrevy (300 m length, 10 m height)**	
	Volume erosion (m^3)	% of annual retreat	Volume erosion (m^3)	% of annual retreat
July – Aug	4	0.1	27	2
Aug – Sept	1	0.03	51	3
Sept – Oct	3	0.1		
Oct – Nov	35	1	88	6
Nov – Dec	1184	33	54	3
Dec – Jan			499	32
Jan – 2nd Feb	187	5	629	40
2nd Feb-18th Feb	1771	50		
Feb – March	140	4	148	9
March – April	10	0.3	28	2
April – May	18	0.5	20	1
May – June	6	0.2	8	1
June – July	4	0.1	30	2
Total	**3633**		**1582**	

4.5 Discussion

4.5.1 Tidal modulation of cliff-top velocity energy

As mentioned in section 4.1, the cliff top ground velocities tend to agree with previous studies where velocity increases with increasing wave height and tidal elevation (Adams *et al.,* 2002; Adams *et al.,* 2005; Young *et al.,* 2011; Young *et al.,* 2013). In this section, we explore this relationship further and investigate what drives the variability in energy across the spectrum, between the two sites and across the three deployments.

The vertical velocity spectra were averaged for the different deployments for high tide and low tide periods to compare with the average vertical velocity spectra at the inland seismometer. The purpose of this was to identify energy that was from a coastal as opposed to inland source. At all sites, there is a noticeable difference across the spectrum between the inland and coastal velocity energy apart from within the DF range (0.1 – 0.2 Hz) where inland and coastal energy are the same, consistent with other studies. Above this frequency band, there is a similarity in energy from about 0.2 - 1 Hz during all deployments. The DF band (Fig 4.18a and c) for the Porthleven deployments is wider than for the Godrevy deployment. The averaged plots (Fig 4.18) identify a difference between coastal and inland levels, yet across the time series (Fig 4.10 and 4.12 c and d) the energy fluctuated slightly within this frequency range at both the inland and coastal spectra, making it difficult to differentiate between local and regional energy source. At all other frequencies i.e., from 0.005 – 0.1 and 5 – 50 Hz for Porthleven and 0.005 – 0.1 and 1 – 50 Hz for Godrevy the coastal energy levels are much greater than inland. The average difference between IG and HF energy levels between high and low tide is greater at Godrevy than Porthleven, with an average difference of 2 μm^2/Hz between 0.005 and 0.05 Hz and 1 – 2 μm^2/Hz between 10 and 50 Hz . At Porthleven under calm conditions (PLV2: Fig 4.18c) there is very little or no noticeable difference in energy levels between high and low tide for all frequencies. Only under higher energy conditions, is there a slight difference between SF energy between 0.05 and 0.1 Hz (Fig 4.18a).

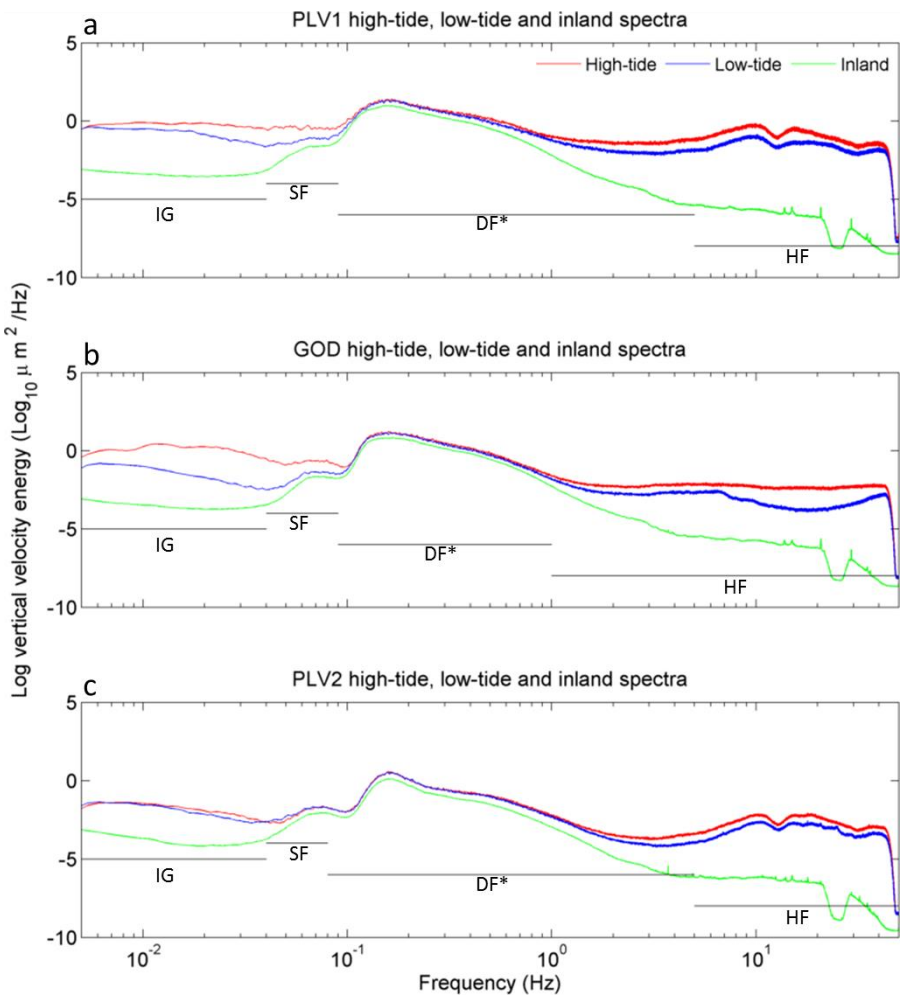

Figure 4.18: Log vertical velocity energy for each deployment a) Porthleven 1, b) Godrevy and c) Porthleven 2. Red and blue lines indicate the average spectra for high tide and low-tide respectively. The corresponding inland average spectrum for the whole deployment period is indicated by the green line. Frequency bands are denoted on each deployment defined according to the full spectra over the time series. * DF includes frequencies noted in the spectra where the inland and coastal energy are very similar.

4.5.2 Cliff-top ground displacements relative to wave climate and water levels

To explore further the physical movement of the ground under wave impacts and varying tidal levels, ground motion is defined here in terms of ground displacement (calculated as the time-integrated velocity) as opposed to velocity. Although both sites experienced extreme storms of similar magnitude, the cliffs responded quite differently. Examples of 1-hr time series of vertical cliff top displacements are presented in Fig. 4.19 for high tide with large and

small waves and low tide, large and small waves under both spring and neap tides for each site.

At Godrevy there is a clear tidal modulation of the signal as displacement almost doubles in magnitude from low to high-tide, regardless of wave conditions and tidal range. A noticeable increase in magnitude (by about double) also occurs from small waves to large waves (from 2 – 3 m H_s to 7 m H_s) (Fig 4.19a and b). Displacements during neap conditions are slightly greater in magnitude than those during spring tide. This is likely to be because the storm that coincided with neap tide on the 8th February was slightly greater in wave energy (~7 m H_s, 20 s. T_p) than the storm that peaked around spring mid-tide on the 15th February (~6 m H_s, 16 s. T_p). Likewise, the displacements under 'calm' wave conditions were greater during neaps than springs, which again is likely to be a result of higher energy wave conditions during that particular tide.

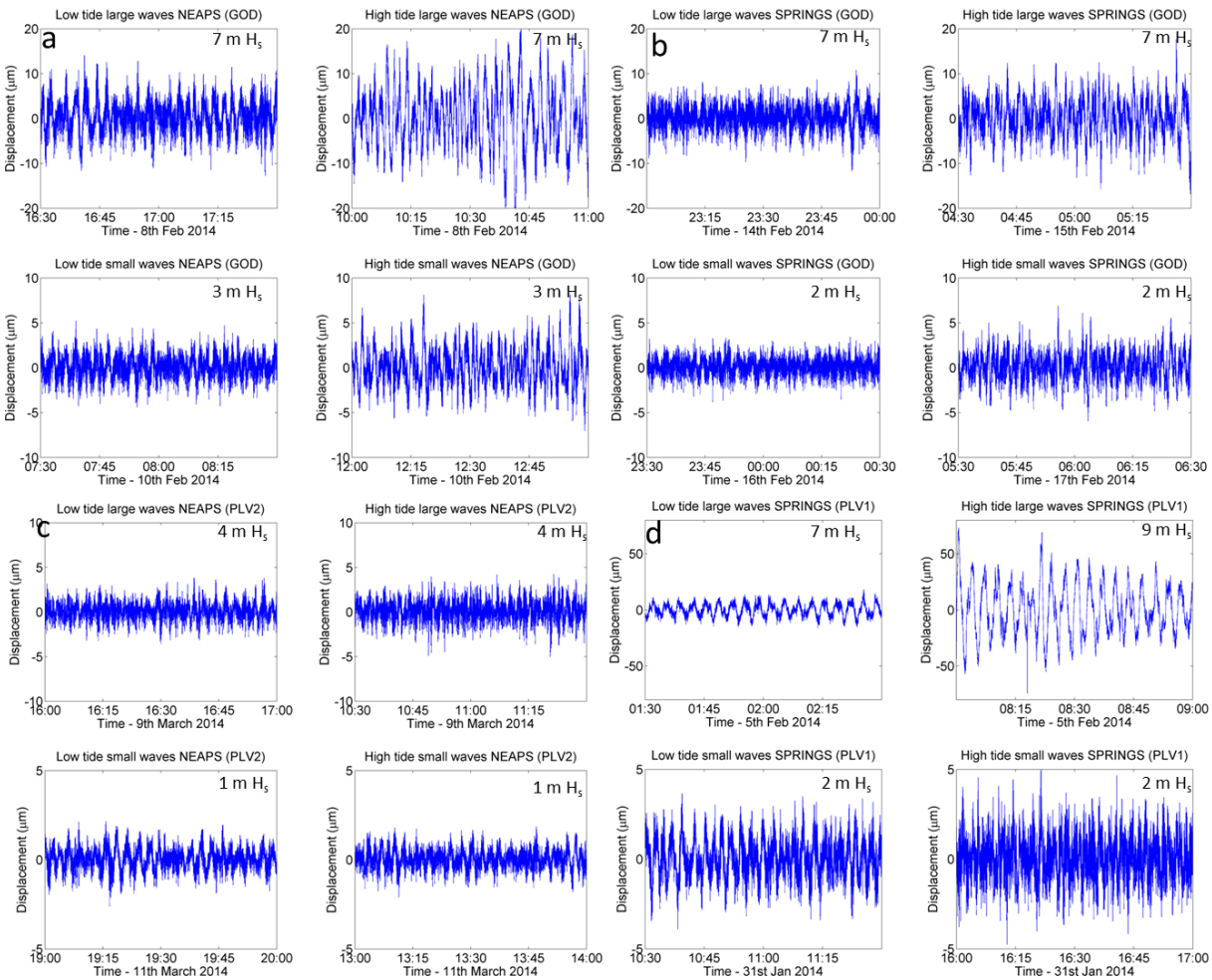

Figure 4.19: Example 1-hr time series of vertical displacements (0.005 – 50 Hz) excluding DF for varying tidal and wave conditions for a) Godrevy during neap tide (3 m range) and b) spring tide (6 m range) an c) Porthleven during neap tide (3 m range) and d) spring tide (7 m range). Significant wave heights represent the inshore wave climate. Note y-axis range is variable depending on energy conditions.

At Porthleven the tidal modulation of the signal is only apparent under spring tidal range conditions. During neap conditions, the displacement signal remains around 2 μm (1 – 4 m H_s). The exceptional nature of the storm on the 5th February is reflected in the massive increase in displacement magnitude from 10 μm under 7 m H_s wave conditions during low tide to 80 μm at high tide when the maximum energy in the storm occurred with waves reaching 9 – 10 m H_s. The storm on the 5th February that affected the south coast and the storm on the 15th that affected the north coast were of a similar magnitude (6 – 8 m H_s) and reached their maximum energy at spring high tide, yet the displacements recorded at Porthleven were almost an order of magnitude greater than those at Godrevy.

4.5.3 Ground motion across the frequency bands

The total hourly vertical displacement energy for all deployments is a function of both incident wave energy and the tidal stage. Figures 4.20, 4.21 and 4.22 illustrate the relationship between tidal elevation, wave energy and cliff top displacement energy. Each 1-hr time series of cliff-top displacement energy is placed within the wave energy and tidal elevation space and each point is scaled by size according to the displacement energy. At PLV1 lower energy values are seen at all states of tide, yet only associated with lower wave energy flux (< 100 kW/m). The highest velocity energy (an order of magnitude greater than 'normal') only occurs during very energetic wave conditions and during mid-high tide (where cliff top displacements exceed 1000 μm/s/Hz and wave power exceeded 200 kW/m). The largest contribution during energetic wave conditions and at higher states of tide is from energy at infragravity frequencies. The hours where there is significant displacement energy during the storms is very clear in the infragravity band (Fig 4.20 a and d), so much so, that these displacement energy values have been down-scaled (divided by 50) in order to plot the points onto the same scale as deployments GOD and PLV2.

At Godrevy, the hourly displacement energy values are more tidally modulated than Porthleven, as displacement energy increases with tidal stage, particularly in the infragravity frequencies (Fig 4.21d). HF and SF displacement energy occurs under all states of tide and wave conditions, and is of a much smaller contribution to the total displacement energy (Fig 4.21 b and c).

Comparatively, under calm conditions at Porthleven (PLV2), the total displacement energy and wave energy is greatly reduced (Fig 4.22) and does not appear to be tidally modulated or regulated by wave climate as seen in Fig 4.12.

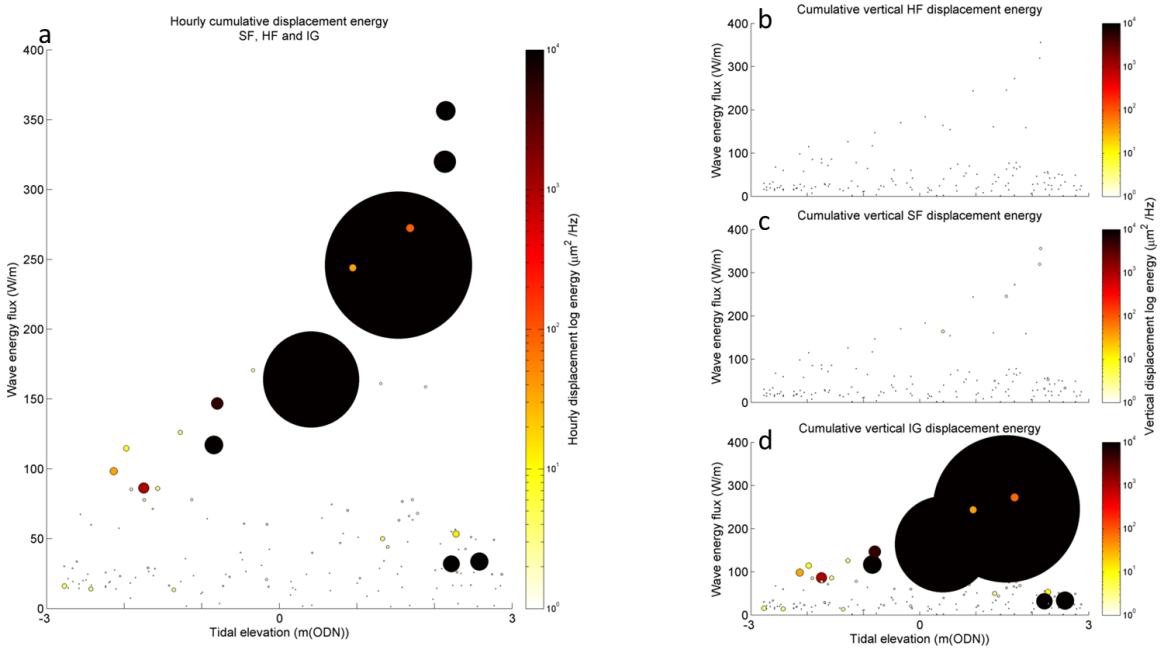

Figure 4.20: Scatter plots of a) total hourly log vertical displacement energy (between 50 – 0.005 Hz) excluding double frequencies (1 – 0.1 Hz) at various states of tide for PLV1. Plots b, c and d represent the total hourly vertical displacement power for the HF, SF and IG bands respectively. Vertical displacement energy is scaled by colour and size of the bubble and plotted logarithmically as the energy increases by orders of magnitude during the extreme events.

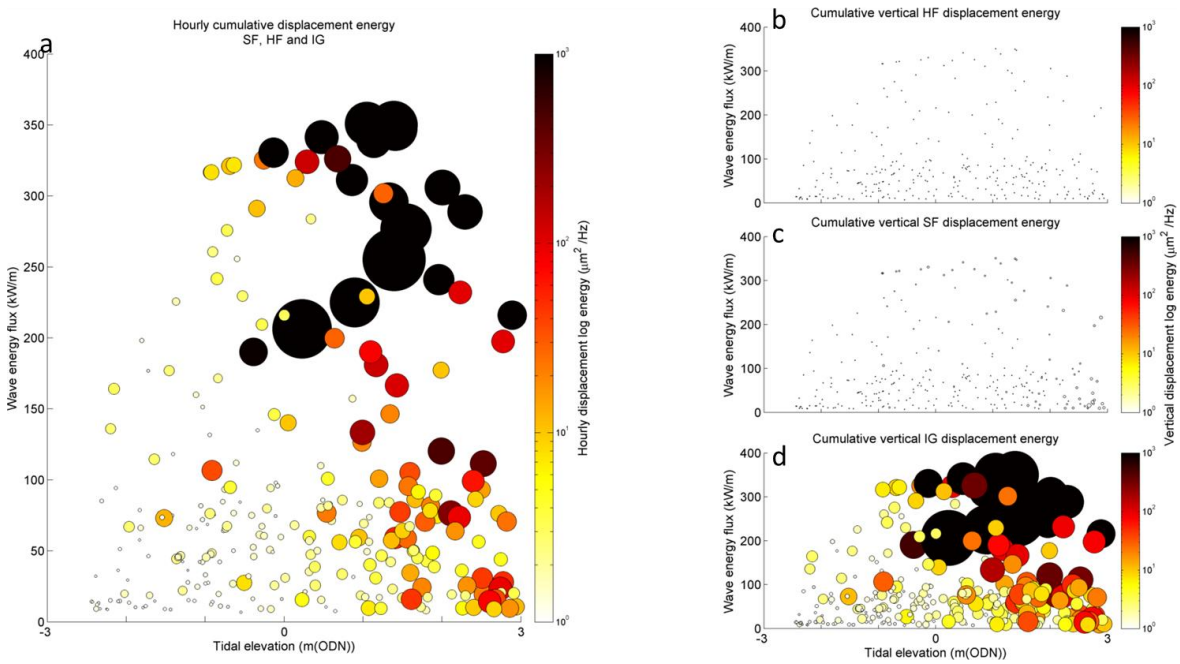

Figure 4.21: Scatter plots of a) total hourly log vertical displacement energy (between 50 – 0.005 Hz) excluding double frequencies (1 – 0.1 Hz) at various states of tide for GOD. Plots b, c and d represent the total hourly vertical displacement power for the HF, SF and IG bands respectively. Vertical displacement energy is scaled by colour and size of the bubble and plotted logarithmically as the energy increases by orders of magnitude during the extreme events.

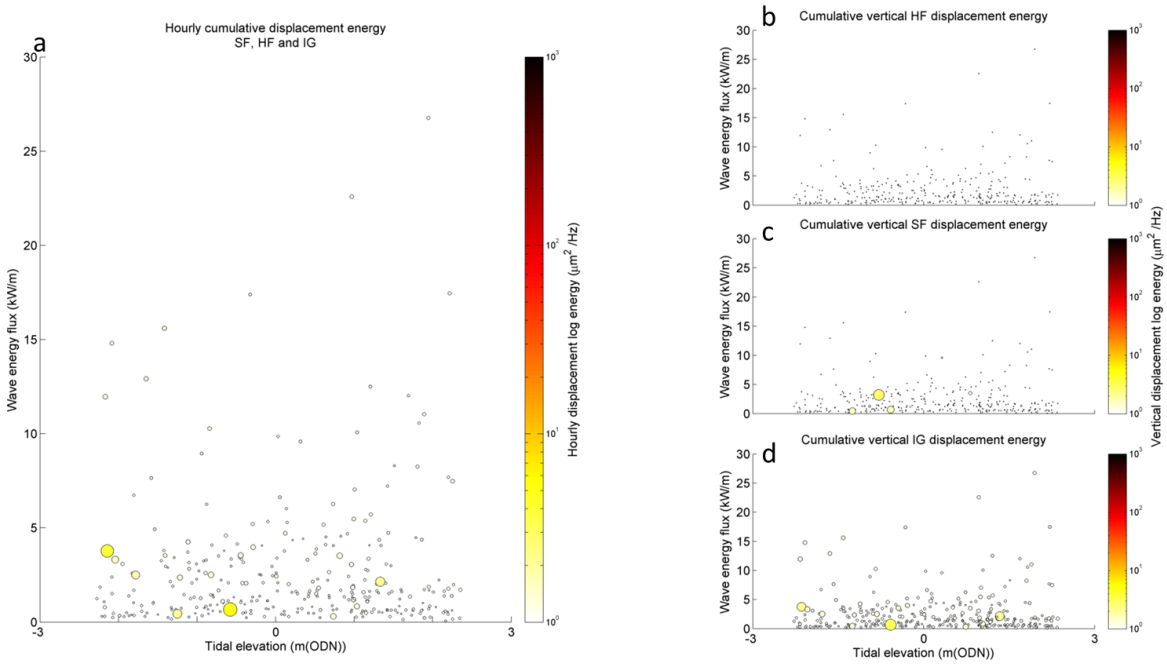

Figure 4.22: Scatter plots of a) total hourly log vertical displacement energy (between 50 – 0.005 Hz) excluding double frequencies (1 – 0.1 Hz) at various states of tide for PLV2. Plots b, c and d represent the total hourly vertical displacement power for the HF, SF and IG bands respectively. Vertical displacement energy is scaled by colour and size of the bubble and plotted logarithmically as the energy increases by orders of magnitude during the extreme events.

4.5.4 Coastal setting

The main difference in ground motion magnitude between the two sites that may be responsible for variation in displacement behaviour is the slope of the beach fronting the cliffs. At Godrevy a large amount of wave energy is dissipated across the shallow intertidal zone before the waves reach the cliffs, whereas at Porthleven the steep beach and steeply shelving bathymetry mean that larger waves break closer inshore and deliver their energy directly onto the beach and the cliffs (Fig 4.23a) (Chapter 3). This is also reflected in the seismic data at both sites where the higher frequencies are apparent in the Porthleven spectra (Fig 4.10c and 4.12c) but lacking in that of Godrevy (Fig 4.11c), suggesting that incident waves tend to impact the beach/cliff more so on reflective as opposed to dissipative beaches. Likewise, the infragravity energy clearly dominant in the Godrevy spectra (Fig 4.11c) is not as obvious in that of Porthleven, which tends to agree with the notion of infragravity energy dominance as beaches become more dissipative (Guza, 1984).

The nature of the beach at Porthleven (coarser material and steeply sloping beach) results in rapid changes to the beach over a short period of time according to the wave conditions.

Energetic, destructive waves, like those seen under the extreme events, remove material from the beach and take it offshore. This lowering of the beach allows formore frequent inundation and therefore prolonged cliff face/toe impacts (Fig 4.13 and Fig 4.22). Under calmer conditions, constructive waves cause the beach to recover very rapidly (Fig 4.15), providing protection to the toe of the cliff via a higher beach elevation and a steeper beach slope. At Godrevy, the changes seen over the storm period indicate an erosion/recovery phase but on a smaller scale than that at Porthleven. This is due, for the most part, to the waves expending most of their energy across the dissipative intertidal zone before they reach the cliffs.

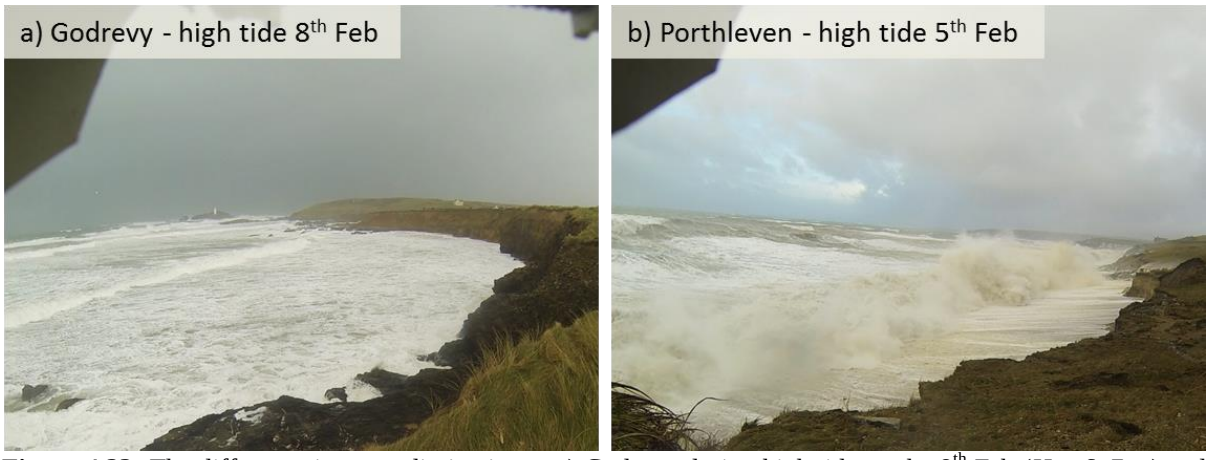

Figure 4.23: The difference in wave dissipation at a) Godrevy during high tide on the 8th Feb (H_s ~ 6–7 m) and b) Porthleven at high tide on the 5th Feb (H_s ~ 8–9 m).

4.5.5 Nearshore hydrodynamics and cliff-top ground motion.

The nearshore wave energy spectra were only available for the second two deployments (GOD and PLV2). During the beginning of the deployment period at GOD, the increase in wave height (and surge) over this stormy period led to the pressure sensor remaining submerged. At PLV2, calm conditions meant the sensor only captured the mid-high-mid tide period. The logistics of deploying nearshore hydrodynamic equipment in a high energy environment made co-locating the seismometer and the pressure sensors impossible and the two signals could not be cross correlated, especially in terms of the phase. However, comparison of the two spectra highlights the agreement between the nearshore wave energy and cliff top displacement energy within the different frequency bands.

At both sites, the most prominent peak in the wave spectra that correlates with the seismometer is within the SF range, between 0.08 and 0.04 Hz. The variability of this peak in the wave spectra as wave period varies across the deployment period is mimicked in the seismic spectra. Under energetic conditions (Fig 4.23a (8th–10th Feb)) the storminess detected in the seismometer between 0.005 and 0.4 Hz is also apparent in the wave spectra. At Porthleven however, the IG energy seen in the nearshore wave energy spectra is not as pronounced in the cliff top. As infragravity energy is a function of deep water wave height (Komar 1998; Guza and Thornton, 1985) this is to be expected at Porthleven under calm conditions. At Godrevy, the infragravity energy in wave spectra dominates the signal under all conditions (Fig 4.24), typical of dissipative beaches, and appears to be less prominent at Porthleven as the steep slope of the beach tends to reflect the infragravity signal (Guza *et al.*, 1984) (Fig 4.25).

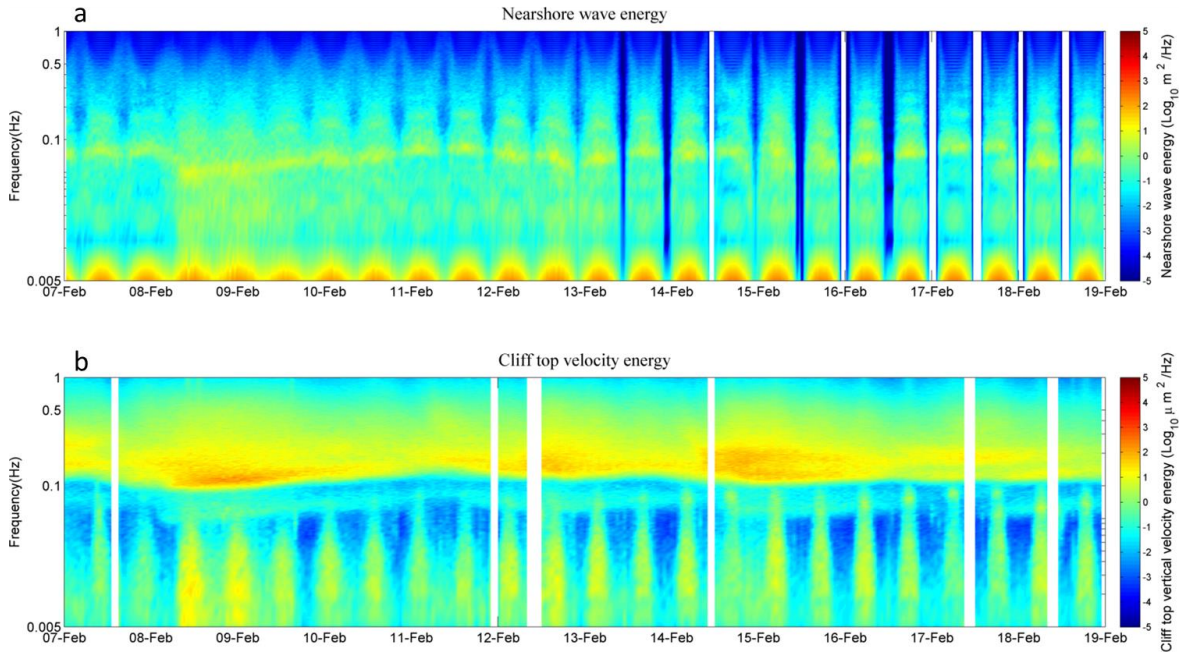

Figure 4.24: a) Wave energy spectra obtained from the nearshore pressure sensor and b) cliff top vertical velocity spectra at GOD.

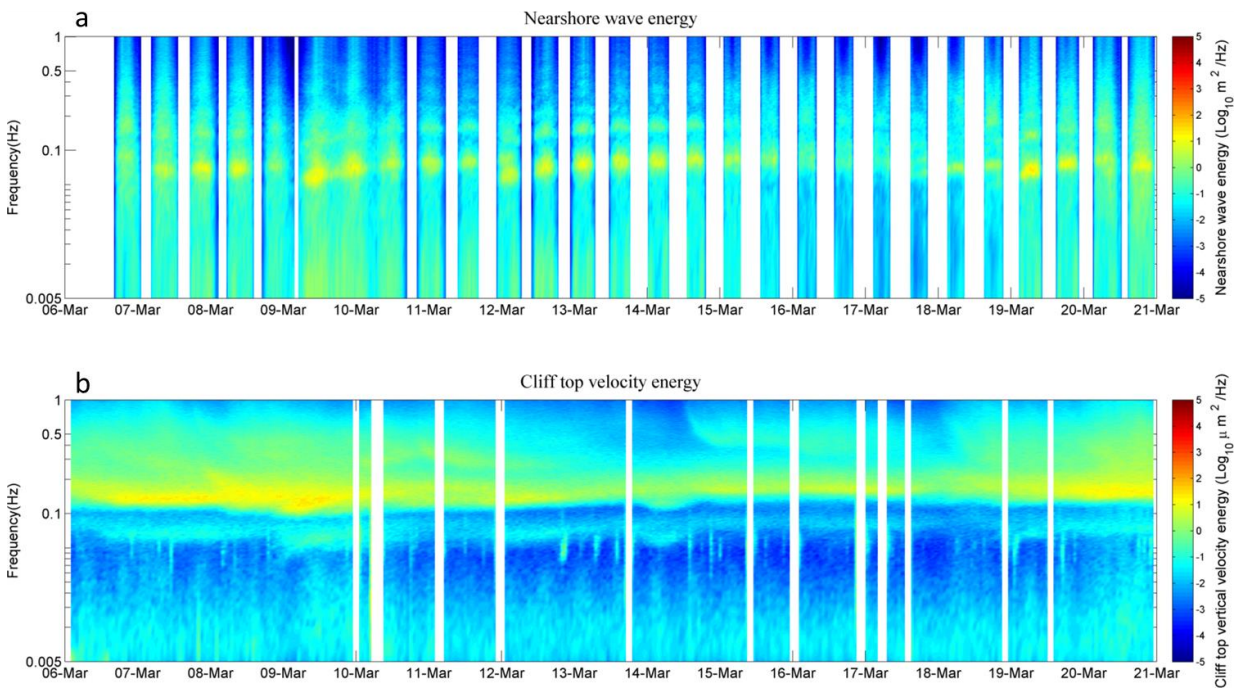

Figure 4.25: a) Wave energy spectra obtained from the nearshore pressure sensor and b) cliff top vertical velocity spectra at PLV2.

4.5.6 Displacements under extreme wave conditions

Although there are no nearshore wave data available for the PLV1 deployment, the camera footage captured during the 5th February storm event at Porthleven shows different periods of wave conditions including: (1) waves breaking on the beach (e.g. Fig 4.27a *09:26:55*); (2) waves breaking at the cliff toe (e.g. Fig 4.27a *09:05:28*); and (3) overtopping of the entire cliff elevation (e.g. Fig 4.27a *08:17:57*) and (Fig. 4.26a).

During each overtopping event, the camera footage showed large volumes of water impacting the top of the cliff and cascading down the cliff face for a number of seconds, the duration of which depends on the scale of overtopping (Fig. 4.26a). The largest vertical displacements (Fig. 4.26b) are coincident with time periods of successive cliff overtopping; suggesting wave loading on the cliff top induces cliff motion and the associated strains and flexure mechanisms during times of wave overtopping. Peaks in IG and HF signals also coincide with time periods of successive overtopping and subsequent cascading events where overtopped water pours down the face of the cliff (Fig. 4.26c and e at 08:15 and 09:05 hrs.). However, not all overtopping events caused significantly elevated seismic signals. Elevated

SF signals occured during some periods of wave overtopping, but the signal variation is less clear compared to timings of the peaks in the IG and HF signals.

The camera footage commenced 30-mins prior to the peak of the high-tide. Wave overtopping was recorded from this point and for up to 90-mins after the peak of the tide. Although cliff collapses cannot be directly coupled with ground displacements, there appeared to be a period of time around the high tide where the majority of failures and wave overtopping occurred. Ground displacement increased in magnitude over this period of elevated tidal levels, suggesting that the cliff underwent an amplified series of strains and flexure mechanisms during times of wave overtopping. Although the timings of the intensive ground displacements did not coincide exactly with the cliff failures, the period of energetic cliff motion coincided with the period of frequent cliff failures.

At Godrevy, no wave overtopping occurred throughout the camera deployment. Waves continually reached the toe of the cliffs with limited impact. The GOD camera was deployed during the most energetic period (high tide 8th Feb); therefore it is unlikely that overtopping occurred during the other extreme events.

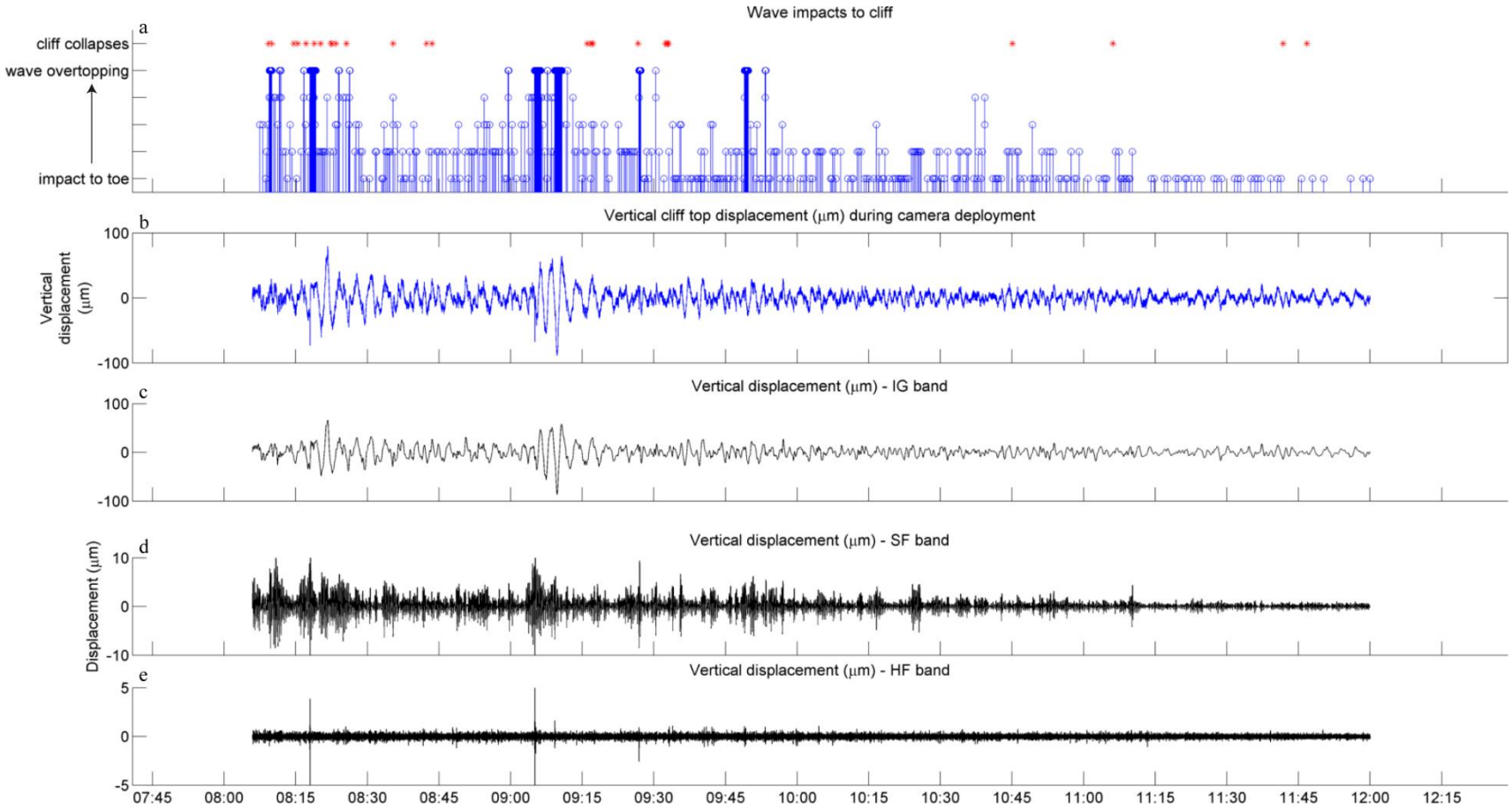

Figure 4.26 (a) PLV1 - Wave impacts to the cliff characterised using the video camera footage, *y*-axis represents a gradual increase in height of wave impact up cliff face, from impact to the toe to overtopping cliff-top, red dots indicate timings of cliff failures. Time series of vertical cliff-top displacement during camera deployment period (08:00 to 12:30 hrs. on 5th February 2014): (b) across all frequency bands (0.005 – 50Hz), (c) infragravity band IG (0.005 – 0.5 Hz), (d) single-frequency band SF (0.1 – 0.05 Hz) and (e) high-frequency band HF (1 – 50 Hz). High-tide on the 5th Feb occurred at 8.31am.

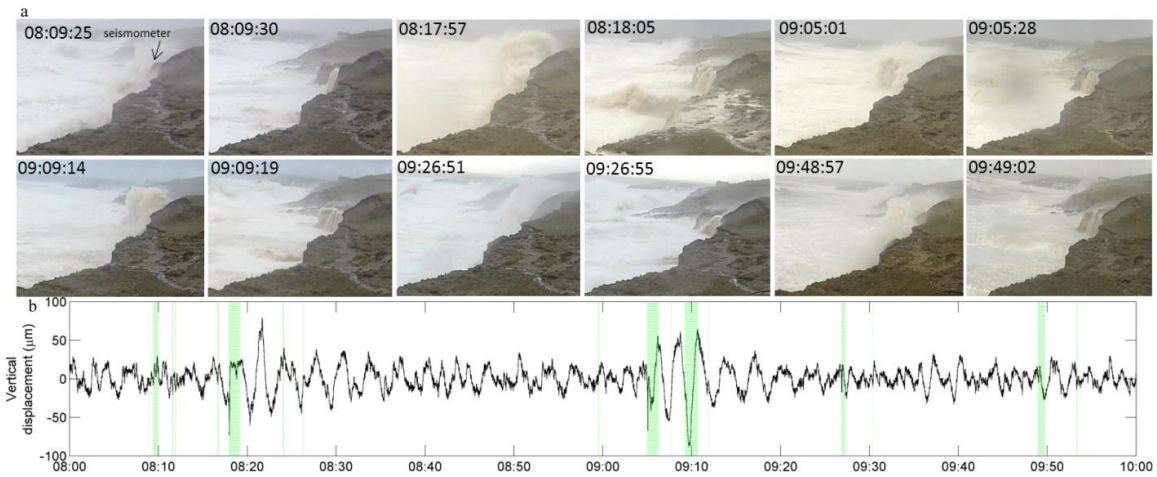

Figure 4.27: (a) Stills from camera footage, illustrating successive wave overtopping and subsequent drainage events on the 5th February 2014 from 08:09 to 09:49 hrs. Overtopped water cascading down the cliff-face seen in the stills corresponds with the shaded regions of plot b. (b) Vertical displacement during this period. A 60-sec movie clip during the camera deployment is provided as supplementary material for Earlie *et al.*, (2015).

4.5.7 Geomorphic perspective and relation to cliff face development

The consequences of these unusually large-scale cliff-top displacements (50 – 100 μm) under the largest wave conditions seen in 60-yrs in terms of rock damage from coastal flexing are unknown. However, previous research has suggested that although displacements under 'normal' conditions are not likely to contribute towards weakening of rock structures, episodic displacements caused by extreme wave conditions may contribute as a fracture mechanism that may be responsible for failure in metasedimentary cliffs (Brain *et al.*, 2014).

Alongside cliff face volume changes, the location of erosion across the cliff face can be detected. At both sites, the cliff decreases in resistance with height, with softer less resistant quaternary head deposit overlaying more resistant bedrock. This upper unit is more susceptible to erosion/weathering due to rainfall (Shail *et al.*, 2010) as an increase in pore water pressures can lead to slope failure. This erosion pattern tends to occur at both sites in the monthly volume difference plots in Chapter 3.

The long-term annual retreat rate for Porthleven, obtained from aerial photography and averaged over 50 yrs (Ridgewell and Walkden, 2009), is 0.1 myr^{-1}. This value was also found by Earlie *et al.* (2014) using airborne LiDAR over a 3.5 year period (0.09 m yr^{-1}). Assuming a cliff height of 10 m, a long-term cliff recession rate of 0.1 m yr^{-1} equates to an annual cliff volumetric loss of 1 m^3 per m length of cliff. Terrestrial laser scans over the 2-week storm

period show that the 300-m long cliff section eroded 1350 m^3 (Fig 4.28a), which represents 5.9 m^3 average erosion volume per m length of cliff over the 2-week period, or an annual cliff volumetric loss of 113 m^3 per m length of cliff. The annual cliff volumetric loss over the 2-week storm period is therefore more than two orders of magnitude greater than volumetric loss based on the long-term cliff recession (i.e., 113 m^3 m^{-1} yr^{-1} *versus* 1 m^3 m^{-1} yr^{-1})(Table 4.3).

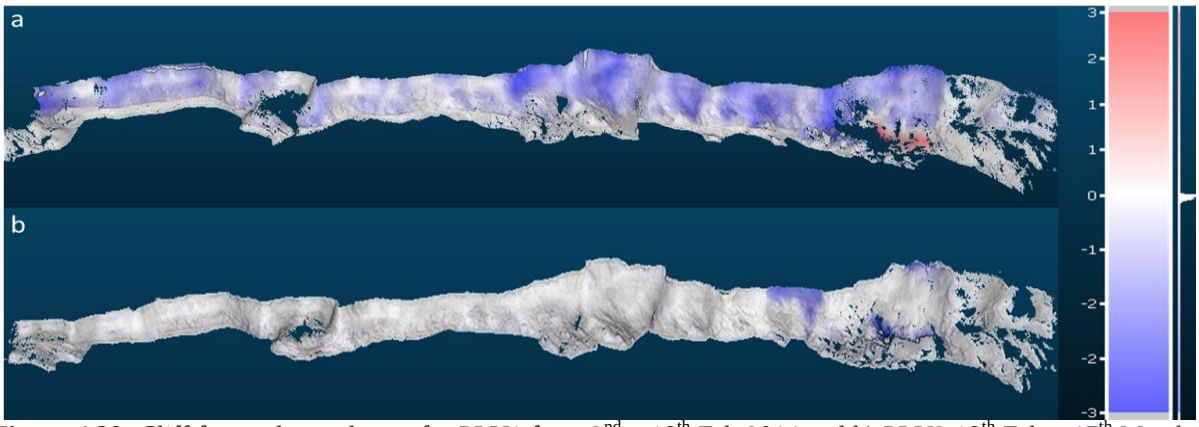

Figure 4.28: Cliff face volume change for PLV1 from 2nd – 18th Feb 2014 and b) PLV2 18th Feb – 17th March. Erosion scale is in m, measured normal to the direction of the surface

At Godrevy, the long term erosion rate is 0.04 myr^{-1} equating to an annual cliff volumetric loss of 0.4 m^3 per m of cliff per year. Over the deployment period (Jan – Feb 2014) the cliff face eroded 629 m^3, representing 40% of the total annual retreat and an annual rate of 25 m^3 per m cliff length per year. At Godrevy under extreme conditions, the failures are again typically focused towards the softer material in the cliff. During this particular month the main cliff failure occurred towards the northern end of the beach where the boundary between the two units falls almost to beach level. As this section of the cliff is mainly comprised of quaternary material and blown sand it is more likely to be eroded by rainfall or saturation of the cliff profile as opposed to wave overtopping and wave impacts weakening the integral structure of the bedrock itself.

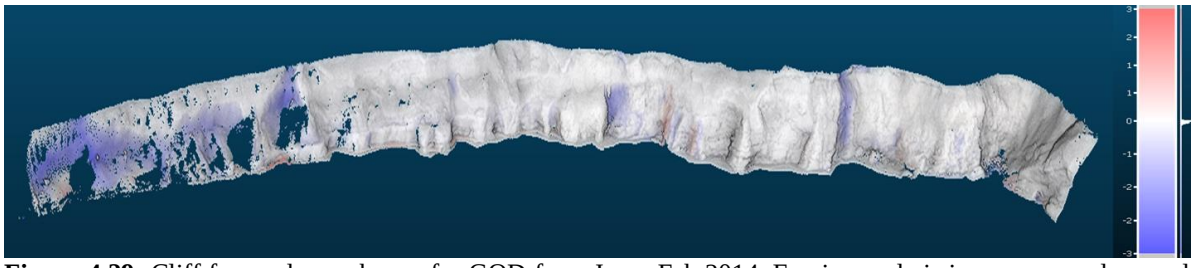

Figure 4.29: Cliff face volume change for GOD from Jan – Feb 2014. Erosion scale is in m measured normal to the direction of the cliff surface

Under calmer conditions at Porthleven (PLV2), much like the cliffs at Godrevy, failure is focused mainly on the softer upper unit, as a result of weathering and rainfall induced erosion (Chapter 3). During the stormy period at Porthleven (PLV1), the volume change was two orders of magnitude greater than the typical monthly erosion volume and erosion occurred across the entire cliff face. The video footage captured constant wave impacts and overtopping during this time, saturating the cliffs and leading to failure. The volume loss measured over this time period is therefore a direct consequence of the extreme wave activity.

At Porthleven, during the 4.5-hour camera deployment the video footage clearly shows failure of cliff material throughout with over 30 failures recorded when energetic wave conditions and regular cliff overtopping prevailed; such cliff failure is not observed under calmer conditions, even at high-tide. This strongly suggests that the observed cliff failures have been triggered by the direct combination of wave impacts and overtopping, and possibly facilitated by the weakening of the cliff through microcrack density growth, such as suggested by Adams *et al.* (2005) and Brain *et al.* (2014). The significance of these extreme wave events on erosion cliff morphology is further highlighted by the observation that the total erosion volume over the 2-week storm period not only exceeds the long-term erosion rate by two orders of magnitude but also accounts for more than half (50%) of the total volumetric loss for the year 2013 – 2014 with reportedly the most severe winter wave conditions on record.

4.6 Conclusions

Vertical cliff top ground motions measured at two locations during an exceptionally stormy winter period in the UK were found to increase with increasing H_s and tidal elevation. Cliffs fronted by a reflective beach along the south coast of the UK, during extreme wave conditions (H_s exceeding 6 m) experienced vertical ground displacements increasing by an order of magnitude from 10 μm to 100 μm. Cliffs along the north coast fronted by a dissipative beach saw ground displacements increase from 2 – 5 μm to 5 – 20 μm. During calm conditions at both sites displacements reduced to ‘normal’ levels consistent with previous studies (0.5 – 10 μm).

Magnitudes of cliff top ground motions were found to be modulated differently according to the nearshore hydrodynamics and water levels, but according to the beach type fronting the

cliffs, with a higher proportion of IG energy in dissipative beaches compared with reflective, with the exception of periods of very high energy waves. Real time cliff top video capture and *in-situ* wave monitoring equipment during exceptionally energetic periods allowed for association of the large ground displacements with the nearshore hydrodynamics, as well as cliff-top wave overtopping events at one site. During this time the greatest ground motion contribution (~100 μm) originated from displacements in the IG frequencies (0.005 – 0.05 Hz). The displacement peaks in the SF (0.05 – 0.1 Hz) of 10 μm and HF (1 – 50 Hz) of 5 μm also coincided with the timings of the wave overtopping events captured with the video camera.

Cliff-face volume erosion measured over the deployment periods showed that during the extreme events on the southwest coast with cliffs fronted by a reflective beach, the long-term erosion rate was exceeded by more than two orders of magnitude (i.e., 113 m^3 m^{-1} yr^{-1} *versus* 1 m^3 m^{-1} yr^{-1}) and accounted for over half the total volume loss for the year. On the north coast with cliffs fronted by an intermediate beach, with storms of similar magnitude impacting the coastline, erosion volumes were one and a half orders of magnitude greater than the long term erosion rate (i.e., 25 m^3 m^{-1} yr^{-1} *versus* 0.4 m^3 m^{-1} yr^{-1}) (Ridgewell and Walkden, 2009; Earlie *et al.,* 2014), thus providing a geomorphic link between energetic cliff-top ground displacements and cliff failure.

This is the first time that remote (camera) and *in-situ* (seismometer) observations of cliff top ground measurements coupled with wave impacts been accomplished under such energetic wave conditions. Capturing these events during one of the stormiest periods the region has seen in 60 years, highlights the role extreme events play in contributing towards coastal cliff morphology.

Chapter 5

Discussion and Synthesis

5.1 Broad aims and outcomes

The overall aim of this thesis has been to develop a quantitative understanding of cliff erosion rates around a rocky coastline and relate the variability in erosion to the geomorphic controls and physical processes. This has been addressed by considering cliff change within a range of spatial and temporal scales, and adopting techniques to measure change appropriate to those scales. Throughout the thesis, the research has specifically drawn on the influence of the wave climate and on cliff erosion volumes. Furthermore, the results have highlighted how the offshore bathymetry and beach morphology fronting the cliffs modulate the dissipation of wave energy and therefore play a crucial role in limiting the extent of wave-cliff interaction. In coastal cliff environments, waves are typically understood to erode the toe of the cliffs, forming wave-cut notches leading to cantilever failure of upper cliff material (Trenhalie, 1987; Sunamura, 1992). Recent field observations (Norman, 2012; Vann Jones *et al.*, 2015), along with the results of this study, have found that wave action is responsible for the erosion of the entire cliff face, in the form of slope-over-wall failure, rotational sliding and planar/wedge failure and abrasion/quarrying of the entire cliff face as well as the cliff-toe, particularly under extreme storm conditions. A key theme running throughout the thesis is the importance of understanding and measuring localised changes that ensue as a result of seasonal conditions and extreme storm events. With the potential for increased storminess associated with climate change (Dodet *et al.*, 2010); it will become more and more prudent to understand the processes occurring under such conditions (i.e., wave-cliff impacts and overtopping, morphology of the beach and volumes of cliff erosion) for future coastal management purposes.

5.2 The broader context

The findings of this thesis are important for two main reasons. Firstly, this research contributes towards the broader geomorphological understanding of the behaviour of cliffed coastlines. There is a limited amount of research on rocky coastlines (Naylor *et al.*, 2010) and

studies that do exist, in the UK, tend to focus on softer rock cliffs (Lee, 2008; Lim *et al.*, 2011; Carpenter *et al.*, 2014). Few studies consider hard-rock coastlines or composite cliffs, (vertically variable in their resistance to erosion), such as the cliffs of the southwest of England. Only recently have cliff erosion studies begun to focus on the interaction between waves and cliff-top ground motions (Adams *et al.*, 2002; 2005; Young *et al.*, 2011; Dickson and Pentney, 2012; Norman, 2012; Young *et al.*, 2012; 2013, Vann Jones *et al.*, 2015), and until this thesis, particularly highly energetic conditions have never before been captured. The rarity of field based wave-cliff interaction investigations means that most proxies for wave-cliff interaction remain theoretical. It is proposed that the results of this study will contribute towards refining our understanding of how waves, beaches and cliff systems interact and may ultimately feed into process-based cliff erosion models. Secondly, it is intended that a more comprehensive understanding of how rocky coasts evolve and how the whole coastal system interacts, particularly under extreme storm conditions, will help to inform more sustainable coastal management decisions in the future.

5.3 Thesis approach

The approach of the thesis has been to consider three different time and spatial scales, dividing the main body of the research into three core chapters. Although each of these chapters can be considered a stand-alone project in isolation, the results of each chapter defines the direction of the next, with key themes evolving throughout the thesis, based on the initial research questions:

1. What factors explain the spatial variability in erosion around a rocky coastline? (*Chapters 2, 3 and 4*)

2. How useful are remote sensing techniques such as airborne LiDAR (*Chapter 2*) and terrestrial laser scanning at capturing coastal cliff change? (*Chapter 3*)

3. What role do the nearshore hydrodynamic regime, offshore bathymetry and beach type play in the variability of cliff erosion? (*Chapters 2, 3 and 4*)

4. How do the cliffs respond to a highly energetic wave environment and which factors contribute to controlling the energy expended on the cliffs? (*Chapters 3 and 4*)

5. How do wave induced cliff-top ground motions respond to waves under different coastal settings i.e., cliffs fronted by a reflective versus a dissipative/intermediate beach? (*Chapter 4*)

Some of the questions are pertinent to all of the chapters (i.e. questions 1 and 3) within the context of the relevant time and spatial scales, whereas other questions are related specifically to a particular scale (i.e. questions 2, 4 and 5). This chapter aims to synthesise the main findings of the thesis in the context of these research questions. Figure 5.1 illustrates the flow of the thesis, summarising the main aims and outcomes within each chapter.

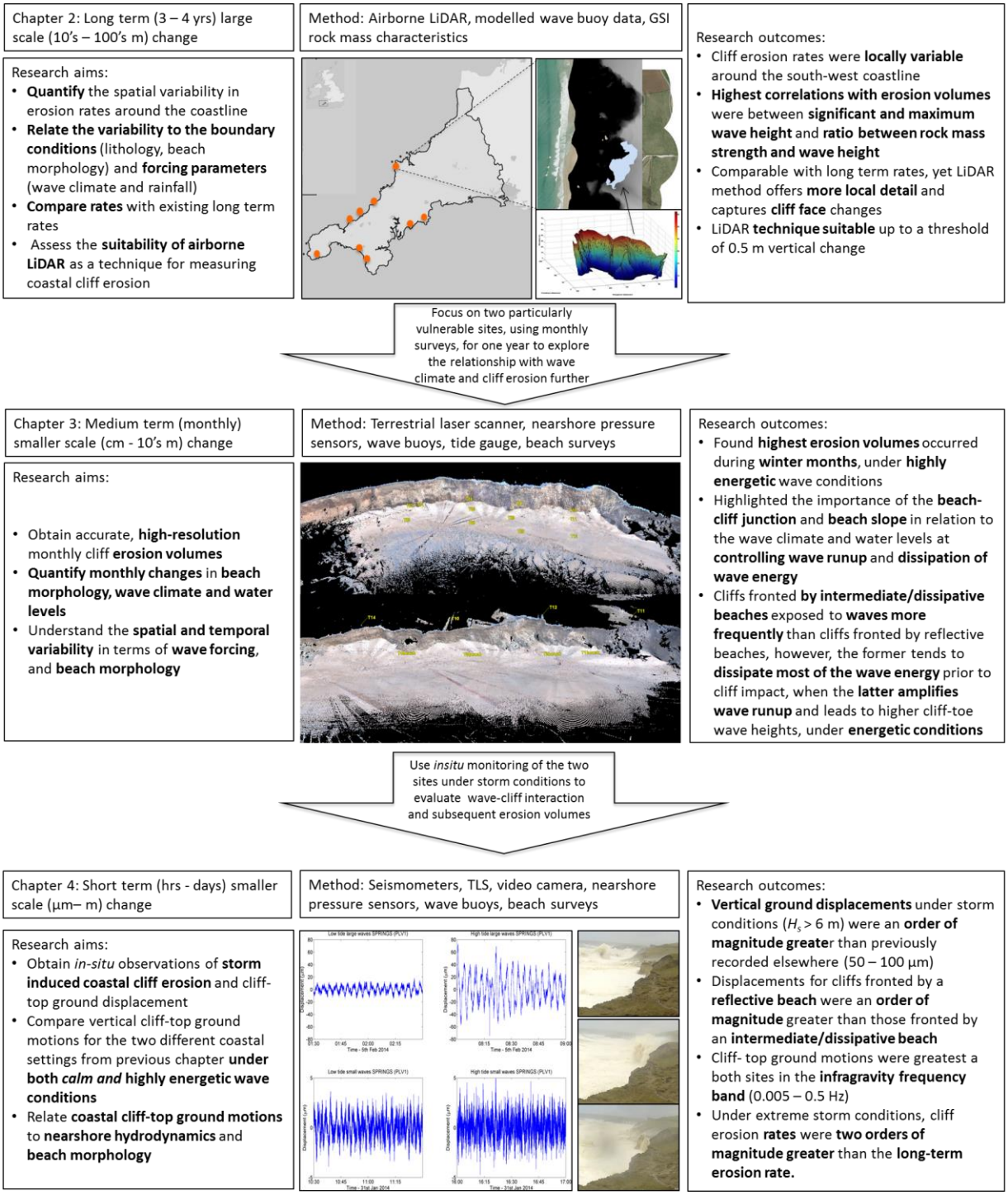

Figure 5.1: Flow diagram summarising the aims and conclusions of the three main data chapters. Major themes and findings are highlighted in bold text. All figures are taken from the relevant chapters.

5.4 Thesis themes

5.4.1 An issue of scale: temporal and spatial scales of measurement and change

The first research question is regarding the processes which govern the variability of erosion rates around the coastline. This question is mainly addressed in Chapter 2, yet these processes are examined throughout the entire thesis. A topic that arises from this and the second research question (regarding the suitability of various methods), is the issue of scale, both temporally and spatially. When considering change at a certain scale it is important to adopt a method of measurement that captures change appropriate to that scale. Likewise, when investigating the evolution of rocky coasts, it is beneficial to consider a range of scales, allowing for the inclusion and comparison of the variety of processes which operate at different scales (Naylor *et al.,* 2010). Adopting different techniques and comparing results is a way of assessing the suitability of a particular technique at measuring change at a particular scale. This section summarises how the issue of scale has been addressed throughout the thesis and discusses the advantages and limitations of each of the methods.

The variability of erosion rates is addressed firstly in Chapter 2, where erosion is considered on a large spatial scale, 10's to 100's of metres of cliff length, at nine sites, around a peninsula covering c. 850 km of coastline (Ridgewell and Walkden, 2009). Long-term coastal cliff erosion rates used for shoreline management purposes are typically based on comparisons of aerial photographs or historic maps, encompassing decadal change (Ridgewell and Walkden, 2009; Earlie *et al.,* 2012). This large-scale, very long-term method (50–100 yrs) integrates both continuous, high-frequency, low-magnitude and sporadic high-magnitude, low-frequency changes, averaged out over a long period of time. Although this provides an indication of changes occurring over decades, it lacks both the spatial detail and temporal resolution required to; a) differentiate between the continuous and sporadic changes b) relate forcing mechanisms to failure.

Chapter 2 considers changes which have occurred in a 3–4 yr. time scale (2007/2008–2010/2011), referred to in this thesis as the *longer-term* time scale. The LiDAR technique adopted in this chapter was suitable for obtaining large scale, high-resolution, three-

dimensional surface models of the cliff (0.5–1 m) and comparing change over a shorter, *long* time scale. Using this technique, both sporadic and continuous changes were identified within the DEM's (Digital Elevation Models) within this time frame, under this spatial scale. Overall erosion/weathering was detected via a gradual retreat of the cliff face (provided the erosion is greater than the error associated with the technique (Chapter 2)) as well as regions where larger scale failure has occurred. Erosion rates established using LiDAR were comparable to the long term erosion rates, yet offered additional insight into the failure occurring to the cliff face that is lacking in cliff-top evolution methods, such as historic map and aerial photograph analysis. The results of this chapter indicated that although the detail provided using this method was appropriate to the time and spatial scale considered, a furthered understanding of the relationship between forcing mechanisms and failure would be facilitated by using a more refined method of cliff-face data capture, over a higher resolution time scale. The results also indicated that although a general overview of the wave climate was appropriate to the scale used, the time step between the DEM comparisons was too large to directly couple failure with forcing events (storms). Beach-cliff junction elevations were taken as an average value from each of the LiDAR surveys. Chapters 3 and 4 concluded however, that it was not only the elevation of the beach-cliff junction and the slope of the beach that were major drivers in controlling wave-cliff interaction, but also the variability of this beach morphology over time.

The limitations associated with using LiDAR data emphasised the importance of down-scaling field observations both spatially and temporally, in order to understand the processes causing cliff erosion. Chapter 3 therefore focussed on two rather than nine sites and monitored change on a smaller spatial (cm – 10's of metres) and time scale (monthly). Monthly beach and cliff surveys were carried out for one year at both sites, and continuous wave and water level data were obtained from inshore wave buoys (10 m water depth), nearshore pressure sensors and tide gauges. The monthly wave climate averages, erosion volumes and beach elevations meant that failure could be implicitly linked to forcing within the time frame of one month. Terrestrial Laser Scanning (TLS) was a suitable technique for the medium-term time scale as it provided the spatial resolution required to confidently capture smaller scale (cm's) changes to the cliff face, which were likely to be occurring within this time scale. In a long-term time scale, one year is typically not a sufficient enough length of time to capture extreme events, as such events that could cause catastrophic failure

tend to occur over a longer return period (e.g. 1:10–1:100 yr. event). Although monitoring change for a one-year period limits the likelihood of capturing an extreme storm event, 2013–2014 happened to be one of the stormiest years the region had experienced in 60 years. Not only did this provide extreme storm conditions within the data set, but it also meant that over the year, a wide range of hydrodynamic and morphological conditions were measured. Monthly cliff surveys provided insight into the failure occurring over the year and allowed for linking the timing of failure to the associated average wave and beach conditions. The results, however, indicated that the monthly time scale of the surveys, in particular the beach surveys, was too coarse to evaluate the role of beach morphology on controlling wave-cliff impacts. In addition to this, more frequent cliff scanning surveys, especially during extreme events, would have helped to determine timings of failure more accurately.

Point cloud data comparisons provided evidence of failure locations across the cliff face, which proved to be indicative of the forcing mechanisms. Point cloud difference plots revealed whether the bedrock or the superficial material had been eroded, and when (to within a month). For example, at Godrevy, heavy rainfall and stormy conditions during December 2013 and January 2014 proved to be conducive to slope-over-wall and rotational failure of superficial material and at Porthleven a two week survey period over the storms of February 2014 led to the erosion of 85% of the entire cliff face. These monthly surveys captured cliff volume changes at a range of scales (cm – m) and were able to determine the cause of the failure with confidence. The surveys showed a strong correlation of failure with periods of extreme wave energy flux and highlighted the significance of understanding wave-cliff interaction on a shorter-term time scale to understanding cliff failure processes.

The same method of cliff face data capture (TLS) was adopted for Chapter 4, to monitor wave-cliff interaction on a very short-term time scale and at a high spatial resolution. An interim scan was carried out at Porthleven, during the stormy period between Jan and Feb 2014. This two-week scan captured a massive amount of cliff erosion (1771 m^3 of erosion, equating to 50% of the erosion for the whole year), which indicated that during highly energetic conditions, even higher frequency cliff scans (perhaps every low tide) should be undertaken to directly couple forcing with failure.

The vertical displacement of the cliff top that results from waves loading/unloading/reflecting from the foreshore and from wave-cliff interaction was measured at a high frequency 100 Hz

with a broadband seismometer. This instrument was deployed at the same two sites (Godrevy and Porthleven) over a 4–5 week period. This method captured potential structurally influential changes to the cliffs with cliff top displacements in excess of 50 μm during an extreme storm event. Although this is very small scale movement, it has been hypothesised that repetitive flexure of the cliff (Adams *et al.,* 2005; Brain *et al.,* 2014; Earlie *et al.,* 2015), combined with ground saturation from waves overtopping the cliffs led to the large volume of erosion during this time. At one of the sites (Porthleven) three beach surveys were carried out over a 36-hr period during one of the extreme storm events (1st–2nd Feb 2014). Beach elevations fluctuated by > 3 m over this short time period, and for the low tide of 2nd Feb (am) the beach elevation was lower than the elevation of the access point, preventing access to the beach to carry out the survey. This high-magnitude fluctuation of beach level occurring over a short time period suggests that over particularly energetic periods, some form of continuous, or high-frequency monitoring of beach elevations is required to accurately quantify wave runup and wave-cliff impacts.

During the most destructive of the 2014 winter storms (5th Feb at Porthleven), remote sensing (using video cameras) provided additional detail of wave-cliff interaction that could not be captured using *in-situ* instrumentation (Earlie *et al.,* 2015). Due to the highly energetic nature of the storm, all wave and water level monitoring instruments malfunctioned. The video footage recorded direct wave-cliff impacts, cliff top wave overtopping and failure of cliff material. This meant that a coupling of wave action and the seismic signal could be approximated. Using higher resolution, georeferenced remote sensing equipment (such as ARGUS-style cameras) this relationship could be explored further in future studies, especially under extreme events when direct wave-cliff measurements are hampered by stormy conditions.

5.4.2 Environmental controls on cliff erosion

5.4.2.1 Consideration of environmental controls over the three time and spatial scales

Coastal cliff erosion studies require a robust examination of the environmental controls on cliff erosion, i.e. the assailing forces (waves and weather) in relation to the resisting forces (geology, bathymetry, beach morphology, rock mass characteristics) (Trenhaile, 1987; Sunamura, 1992; Naylor *et al.,* 2010). For the long term time scale (Chapter 2) the wave

climate (significant wave height and wave period) was averaged over the year to obtain a generalised view of the regional assailing forces at each site. Rainfall was not considered in this chapter, as there was little variability in total rainfall values over all of the sites, over a 3–4-yr period. Cliff geology, and rock mass characteristics were quantified based on the Hoek *et al.* (1998) Geological Strength Index, and average cliff heights and beach-cliff elevations were identified from aerial photographs and LiDAR data. Although these were approximations of the environmental controls, they offered sufficient detail to enable a comparison of controls at each site with the erosion rates. In Chapter 3, the environmental controls were quantified using higher resolution data at shorter time steps. The wave climate and rainfall were examined in line with the time scales of the cliff scans (TLS) and beach survey data; where continuous data were averaged (waves) or summed (rainfall) over the survey periods. Monthly approximations of beach slope were determined from GPS beach surveys and beach-cliff junction elevations were estimated from TLS point cloud data. These field data provided a comprehensive time series over a 1-year period at two different sites in order to establish on a monthly basis how the beach, waves and water level were influencing the erosion of the cliffs. Consideration of the resisting forces, in terms of geological controls, was approached in a more geotechnical manner in Chapter 3, examining the failure mechanisms occurring from month to month, as opposed to the structure and characteristics of the rocks themselves. The topic of environmental controls was taken a step further in Chapter 4, where the interplay between the assailing and resisting forces was explored by examining the interaction between the cliff-top vertical ground motion and the nearshore wave spectra at two different sites under similar forcing conditions (tides, waves). Differences in the energy spectra for the cliff top ground displacements between the two sites revealed the importance of the dissipation of wave energy prior to wave-cliff impact.

5.4.2.2 Geological controls

The geological control on coastal cliff erosion has been approached in a qualitative way throughout the thesis. In Chapter 2, however, the rock mass strength of each of the nine sites is based on a visual analysis of the bedrock joint characteristics (GSI, Hoek *et al.*, 1998). The purpose of this was to determine the spatial variability in rock mass strength at each site and to correlate this with the spatially variable erosion rates (r value 0.66). A stronger relationship occurred however, when the ratio between the rock mass strength and the significant wave

height was correlated with erosion rates (0.77), supporting the notion that cliff erosion occurs when the assailing forces exceed the resisting forces (Sunamura, 1992).

For the experiments involving the two sites (Chapters 3 and 4) a qualitative geological description of the cliffs was sufficient to explain the volumes of erosion and failure mechanisms at each site. Without carrying out extensive geotechnical analysis of the cliffs it is difficult to assess the detailed structural controls of the rocks; such analysis is beyond the scope of this thesis. Locations of failure were visible in the TLS scans, from which approximate failure mechanisms could be determined. At Godrevy the elevation of the boundary between the bedrock and the superficial material proved to be the key geological control of cliff failure. Towards the northern end of the cliffs, the boundary falls to almost beach level and rises to the full height of the cliff at the southern extent. Erosion was constrained to this upper, less resistant unit throughout the survey year (Jul 2013–Jul 2014), with erosion occurring via slope-over-wall or rotational failure, apart from under extreme wave conditions, when quarrying of the lower bedrock occurred. At Porthleven, very little erosion occurred during the autumn, spring and summer and was limited to spalling of the upper, superficial unit. During the winter, however, erosion of both upper superficial and lower bedrock occurred. The failure mechanism was difficult to determine as the entire cliff face appeared to retreat homogenously alongshore and vertically.

5.4.2.3 Meteorological controls

In the absence of detailed slope stability analysis and *in-situ* measurements of pore water pressures (Wyllie and Mah, 2004; Duperret *et al.*, 2005), daily rainfall data were used as a proxy for ground saturation for the monthly and short term investigations (Chapters 3 and 4). Rainfall totals were not included in the long term study (Chapter 2) due to issues with scale, i.e. the time step between LiDAR surveys was too large to correlate with rainfall event data or totals. In previous studies wind has been adopted as a proxy for wave climate due to lack of modelled or measured wave and correlated with cliff top ground motions (Lim *et al.*, 2011; Norman, 2012; Vann Jones *et al.*, 2015). As this thesis uses nearshore and offshore wave data for the sites under consideration, the influence of the wind has been disregarded.

5.4.2.4 Hydrodynamics, offshore bathymetry and beach morphology

The previous two chapters of this thesis include an analysis of the relationship between the beach and nearshore water levels with the erosion volumes (Chapter 3) and cliff-top ground motion (Chapter 4). The results demonstrated that Godrevy, along the north facing coast experienced less than half the erosion measured at Porthleven, along the south-west facing coast. The erosion volumes over the year equated to a retreat rate of 0.5 m yr^{-1} at Godrevy and 1.1 m yr^{-1} at Porthleven, with 81% of erosion occurring over the winter months (Nov 2013–Mar 2014) at Godrevy and 98% at Porthleven. Inshore significant wave heights (10 m water depth) exceeded 5 m H_s and peak wave periods T_p exceeded 15 s on seven occasions between Nov and Mar at both Godrevy and Porthleven. Over the remainder of the year (Jul–Nov 2013 and Apr–Jul 2014) monthly erosion volumes ranged between 10–80 m^3 at Godrevy and 4–35 m^3 at Porthleven, normalised according to the length of the cliff face, (~300 m at both sites) equated to a monthly volume loss of 0.03–0.3 m^3 per length of cliff at Godrevy (or the equivalent of 0.04–0.32 m yr^{-1}) and 0.01–0.12 m^3 per length of cliff face at Porthleven (0.02–0.14 m yr^{-1}). During these times, inshore conditions were relatively calm at both sites with significant wave heights and wave periods averaging 1.3 m and 11 s at Godrevy and 1.1 m and 9 s at Porthleven.

During the winter, both sites were exposed to a number of extreme storms over a short period of time, however, out of the seven large wave events, three of these measured > 8 m H_s and > 20 s T_p at Porthleven only. The volume of erosion measured at Porthleven during this winter period was three times greater than Godrevy, suggesting this particularly energetic wave climate along the south-west coast may have been responsible for the large difference in erosion volumes between the sites.

Although the wave climate provides an indication of energy transfer at the coastline, and hence possible cliff erosion, the potential for wave energy to reach the cliffs depends on tidal elevations and beach characteristics as well as the wave climate itself. A recent study by Vann Jones *et al.* (2015) compared the rockfall activity along a coastal cliff in north east England with modelled cliff-toe inundation durations and cliff-top ground motions. They concluded that the relationship between the nearshore wave climate and the transfer of wave energy leading to rockfalls is more complex than tidal inundation duration alone. This notion is echoed in this thesis, where the complexity in the inundation duration at the toe of the cliffs

is both a function of the nearshore wave climate and tidal elevations and more importantly the beach and offshore slope and the beach-cliff junction elevation, and related/ resulting wave runup. Offshore bathymetry and beach slope play an important role in wave breaking and, hence, wave energy dissipation. The beach slope and variability of elevation of the beach-cliff junction fluctuates greatly between the two main sites. Porthleven is fronted by a reflective beach (tan β = 0.12) and Godrevy, an intermediate beach (tan β = 0.01) (Chapter 3). The slope and hence the beach-cliff junction elevation varies by up to 3 m at Porthleven and Godrevy.

Linear wave theory states that wave shoaling (increase in wave height as waves enter intermediate/shallow water) across wide shallow shelves results in a decrease in wave height due to bed friction, resulting in less energetic nearshore than deep water conditions. Steeply shelving coastlines, however, may experience breaking wave heights greater than deep water wave heights as no or little energy is lost due to bed friction (Komar, 1998; Masselink and Hughes, 2003). Wave breaking in the surf zone can be characterised by the dimensionless parameter, the Iribarren number (ξ) (Battjes, 1974) where the wave breaker type (spilling, plunging or surging) is a function of the slope of the beach and the square of the wave steepness. Breaker types (based on three different beach slope *scenarios* (Chapter 3)) were determined for each month during the one year survey period at each site. At Godrevy, under a mean and minimum beach slope scenario Irribarren numbers were $\xi < 0.4$ indicating spilling breakers and only exceeding 0.4 (plunging) under a maximum beach slope scenario, during more energetic periods in the winter months. At Porthleven, Iribarren numbers between 1 and 2 indicated plunging waves under a minimum beach slope scenario and surging waves ($\xi > 2$) under a mean and maximum scenario.

The difference in wave breaking is reflected in the vertical cliff-top ground motion spectra in Chapter 4. Waves breaking on the foreshore are generally associated with a peak in the higher frequencies (1–50 Hz) as the ground/cliff rings in response to wave breaking (Young *et al.*, 2011a; 2012; 2103). At Porthleven, the plunging and surging wave signal is apparent in the higher frequencies of the spectra under both energetic (Fig 4.10) and calm wave conditions (Fig. 4.12), as waves plunge onto the beach or surge into the cliffs, with more energy during high tide. This high frequency peak is not as pronounced in the Godrevy cliff top spectra (Fig. 4.11) under calm wave conditions, supporting the presence of gently spilling breakers, yet higher energy is present during high tide with large wave conditions, when the Iribarren

numbers tend to represent plunging waves. At Godrevy the peak at the infragravity frequencies is visible in both the nearshore pressure sensor spectra and the cliff-top ground motion spectra between 0.005–0.05 Hz, and is less pronounced at Porthleven under calm conditions and contains the highest amount of energy during stormy conditions.

An important parameter that influences wave-cliff interaction (identified in Chapters 3 and 4) is the wave runup extent. On beaches where the Iribarren number lies between 0.3 and 1.25 (i.e. at Godrevy) wave runup is calculated using equation 3.2. For beaches where the Irribarren number is greater than 1.25, this approximation underrepresents wave runup by an order of 2 (Masselink *et al.*, in press); therefore for Porthleven where Irribarren numbers are between 1 and 3, a modified version of the Stockdon et al. (2006) equation is used where the fitting parameter K is increased from 1.1 to 2 (Chapter 3). The differences in wave runup for Godrevy and Porthleven (Chapter 3) demonstrates the interplay between the beach morphology, wave conditions and the wave runup. At Godrevy, wave energy dissipation occurs across the shallow shelf (offshore tan β = 0.017) and intertidal zone (beach face tan β = 0.022) resulting in a decrease in run up with a decrease in beach slope. At Porthleven (offshore tan β = 0.05, beach face tan β = 0.2), little wave energy is dissipated during shoaling and wave runup *amplitude* increases at the shore to 1.5–2 times the offshore wave height, increasing with an increasing beach slope. Godrevy experiences wave-cliff interaction every high tide, under a mean and minimum beach cliff junction elevation as horizontal runup *excursion* increases with a decreasing beach slope, however Porthleven cliff-toe is only inundated every high tide under a minimum beach cliff junction elevation and during large wave events only under a maximum and mean junction scenario. The lower erosion rates at Godrevy supports the findings of Vann Jones *et al.* (2015) where cliff failure is not necessarily a function of inundation duration alone, but the energy expended on the cliffs during inundation.

The differences in cliff response, in terms of cliff top ground motion and erosion between two very similar sites, under similar forcing conditions, indicates that understanding the interplay between the wave climate, water levels and beach morphology on a site by site basis is key to understanding the processes that govern cliff erosion.

5.4.3 Estimations of wave-cliff interaction

Scaling down temporally and spatially helped to determine the main drivers and processes contributing towards variability in cliff erosion (Chapters 3 and 4). This section, revisits the results of the long term study (Chapter 2), and using the knowledge gained from the previous two chapters, allows conclusions to be drawn between the assailing and resisting forces around the southwest coastline. As Chapter 2 involved a desk based assessment of the historic (2007/8–2010/11) erosion rates around the coastline, it is not possible to carry out detailed analysis of the variability of the beach morphology and the nearshore wave climate in relation to the erosion. Estimations can be made, however, which revisit the erosion rates at each of the sites, and use beach characteristics and tidal elevations to infer the typical inundation of the cliffs and more importantly, describe how the morphology of the beach modulates the energy expended on the cliffs during these times of inundation.

Six out of the nine beaches are classified as intermediate, low-tide terrace/ low tide bar/rip (Scott, 2012), with the exception of Porthleven, (reflective), Trevellas (rocky platform) and Bedruthan Steps (intermediate/dissipative). All are exposed to a similar wave climate, with the south coast generally experiencing calmer conditions on average, compared to the north-west and south-west facing coasts. In terms of wave breaking, three of the sites experience spilling breakers (on average) (Godrevy, Portreath and Bedruthan Steps), and the remainder are subject to plunging/surging. The influence these waves have on the cliffs, however, is determined by the beach-cliff junction elevation. The beach-cliff junction elevations in Table 5.1 are taken from an average between two LiDAR surveys and are only suggestive of the frequency of cliff toe inundation, e.g., Porthleven is less frequently inundated than Bedruthan Steps. However, the results of this thesis emphasise how variable this junction along with the beach slope can be, and how crucial this variability is in influencing a) the wave runup extent and b) the cliff exposure to inundation.

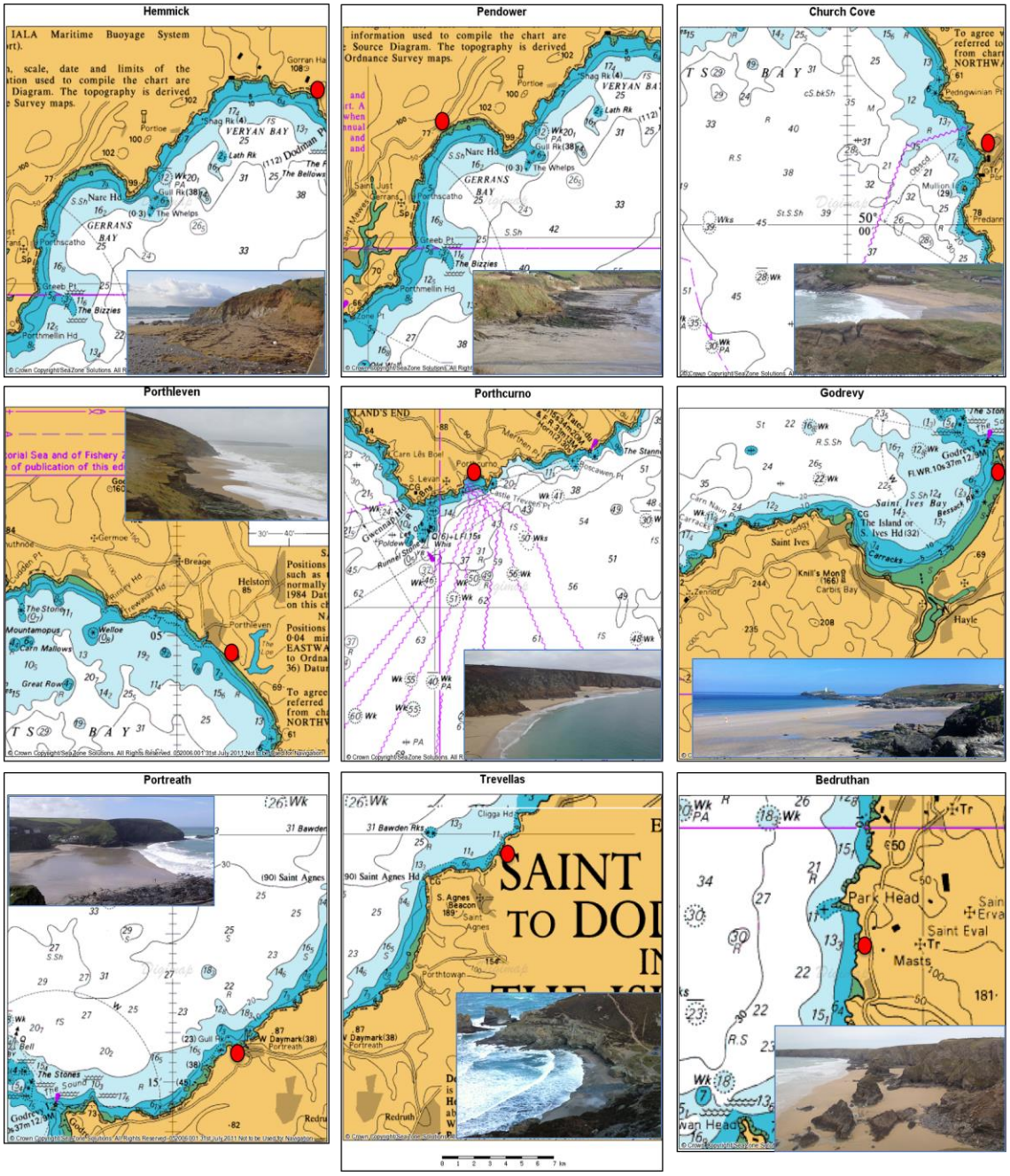

Figure 5.2: Admiralty charts for all nine sites (red circles). Offshore bathymetry has been estimated in Table 5.1 using the average depth directly offshore over a 10 km distance. Photographs of the cliffs and foreshore for each site illustrate the variety of beach types.

Without a time series of beach morphology, water levels and wave climate, it is difficult to establish the exact frequency of inundation and wave exposure for all nine sites; however, inferences can be made about the exposure of the cliffs to wave energy. The isobaths from Admiralty charts illustrate the shallow/steepness of the offshore profile and hence indicate the wave exposure. Porthcurno, for example is fronted by a steeply shelving coastal slope and beach face, experiences frequent tidal inundation (b/c junction 0.7 m and MHWS 3 m) with

an average Iribarren number of 0.9 (plunging breakers). Despite this frequent and energetic inundation, Porthcurno experiences the lowest erosion out of all of the sites. This is highly likely to be due to the high rock mass strength of the cliffs, resulting in the resisting forces exceeding assailing forces. In contrast, Porthleven has very infrequent inundation with the beach-cliff junction, on average much higher than the MHWS (5.3 m compared to 2.5 m) and a steeply sloping coastal slope and beach face. The rock mass strength is relatively low compared with other sites, which may explain the higher erosion rate (0.09 m yr^{-1}). Additionally, the results have also demonstrated the significance of extreme storm events on nearshore wave conditions, beach elevations and water levels, and during the LiDAR survey period (Chapter 2), conditions remained *calm* (< 5 m H_s) compared to conditions in Chapters 3 and 4. This thesis has demonstrated the complexity of the relationship between the nearshore environment and coastal cliff erosion, where a range of parameters and processes are responsible for the rates of cliff erosion around a coastline (Table 5.1).

Table 5.1: Summary of beach and wave characteristics for nine sites in Chapter 2. Beach type abbreviations: LTT (low tide terrace), LTBR (low tide bar-rip), Diss (dissipative), Ref (reflective). Offshore slopes estimated from Admiralty charts (UKHO, 2012); beach slopes from beach profile data (CCO, 2015) where available. Estimates determined from photographic comparison with other beaches. Beach-cliff junction elevations (b/c junct) averaged from LiDAR data. MHWS (mean high water spring tidal elevation) from UKHO, 2012. Significant wave height (H_s) and wave period (T_p) averaged from SWAN modelled wave data and erosion rates taken from Chapter 2. Iribarren number (ξ) calculated using ($\frac{\tan\beta}{\sqrt{H_0/L_0}}$) (Battjes, 1974). Erosion rates are based on the *longer term* LiDAR analysis results (Chapter 2).

Site	Beach type	GSI	Offshore (tan β)	Beach face (tan β)	b/c junct (mODN)	MHWS (mODN)	H_s (m)	T_p (s)	ξ	Rate (m yr^{-1})
Hemmick	LTT	55 – 58	0.003	0.05	2.7	2.4	0.87	5	0.5	0.03
Pendower	LTT	37 – 40	0.004	0.09	1.7	2.5	0.87	5	0.8	0.01
Church Cove	LTBR/ LTT	30 – 35	0.004	0.05	1.8	2.4	1.33	8	0.5	0.29
Porthleven	Ref	25 – 30	0.004	0.12	5.3	2.5	1.33	8	1.1	0.09
Porthcurno	LTT/ LTBR	70 – 75	0.006	0.08 (estimated)	0.7	3.0	1.1	6	0.9	0.00
Godrevy	LTBR	40 – 50	0.002	0.02	4.8	3.2	1.01	9	0.3	0.04
Portreath	LTT/ LTBR	45 – 50	0.003	0.03	3.5	3.5	1.36	9	0.3	0.06
Trevellas	Rocky platform	33 – 36	0.003	0.05 (estimated)	2.7	3.5	1.36	9	0.5	0.08
Bedruthan Steps	LTBR/ Diss	30 – 34	0.003	0.01	0.5	3.5	1.42	9	0.1	0.17

5.4.4 Significance of low-frequency, high-magnitude events

The erosion rates at Porthleven and Godrevy, calculated over the year survey period (Chapter 3) (GOD = 0.5 m yr^{-1}, PLV = 1.1 m yr^{-1}) were an order of magnitude greater than the long term rates established using LiDAR (Chapter 2) (GOD = 0.04 m yr^{-1}, PLV = 0.09 m yr^{-1}).

Firstly this emphasises the need for a site by site assessment for accurate cliff erosion volumes and secondly, due to the unprecedented conditions during that year, accentuates the importance of extreme storm events in coastal cliff erosion volumes (Fig 5.3).

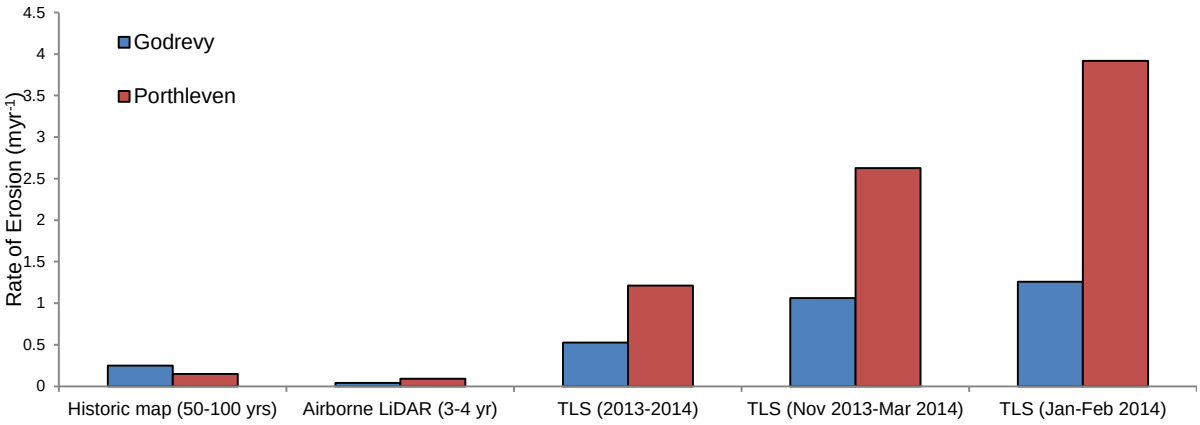

Figure 5.3: All erosion rates derived in this thesis for Porthleven and Godrevy. Historic map rates from (Ridgewell and Walkden, 2009) Airborne LiDAR from Chapter 2 and Earlie *et al.*(2013;2014), TLS rates from monthly scans over a 1-yr period (Chapter 3) and the contribution of the winter erosion volumes (Nov-Mar) and storm period (Jan-Feb) to the total erosion from the year 2013-2014.

High magnitude, low frequency events could become more frequent in the future with the risk of increased storminess associated with climate change (Dodet *et al.*, 2010). Failure detected during such events can account for up to and perhaps more than two orders of magnitude more than the long term erosion rate. The results captured using remote sensing (video cameras, TLS) and *in-situ* instrumentation (pressure sensors, seismometers) (Chapter 4) proved that site specific investigations of extreme storms on coastal cliffs and the interaction of waves with the beach and cliffs are not only obtainable, but essential in understanding how these rare events affect our coastline.

5.4.5 Recommendations for future research

The scaled approach to this research allowed for a range of instruments/methods/techniques to be tested and adopted in the field. The results, however, suggest that if we are to understand the interaction between wave impacts and cliff response in finer detail, higher frequency beach surveys and cliff scans are required to directly link forcing with failure. Fluctuation of the beach profile has proved to be highly influential in limiting wave-cliff interaction. In some cases, i.e., Porthleven, under extreme wave conditions, the beach elevation lowered beyond the point of access, hampering field measurements. A useful

method of obtaining remotely sensed, continuous beach morphological and wave runup data is via the deployment of a laser scanner at the top of the cliff (Almeida *et al.,* 2015). Difficulties with this method, however, may occur under extreme wave conditions with the risk of waves overtopping the cliff-top. An alternative remotely sensed method of obtaining continuous beach; wave and runup data is using video cameras. This proved effective, even under extreme storm conditions (Chapter 4; Earlie *et al.,* 2015) and could be explored further with an automated method of detecting cliff impacts/failures, for long time series. These data could then be cross correlated with the seismic signal and the nearshore pressure sensor for an additional level of wave-cliff impact detail.

The approach of this thesis was from a marine perspective; therefore the role of the underlying geology, the cliff lithology and the influence of meteorology has been simplified. Slope stability analysis, monitoring pore water pressures and performing kinematic analysis on the cliffs would improve the understanding of the observed and perhaps anticipated failure mechanisms of the cliffs.

An experiment involving the combined field data discussed above would provide a high-resolution time series of seismically sensed and visually observed impacts of waves at the cliff-face and would enable a direct coupling of wave-cliff interaction. The results of this study could help to refine processed based models (e.g., SCAPE, *Soft-Cliff and Platform Erosion*) (Walkden and Hall, 2005; Walkden and Hall, 2011; Carpenter *et al.,* 2014) and incorporate localised metrics for beach morphology and wave runup to help explain the spatial variability in cliff erosion under a variety of environmental settings and forcing conditions.

5.5 Thesis conclusions

The first part of this study tested the suitability of using Airborne LiDAR on a regional scale over 3–4 yrs at nine different sites, to determine volumetric changes to the cliff-face and calculate linear rates of retreat for a slowly eroding geologically ‘resistant’ coastline exposed to a highly energetic wave climate. Rates of retreat around the Cornish coastline ranged from 0.01–0.37 m yr^{-1} and were found to vary according to the spatially varying boundary conditions (rock mass characteristics, beach elevation/ cliff toe exposure) and forcing parameters (significant wave height and peak wave period). The strongest correlations were

apparent between the rate of retreat and a) the significant wave height (H_s) (0.78) b) the 10% exceedance wave height (H_{10}) (0.76) and c) the ratio between the rock mass strength and H_s (0.77) (GSI/H_s). The overall rates of retreat determined using LiDAR data were similar to the long term rates used for shoreline management, yet provided an additional level of detail that the historic map analysis method was not able to provide. This method indicated that localised studies are vital to obtaining a more accurate understanding of the rates of erosion on a shorter time scale, especially in hard rock coastlines where failure is often episodic.

Following the results of this analysis, two sites were selected to examine these findings in further detail on a shorter timescale. Monthly surveys of cliff erosion volumes at two particularly vulnerable sites indicated that the variability from month-to-month was dependent on a combination of rainfall totals and offshore wave climate, where stormy conditions during the winter months produced an increase in rainfall together with an increase in wave energy, leading to elevated rates of erosion. As well as considering the influence of offshore wave conditions, this study examined the interplay between the morphology of the beach and the wave climate. It was found that although Porthleven and Godrevy have similar physical settings, i.e., similar lithology, cliff height, exposure to waves and weather conditions (exposed to highly energetic Atlantic swell), the beaches fronting the cliffs are very different; with a reflective beach at Porthleven and intermediate/dissipative beach at Godrevy. Beach slope, wave breaker type and the elevation of the beach-cliff junction were found to directly control the extent of wave energy flux reaching the cliff toe and resultant erosion volumes at both sites. Cliffs fronted by an intermediate/dissipative beach were less vulnerable to wave energy reaching the cliffs as wave energy under larger wave conditions was dissipated offshore, before reaching the cliff toe. Cliffs fronted by a reflective beach, however were more vulnerable under highly energetic wave conditions as beach elevation fluctuations amplified wave runup and waves with greater energy were able to reach the toe of the cliffs.

The final stage of the thesis scaled-down further to consider vertical cliff top ground motions at two locations during an exceptionally stormy winter period in the UK. Cliff-top displacements were found to increase with increasing H_s and tidal elevation. Cliffs fronted by a reflective beach along the south coast of the UK, during extreme wave conditions (H_s exceeding 6 m) experienced vertical ground displacements increasing by an order of magnitude from 10 μm to 100 μm. Cliffs along the north coast fronted by a dissipative beach

saw ground displacements increase from 2 – 5 μm to 5 – 20 μm. During calm conditions at both sites displacements reduced to 'normal' levels consistent with previous studies (0.5 – 10 μm).

Cliff-top ground motions were found to be modulated differently according to the nearshore hydrodynamics and water levels, but again, according to the beach type fronting the cliffs. Under these energetic conditions, a higher proportion of IG energy was apparent in dissipative beaches compared with reflective, with the exception of periods of very high energy waves. Real time cliff-top video capture and *in-situ* wave monitoring equipment during exceptionally energetic periods allowed for association of the large ground displacements with the nearshore hydrodynamics and rare, cliff-top wave overtopping events. During this time the greatest ground motion contribution (~100 μm) originated from displacements in the IG frequencies (0.005 – 0.05 Hz). The displacement peaks in the SF (0.05 – 0.1 Hz) of 10 μm and HF (1 – 50 Hz) of 5 μm also coincided with the timings of the wave overtopping events captured with the video camera.

Cliff-face volume erosion measured over the deployment periods showed that during the extreme events on the southwest coast with cliffs fronted by a reflective beach, the long-term erosion rate was exceeded by over two orders of magnitude (i.e., 113 m^3 m^{-1} yr^{-1} *versus* 1 m^3 m^{-1} yr^{-1}) and accounted for over half the total volume loss for the year. On the north coast with cliffs fronted by an intermediate beach, with storms of similar magnitude impacting the coastline, erosion volumes were one and a half orders of magnitude greater than the long term erosion rate (i.e., 16 m^3 m^{-1} yr^{-1} *versus* 0.4 m^3 m^{-1} yr^{-1}), thus providing a geomorphic link between energetic cliff-top ground displacements and cliff failure.

In terms of understanding hard rock cliff erosion, this study has emphasised the complexity of these coastal systems. This thesis forms one of the first scaled-approach studies, investigating cliff erosion rates around a rocky coastline; using a variety of techniques and methods of measurement allowing for the detail in these complex processes to be revealed. The variety of factors that influence the rates of erosion means there is no single factor causing cliff erosion; the whole system of the physical interactions must be considered holistically in order to understand their evolution.

This is also the first time that remote (camera) and *in-situ* (seismometer) observations of cliff top ground measurements coupled with wave impacts been accomplished under such energetic wave conditions. Capturing these events during one of the stormiest periods the region has seen in 60 years and comparing the results with processes occurring under *normal* conditions, highlights the role extreme events play in contributing towards coastal cliff morphology. Having recorded microseismic cliff-top motion and captured cliff volume change on this temporal and spatial scale for the first time and determined an effective method of monitoring wave impacts *in-situ*, emphasises how investigation of cliff behaviour is not only obtainable, but paramount to understanding coastal evolution.

References

ABPMer (2015) *WEBvision –Renewables (Tide and Waves)* [Online] Available from: http://vision.abpmer.net/renewables/map_default.phtml?config=tide&resetsession=groups,resultlayers (Accessed April 2015)

Abellan, A., Calvet, J., Vilaplana, J. M., and Blanchard, J. (2010) Detection and spatial prediction of rockfalls by means of terrestrial laser scanner monitoring, *Geomorphology,* 119, 162–171.

Abellan, A., Vilaplana, J. M., Calvet, D., Garcia-Selles, D., and Asensio, E. (2011) Rockfall monitoring by Terrestrial Laser Scanning – case study of the basaltic rock face at Castellfollit de la Roca (Catalonia, Spain), *Natural Hazards earth System Science* 11, 829–841.

Adams, P. N., Anderson, R. S., and Revenaugh, J. (2002) Microseismic measurement of wave-energy delivered to a rocky coast, *Geology,* 30, 895–898.

Adams, J. C., and Chandler, J. H. (2002) Evaluation of LiDAR and medium scale photogrammetry for detecting soft-cliff coastal change. *Photogrammetric Record* 17, 405–418.

Adams, P. N., Storlazzi, C. D. and Anderson, R. S. (2005) Nearshore wave-induced cyclical flexing of sea cliffs. *Journal of Geophysical Research*, 110 DOI:10.1029/2004JF000217.

Agnew, D. C., and Berger, J. (1978) Vertical seismic noise at very low frequencies, *Journal of Geophysical Research*, 83, 5420–5424.

Alexander, A. C., and Shail, R. K. (1995) Late Variscan structures on the coast between Perranporth and St. Ives, south Cornwall, *Proceedings of the Ussher Society,* 8, 398–404.

Alexander, A. C. and Shail, R. K. (1996) Late-to post-Variscan structures on the coast between Penzance and Pentewan, south Cornwall, *Proceedings of the Ussher Society,* 9, 072–078.

Alho, P., Vaaja, M., Kukko, A., Kasvi, E., Kurkela, M., Hyyppa, J., Hyyppa, H., and Kaartinen, H. (2011) Mobile laser scanning in fluvial geomorphology: mapping and change detection of point bars, *Zeitschrift fur Geomorphologie,* 55, 31–50.

Almeida, L.P., Masselink, G., Russell, P.E., Davidson, M.A. (2015) Observations of gravel beach dynamics during high energy wave conditions using a laser scanner, *Geomorphology,* 228, 15–27.

Arber, M. A. (1949) Cliff profiles of Devon and Cornwall, *The Geographical Journal,* 114, 191-197.

Ardhuin, F., Gualtieri L., Stutzmann E. (2015) How ocean waves rock the Earth: two mechanisms explain microseisms with periods 3 to 300 s. *Geophysical Research Letters*, 42(3), 765-772. http://dx.doi.org/10.1002/2014GL062782

Ashton, A. D., Walkden, M. J. A. and Dickson, M. E. (2011) Equilibrium responses of cliffed coasts to changes in the rate of sea level rise. *Marine Geology*, 284(1-4), 217–229.

Austin, M. J., Scott, T. M., Russell, P. E., Masselink, G. (2012) Rip current prediction: development, validation, and evaluation of an operational tool. *Journal of Coastal Research*, 29(2): 283–300

Barlow, J., Lim, M., Rosser, N., Petley, D., Brain, M., Norman, E., Geer, M. (2012) Modelling cliff erosion using negative power law scaling of rockfalls, *Geomorphology*, 139–140, 416–424.

Battjies, J. A. (1974), Surf similarity, *Proceedings of the 14th Conference of Coastal Engineering*, ASCEm 446–480.

BBC (2012) *BBC news: Rain causes 'unprecedented' landslips in south-west England* [Online] Available from: http://www.bbc.co.uk/news/uk-22365093 (Accessed May 2013)

BGS (2013) *British Geological Survey: Coastal landslides and coastal erosion.* [Online] Available from: http://www.bgs.ac.uk/landslides/coastal.html (Accessed May 2013).

Bird, E. C. F. (1998) The *Coasts of Cornwall: Scenery and Geology with an Excursion Guide.* Alexander Associates.

Brain, J. M., Rosser, N. J., Norman, E. C. and Petley, D. N. (2014) Are microseismic ground displacements a significant geomorphic agent? *Geomorphology*, 207, 161–173.

Brock, J. C., and Purkis, S. J. (2009) The emerging role of LiDAR remote sensing in coastal research and resource management. *Journal of Coastal Research*, SI(53), 1–5.

Brodu, N., and Lague, D. (2012) 3D terrestrial LiDAR data classification of complex natural scenes using a multi-scale dimensionality criterion: applications in geomorphology, *ISPRS Journal of Photogrammetry and Remote Sensing*, 68, 121–134.

Bromirski, P. D., Duennebier, F. K. (2002) The near-coastal microspectrum: Spatial and temporal wave climate relationships, *Journal of Geophysical Research*, 107, doi:10.1029/2001JB000265

Bromirski, P. D., Flick, R. E., Graham, N. (1999) Ocean wave height determined from inland seismometer data: Implications for investigating wave climate changes in the NE Pacific, *Journal of Geophysical Research*, 104, 20,753–20,766.

Brooks, S. M. and Spencer, T. (2010) Temporal and spatial variations in recession rates and sediment release from soft rock cliffs, Suffolk coast, UK. *Geomorphology* 124(1-2), 26–41.

Brooks, S. M., Spencer, T., and Boreham, S. (2012) Deriving mechanisms and thresholds for cliff retreat in soft-rock cliffs under changing climates: Rapidly retreating cliffs of the Suffolk coast, UK. *Geomorphology* 153–154, 48–60.

Buckley, S. J., Mills, J. P., Clarke, P. J., Edwards, S. J., Pethick, J., and Mitchell, H. L., (2002) Synergy of GPS, Photogrammetry and INSAR for coastal zone monitoring, *Symposium on Geospatial Theory, Processing and Applications*, Ottawa.

Buscombe, D. D., and Scott, T. M. (2008) *The coastal geomorphology of north Cornwall: St. Ives Head to Trevose Head, Wave Hub impact on seabed and shoreline processes (WHISSP),* University of Plymouth, U.K.

Cai, M., Kaiser, P. K., Uno, H., Tasaka, Y., and Minami, M (2004) Estimation of rock mass deformation modulus and strength of jointed hard rock masses using the GSI system, *International Journal of Rock Mechanics & Mining Sciences,* 41, 3–19.

Caplain, B., Astruc, D., Regard, V., and Moulin, F. Y. (2011) Cliff retreat and sea bed morphology under monochromatic wave forcing: Experimental study, *Comptes Rendus Geoscience,* 343(7), 471–477.

Carpenter, N. E., Dickson, M. E., Walkden, M. J. A., Nicholls, R. J. and Powrie, W. (2014) Effects of varied lithology on soft-cliff recession rates, *Marine Geology,* 354, 40–52.

Castedo, R., Murphy, W., Lawrence, J., Paredes, C. (2012) A new process-response coastal recession model under soft rock cliffs, *Geomorphology,* 177–178, 128–143.

CCO, (2015) *Channel Coastal Observatory, Map viewer and data catalogue.* [Online] Available from: http://www.channelcoast.org/data_management/online_data_catalogue/ (Accessed Feb 2015)

Coggan, J. S., Pine, R. J., and Stead, D. (2001) A proposed methodology for rockfall risk assessment along coastlines, *Geoscience in south-west England,* 10.

Collins, B. D., and Sitar, N. (2008) Processes of coastal bluff erosion in weakly lithified sands, Pacific, California, USA., *Geomorphology,* 97(3-4), 483–501.

Cosgrove, A. R. P., Bennett, M. R., and Doyle, P. (1998) The rate and distribution of coastal cliff erosion in England: A cause for concern? In: Bennett, M.R. and Doyle, P. (Eds), *Issues in Environmental Geology: A British Perspective*. The Geological Society, London.

Damgaard, J. S., and Dong, P. (2004) Soft cliff recession under oblique waves: physical model tests, *Journal of Waterway, Port, Coastal and Ocean Engineering,* 130(5), 234–242.

Dawson, R. J., Dickson, M. E., Nicholls, R. J., Hall, J. W., Walkden, M. J. A., Stansby, P. K., Mokrech, M., Richards, J., Zhou, J., Milligan, J., Jordan, A., Pearson, S., Rees, J., Bates, P. D., Koukoulas, S. and Watkinson, A. R. (2009) Integrated analysis of risks of coastal flooding and cliff erosion under scenarios of long term change. *Climatic Change,* 95: 249–288.

De la Beche, H. T. (1839) *Report on the geology of Cornwall, Devon and West Somerset,* Longman, Orme, Brown, Green and Longmans, London.

Dewez, T., Chamblas, G., Lasseur, E., Vandromme, and R. (2009) Five seasons of chalk cliff face erosion monitoried by terrestrial laser scanner: from quantitative description to rock fall probabilistic hazard assessment, *EGU General Assembly Conference Abstracts,* 11, 8218.

Dewez, T. J. B., Rohmer, J., Regard, V., and Cnudde, C. (2013) Probabilistic coastal cliff collapse hazard from repeated terrestrial laser surveys: case study from Mesnil Val (Normandy, northern France), *In:* Conley, D.C., Masselink, G., Russell, P.E. and O'Hare, T.J. (eds.), *Proceedings 12th International Coastal Symposium* (Plymouth, England), *Journal of Coastal Research*, SI(65), 702–707.

Dickson, M. E., Kennedy, D. M., and Woodroffe, C. D. (2004) The influence of rock resistance on coastal morphology around Lord Howe Island, Southwest Pacific, *Earth Surface Processes and Landforms*, 29, 629–643.

Dickson, M. E. and Pentney, R. (2012) Micro-seismic measurements of cliff motion under wave impact and implications for the development of near-horizontal shore platforms. *Geomorphology*, 151–152, 27–38.

Dodet, G., Bertin, X. and Taborda, R. (2010) Wave climate variability in the North-East Atlantic Ocean over the last six decades. *Ocean Modelling*, 31, 120–131.

Dong, P., and Guzzetti, F. (2005) Frequency-size statistics of coastal soft-cliff erosion, *Journal of Waterway, Port, Coastal and Ocean Engineering*, 131(1), 37–42.

Dornbusch, U. and Robinson, D. (2005) *Controls on chalk cliff erosion in the eastern channel.* BAR Phase 1 report, University of Sussex.

Duperret, A., Taibi, S., Mortimore, R. N. Daigneault, M. (2005) Effect of groundwater and sea weathering cycles on the strength of chalk rock from unstable coastal cliffs of NW France, *Engineering Geology*, 78, 321–343.

Earlie, C. S., Guthrie, G. and Clipsham, V. (2012) *West of Wales Shoreline Management Plan 2: Cardigan Bay and Ynys Enlli to the Great Orme Coastal Groups, Introduction and Glossary*, Pembrokeshire County Council, Peterborough.

Earlie, C. S., Masselink, G., Russell, P.E., Shail, R.K. (2013) Sensitivity analysis of the methodology for quantifying cliff erosion using airborne LiDAR – examples from Cornwall, UK., *In:* Conley, D.C., Masselink, G., Russell, P.E. and O'Hare, T.J. (eds.), *Proceedings 12th International Coastal Symposium* (Plymouth, England), *Journal of Coastal Research*, SI(65): 470–475.

Earlie, C. S., Masselink, G., Russell, P. E., Shail, R. K. (2014) Application of airborne LiDAR to investigate rates of recession in rocky coast environments, *Journal of Coastal Conservation: Planning and Management*, DOI:10.1007/s11852-014-0341.

Earlie, C. S., Young, A. P., Masselink, G., Russell, P.E. (2015) Coastal cliff ground motions and response to extreme storm waves, *Geophysical Research Letters*, 42, DOI: 10.1002/2014GL062534.

EDF R&D, T. P. (2011) *CloudCompare (version 2.3) GPL software*. [Online] Available from: http://www.danielgm.net/cc/ (Accessed Nov 2012).

Emery, K. O. and Kuhn G. G. (1982) Sea cliffs: Their processes, profiles and classification, *Geological Society of America Bulletin*, 93, (644–654), DOI:10.1130/0016-7606(1982)93<644:SCTPPA>2.0CO;2

ESRI, (2011) *Mapping and analysis for understanding our world.* [Online] Available from: http://www.esri.com/software/arcgis/index.html (Accessed May 2012)

Fenton J. D. and McKee, W. D. (1990) On calculating the lengths of water waves, *Coastal Engineering*, 14, 499–513.

Geomatics Group, (2012) *Geomatics Group; Integrated spatial data.* [Online] Available from: https://www.geomatics-group.co.uk/geocms/ (Accessed Feb 2012)

Girardeau-Montaut, D., Roux, M., Marc, R., Thibault, G. (2005) Change detection on point cloud data acquired with a ground laser scanner. *International Archives of Photogrammetry, remote Sensing and Spatial Information Sciences*, 36 (part 3), 30–35.

Girardeau-Montaut, D. (2014) *CloudCompare Forum* [Online] Available from: http://www.danielgm.net/cc/forum/viewtopic.php?f=9&t=755&p=2523&hilit=comparison+cloud+to+cloud+cylinder+overlap#p2523 (Accessed, Feb 2014)

Grazier, V.M., (2006) Tilts in strong ground motion, *Bulletin of the Seismological Society of America* 96:6, 2090–2102.

Gutenberg, B. (1931) Bulletin of the Seismological Society of America, 21, 1.

Guza, R. T., Thornton, E. B., Holman, R. A. (1984) Swash on steep and shallow beaches, *Coastal Engineering*, 49, 708–723.

Guza, R. T., and Thornton, E. B. (1985) Observations of Surf Beat, *Journal of Geophysical Research*, 90, 3161–3172.

Hack, R., and Huisman, M. (2002) Estimating the intact rock strength of a rock mass by simple means. *Engineering Geology for Developing Countries* (Proceedings of the 9th Congress of the International Association for Engineering Geology and the Environment) Durban South Africa.

Hall, J. W., Meadowcroft, I. C., Lee, E.M., and van Gelder, P.H.A.J.M. (2002) Stochastic simulation of episodic soft coastal cliff recession. *Coastal Engineering*, 46, 159–174.

Hladik, C. and Alber, M. (2012) Accuracy assessment and correction of a LiDAR-derived salt marsh digital elevation model. *Remote Sensing of Environment*, 121, 224–235.

Hoek, E., Marinos, P. and Benissi, M. (1998) Applicability of the Geological Strength Index (GSI) classification for very weak and sheared rock masses. The case of the Athens Schist Formation. *Bulletin of Engineering Geology and the Environment*, 57, 151-160.

Jaboyedoff, M., Demers, D., Locat, J., Locat, A., Locat, P., Oppikofer, T., Robitalle, D. and Turmel, D. (2009). Use of terrestrial laser scanning for the characterization of retrogressive landslides in sensitive clay and rotational landslides in river banks, *Canadian Geotechnical Journal*, 46, 1379–1390.

Jaboyedoff, M., Oppikofer, T., Abellan, A., Derron, M.H., Loye, A., Metzger, R., and Pedrazzini, A. (2012) Use of LIDAR in landslide investigations: a review. *Natural Hazards* 61, 5–28.

Jenkins, G., M., Watts, D. G. (1968) *Spectral analysis and its applications,* Holden-Day, San Francisco.

Kennedy, D. M., Paulik, R., and Dickson, M. E. (2011) Subaerial weathering versus wave processes in shore platform development: reappraising the Old Hat Island evidence, *Earth Surface Processes and Landforms,* 36, 686–694.

Kidner, D. B., Thomas, M., Leight, C., Oliver, R., and Morgan, C. (2004) Coastal monitoring with LiDAR: Challenges, problems and pitfalls. Remote Sensing for Environmental Monitoring, Gis Applications, and Geology. Edited by M. Ehlers, F. Posa, H. J. Kaufmann, U. Michel and G. DeCarolis. Bellingham, *Spie-Int Soc Optical Engineering*. 5574, 80–89.

Komar, P.D. (1998) *Beach Processes and Sedimentation,* 2nd edn. Upper Saddle River, NJ: Prentice-Hall.

Kuhn, D. and Prufer, S. (2014) Coastal cliff monitoring and analysis of mass wasting processes with the application of terrestrial laser scanning: A case study of Rugen, Germany, *Geomorphology,* 213, 153–165.

Lague, D., Bonnet, S., Brodhu, N., Davies, T., and Leroux, J. (2012) High precision terrestrial laser scanning: measuring the individual impact of floods and landslides on meandering bedrock river dynamics (Rangitikei river, New Zealand), *Geophysical research Abstracts,* EGU General Assembly, 14.

Lague, D., Brodu, N., and Leroux, J. (2013) Accurate 3D comparison of complex topography with terrestrial laser scanner: application to the Rangitikei canyon (NZ), *ISPRS Journal of Photogrammetry and Remote Sensing* DOI:10.1016/j.isprsjprs.2013.04.00.

Lee, E. M., Hall, J. W., and Meadowcroft, I. C. (2001) Coastal cliff recession: the use of probabilistic prediction methods, *Geomorphology,* 40, 253–269.

Lee, E. M. (2002) *Soft Cliffs: Prediction of recession rates and erosion control techniques,* DEFRA/ Environment Agency, Flood and Coastal Defence R & D Programme, DEFRA Flood and Management Division, London.

Lee, E. M. (2008) Coastal cliff behaviour: Observations on the relationship between beach levels and recession rates, *Geomorphology,* 101(4), 558–571.

Leica (2015) *Leica Cyclone, 3D point cloud processing software* (version 8.1) [Software]. Available from http://hds.leica-geosystems.com/en/Leica-Cyclone_6515.htm

Leigh, C. L., Kidner, D. B., and Thomas, M.C. (2009) The Use of LiDAR in Digital Surface Modelling: Issues and Errors. *Transactions in GIS*, 13, 345–361.

Leveridge, B., and Hartley, A.J. (2006) The Variscan Orogeny: the development and deformation of Devonian/Carboniferous basins in SW England and South Wales. In: Brenchley, P.J.; Rawson, P.F., (eds.) *The Geology of England and Wales.* London, Geological Society of London, 225–255.

Leveridge, B. E. and Shail, R. K. (2011) The Gramscatho Basin, south Cornwall, UK: Devonian active margin successions. *Proceedings of the Geologists' Association*, 122, 568–615.

Lim. D. I., Choi, J. Y., and Jung, H. S. (2009) Sea-cliff erosion and retreat in semi-enclosed macrotidal embayment: Hampyung Bay, West coast of Korea, *Journal of Coastal Research*, (Proceedings of the 10th International Coastal Symposium) Lisbon, Portugal, SI(56): 732–736,

Lim, M., Rosser, N.J., Allison, R.J. and Petley, D.N. (2010) Erosional processes in the hard rock coastal cliffs at Staithes, North Yorkshire. *Geomorphology*, 114(1-2), 12–21.

Lim, M., Rosser, N. J., Petley, D. N. and Keen, M. (2011) Quantifying the Controls and Influence of Tide and Wave Impacts on Coastal Rock Cliff Erosion. *Journal of Coastal Research*, 27(1), 46–56.

Longuet-Higgins, M. S., 1950, A theory of the origin of microseisms, *Philosophical transactions of the Royal society of London. Series A, Mathematical and Physical Sciences*, 243, 1–35.

Marks, A. (1999) Interpreting geology at Portreath, Cornwall: a resource for geological education, *Geology Today*, 149.

Masselink, G., Austin, M. J., Scott, T. M., Poate, T. G., Russell, P. E. (2014) Role of wave forcing, storms and NAO in outer bar dynamics on a high-energy, macro-tidal beach, *Geomorphology*, 226, 76–93.

Masselink, G. and Hughes, M.G. (2003) *Introduction to Coastal Processes and Geomorphology*. London, Arnold.

Masselink, G., and Russell, P. (2013) Impacts of climate change on coastal erosion, *Marine climate change impacts partnership: science review*, 71–86, DOI: 10.14465/2013.arc09.071-086

Masselink, G., Scott, T., Poate, T., Almeida, P., Inch, K., Davidson, M., Russell, P. and Conley, D., in press, Measuring extreme storm dynamics and response on sandy and gravel beached: regional monitoring and storm surveys, *submitted to Earth Surface Processes and Landforms*

MathWorks (2013) *MATLAB* (Version R2013a) [Software]. Available from http://uk.mathworks.com/products/matlab/

Met Office (2012) *South West England: Climate*. [Online] Available from: http://www.metoffice.gov.uk/climate/uk/sw/print.html. (Accessed Feb 2015).

Milheiro-Oliverira, P. (2007) Bayesian statistical methods for modelling and prediction of major landslides in coastal cliffs, *Coastal Engineering Journal*, 49, 45–61.

Montreuil, A. L., Bullard, J., and Chandler, J. (2013) Detecting seasonal variations in embryo dune morphology using a Terrestrial Laser Scanner. *In:* Conley, D.C., Masselink, G., Russell, P.E. and O'Hare, T.J. (eds.), *Proceedings 12th International Coastal Symposium* (Plymouth, England), *Journal of Coastal Research*, SI(65) 1313–1318.

Nanometrics (2011) *Trillium Compact User Guide*, Nanometrics Seismological Instruments, Ontario, Canada.

Naylor, L., Stephenson, W., and Trenhaile, A.S. (2010) Rock coast geomorphology: recent advances and future research directions. *Geomorphology*, 114 (1-2), 3-11.

NOAA (2014) *National Oceanographic and Atmospheric Administration, National Data Buoy Centre, Station 62107 – Sevenstones Lightship* [Online] Available from: http://www.ndbc.noaa.gov/station_page.php?station=62107 (Accessed March 2014)

Norman, E. C. (2012*) Microseismic monitoring of the controls on coastal rock cliff erosion*, PhD thesis, Department of Geography, Durham University.

Norman, E. C., Rosser, N. J., Brain, M. J., Petley, D. N., Lim, M. (2013) Coastal cliff-top ground motions as proxies for environmental processes. *Journal of Geophysical Research – Oceans*, 118, 6807–6823.

NTSLF (2014) *National Tidal and Sea Level Facility* [Online] Available from: https://www.ntslf.org/ (Accessed Jan 2014).

Nunes, M., Ferreira, O., Loureiro, C. and Baily, B. (2011) Beach and cliff retreat induced by storm groups at Forte Novo, Algarve (Portugal). *Journal of Coastal Research*, SI (64), 795–799.

Ogawa H., Dickson, M. E. and Kench, P. S. (2015) Hydrodynamic constraints and storm wave characteristics on a sub-horizontal shore platform, *Earth Surface Processes and Landforms*, 40, 65–77.

ORFEUS (2014) *Observatories and research facilities for European Seismology, European Integrated Data Archive,* [Online] Available from: http://145.23.252.222/eida/webdc3/ (Accessed June 2014).

Orford, J., Burgess, K., Dyer, K., Townend, I. and Balson, P. (2002) 'FUTURECOAST' - The Integration of Knowledge to Assess Future Coastal Evolution at a National Scale' Paper presented at 28th International Conference on Coastal Engineering, Cardiff, 3221–3233.

Pethick, J. (1984) *An Introduction to Coastal Geomorphology*, London, Arnold.

Pethick, J. S., Crooks, S. (2000) Development of a coastal vulnerability index: a geomorphological perspective, *Environmental Conservations*, 27(4), 359–367.

Pierre, G. and Lahousse, P. (2006) The role of groundwater in cliff instability: an example at Cape Blanc-Nez (Pas-de-Calais, France). *Earth Surface Processes and Landforms*, 31(1), 31–45.

Poate, T., Kingston, K., Masselink, G., and Russell, P. (2009) Response of high-energy, macrotidal beaches to seasonal changes in wave conditions: Examples from North Cornwall, UK, *Proceedings of the 10th International Coastal Symposium* (Lisbon, Portugal) *Journal of Coastal Research*, Special Issue 56, 747–751.

Poate, T., Masselink, G., Russell, P. and Austin, M. (2014) Morphodynamic variability of high-energy macrotidal beaches, Cornwall, UK, *Marine Geology*, 350, 97–111.

Poulton, C. V. L., Lee, J. R., Hobbs, P. R. N., Jones, L., and Hall, M. (2006) Preliminary investigation into monitoring coastal erosion using terrestrial laser scanning: case study at Happisburgh, Norfolk, *Bull. Geol. Soc. Norfolk*, 56, 45–64.

Quinn, J. D., Rosser, N. J., Murphy, W., Lawrence, J. A. (2010) Identifying the behavioural characteristics of clay cliffs using intensive monitoring and geotechnical numerical modelling, *Geomorphology*, 120, 107–122.

Ramirez, J. E. (1940) An experimental investigation of the nature and origin of microseisms at St. Louis, Missouri. *Bulletin of the Seismological Society of America*. 30, 35 – 84, 139–178.

RBR (2013), *RBR logger configuration and analysis software: Ruskin* (Version 1.10.0) [Software]. Available from http://www.rbr-global.com/support/software

Ridgewell, J., and Walkden, M. (2009) *Cornwall and Isles of Scilly SMP2 Sub-cells Review of Coastal Processes and Geomorphology*, Royal Haskoning Ltd, Peterborough.

Rodgers, P. W. (1968) Response of horizontal pendulum seismometer to rayleigh and love waves tilt and free oscillations of Earth, *Bulletin of the Seismological Society of America*, 58(5), 1384–1406.

Rogers, J., Baptiste, A., and Jeans, K. (2009) National Coastal Erosion Risk Mapping – The final furlong. *Proceedings of the 44th Flood and Coastal Risk Management Conference*, Telford UK.

Rohmer, J., and Dewez, T. (2013) On the deviation of extreme sea-cliff instabilities from the power-law frequency-volume distribution: practical implications for coastal management, *In:* Conley, D.C., Masselink, G., Russell, P.E. and O'Hare, T.J. (eds.), *Proceedings 12th International Coastal Symposium* (Plymouth, England), *Journal of Coastal Research*, SI(65), 1698–1703.

Rosser, N., Lim, M., Petley, D., Dunning, S., and Allison, R. (2007) Patterns of precursory rockfall prior to slope failure. *Journal of Geophysical Research-Earth Surface* 112, DOI:10.1029/2006JF000642.

Rosser, N. J., Petley, D. N., Lim, M., Dunning, S. A. and Allison, R. J. (2005) Terrestrial laser scanning for monitoring the process of hard rock coastal cliff erosion. *Quarterly Journal of Engineering Geology and Hydrogeology*, 38(4), 363–375.

Rosser, N. J., Brain, M. J., Petley, D. N., Lim, M., Norman, E. C. (2013) Coastline retreat via progressive failure of rocky coastal cliffs, *Geology*, 41(8), 939–942.

Ruggerio, P., Holman, R. A., and Beach, R. A. (2004) Wave runup on a high-energy dissipative beach, *Journal of Geophysical Research*, 109, doi:10.1029/2003JC002160.

Ruggerio, P., Komar, P. D., McDougal, W. G., Beach, R. A. (1996) Extreme water levels, wave runup and coastal erosion, *25th International Conference on Coastal Engineering, Am. Soc. of Civ. Eng.* Orlando, Florida.

Ruggerio, P., Komar, P. D., McDougal, W. G., Marra, J. J. and Beach, R. A. (2001) Wave runup, extreme water levels and the erosion of properties backing beaches, *Journal of Coastal Research*, 17, 2, 407–419.

Runyan, K., and Griggs, G. B. (2003) The effects of armouring sea-cliffs on the natural sand supply to the beaches of California, *Journal of Coastal Research*, 19, 336–347.

Sallenger Jr., A. H., Krabill, W. B., Swift, R. N., Brock, J., List, J., Hansen, M., Holman, R. A., Manizade, S., Sontag, J., Meredith, A., Morgan, K., Yunkel, J. K., Frederick, E. B., Stockdon, H. (2003) Evaluation of Airborne Topographic Lidar for quantifying beach changes, *Journal of Coastal Research*, 19, 125–133.

Santana, D., Corominas, J., Mavrouli, O., and Garcia-Selles, D. (2012) Magnitude-frequency relation for rockfall scars using Terrestrial Laser Scanner, *Engineering Geology*, 145–146, 50–64.

SBE (2002) *Conversion of Pressure to Depth, Seabird Electronics* [Online] Available from: http://www.seabird.com/sites/default/files/documents/appnote69.pdf (Accessed Dec 2013)

Schmidt, K. A., Hadley, B. C., and Wijekoon, N. (2011) Vertical Accuracy and Use of Topographic LIDAR Data in Coastal Marshes. *Journal of Coastal Research* 27, 116–132.

Schurch, P., Densmore, A. L., Rosser, N. J., Lim, M., McArdell, B. W. (2011) Detection of surface change in complex topography using terrestrial laser scanning: application to the Illgraben debris-flow channel, *Earth Surface Processes and Landforms*, 36, 1847–1859.

Scott, T., Masselink, G., Russell, P. (2011) Morphodynamic characteristics and classification of beaches in England and Wales, *Marine Geology*, 286, 1–20.

Scott, T. M. (2012) UKBSAM: Database of physical hazards at designated UK bathing beaches. RNLI risk assessment database.

Shail, R., Coggan, J., and Stead, D. (1998) Coastal landsliding in Cornwall, UK: Mechanisms, modelling and implications. *Proceedings of the 8th International Congress of the International Association for Engineering Geology and the Environment*, (Vancouver, Canada), 1323–1330.

Shail, R. K., and Coggan, J.S. (2010) *Godrevy coastal recession baseline survey* 2009-2010, Camborne School of Mines, University of Exeter.

Shail, R. K. and Leveridge, B. E. (2009) The Rhenohercynian passive margin of SW England: Development, inversion and extensional reactivation, *C.R Geoscience*, 341, 140–155.

Shail, R. K., and Wilkinson, J. J. (1994) Late to post-Variscan extensional tectonics in south Cornwall, *Proceedings of the Ussher Society*, 8, 228–236.

Shih, S. M., Komar, P. D., Tillitson, K. J., McDougal, W. G., Ruggerio, P. (1994) Wave runup and sea-cliff erosion, *Proceedings 24th Coastal Engineering Conference, American Society of Civil Engineers*, 2170–2184.

Steers, J. A. (1964) *The Coastline of England and Wales*, Cambridge University Press, Cambridge.

Stephenson, W. J. (2006) *Coastal Geomorphology*. Progress in Physical Geography 30: 122–132.

Stephenson, W. J. and Kirk, R. M. (2000) Development of shore platforms on Kaikoura Peninsula, South Island, New Zealand Part One: The role of waves, *Geomorphology,* 32, 21–41.

Stephenson, W. J., Kirk, R. M., Kennedy, D. M., Finlayson, B. L., and Chen, Z. (2012) Long term shore platform surface lowering rates: Revisiting Gill and Lang after 32 years, *Marine Geology*, 299–302, 90–95.

Stockdon, H. F., Holman, R. A., Howd, P. A., Sallenger Jr, A. H. (2006) Empirical parameterization of setup, swash and runup, *Coastal Engineering,* 53, 573–588.

Sunamura, T. (1992) *Geomorphology of Rocky Coasts,* John Wiley and Sons Ltd., Chichester, UK.

SWCP (2014) *Southwest coast path: Latest news on path diversions* [Online] Available from: http://www.southwestcoastpath.com/newsapp/article/57/ (Accessed May 2014)

Taibi, S., Duperret, A., Fleureau, J. M. (2009) The effect of suction on the hydro-mechanical behaviour of chalk rocks, *Engineering Geology,* 106, 40–50.

Tillotson, K., and Komar, P.D. (1997) The wave climate of the Pacific Northwest (Oregon and Washington): A comparison of data sources: Journal of Coastal Research, 13, 440–452.

Traer, J., Gerstoft, P., Bromirski, P. D., Shearer, P. M. (2012) Microseisms and hum from ocean surface gravity waves, *Journal of Geophysical Research,* 117, DOI: 10.1029/2012JB009550.

Travelletti, J., Malet, J. P., Delacourt, C. (2014) Image-based correlation of Laser Scanning point cloud time series for landslide monitoring, *International Journal of Applied Earth Observation and Geoinformation,* 32, 1–18.

Trenhaile, A. S. (1987) *The Geomorphology of Rock Coasts,* Oxford, Clarendon Press.

Trimble (2012) *Trimble Business Centre* (Version 2.70) [Software] Available from: http://www.trimble.com/Survey/trimble-business-center.aspx

UKHO, (2012) *UK Hydrographic Office; Products and Services*. [Online] Available from: http://www.ukho.gov.uk/ProductsandServices/Pages/Home.aspx. (Accessed May 2012)

USGS. (2012) *Digital Shoreline Analysis System* [Online] Available from: http://woodshole.er.usgs.gov/project-pages/dsas/ (Accessed April 2012).

USGS (2014) *Earthquake Hazards Program,* [Online] Available from: http://comcat.cr.usgs.gov/earthquakes/eventpage/usc000mfuh#pager (Accessed Oct 2014).

Vaaja, M., Hyyppa, J., Kukko, A., Kaartinen, H., Hyyppa, H., and Alho, P. (2011) Mapping topography changes and elevation accuracies using a mobile laser scanner, *Remote Sensing,* 3, 587–600.

Vann Jones, E.C., Rosser, N.J., Brain, M.J., Petley, D.N. (2015) Quantifying the environmental controls on erosion of a hard rock cliff, *Marine Geology,* 363, 230–242.

Vetterling, W. T., Press, W. H., Teukolsky, S. A. and Flannery, B. P. (1988) *Numerical recipes: example book (C)* Cambridge University Press, New York, NY.

Walkden, M. J., and Dickson, M. (2008) Equilibrium erosion of soft rock shores with a shallow or absent beach under increased sea level rise, *Marine Geology,* 251, 75–84.

Walkden, M. J., and Hall, J. W. (2005) A predictive Mesoscale model of the erosion and profile development of soft rock shores, *Coastal Engineering,* 52, 535–563.

Walkden, M. J., and Hall, J. W. (2011) A mesoscale predictive model of the evolution and management of a soft-rock coast. *Journal of Coastal research,* 27, 529–543.

Wangensteen, B., Eiken, T., Odegard, R. S., and Sollid, J. L. (2007) Measuring coastal cliff retreat in the Kongsfjorden area, Svalbard, using terrestrial photogrammetry, *Polar Research,* 26, 14–21.

Waters B. E., and Payne, H. R. (2006) Meeting report: Soft coastal cliff: Understanding and managing retreat, *Maritime Engineering,* (Proceedings of the Institution of Civil Engineers) 159, 77–79.

Westgate, B. M., Coggan, J. S., Pine, R. J. (2003) Development of a risk-based approach to coastal slope instability assessment in Cornwall. *Geoscience in south-west England,* 10, 390–396.

Westoby, M.J., Brasington, J., Glasser, N.F., Hambrey, M.J., Reynolds, J.M., (2012) 'Structure-from-Motion' photogrammetry: A low-cost, effective tool for geoscience applications, *Geomorphology,* 179, 300–310

Wood, J. D. and Fisher P. F. (1993). Assessing interpolation accuracy in elevation models. *Computer Graphics and Applications, IEEE* 13, 48–56.

Wyllie, D.C., and Mah, C.W. (2004) *Rock Slope Engineering: Civil and Mining*. (4th edition), Spon Press, London.

Xeidakis, G. S., Delimani, P., and Skias, S. (2007) Erosion problems in Alexandroupolis coastline, North-Eastern Greece, *Environmental Geology,* 53, 835–848.

Xhardé, R., Long, B. F., and Forbes, D. L. (2006) Accuracy and limitations of airborne LiDAR surveys in coastal environments. In: 2006 *International Geoscience and Remote Sensing Symposium* 2412–2415. Denver, CO: IEEE.

Young, A. P., Adams, P., O'Reilly, W. C., Flick, R. E., Guza, R. T. (2011a) Coastal cliff ground motions from local ocean swell and infragravity waves in southern California, *Journal of Geophysical Research,* 116, DOI: 10.1029/2011jc007175.

Young, A. P. and Ashford, S. A. (2006) Application of airborne LiDAR for seacliff volumetric change and beach-sediment budget contributions. *Journal of Coastal Research* 22, 307–318.

Young, A. P., Flick, R. E., Gutierrez, R., and Guza R.T. (2009) Comparison of short-term seacliff retreat measurement methods in Del Mar, California. *Geomorphology* 112, 318–323.

Young, A. P., Guza, R. T., Adams, P. N., O'Reilly, W. C., Flick, R. E. (2012) Cross-shore decay of cliff top ground motions driven by local ocean swell and infragravity waves, *Journal of Geophysical Research,* 117, DOI: 10.1029/2012JC007908.

Young, A. P., Guza, R. T., Dickson, M.E., O'Reilly, W. C., Flick, R. E. (2013) Ground motions on rocky, cliffed, and sandy shorelines generated by ocean waves, *Journal of Geophysical Research: Oceans,* 118, 6590 – 6602, DOI: 10.1002/2013JC008883.

Young, A. P., Guza, R. T., O'Reilly, W. C., Flick, R. E., and Gutierrez, R., (2011b) Short-term retreat statistics of a slowly eroding coastal cliff. *Natural Hazards and Earth System Sciences* 11, 205–217.

Zhang, K., Whitman, D., Leatherman, S., and Robertson, W. (2005) Quantification of beach changes caused by Hurricane Floyd along Florida's Atlantic coast using airborne laser surveys. *Journal of Coastal Research,* 21, 123–134.

Zopf, D.O., Creech, H.C., and Quinn, W.H. (1976) The wavemeter: A land-based system for measuring nearshore ocean waves: *Marine Technological Society Journal*, 10, 19–25.

Appendix

Appendix 1 – Point cloud comparison method: M3C2 scales explained

Normal Scale

The normal scale is defined as the scale or distance to which the first point cloud looks for change in the next. In three-dimensional complex surfaces this is complicated by the fact that the surface normal for every point changes according to the surface roughness. If the normal scale is smaller than or of a similar scale to the surface roughness, the orientation will fluctuate strongly and result in an overestimation of distance between the two clouds (Fig 3.7b). The algorithm offers two options, to either choose a uniform normal scale for the entire point cloud or provide a range of normal scales which the algorithm can apply iteratively to the point cloud. Choosing a uniform normal scale, although more efficient for processing, may lead to a surface smoothing effect and may miss changes in surface orientation. By using a gradually increasing normal scale (in this case from 2 m incrementing at 1 m intervals to 10 m) the most suitable scale at which the plane best fits the surface is selected. This scale is selected based on Principal Component Analysis (PCA) of the coordinates of the nearest neighbours of a point (*i*, Fig 3.7a) within a sphere of radius *d* (Fig 3.7a). The PCA provides the eigenvector and eigenvalues of the covariance matrix of the three dimensional data within the sphere. The three eigenvalues resulting from the PCA account for the variance within the matrix, ordered by decreasing magnitude. If only the first eigenvalue is considered, this only accounts for the variance in one dimension, and the second, two dimensions. In order to consider the data in three dimensions, three eigenvalues are considered and the proportion of each eigenvalue to the total variance defines how 1D, 2D or 3D the cloud appears at a given scale. The scale chosen is that at which the third component is the smallest, hence the scale normal to the surface of the cliff, with its origin oriented towards the scanner. Performing PCA on a gradually increasing normal scale allows the algorithm to determine the optimum scale when the surface roughness is at its minimum (Brodhu and Lague, 2012; Lague *et al.*, 2013).

Projection Scale

The projection scale is essentially the diameter of the base of the 'cylinder' that is projected from one cloud to another to estimate surface change (Lague *et al.*, 2013) (Fig 3.7a). The surface distance will only be calculated if this cylinder contains more than 4 points in either point cloud (n_1 and n_2). For greater statistical significance, Lague *et al.* (2013) stated that the projection scale should be large enough to contain an average minimum of 20 points, but small enough to not degrade the spatial resolution by spatial averaging. On this basis sensitivity analysis was carried out on two consecutive point clouds to determine the optimum projection scale at each site.

Projection depth

This is the maximum projection distance to which one cloud is projected onto the next. It is assigned to speed up the calculation and in this case is 4 m. It is unlikely that the monthly difference between the two point clouds will exceed this value.

Registration error

This varies for each point cloud according to the accuracy of the georeferenced targets and hence the validity of the point cloud registration. The registration is performed using the point cloud processing software *Cyclone* and a mean absolute registration error is computed according to the root mean squared error of the registered ScanWorld.

Due to computational times and inability to calculate changes for very large data sets (>20 million points) the surface change analysis was initially performed on point clouds reduced from 2 cm resolution to 20 cm resolution. Upon analysis, it appeared that smoothing the surface in such a way was missing out the very changes that were occurring at this scale. A 10 cm resolution was suitable for capturing the surface detail yet allowing for ease of computation.

It is important to use the highest resolution that the software can cope with in order to optimise the changes seen on a surface such as complex topography. In order to do this, the point cloud was halved for analysis in M3C2 and then merged back together for analysis in Matlab.

Distance calculation

Once the appropriate normal scale and projection scales are defined, the intercept of each cloud within the cylinder results in two sets of points, one for each point cloud. The average position of the points in each cloud (i_1 and i_2) is calculated along the normal and the standard deviations of the points (σ_1 *(d)* and σ_2 *(d)*) provides the surface roughness along the normal direction (Fig 3.7b).

Level of Detection – Confidence interval

The algorithm also incorporates a spatially variable confidence interval for each distance calculated. This confidence interval, defined at 95%, determines the measurement accuracy dependant on the registration error (*reg*) and the surface roughness (σ_1 and σ_2) and informs us whether or not a statistically significant chance is detected. This value is provided in the output file of the algorithm, referred to as the Level of Detection$_{95\%}$ (LOD$_{95\%}$) (Lague *et al.*, 2013) (Eqn A1). This then provides us with data that is a) a statistically significant change and b) actual change as opposed to registration error or error due to surface roughness.

$$LOD_{95\%}(d) = \pm 1.96\left(\sqrt{\frac{\sigma_{1(d)^2}}{n_1} + \frac{\sigma_{2(d)^2}}{n_2}} + reg\right) \qquad \text{Equation A1}$$

The resultant output from the M3C2 algorithm batch file provides the following data:

- The original coordinates from the core point file and the projected coordinates on the second point cloud
- The distance between the two clouds along the normal vectors L_{M3C2}
- The upper limit of the confidence interval, the local LOD$_{95\%}$
- Whether or not the difference is statistically significant at the LOD$_{95\%}$
- The number of points within each cylinder on each point cloud
- The standard deviation of points from the plane thought the point cloud (surface roughness)

Appendix 2 – Seismic transfer function correction

The transfer function used to determine the instrument output correction values was calculated using the poles and zeros provided in the instrument manual (Nanometrics, 2011).

Table A2a: Poles and Zeros for transfer function for Trillium Broadband Seismometer

Symbol	Parameter	Nominal values	Units
z_n	Zeros	0 0 -434.1	rad/s
p_n	Poles	-0.03691 +/- 0.037121i -371.2 -373.9 +/- 475.5i -588.4 +/- 1508i	rad/s
k	Normalisation factor	8.184×10^{11}	$(rad/s)^4$
f_0	Normalisation frequency	1	Hz
S	Ground motion sensitivity at f_0	749.1	V s/m

These values are used as inputs for the Matlab 'zpk' function to define the transfer function according to the equation

$$F(s) = S.k.\frac{\prod_n(s - z_n)}{\prod_n(s - p_n)}$$ Equation A2a

$$where \quad k = \left|\frac{\prod_n(i2\pi f_0 - p_n)}{\prod_n(i2\pi f_0 - z_n)}\right|$$ Equation A2b

The inland seismic data were corrected using the same method. The instruments are different models and therefore their output responses also differ. The poles and zeros used to correct the inland seismic data are provided in the table below (BGS, 2014).

Table A2b: Poles and Zeros for transfer function for BGS Seismometer

Symbol	Parameter	Nominal values	Units
z_n	Zeros	0 0 -161 -108	rad/s
p_n	Poles	-0.01815 +/- 0.01799i -173.0 -196.0 +/- 231.0i -732.0 +/- 1415.0i	rad/s
k	Normalisation factor	2.3132×10^9	$(rad/s)^4$
f_0	Normalisation frequency	1	Hz
S	Ground motion sensitivity at f_0	749.1	V s/m

Appendix 3 – 'Apparent' horizontal ground motions from seismometer deployments

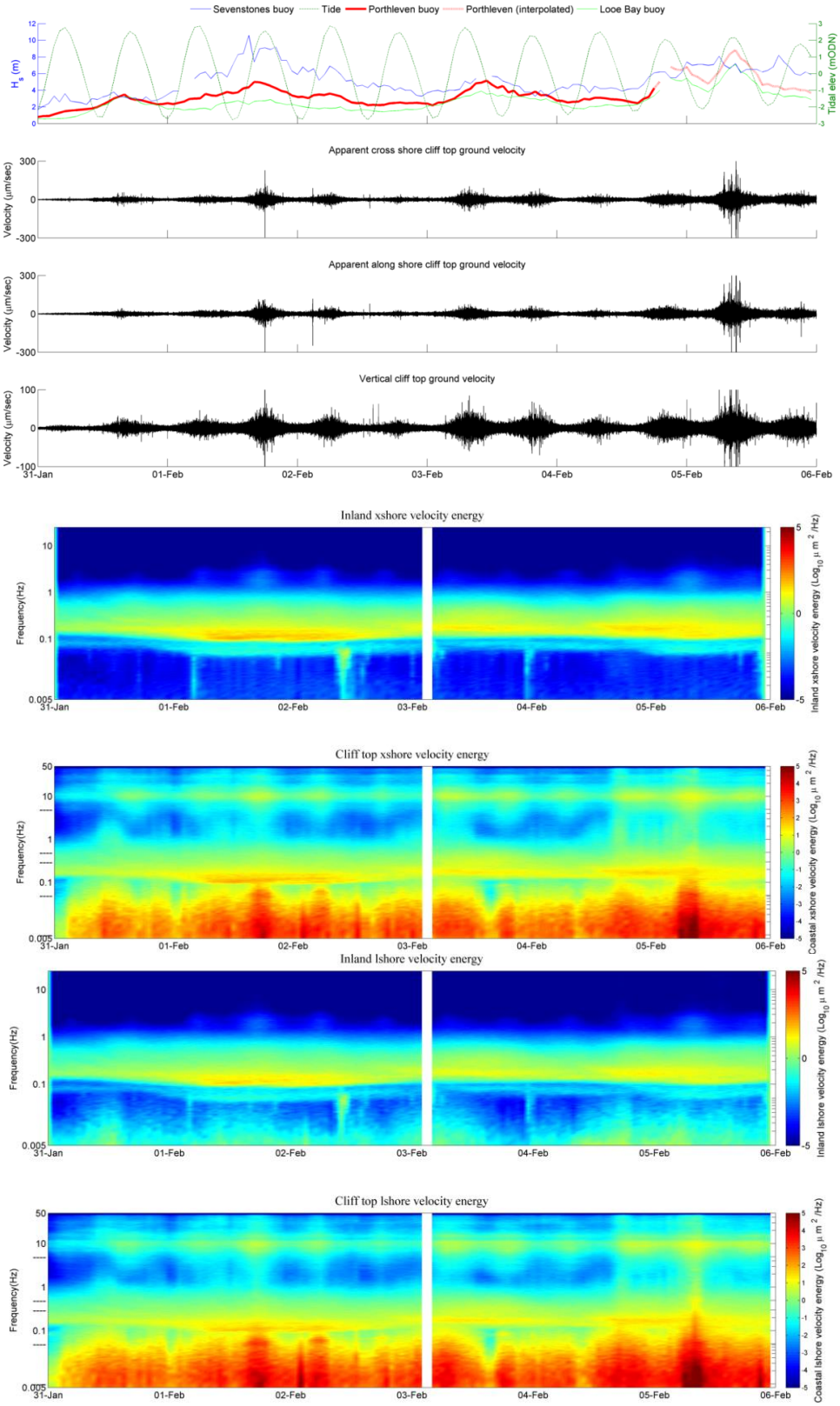

Figure A3a: Apparent cross shore and alongshore cliff top and inland seismometer velocity and energy (PLV1)

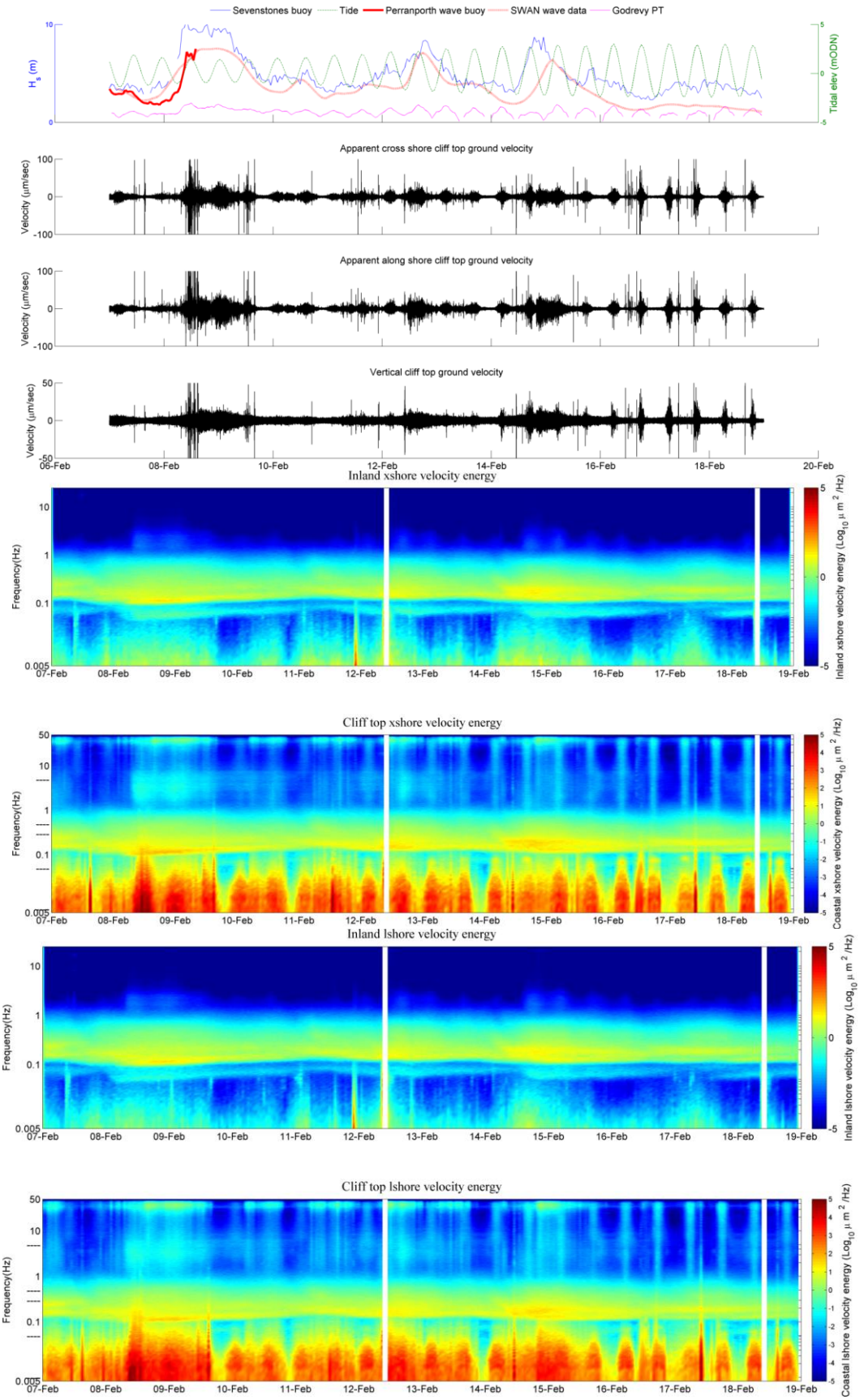

Figure A3b: Apparent cross shore and alongshore cliff top and inland seismometer velocity and energy (GOD)

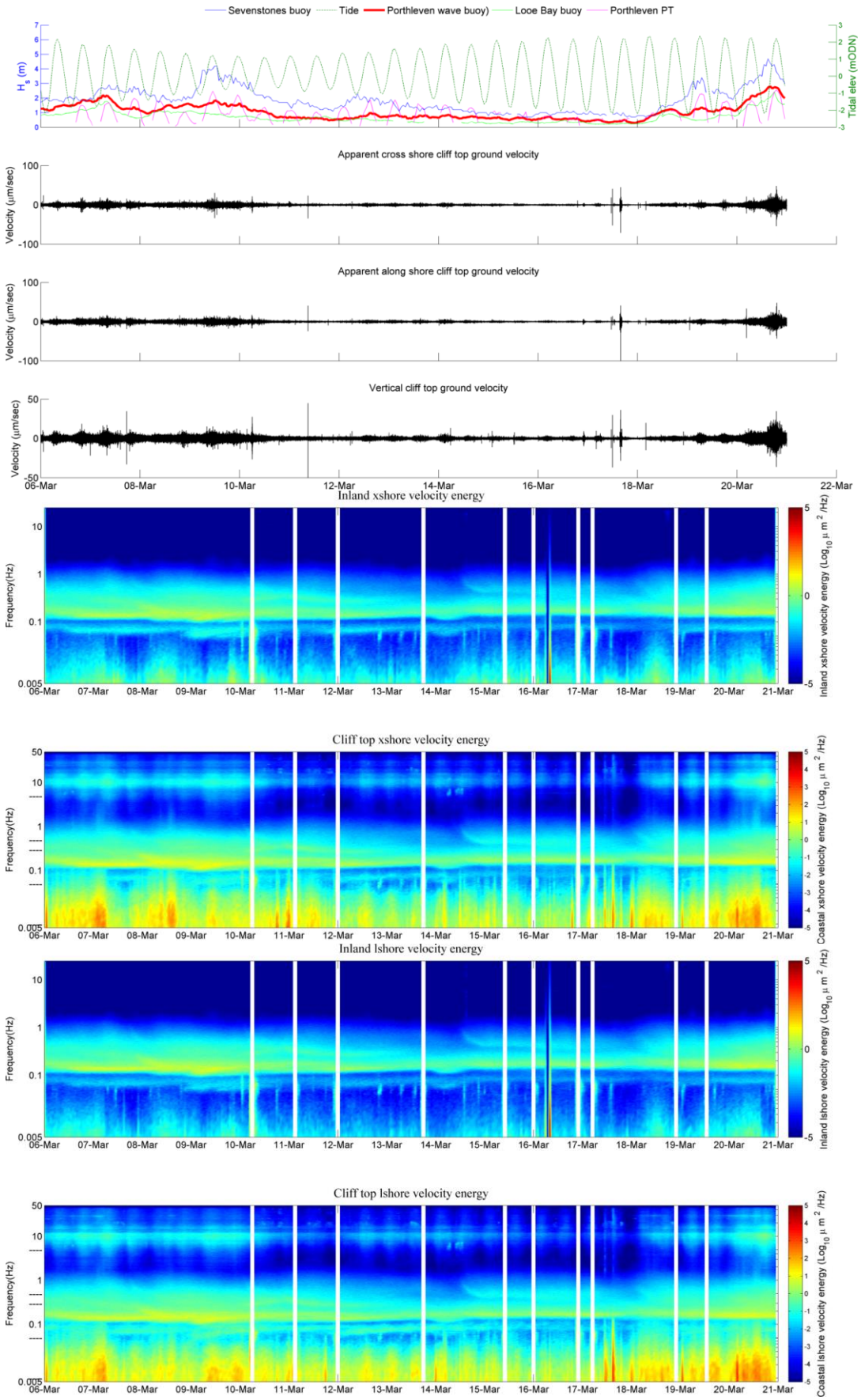

Figure A3c: Apparent cross shore and alongshore cliff top and inland seismometer velocity and energy (PLV2)

Appendix 4

Earlie, C.S., Young, A.P., Masselink, G., Russell, P.E. (2015) Coastal cliff ground motions and response to extreme storm waves. *Geophysical Research Letters*, DOI: 10.1002/2014GL062534

Appendix 5

Earlie, C.S., Masselink, G., Russell, P.E., Shail, R.K. (2014) Application of airborne LiDAR to investigate rates of recession in rocky coast environments, *Journal of Coastal Conservation*, DOI: 10.1007/s11852-014-0340-1

Appendix 6

Earlie, C.S., Masselink, G., Russell., P.E., Shail., R.K. (2013) Sensitivity analysis of the methodology for quantifying cliff erosion using airborne LiDAR – examples from Cornwall, UK., *In:* Conley, D.C., Masselink, G., Russell, P.E., and O'Hare, T.J. (Eds), *Proceedings 12th International Coastal Symposium, Plymouth, UK. Journal of Coastal Research*, SI (65): 470-475.